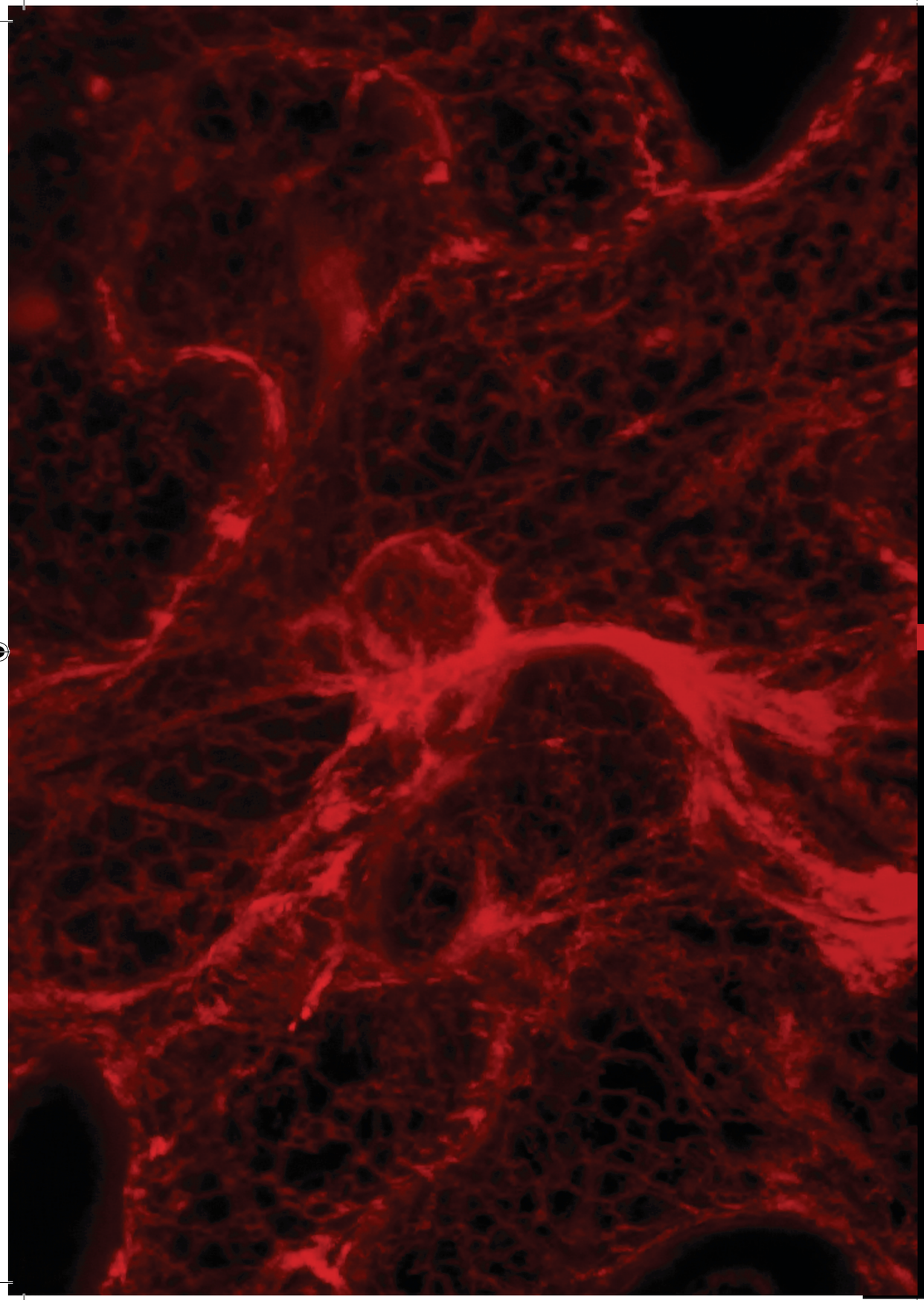

Visualizing brassinosteroid receptor hetero-oligomers in *Arabidopsis* roots C.A. BÜCHERL 2013

Visualizing brassinosteroid receptor hetero-oligomers in *Arabidopsis* roots

Christoph A. Bücherl

Visualizing brassinosteroid receptor hetero-oligomers in *Arabidopsis* roots

Christoph Albert Bücherl

THESIS COMMITTEE

Promotor
Prof. Dr S.C. de Vries
Professor of Biochemistry
Wageningen University

Co-promotor
Dr ing J.W. Borst
Assistant Professor, Laboratory of Biochemistry
Wageningen University

Other members
Dr A.I. Caño-Delgado, Centre de Recerca en Agrigenòmica, Barcelona, Spain
Dr J.C. Hohlbein, Wageningen University
Prof. Dr M.E. Janson, Wageningen University
Dr S. Robatzek, The Sainsbury Laboratory, Norwich, England

This research was conducted under the auspices of the Graduate School of Experimental Plant Sciences.

Visualizing Brassinosteroid Receptor Hetero-oligomers in *Arabidopsis* Roots

Christoph A. Bücherl

Thesis

submitted in fulfillment of the requirements for the degree of doctor
at Wageningen University
by the authority of the Rector Magnificus
Prof. Dr M.J. Kropff,
in the presence of the
Thesis Committee appointed by the Academic Board
to be defended in public
on Wednesday 11 September 2013
at 11 a.m. in the Aula.

Christoph A. Bücherl
Visualizing brassinosteroid receptor hetero-oligomers in *Arabidopsis* roots, 201 pages.

PhD thesis, Wageningen University, Wageningen, NL (2013)
With references, with summaries in Dutch, English, and German

ISBN 978-94-6173-654-3

Layout and printing: Optima Grafische Communicatie, Rotterdam, The Netherlands

For my Family

TABLE OF CONTENTS

Chapter 1

General Introduction

Christoph A. Bücherl

"Living matter evades the decay to equilibrium" (Schrödinger, 1951). This is how Erwin Schrödinger defined living objects at a lecture at the Trinity College of Dublin in 1943. And indeed, also nowadays living matter is characterized as a dissipative system (Dehmelt and Bastiaens, 2010). As such, microbes, animals and plants continuously exchange energy and matter with their environment to avoid equilibrating with the surroundings, which would result in death. This also implies that every organism and each cell has to sense its habitat to adapt to external and internal dynamics. Therefore cells are equipped with a wide array of cell surface and intracellular receptors (Gómez-Gómez and Boller, 2002), which allow the perception of signals that in turn dictate the physiological condition of the cell. Collectively, signal perception by receptors, the subsequent intracellular signal relay, and the generation of adequate cellular responses form so-called signal transduction pathways.

Traditionally, these signaling pathways or cascades have been considered as linear sequences of biochemical reactions that relay the signal, being a ligand or stimulus perception, to downstream components, which ultimately regulate gene transcription (Dehmelt and Bastiaens, 2010). However, this concept only provides a very limited representation of the actual conditions cells and organisms are embedded in. Living matter is continuously confronted with a plethora of signals like light, temperature, nutrient availability, hormones, or the presence of pathogens. The identification of key regulators like mitogen-activated protein (MAP) kinases that participate as core machineries in many different signaling responses therefore led to a conceptual change and the hourglass model for signal transduction pathways was introduced (Citri and Yarden, 2006). This model describes the perception of a wide array of signals, which are integrated via core machineries or central nodes that in turn enable the generation of tailor-made cellular outputs according to the input composition. Recent advances in systems biology and application of cross-disciplinary experimental approaches provided an even more holistic view of signaling processes (Dehmelt and Bastiaens, 2010). Nowadays, most signaling circuits are seen as part of an interconnected signaling network that allows signal integration at different levels (Dehmelt and Bastiaens, 2010; Wang et al., 2012; Zhu et al., 2013). Often these networks are bistable, thus maintain two steady states, which are interconverted by signal perception (Citri and Yarden, 2006). As a consequence of system bistability also the cellular responses are often binary and allow a cell to survive or die, divide or differentiate, or to activate and repress specific genes. Essential determinants for the final cellular output are already the receptor complexes that perceive the input signals, the very first constituents of signal transduction. Differential homo- and hetero-oligomerization of the respective ligand-binding receptors and associated coreceptors or regulatory components provides plentiful possibilities of signaling specificity within an integrated signaling network (Mellado et al., 2001; Springael et al., 2005; Wang and Norcross, 2008; Rozenfeld and Devi, 2010; Ehrlich et al., 2011; Liebmann, 2011).

In plants, brassinosteroid (BR) signaling represents one of the most prominent signal transduction cascades or networks (Zhu et al., 2013). BRs form a ubiquitous class of phytohormones (Kutschera and Wang, 2012), which are structurally similar to animal steroids (Grove et al., 1979). In analogy to their animal counterparts, BRs influence several aspects of plant growth and development (Clouse, 2011; Wang et al., 2012). Mutants, which are impaired in BR biosynthesis or BR perception, show dwarfed stature, dark-green color and de-etiolated phenotypes when grown in darkness (Kutschera and Wang, 2012). Recent studies revealed that BRs coregulate a wide range of other hormonal and environmental signals, which places them high in the hierarchy of the plant regulatory system (Wang et al., 2012).

Leucine-rich repeat receptor-like kinases

The BR signaling cascade involves several plasma membrane (PM)-located receptors, all belonging to the family of receptor-like kinases (RLKs). RLKs form the largest family of plant cell surface receptors with more than 600 members in Arabidopsis thaliana (Shiu and Bleecker, 2001b). These receptors comprise an extracellular domain, which can function as a ligand-binding domain, a single-pass transmembrane region, and an intracellular domain composed of a juxtamembrane domain, a kinase domain and an auto-inhibitory C-terminal tail (Gish and Clark, 2011). According to their kinase phylogeny, extracellular domains, and intron information, the family of RLKs was divided into 46 subfamilies (Shiu and Bleecker, 2003). The largest clade among these subfamilies, with more than 230 members in Arabidopsis thaliana, is formed by RLKs with a leucine-rich repeat extracellular domain (Lehti-Shiu et al., 2009). Members of this RLK subfamily fulfill diverse functions ranging from growth and development to abiotic and biotic stress responses (Shiu and Bleecker, 2001a).

Structurally LRR-RLKs are similar to animal receptor tyrosine kinases (RTKs) like the epidermal growth factor receptor (EGFR) (Walker, 1994). In contrast to their animal analogs, plant LRR-RLKs are based on phylogenetic and biochemical analyses generally classified as Ser/Thr kinases, not unlike the five cytosolic animal kinase homologs Pelle (Drosophila melanogaster), Pelle-like kinase (Caenorhabditis elegans) and the three human interleukin 1-receptor associated kinases (IRAKs) (Shiu and Bleecker, 2001b). However, there are also exceptions. For example, for two members of the Somatic embryogenesis receptor-like kinase (SERK) family and the BR-perceiving receptor Brassinosteroid insensitive 1 (BRI1) dual-specificity was reported (Shah et al., 2001; Oh et al., 2009; 2010). These three LRR-RLKs cannot only phosphorylate Ser and Thr residues, but also Tyr moieties. Interestingly, these three PM-located receptors are involved in the same signal transduction pathway, the BR signaling cascade (Li et al., 2002; Nam and Li, 2002; Karlova et al., 2006; Albrecht et al., 2008), as illustrated in the following sections.

The multi-tasking SERK family

The first SERK gene was discovered in carrots (Daucus carota) as a marker for single embryogenic cells in culture (Schmidt et al., 1997). Subsequently, phylogenetic analysis led to the identification of the Arabidopsis thaliana SERK protein family, which comprises the five members SERK1 to SERK5 and belongs to the LRR-RLK subfamily II (Hecht et al., 2001). SERKs are characterized by an N-terminal leucine-zipper (LZ) domain, five LRRs (of which the most N-terminal one is truncated) and a proline-rich (SPP) region just upstream of the transmembrane domain (Baudino et al., 2001). The schematic domain architecture of SERK3, also known as BRI1-associated kinase 1 (BAK1) (Nam and Li, 2002; Li et al., 2002), as an example for the SERK family is shown in Figure 1.

A hallmark of the SERK proteins is their multi-tasking ability (Chinchilla et al., 2009; Li, 2010; Kim et al., 2013). Even though no ligand-binding activity has been demonstrated to date, for all SERK family members, except SERK5, which most likely is kinase inactive (He et al., 2007), functions in diverse physiological pathways were discovered. SERK1 to SERK4 were all associated with plant immunity (Chinchilla et al., 2007; Kemmerling et al., 2007; Heese et al., 2007; Roux et al., 2011). Additionally, a role for SERK1 in abscission (Lewis et al., 2010), in somatic embryogenesis (Hecht et al., 2001) and redundantly with SERK2 in male sporogenesis was reported (Albrecht et al., 2005). SERK3 and SERK4 moreover function in cell death regulation (Kemmerling et al., 2007; He et al., 2007) and together with SERK1

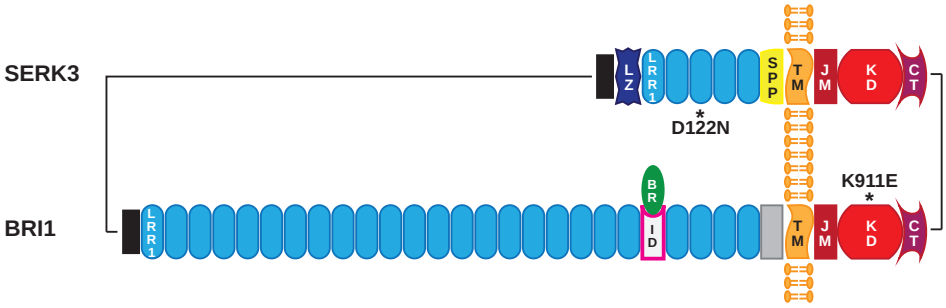

Figure 1: Schematic domain architecture of SERK3 and BRI1.
The extracellular domain of SERK3 comprises a leucine zipper domain (LZ), five leucine-rich repeats (LRR), and a proline-rich region (SPP). A single-pass transmembrane domain (TM) connects the extracellular domain to the intracellular SERK3 domain composed of a juxtamembrane region (JM), a kinase domain (KD), and C-terminal tail (CT). BRI1 consists of 25 LRRs, which enclose the island domain (ID) responsible for brassinosteroid (BR) binding, a TM domain, followed by the intracellular JM region, KD, and the CT. The signal peptide regions of both LRR-RLKs are presented as black boxes. The gray box represents an unassigned region.
Many different studies showed interaction between BRI1 and SERK3, a process in which both the extracellular LRR domains and intracellular kinase domains are involved (Jaillais et al., 2011a; Nam and Li, 2002; Li et al., 2002), as indicated by the black lines. The point mutant D122N in the third LRR of SERK3 enhances oligomerization (Jaillais et al., 2011a), whereas the point mutant K911E in the BRI1 kinase domain compromises the interaction between the two plasma membrane receptors (Wang et al., 2008). (Adapted from Kim and Wang, 2010)

control BR signal transduction (Nam and Li, 2002; Li et al., 2002; Albrecht et al., 2008; Gou et al., 2012). Their participation in various signaling pathways illustrates that SERKs show a certain degree of redundancy, but also have specific functions (Albrecht et al., 2008).

The specificity of SERK proteins is accomplished by differential hetero-oligomerization with ligand-binding receptors like EMS1/EXS for male sporogenesis (Canales et al., 2002; Zhao et al., 2002), EFR and FLS2 for plant immunity (Chinchilla et al., 2007; Kemmerling et al., 2007; Heese et al., 2007; Schwessinger et al., 2011; Roux et al., 2011), or BRI1 for BR signal transduction (Nam and Li, 2002; Li et al., 2002; Gou et al., 2012). In these receptor complexes SERKs act as coreceptors or regulators that enhance or enable downstream signaling (Wang et al., 2008; Gou et al., 2012).

Most likely due to their redundant functions, single loss-of-function serk mutants do not show clear phenotypes (Albrecht et al., 2008). An exception is SERK3. This most prominent member of the SERK family appears to be a key regulator of several physiological pathways (Chinchilla et al., 2009). Loss-of-function mutants of serk3 gave rise to uncontrolled cell death (Kemmerling et al., 2007; Heese et al., 2007), compromised plant immunity (Chinchilla et al., 2007; Kemmerling et al., 2007; Heese et al., 2007) and BR-related phenotypes (Nam and Li, 2002; Li et al., 2002; Kemmerling et al., 2007; Albrecht et al., 2008; Gou et al., 2012). Therefore it was speculated that SERK3 may act as integrator for the different signaling pathways and may form the molecular interface for pathway cross talk. In contrast to Belkhadir et al. (2012), who proposed SERK3-mediated cross talk for immune and BR signaling, Albrecht et al. (2012) reported that SERK3 is not rate limiting for the physiological responses of these two pathways and that cross talk occurs downstream or independently of the hetero-oligomerization between SERK3 and the respective ligand-binding receptors. Instead, separate cellular SERK3 pools for the different signaling routes were proposed (Albrecht et al., 2012). Based on semi-quantitative coimmunoprecipitation experiments it was concluded that approximately 5% of total SERK3 protein participates in BRI1-mediated BR signal transduction (Albrecht et al., 2012).

To understand why SERK3 or SERKs in general are employed by multiple distinct signal transduction pathways, it is important to reveal their precise mode of action. Here, we will focus on BR signaling and the concerted action of SERK3 and BRI1, the receptor that perceives BRs at the cell surface of plant cells (He et al., 2000; Kinoshita et al., 2005).

BRI1, the signal perceiving receptor

As mentioned above, SERK3 is an essential component of BR signaling and acts in this particular pathway as a coreceptor of the ligand binding receptor BRI1 (Nam and Li, 2002; Li et al., 2002; Jaillais et al., 2011a; Albrecht et al., 2012; Gou et al., 2012). BRI1 was identified in the mid 1990s in a BR-insensitive Arabidopsis mutant (Clouse et al., 1996) and belongs, like the SERK proteins, to the family of LRR-RLKs (Li and Chory, 1997; Shiu and Bleecker, 2001b). In contrast to the SERKs with only five LRRs, the extracellular domain of

BRI1 comprises 25 repeats (Li and Chory, 1997) (Figure 1). The BR binding site, the so-called island domain, is located between the LRRs 21 and 22 of the BRI1 ectodomain (Kinoshita et al., 2005). The crystal structure of this domain revealed that the 25 LRRs are arranged in a superhelix with the island domain shielded in the interior of this domain architecture (Hothorn et al., 2011; She et al., 2011). Surprisingly, the crystallographic studies revealed that ligand binding did not induce a change in the overall BRI1 ectodomain (Zhu et al., 2013; Hothorn et al., 2011; She et al., 2011).

This finding contradicted the proposed BRI1 mode of action. Several reports showed a homodimeric BRI1 configuration (Wang et al., 2005; Hink et al., 2008; Wang et al., 2008) and suggested that ligand binding would cause a conformational change that leads to kinase activation (Wang et al., 2008; Jaillais et al., 2011a). That this scenario is unlikely was supported by the observation of solely monomeric BRI1 ectodomains during the crystallization process (Hothorn et al., 2011; She et al., 2011). Moreover computational modeling indicated that a head-to-head arrangement of two BRI1 monomers would lead to a substantial distance between the intracellular kinase domains (Hothorn et al., 2011).

However, the structural analysis elucidated a small rearrangement of the BR binding pocket upon BR addition and these structural changes create a hydrophobic surface, which may function as a docking site for interaction partners (Hothorn et al., 2011; She et al., 2011). Intriguingly, this possible interaction platform is located about five LRRs above the membrane surface and is therefore close to the N-terminal end of the SERK ectodomains (She et al., 2011).

In the following section, we will elaborate on how the regulation of BRI1-SERK3 interactions is currently envisioned by introducing the signal transduction pathway initiated by binding of BRs to the extracellular BRI1 island domain.

The BR signaling pathway

Based on genetic, proteomic and biochemical approaches most major components of the BR signal transduction pathway have been identified (Wang et al., 2012). In contrast to animal steroid signaling, plants perceive BRs at the cell surface (Wang et al., 2012). In the absence of ligand, PM-located BRI1 is suggested to remain inactive due to a double-lock mechanism, accomplished by kinase inhibition and prevented association with SERK3 (Jaillais et al., 2011a). Binding of BRs to the extracellular domain of BRI1 (He et al., 2000; Kinoshita et al., 2005) is thought to induce basal BRI1 kinase activity (Wang et al., 2008). BR-activated BRI1 in turn trans-phosphorylates BRI1 kinase inhibitor 1 (BKI1), which subsequently dissociates from the intracellular BRI1 kinase domain into the cytoplasm (Jaillais et al., 2011b). BKI1 prevents hetero-oligomerization of BRI1 and SERK3 in vitro (Wang et al., 2008; Jaillais et al., 2011b), suggesting that BKI1 release is required for the initiation of downstream signaling. Sequential trans-phosphorylation events within the BRI1-SERK3 receptor complex (Wang et al., 2008) result in the phosphorylation-mediated activation of

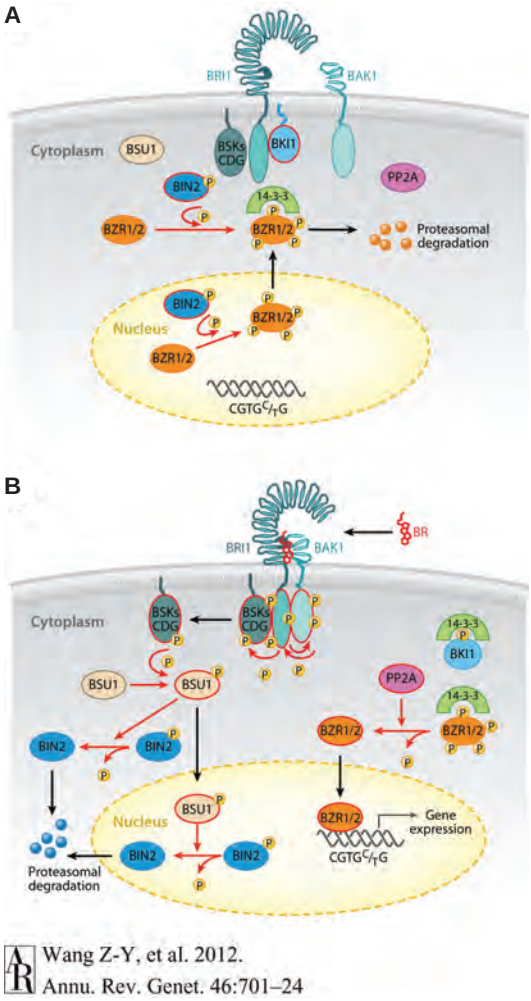

Wang Z-Y, et al. 2012.
Annu. Rev. Genet. 46:701–24

Figure 2: The brassinosteroid signal transduction pathway.
(A) In the absence of brassionsteroid (BR) ligands, BRI1 kinase activity and association with SERK3(BAK1) is inhibited by BKI1. Additionally, BRI1 is associated with BSKs/CDG1. Active BIN2 kinase phosphorylates the transcripton factors BZR1 and BES1(BZR2), which results in loss of DNA binding activity, transport out of the nucleus, cytoplasmic retention by 14-3-3 proteins and proteasomal degradation.
(B) In the presence of BRs, ligand binding to the BRI1 ectodomain leads to the dissociation of BKI1, followed by the association of BRI1 with SERK3(BAK1). Sequential phosphorylation events within the BRI1-SERK3(BAK1) receptor hetero-oligomers result in full activation of the BRI1 kinase. Subsequently, BSKs/CDG1 are trans-phosphorylated and released from the receptor complex. Activated BSKs/CDG1 in turn phosphorylate and activate the BSU1 phosphatase, which results in the dephosphorylation and deactivation of the BIN2 kinase. Dephosphorylation and thereby activiation of the transcription factors BZR1 and BES1(BZR2) is conducted by the PP2A phosphatase.
Red lines indicate active signaling components, red arrows indicate phosphorylation and dephosphorylation events, and black arrows indicate the movement of proteins. (This figure was taken and adapted from Wang et al., 2012)

BR signaling kinases (BSKs) (Tang et al., 2008) and constitute differential growth 1 (CDG1) (Kim et al., 2011). These receptor-like cytoplasmic kinases (RLCKs) relay BR signaling by phosphorylating the BRI1-suppressor 1 (BSU1) phosphatase (Kim et al., 2011). Phosphorylation of BSU1 promotes the interaction with and the inactivation of the BR insensitive 2 (BIN2) kinase, a negative regulatory entity of BR signaling (Tang et al., 2008; Kim et al., 2011). In the absence of activating BRs, BIN2 maintains the BR transcription factors brassinazole resistant 1 (BZR1) and BRI1 EMS suppressor 1 (BES1) in a phosphorylation-dependent inactive state (Yin et al., 2002; He et al., 2002). However, inactivation of BIN2 by BSU1 results in dephosphorylation of the two transcription factors and translocation into the nucleus followed by BR-mediated transcriptional regulation (Yin et al., 2002; He et al., 2002; Sun et al., 2010; Tang et al., 2011; Yu et al., 2011). An overview of the BR signaling pathway is shown in Figure 2.

Thus, various multi-disciplinary approaches have revealed a comprehensive set of molecular components linking BR perception at the cell surface to nuclear transcriptional regulation (Kim and Wang, 2010; Clouse, 2011; Wang et al., 2012). But even though the molecular determinants of BR signaling have been established, many mechanistic questions remain unanswered. For example, what is the mechanism behind the observed stimulatory and inhibitory growth effects under low and high exogenous BR concentrations, respectively (van Esse et al., 2012)? Since the structural analysis of the BRI1 ectodomain does not appear to favor homodimers and did not reveal overall domain changes upon BR addition (Hothorn et al., 2011; She et al., 2011), how is the binding of BRs to the island domain of BRI1 transmitted to the cell interior? Is SERK3 a component of the hormone perceiving complex as speculated by She et al. (2011)? Moreover, where does BR signaling occur? And how do the BRI1-like (BRL) LRR-RLKs BRL1 and BRL3, which also can bind BRs (Caño-Delgado et al., 2004), contribute to the overall BR response? Are there organ, tissue, or cell type specific BR signaling circuits? And in which cellular compartment does BR signaling actually take place?

The interplay between location and signaling

Some of the above-mentioned questions have already been investigated and a fundamental role of the epidermal cell layer for executing BR signaling and regulating BR-related developmental processes in shoot and root was established (Savaldi-Goldstein et al., 2007; Hacham et al., 2011). To zoom in further and to address which cellular compartments exhibit BRI1-mediated signal transduction it is worthwhile to take a closer look on the subcellular localization patterns of BRI1 and SERK3.

In Arabidopsis thaliana, both LRR-RLKs are ubiquitously expressed and typically reside in the PM (Friedrichsen et al., 2000; Nam and Li, 2002; Li et al., 2002; Geldner et al., 2007). However, how do BRI1 and SERK3 arrive at the site of BR perception? And what happens

after fulfilling their signaling task? Popescu et al. (2012) recently proposed a model for the biogenesis and the anterograde transport of PM receptors.

The biosynthesis of cell surface receptors is initiated at the endoplasmic reticulum (ER) (Popescu, 2012). Here, after translation folding of the nascent polypeptide chain, positioning in the membrane, addition of post-translational modifications, and ER quality control occur (Jürgens, 2004; Staehelin and Kang, 2008; Popescu, 2012). Targeted transport directs the newly synthesized and correctly processed receptor molecules to the Golgi apparatus, where additional post-translational modifications take place (daSilva et al., 2004; Langhans et al., 2012). Successfully processed PM receptors leave the Golgi by vesicle budding and are sorted within the trans-Golgi network (TGN) for subsequent PM transport and insertion (Richter et al., 2009). Fusion of TGN-derived vesicles with the PM eventually completes the anterograde or secretory trafficking route.

In plants, the TGN fulfills a dual function. It represents a hub for biosynthetic and retrograde transport (Reyes et al., 2011). Therefore the plant TGN is equivalent to the early endosome (EE) compartment (Dettmer et al., 2006; Lam et al., 2007) and initially receives endocytosed PM receptors. Here, the endocytosed cargo is either sorted for recycling back to the PM or follows a route towards degradation (Reyes et al., 2011). Degradative sorting results in the formation of late endosomes (LEs) or multi-vesicular bodies (MVBs), which mature from EEs (Reyes et al., 2011). Fusion of LEs/MVBs with the tonoplast results in the release of cargo into the vacuolar lumen and finally protein degradation (Reyes et al., 2011) (Figure 3).

BRI1 localizes to most of the anterograde and retrograde compartments. Live-cell imaging (Geldner et al., 2007; Viotti et al., 2010; Irani et al., 2012) and electron microscopy (Viotti et al., 2010) revealed the presence of BRI1 in Golgi, TGN, and luminal MVB vesicles. Moreover, Geldner et al. (2007) reported that BRI1 constitutively recycles between PM and TGN. In contrast, little is known about the subcellular distribution of SERK3. Only the presence in EEs was speculated about for this coreceptor (Russinova et al., 2004). Taking into account that BRs are perceived at the PM and that initiation of BR signal transduction requires the sequential trans-phosphorylation within a BRI1-SERK3 hetero-oligomer, the localization patterns of BRI1 and SERK3 hint towards the cell surface and EEs as possible sites of BR signaling activity. And in fact, experimental evidence for endosomal and PM BR signal transduction was provided.

Geldner et al. (2007) reported increased BR signaling upon application of brefeldin A (BFA), a fungal toxin. Since BFA inhibits the recycling pathway at the stage of TGN (Nebenführ et al., 2002), Geldner et al. (2007) concluded that the elevated BR signaling outputs arise from endocytosed and intracellularly trapped BRI1 receptors. However, a recent report revealed an additional feature of BFA. Besides inhibiting recycling, this fungal toxin also stabilizes BRI1 at the PM (Irani et al., 2012). Subsequent analysis showed that this second effect actually attributes most to the BFA-induced BR signaling activity (Irani et

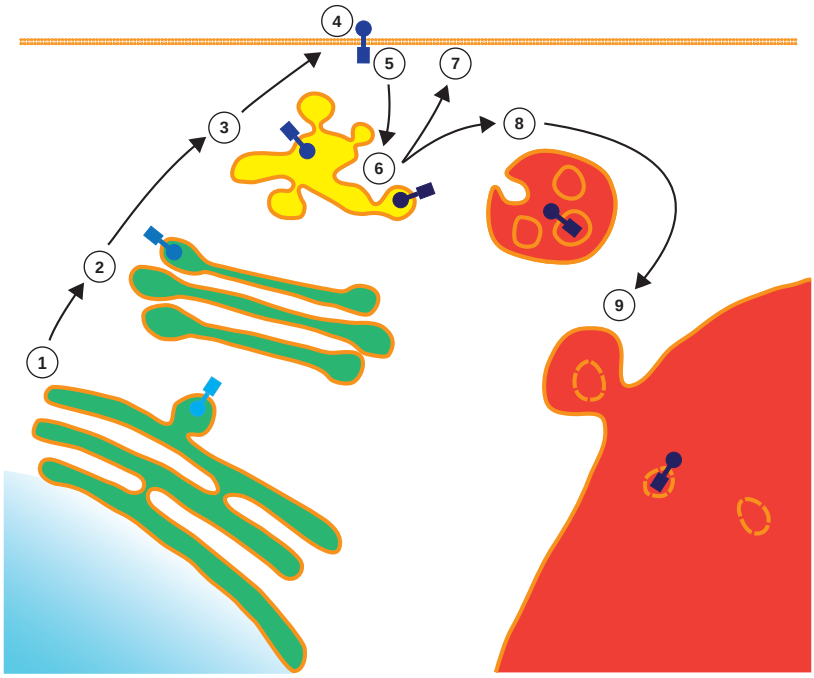

Figure 3: Anterograde and retrograde trafficking of plasma membrane receptors.
The biogenesis of plasma membrane receptors starts with the biosynthesis of nascent polypeptide chains in the ER (1). Folded and matured receptor proteins are transported to the Golgi apparatus, where further post-translational modifications are processed (2). Receptors that passed quality control shuttle to the trans-Golgi network (TGN) and are sorted for transport to the plasma membrane (3). Fusion of TGN-derived vesicles with the plasma membrane results in the insertion of matured and signaling competent receptor proteins (4). After endocytosis receptors (5) are again targeted to the TGN, which in plants is equivalent to the early endosome (EE) compartment (6). Here, receptor proteins can be sorted for recycling back to the plasma membrane (7) or via late endosomes (LE)/multivesicular bodies (MVBs) for the degradative pathway (8). Fusion of MVBs with the tonoplast releases the protein cargo into the vacuolar lumen and culminates in protein degradation (9). (Adapted from Reyes et al., 2011)

al., 2012). Thus, BRI1 may be able to signal from endosomes, but the main site of BR signal transduction is at the PM (Irani et al., 2012).

Collectively, the most prominent sites of BR signaling activity seem to be the PMs of epidermal plant cells. But these findings based on downstream signaling outputs and phenotypic analyses still leave open how the very first steps of BR signaling, the transmission of the BR binding signal across the PM and the initiation of BRI1 and SERK3 kinase activity, are regulated.

Lessons from animal signaling

Similar findings as observed for BRI1, have also been reported for its animal counterpart EGFR. This RTK is able to signal from endosomal compartments (Lai et al., 1989; Vieira et al., 1996), but the main signaling activity stems from PM-localized receptors (Sousa et al.,

2012). Structural analysis additionally revealed that ligand binding does not result in drastic changes of the ectodomain architecture and that the domain assembly is too flexible to transmit the signal of ligand binding across the PM within an EGFR monomer (Lu et al., 2010). This implies that at least a dimeric receptor configuration is required for intracellular kinase activation. Indeed, structural and biochemical evidence provided proof for this scenario as extensively reviewed by Lemmon and Schlessinger (2010). However, where or when are these receptor oligomers, which enable kinase activation and downstream signaling, established?

Initial studies addressing this question revealed ligand-induced EGFR dimerization (Yarden and Schlessinger, 1987; Cochet et al., 1988). Ligand-mediated recruitment models were also proposed for other classes of PM animal receptors like the G protein-coupled receptors (GPCRs) (Vila-Coro et al., 2000; Mellado et al., 2001) or the transforming growth factor β receptors (TGFβRs) (Wrana et al., 1994). Most of these studies were based on protein gel analysis, cross-linking experiments, or immunoprecipitation. In parallel to the development of more specific techniques like coimmunoprecipitation and in particular imaging approaches, ligand-induced receptor recruitment models have evolved. More detailed studies revealed ligand-independent and thus preformed receptor complexes for EGFR (Gadella and Jovin, 1995; Bader et al., 2009), GPCRs (Hernanz-Falcón et al., 2004; Van Craenenbroeck et al., 2011; Springael et al., 2005), TGFβRs (Gilboa et al., 1998; Ehrlich et al., 2012), and bone morphogenic protein receptors (BMPRs) (Gilboa et al., 2000; Ehrlich et al., 2012).

Besides the identification of preformed receptor complexes also functional consequences have been reported. For BMPRs it was shown that preformed and ligand-induced receptor oligomers follow different endocytic routes (Hartung et al., 2006) and exhibit differential signaling (Nohe et al., 2002). Moreover, receptor preformation was not only associated with downstream signaling, but it was postulated that oligomerization may already affect the biogenesis of the PM receptors.

This hypothesis is based on observations of receptor complexes shortly after biosynthesis in the ER. One of the first examples was presented by Gilboa et al. (1998), who showed that TGFβR oligomers are formed in the ER and persist at the PM. Using imaging approaches similar findings were obtained for kainate receptors (Ma-Högemeier et al., 2010) and different members of the GPCR family (Springael et al., 2005; Van Craenenbroeck, 2012). In particular for GPCRs, an influence of receptor oligomerization in the ER on their biogenesis and anterograde trafficking was revealed. For γ-aminobutyric acid B ($GABA_B$) receptors it was shown that complex formation results in masking of an ER-retention signal and thus receptor oligomerization is necessary to enter the secretory transport route (Margeta-Mitrovic et al., 2000). Furthermore, van Craenenbroeck et al. (2011) hypothesized a chaperone-like function for ER oligomerization of PM receptors.

Consequently, preformed receptor complexes seem to fulfill essential regulatory functions for PM receptor signaling. In contrast to the animal field, where PM receptor complex

preformation is nowadays an established concept, there is only one example in the plant field, the chitin-sensing receptor system of rice (Shimizu et al., 2010). Interestingly, Wang et al. (2005) hypothesized that also BRI1 and SERK3, the BR signaling components, may form ligand-independent hetero-oligomers.

This discrepancy between animal and plant receptor signaling models is surprising given the tremendous number of plant PM receptors as illustrated earlier. Of course, this large repertoire of plant surface receptors offers a plethora of possible molecular interactions involving various different regulatory principles. However, biology in general favors simplicity (Alon, 2007). Recent research revealed that actually only a few regulatory patterns or motifs are used, which are repeated and interconnected to generate robust and "economic" signaling circuits (Alon, 2007).

A possible explanation for the differences between the proposed signaling modes in animals and plants may be given by the experimental approaches applied. Mainly the use of low invasive and spatiotemporally resolving imaging techniques contributed to the conceptual changes for animal receptor signaling models (Springael et al., 2005; Ciruela et al., 2010; Ehrlich et al., 2011; 2012; Van Craenenbroeck, 2012), methods that are still underrepresented in the plant field.

Fluorescence microscopy as a tool for investigating signaling events

Signaling processes involve the assembly and disassembly of molecular complexes, which is often accompanied by the physical repositioning of complex components within the cellular matrix (Day et al., 2005). For gaining access to the fundamental principles of signal transduction that communicate information in the form of protein activities through space, imaging approaches offer very good possibilities (Dehmelt and Bastiaens, 2010). In particular fluorescence microscopy provides a large portfolio of techniques, which allow elucidating the spatial distribution as well as the oligomerization patterns of proteins participating in signal transduction cascades, as recently exemplified for the plant LRR-RLK Clavata1 (CLV1) (Stahl et al., 2013).

Independent of the approach applied a prerequisite of fluorescence microscopy is the presence of fluorescent probes in the investigated biological system. However, most proteins are not per se fluorescent in the visible spectrum. Therefore visualizing proteins of interest often requires labeling with chemical or biological fluorophores. The introduction of the GFP technology (Gerdes and Kaether, 1996; Ehrhardt, 2003; Chudakov et al., 2005) has provided a vast range of visible fluorescent proteins (VFPs) that can be used to genetically tag the proteins under investigation (Shaner et al., 2007). This enables dynamic live-cell imaging and protein tracking from single molecule to organism level. Though, due to the size of VFPs and depending on the molecular site of attachment functionality of the tagged protein can be compromised (Ntoukakis et al., 2011). To avoid these adverse effects of VFP-tagging, immuno-labeling with native or secondary fluorophore-

conjugated antibodies can be applied. A drawback of this methodology is that it usually requires fixation of the samples. Alternatively, proteins can be genetically tagged with small epitopes or labeled with endogenously expressed antibodies, which in turn bind synthetic membrane-permeable fluorophores (Farinas and Verkman, 1999; Crivat and Taraska, 2012; Wombacher and Cornish, 2011). This approach allows in vivo imaging, but may suffer from toxicity and unspecific binding of the respective fluorescent agents (Crivat and Taraska, 2012; Wombacher and Cornish, 2011). Most microscopic studies are based on genetic VFP-tagging, both because of its simplicity of sample preparation and applicability to live-cell imaging.

Labeling proteins with fluorescent tags can either be used to report physiological changes caused by signaling activities, thus the tagged proteins function as biosensors, or it can used to directly study the features of the molecular signaling components. Here, we want to focus solely on the latter. Fluorescence microscopy provides various read-outs, like fluorescence intensity, fluorescence lifetime, or fluorescence anisotropy (Yasuda, 2006), to characterize fluorescently labeled molecules. The most straightforward read-out is the measurement of fluorescence intensities, which allows the investigation of localization and colocalization patterns, protein mobility, conformational changes, or protein-protein interactions (Dehmelt and Bastiaens, 2010). The majority of biological studies apply fluorescence microscopy to reveal the localization and colocalization patterns of proteins, as exemplified earlier for BRI1 (Friedrichsen et al., 2000; Geldner et al., 2007; Viotti et al., 2010; Irani et al., 2012) and SERK3 (Nam and Li, 2002; Li et al., 2002; Russinova et al., 2004). (Co)Localization studies are mainly performed in wide-field or confocal mode. The advantage of confocal imaging is the higher precision with a lateral spatial resolution of up to 200-300 nm, the diffraction limit of visible light (Day et al., 2005). Recent technological advances that resulted in the so-called superresolution methods could even break this physical limit. In most-optimal conditions, which unfortunately still require sample fixation, these techniques enable a lateral resolution of up to 20 nm in biological samples (Leung and Chou, 2011). An alternative method, especially for PM or PM-associated proteins, with increased z-resolution compared to confocal imaging is total internal reflection fluorescence (TIRF) microscopy. Since this technique is based on the evanescent field occurring at glass substrate-PM interfaces the imaging depth is restricted to 50-300 nm (Millis, 2012).

TIRF microscopy can additionally be applied for studying the protein mobility within or close to the PM (Millis, 2012). But due to the technical challenges of setting up this method it has so far only been rarely used in plant research. Other approaches enabling the investigation of protein mobility are fluorescence correlation spectroscopy (FCS) and fluorescence recovery after photobleaching (FRAP) (Dehmelt and Bastiaens, 2010; Kwaaitaal et al., 2011; Hink et al., 2008). Both methods have already been successfully applied to study plant PM receptors. Using FRAP a ligand-dependent reduction in PM mobility of FLS2 was reported (Ali et al., 2007). Application of a dual-color variant of FCS,

which is called fluorescence cross-correlation spectroscopy (FCCS), allowed assessing the mobility of SERK1, SERK3, and BRI1 in cowpea protoplasts and determining the molecular composition of respective protein complexes (Hink et al., 2008). Hink et al. (2008) was able to estimate that approximately 15% of SERK1 and around 20% of BRI1 may be in a homodimeric configuration in the PM of the plant cells investigated. It is not clear whether the homodimers observed in that study represent active receptors.

However, most of the fluorescence microscopic techniques that are employed to determine protein oligomerization exploit Förster resonance energy transfer (FRET) (Förster, 1948; Day et al., 2005). This photo-physical process describes the non-radiative transfer of excited-state energy from a donor fluorophore to an acceptor chromophore. Since the energy transfer is accomplished by dipole-dipole coupling of the transition dipole moments of donor and acceptor, this process is limited to distances smaller than 10 nm, which is in the dimension of typical protein sizes (Dehmelt and Bastiaens, 2010). Therefore FRET is a suitable read-out for investigating protein-protein interactions as illustrated in Figure 4.

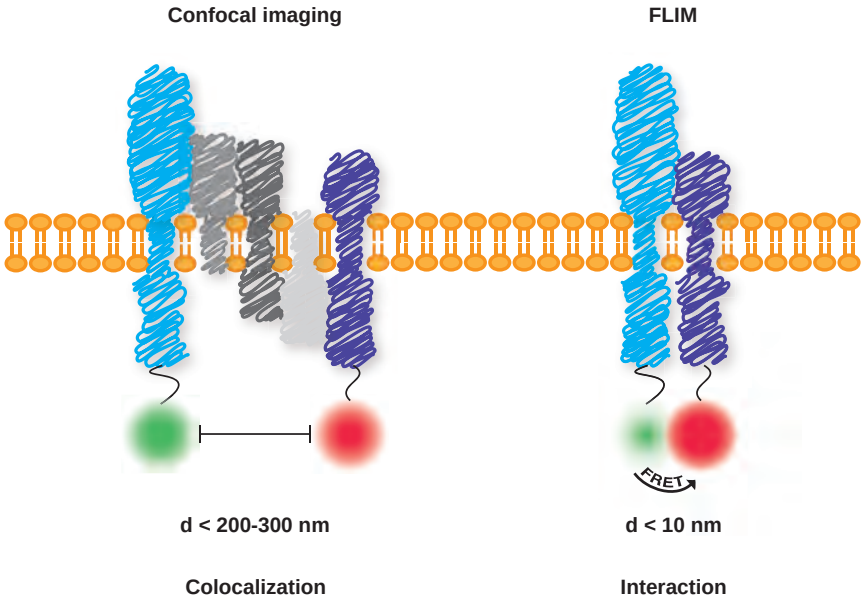

Figure 4: Spatial resolution of different fluorescence microscopic techniques.
Fluorescence microscopy can be used to investigate the spatial correlation between fluorescently labeled proteins. Depending on the applied technique various degrees of distances (d) are resolvable. Here, confocal microscopy and fluorescence lifetime imaging microscopy (FLIM) are compared. Fluorescence intensity images acquired in confocal mode allow resolving distances close to the diffraction limit of light. This spatial resolution enables to reveal the colocalization of two proteins in a dual color image. For studying the oligomerization of proteins FLIM is a suitable method. This imaging technique can detect FRET between the fluorescent tags of fusion proteins. Since FRET can only occur in the range of typical protein dimensions the physical interaction of the two appropriately labeled proteins can be deduced.

Several methods are applicable to detect FRET. Most of them rely on fluorescence intensity measurements like ratio-imaging, acceptor photo-bleaching, or acceptor-sensitized emission (Dehmelt and Bastiaens, 2010; Yasuda, 2006). A drawback of these intensity-based approaches is the dependency on fluorophore concentrations, which are hard to assess in living systems (Yasuda, 2006). Thus, various corrections have to be implemented in the data analysis. To avoid these pitfalls of intensity-based methods, fluorescence lifetime imaging microscopy (FLIM) can be applied for detecting FRET (Yasuda, 2006). The fluorescence lifetime is an intrinsic property of fluorphores and therefore concentration-independent. However, it is sensitive to the immediate environment of the excited molecule. In the presence of an acceptor in the close proximity of an excited donor fluorophore the fluorescence lifetime decreases due to FRET (Day et al., 2005; Borst and Visser, 2010). FRET-FLIM has been applied in several studies to investigate the interaction of plant PM receptors. Russinova et al. (2004) used this methodology to reveal the oligomerization of BRI1 and SERK3 in transiently transfected cowpea protoplasts. Also based on a heterologous expression system the interaction between both PM receptors was shown in Nicotina benthamiana (Caesar et al., 2011).

Collectively, the fluorescence microscopic methods presented here provide an enormous portfolio for uncovering mechanistic details of signal transduction events. Moreover, most of the described techniques are applicable to live-cell imaging and allow the elucidation of spatiotemporal dynamics in the natural habitat of signaling components.

SCOPE OF THE THESIS

Brassinosteroids are key regulators of plant architecture and physiology. They directly influence plant development and growth but moreover affect many other regulatory circuits. The high degree of interconnections between brassinosteroid signaling and processes like light perception or abiotic and biotic stress responses enforces the need for deciphering the fundamental principles underlying brassinosteroid signal transduction. Understanding the regulation of this particular signaling pathway will not only result in a more detailed picture of the overall plant physiology, but will also help to optimize crops for steadily harsher environmental conditions.

Research using genetic, proteomic and biochemical approaches has uncovered the major components of the brassinosteroid signal transduction pathway during the last two decades. It was shown how the information of ligand-activated BRI1 at the plasma membrane is relayed to the cell nucleus via a phosphorylation-dependent cascade. Despite the detailed information of downstream signaling events, the very first steps of brassinosteroid signaling are still elusive. How is the binding of brassinosteroids to the extracellular domain of BRI1 transmitted into the cell interior?

Previous models of brassinosteroid signaling assumed the presence of BRI1 homodimers, which would undergo a conformational change upon ligand binding. This structural change was suggested to induce basal cytoplasmic BRI1 kinase activity followed by subsequent recruitment of SERK proteins to enhance downstream signaling outputs. However, the resolved crystal structure of the BRI1 ectodomain opposes this scenario. Instead it was postulated that a hetero-oligomeric complex could facilitate the cross-membrane signal transmission. Intriguingly, genetic evidence revealed the necessity of SERK1, SERK3, and SERK4 for initiating brassinosteroid signaling. Hence, these SERK family members are ideal candidates for the postulated hetero-oligomeric BRI1 complex, which could transmit ligand binding across the plasma membrane and induce the downstream phosphorylation cascade.

Therefore this thesis focuses on the spatial correlation between BRI1 and SERK3, the main coreceptor of brassinosteroid signaling. Different imaging and image analysis procedures are applied to investigate the colocalization and interaction patterns of the two plasma membrane receptors in their natural and signaling competent habitat, the epidermal cells of Arabidopsis thaliana roots.

OUTLINE OF THIS THESIS

After an introduction into signaling and the use of fluorescence microscopy in **Chapter 1**, a protocol for the application of FRET-FLIM on Arabidopsis thaliana mesophyll protoplasts is provided in **Chapter 2**. It describes the theoretical background of the FRET-FLIM methodology in detail employing a transient expression system. The oligomerization of AtCDC48 is used as a biological example to explain how time-resolved fluorescence intensity images are analyzed based on the SPCImage software package (Becker & Hickl). This Chapter illustrates the potential of FRET-FLIM as a light microscopic method to study protein-protein interactions in vivo.

Subsequently, FRET-FLIM and colocalization analysis are used to reveal the spatial distribution of BRI1 and SERK3 in response to brassinosteroids. **Chapter 3** provides evidence for brassinosteroid signaling-dependent colocalization of the two LRR-RLKs in the plasma membrane and cytosol of Arabidopsis thaliana epidermal root cells. Next to increased colocalization, ligand application also results in elevated amounts of plasma membrane-localized BRI1-SERK3 hetero-oligomers. Surprisingly, ligand depletion does not abolish these molecular interactions. Instead, a substantial amount of preformed BRI1-SERK3 receptor complexes is observed in the plasma membrane of root epidermal cells.

Since imaging approaches often suffer from solely qualitative interpretations, **Chapter 4** elaborates on quantitative image analysis procedures. Two colocalization analysis approaches are presented and used to discriminate different colocalizing populations in confocal images. In addition, a novel FRET-FLIM analysis procedure is introduced, which allows the quantification of BRI1-SERK3 hetero-oligomers in time-resolved fluorescence intensity images. Applied to the FRET-FLIM results of Chapter 3, this approach reveals that approximately 70% of BRI1-SERK3 receptor complexes are preformed.

To address where or when these ligand-independent hetero-oligomers are established it is essential to identify the subcellularly resolved colocalization patterns of BRI1 and SERK3. Both LRR-RLKs localize to the common anterograde and retrograde endomembrane compartments and fractions of both receptors also colocalize in the respective cellular structures, as demonstrated in **Chapter 5**. Using the transient expression system of Arabidopsis thaliana mesophyll protoplasts additionally enables to investigate whether BRI1 and SERK3 already hetero-oligomerize prior to their plasma membrane insertion. FRET-FLIM analysis of endoplasmic reticulum residing BRI1 and SERK3 populations indicates that both receptors associate early after biogenesis. This observation is confirmed in Arabidopsis thaliana root epidermal cells, which are fixed shortly after heat-shock induction of the BRI1 receptor. BRI1-SERK3 hetero-oligomers are present in anterograde trafficking organelles prior to plasma membrane fusion, revealed by FRET-FLIM performed on the heat-shock induced and chemical fixed Arabidopsis thaliana roots. Consequently, the biogenesis of BRI1 and SERK3 is accompanied by receptor complexes formation, followed by the anterograde

transport and plasma membrane insertion of preassembled and signaling competent BR signaling units.

In **Chapter 6**, the results of this thesis are summarized and the implications on the current view of brassinosteroid signal transduction and other pathways involving the SERK3 coreceptor are discussed.

REFERENCES

Albrecht, C., Boutrot, F., Segonzac, C., Schwessinger, B., Gimenez-Ibanez, S., Chinchilla, D., Rathjen, J.P., de Vries, S.C., and Zipfel, C. (2012). Brassinosteroids inhibit pathogen-associated molecular pattern-triggered immune signaling independent of the receptor kinase BAK1. Proc. Natl. Acad. Sci. U.S.A. **109**: 303–308.

Albrecht, C., Russinova, E., Hecht, V., Baaijens, E., and de Vries, S. (2005). The Arabidopsis thaliana SOMATIC EMBRYOGENESIS RECEPTOR-LIKE KINASES1 and 2 control male sporogenesis. Plant Cell **17**: 3337–3349.

Albrecht, C., Russinova, E., Kemmerling, B., Kwaaitaal, M., and de Vries, S.C. (2008). Arabidopsis SOMATIC EMBRYOGENESIS RECEPTOR KINASE proteins serve brassinosteroid-dependent and -independent signaling pathways. Plant Physiol. **148**: 611–619.

Ali, G.S., Prasad, K.V.S.K., Day, I., and Reddy, A.S.N. (2007). Ligand-dependent reduction in the membrane mobility of FLAGELLIN SENSITIVE2, an arabidopsis receptor-like kinase. Plant Cell Physiol. **48**: 1601–1611.

Alon, U. (2007). Simplicity in biology. Nature **446**: 497.

Bader, A.N., Hofman, E.G., Voortman, J., en Henegouwen, P.M.P.V.B., and Gerritsen, H.C. (2009). Homo-FRET imaging enables quantification of protein cluster sizes with subcellular resolution. Biophys. J. **97**: 2613–2622.

Baudino, S., Hansen, S., Brettschneider, R., Hecht, V.F., Dresselhaus, T., Lörz, H., Dumas, C., and Rogowsky, P.M. (2001). Molecular characterisation of two novel maize LRR receptor-like kinases, which belong to the SERK gene family. Planta **213**: 1–10.

Belkhadir, Y., Jaillais, Y., Epple, P., Balsemão-Pires, E., Dangl, J.L., and Chory, J. (2012). Brassinosteroids modulate the efficiency of plant immune responses to microbe-associated molecular patterns. Proc. Natl. Acad. Sci. U.S.A. **109**: 297–302.

Borst, J.W. and Visser, A.J.W.G. (2010). Fluorescence lifetime imaging microscopy in life sciences. Meas. Sci. Technol. **21**: 102002.

Caesar, K., Elgass, K., Chen, Z., Huppenberger, P., Witthöft, J., Schleifenbaum, F., Blatt, M.R., Oecking, C., and Harter, K. (2011). A fast brassinolide-regulated response pathway in the plasma membrane of Arabidopsis thaliana. Plant J. **66**: 528–540.

Canales, C., Bhatt, A.M., Scott, R., and Dickinson, H. (2002). EXS, a putative LRR receptor kinase, regulates male germline cell number and tapetal identity and promotes seed development in Arabidopsis. Curr. Biol. **12**: 1718–1727.

Caño-Delgado, A., Yin, Y., Yu, C., Vafeados, D., Mora-Garcia, S., Cheng, J.-C., Nam, K.H., Li, J., and Chory, J. (2004). BRL1 and BRL3 are novel brassinosteroid receptors that function in vascular differentiation in Arabidopsis. Development **131**: 5341–5351.

Chinchilla, D., Shan, L., He, P., de Vries, S., and Kemmerling, B. (2009). One for all: the receptor-associated kinase BAK1. Trends Plant Sci. **14**: 535–541.

Chinchilla, D., Zipfel, C., Robatzek, S., Kemmerling, B., Nürnberger, T., Jones, J.D.G., Felix, G., and Boller, T. (2007). A flagellin-induced complex of the receptor FLS2 and BAK1 initiates plant defence. Nature **448**: 497–500.

Chudakov, D.M., Lukyanov, S., and Lukyanov, K.A. (2005). Fluorescent proteins as a toolkit for in vivo imaging. Trends Biotechnol. **23**: 605–613.

Ciruela, F., Fernández-Dueñas, V., Sahlholm, K., Fernández-Alacid, L., Nicolau, J.C., Watanabe, M., and Luján, R. (2010). Evidence for oligomerization between GABAB receptors and GIRK channels containing the GIRK1 and GIRK3 subunits. Eur. J. Neurosci. **32**: 1265–1277.

Citri, A. and Yarden, Y. (2006). EGF–ERBB signalling: towards the systems level. Nat. Rev. Mol. Cell Biol. **7**: 505–516.

Clouse, S.D. (2011). Brassinosteroid signal transduction: from receptor kinase activation to transcriptional networks regulating plant development. Plant Cell **23**: 1219–1230.

Clouse, S.D., Clouse, S.D., Langford, M., Langford, M., McMorris, T.C., and McMorris, T.C. (1996). A brassinosteroid-insensitive mutant in Arabidopsis thaliana exhibits multiple defects in growth and development. Plant Physiol. **111**: 671–678.

Cochet, C., Kashles, O., Chambaz, E.M., Borrello, I., King, C.R., and Schlessinger, J. (1988). Demonstration of epidermal growth factor-induced receptor dimerization in living cells using a chemical covalent cross-linking agent. J. Biol. Chem. **263**: 3290–3295.

Crivat, G. and Taraska, J.W. (2012). Imaging proteins inside cells with fluorescent tags. Trends Biotechnol. **30**: 8–16.

daSilva, L.L.P., Snapp, E.L., Denecke, J., Lippincott-Schwartz, J., Hawes, C., and Brandizzi, F. (2004). Endoplasmic reticulum export sites and Golgi bodies behave as single mobile secretory units in plant cells. Plant Cell **16**: 1753–1771.

Day, R.N., Day, R.N., Schaufele, F., and Schaufele, F. (2005). Imaging molecular interactions in living cells. Mol. Endocrinol. **19**: 1675–1686.

Dehmelt, L. and Bastiaens, P.I.H. (2010). Spatial organization of intracellular communication: insights from imaging. Nat. Rev. Mol. Cell Biol. **11**: 440–452.

Dettmer, J., Hong-Hermesdorf, A., Stierhof, Y.-D., and Schumacher, K. (2006). Vacuolar H+-ATPase activity is required for endocytic and secretory trafficking in Arabidopsis. Plant Cell **18**: 715–730.

Ehrhardt, D. (2003). GFP technology for live cell imaging. Curr Opin. Plant Biol. **6**: 622–628.

Ehrlich, M., Gutman, O., Knaus, P., and Henis, Y.I. (2012). Oligomeric interactions of TGF-β and BMP receptors. FEBS Letters **586**: 1885–1896.

Ehrlich, M., Horbelt, D., Marom, B., Knaus, P., and Henis, Y.I. (2011). Homomeric and heteromeric complexes among TGF-β and BMP receptors and their roles in signaling. Cell. Signal. **23**: 1424–1432.

Farinas, J. and Verkman, A.S. (1999). Receptor-mediated targeting of fluorescent probes in living cells. J. Biol. Chem. **274**: 7603–7606.

Förster, T. (1948). Zwischenmolekulare Energiewanderung und Fluoreszenz. Ann. Phys. **2**: 55–75.

Friedrichsen, D.M., Joazeiro, C.A., Li, J., Hunter, T., and Chory, J. (2000). Brassinosteroid-insensitive-1 is a ubiquitously expressed leucine-rich repeat receptor serine/threonine kinase. Plant Physiol. **123**: 1247–1256.

Gadella, T.W. and Jovin, T.M. (1995). Oligomerization of epidermal growth factor receptors on A431 cells studied by time-resolved fluorescence imaging microscopy. A stereochemical model for tyrosine kinase receptor activation. J. Cell Biol. **129**: 1543–1558.

Geldner, N., Hyman, D.L., Wang, X., Schumacher, K., and Chory, J. (2007). Endosomal signaling of plant steroid receptor kinase BRI1. Genes Dev. **21**: 1598–1602.

Gerdes, H.H. and Kaether, C. (1996). Green fluorescent protein: applications in cell biology. FEBS Letters **389**: 44–47.

Gilboa, L., Nohe, A., Geissendörfer, T., Sebald, W., Henis, Y.I., and Knaus, P. (2000). Bone morphogenetic protein receptor complexes on the surface of live cells: a new oligomerization mode for serine/threonine kinase receptors. Mol. Biol. Cell **11**: 1023–1035.

Gilboa, L., Wells, R.G., Lodish, H.F., and Henis, Y.I. (1998). Oligomeric structure of type I and type II transforming growth factor beta receptors: homodimers form in the ER and persist at the plasma membrane. J. Cell Biol. **140**: 767–777.

Gish, L.A. and Clark, S.E. (2011). The RLK/Pelle family of kinases. Plant J. **66**: 117–127.

Gou, X., Yin, H., He, K., Du, J., Yi, J., Xu, S., Lin, H., Clouse, S.D., and Li, J. (2012). Genetic evidence for an indispensable role of somatic embryogenesis receptor kinases in brassinosteroid signaling. PLoS Genet. **8**: e1002452.

Gómez-Gómez, L. and Boller, T. (2002). Flagellin perception: a paradigm for innate immunity. Trends Plant Sci. **7**: 251–256.

Grove, M.D., Spencer, G.F., Rohwedder, W.K., Mandava, N., Worley, J.F., Warthen, J.D., Steffens, G.L., Flippen-Anderson, J.L., and Cook, J.C. (1979). Brassinolide, a plant growth-promoting steroid isolated from Brassica napus pollen. Nature **281**: 216–217.

Hacham, Y., Holland, N., Butterfield, C., Ubeda-Tomas, S., Bennett, M.J., Chory, J., and Savaldi-Goldstein, S. (2011). Brassinosteroid perception in the epidermis controls root meristem size. Development **138**: 839–848.

Hartung, A., Bitton-Worms, K., Rechtman, M.M., Wenzel, V., Boergermann, J.H., Hassel, S., Henis, Y.I., and Knaus, P. (2006). Different routes of bone morphogenic protein (BMP) receptor endocytosis influence BMP signaling. Mol. Cell. Biol. **26**: 7791–7805.

He, J.-X., Gendron, J.M., Yang, Y., Li, J., and Wang, Z.-Y. (2002). The GSK3-like kinase BIN2 phosphorylates and destabilizes BZR1, a positive regulator of the brassinosteroid signaling pathway in Arabidopsis. Proc. Natl. Acad. Sci. U.S.A. **99**: 10185–10190.

He, K., Gou, X., Yuan, T., Lin, H., Asami, T., Yoshida, S., Russell, S.D., and Li, J. (2007). BAK1 and BKK1 regulate brassinosteroid-dependent growth and brassinosteroid-independent cell-death pathways. Curr. Biol. **17**: 1109–1115.

He, Z., Wang, Z.Y., Li, J., Zhu, Q., Lamb, C., Ronald, P., and Chory, J. (2000). Perception of brassinosteroids by the extracellular domain of the receptor kinase BRI1. Science **288**: 2360–2363.

Hecht, V., Vielle-Calzada, J.P., Hartog, M.V., Schmidt, E.D., Boutilier, K., Grossniklaus, U., and de Vries, S.C. (2001). The Arabidopsis SOMATIC EMBRYOGENESIS RECEPTOR KINASE 1 gene is expressed in developing ovules and embryos and enhances embryogenic competence in culture. Plant Physiol. **127**: 803–816.

Heese, A., Hann, D.R., Gimenez-Ibanez, S., Jones, A.M.E., He, K., Li, J., Schroeder, J.I., Peck, S.C., and Rathjen, J.P. (2007). The receptor-like kinase SERK3/BAK1 is a central regulator of innate immunity in plants. Proc. Natl. Acad. Sci. U.S.A. **104**: 12217–12222.

Hernanz-Falcón, P., Rodríguez-Frade, J.M., Serrano, A., Juan, D., del Sol, A., Soriano, S.F., Roncal, F., Gómez, L., Valencia, A., Martínez-A, C., and Mellado, M. (2004). Identification of amino acid residues crucial for chemokine receptor dimerization. Nat. Immunol. **5**: 216–223.

Hink, M.A., Shah, K., Russinova, E., de Vries, S.C., and Visser, A.J.W.G. (2008). Fluorescence fluctuation analysis of Arabidopsis thaliana somatic embryogenesis receptor-like kinase and brassinosteroid insensitive 1 receptor oligomerization. Biophys. J. **94**: 1052–1062.

Hothorn, M., Belkhadir, Y., Dreux, M., Dabi, T., Noel, J.P., Wilson, I.A., and Chory, J. (2011). Structural basis of steroid hormone perception by the receptor kinase BRI1. Nature **474**: 467–471.

Irani, N.G., Di Rubbo, S., Mylle, E., Van den Begin, J., Schneider-Pizoń, J., Hniliková, J., Síša, M., Buyst, D., Vilarrasa-Blasi, J., Szatmari, A.-M., Van Damme, D., Mishev, K., Codreanu, M.-C., Kohout, L., Strnad, M., Caño-Delgado, A.I., Friml, J., Madder, A., and Russinova, E. (2012). Fluorescent castasterone reveals BRI1 signaling from the plasma membrane. Nat. Chem. Biol. **8**: 583–589.

Jaillais, Y., Belkhadir, Y., Balsemão-Pires, E., Dangl, J.L., and Chory, J. (2011a). Extracellular leucine-rich repeats as a platform for receptor/coreceptor complex formation. Proc. Natl. Acad. Sci. U.S.A. **108**: 8503–8507.

Jaillais, Y., Hothorn, M., Belkhadir, Y., Dabi, T., Nimchuk, Z.L., Meyerowitz, E.M., and Chory, J. (2011b). Tyrosine phosphorylation controls brassinosteroid receptor activation by triggering membrane release of its kinase inhibitor. Genes Dev. **25**: 232–237.

Jürgens, G. (2004). Membrane trafficking in plants. Annu. Rev. Cell Dev. Biol. **20**: 481–504.

Karlova, R., Boeren, S., Russinova, E., Aker, J., Vervoort, J., and de Vries, S. (2006). The Arabidopsis SOMATIC EMBRYOGENESIS RECEPTOR-LIKE KINASE1 protein complex includes BRASSINOSTEROID-INSENSITIVE1. Plant Cell **18**: 626–638.

Kemmerling, B., Schwedt, A., Rodriguez, P., Mazzotta, S., Frank, M., Qamar, S.A., Mengiste, T., Betsuyaku, S., Parker, J.E., Müssig, C., Thomma, B.P.H.J., Albrecht, C., de Vries, S.C., Hirt, H., and Nürnberger, T. (2007). The BRI1-associated kinase 1, BAK1, has a brassinolide-independent role in plant cell-death control. Curr. Biol. **17**: 1116–1122.

Kim, B.H., Kim, S.Y., and Nam, K.H. (2013). Assessing the diverse functions of BAK1 and its homologs in arabidopsis, beyond BR signaling and PTI responses. Mol. Cells **35**: 7–16.

Kim, T.-W. and Wang, Z.-Y. (2010). Brassinosteroid signal transduction from receptor kinases to transcription factors. Annu. Rev. Plant Biol. **61**: 681–704.

Kim, T.-W., Guan, S., Burlingame, A.L., and Wang, Z.-Y. (2011). The CDG1 kinase mediates brassinosteroid signal transduction from BRI1 receptor kinase to BSU1 phosphatase and GSK3-like kinase BIN2. Mol. Cell **43**: 561–571.

Kinoshita, T., Caño-Delgado, A., Seto, H., Hiranuma, S., Fujioka, S., Yoshida, S., and Chory, J. (2005). Binding of brassinosteroids to the extracellular domain of plant receptor kinase BRI1. Nature **433**: 167–171.

Kutschera, U.U. and Wang, Z.-Y.Z. (2012). Brassinosteroid action in flowering plants: a Darwinian perspective. J. Exp. Bot. **63**: 3511–3522.

Kwaaitaal, M., Schor, M., Hink, M.A., Visser, A.J.W.G., and de Vries, S.C. (2011). Fluorescence Correlation Spectroscopy and Fluorescence Recovery After Photobleaching to study receptor kinase mobility in planta. Methods Mol. Biol. **779**: 225–242.

Lai, W.H., Cameron, P.H., Doherty, J.J., Posner, B.I., and Bergeron, J.J. (1989). Ligand-mediated autophosphorylation activity of the epidermal growth factor receptor during internalization. J. Cell Biol. **109**: 2751–2760.

Lam, S.K., Siu, C.L., Hillmer, S., Jang, S., An, G., Robinson, D.G., and Jiang, L. (2007). Rice SCAMP1 defines clathrin-coated, trans-golgi-located tubular-vesicular structures as an early endosome in tobacco BY-2 cells. Plant Cell **19**: 296–319.

Langhans, M., MECKEL, T., KRESS, A., LERICH, A., and Robinson, D.G. (2012). ERES (ER exit sites) and the "secretory unit concept". J. Microsc. **247**: 48–59.

Lehti-Shiu, M.D., Zou, C., Hanada, K., and Shiu, S.H. (2009). Evolutionary history and stress regulation of plant receptor-like kinase/pelle genes. Plant Physiol. **150**: 12–26.

Leung, B.O. and Chou, K.C. (2011). Review of super-resolution fluorescence microscopy for biology. Appl. Spectrosc. **65**: 967–980.

Lewis, M.W., Leslie, M.E., Fulcher, E.H., Darnielle, L., Healy, P.N., Youn, J.-Y., and Liljegren, S.J. (2010). The SERK1 receptor-like kinase regulates organ separation in Arabidopsis flowers. Plant J. **62**: 817–828.

Li, J. (2010). Multi-tasking of somatic embryogenesis receptor-like protein kinases. Curr. Opin. Plant Biol. **13**: 509–514.

Li, J. and Chory, J. (1997). A putative leucine-rich repeat receptor kinase involved in brassinosteroid signal transduction. Cell **90**: 929–938.

Li, J., Wen, J., Lease, K.A., Doke, J.T., Tax, F.E., and Walker, J.C. (2002). BAK1, an Arabidopsis LRR receptor-like protein kinase, interacts with BRI1 and modulates brassinosteroid signaling. Cell **110**: 213–222.

Liebmann, C. (2011). EGF receptor activation by GPCRs: an universal pathway reveals different versions. Mol. Cell. Endocrinol. **331**: 222–231.

Lu, C., Mi, L.-Z., Grey, M.J., Zhu, J., Graef, E., Yokoyama, S., and Springer, T.A. (2010). Structural evidence for loose linkage between ligand binding and kinase activation in the epidermal growth factor receptor. Mol. Cell. Biol. **30**: 5432–5443.

Ma-Högemeier, Z.-L., Körber, C., Werner, M., Racine, D., Muth-Köhne, E., Tapken, D., and Hollmann, M. (2010). Oligomerization in the endoplasmic reticulum and intracellular trafficking of kainate receptors are subunit-dependent but not editing-dependent. J. Neurochem.

Margeta-Mitrovic, M., Jan, Y.N., and Jan, L.Y. (2000). A trafficking checkpoint controls GABA(B) receptor heterodimerization. Neuron **27**: 97–106.

Mellado, M., Rodríguez-Frade, J.M., Vila-Coro, A.J., Fernández, S., Martin de Ana, A., Jones, D.R., Torán, J.L., and Martínez-A, C. (2001). Chemokine receptor homo- or heterodimerization activates distinct signaling pathways. EMBO J. **20**: 2497–2507.

Millis, B.A. (2012). Evanescent-wave field imaging: an introduction to total internal reflection fluorescence microscopy. Methods Mol. Biol. **823**: 295–309.

Nam, K.H. and Li, J. (2002). BRI1/BAK1, a receptor kinase pair mediating brassinosteroid signaling. Cell **110**: 203–212.

Nebenführ, A., Ritzenthaler, C., and Robinson, D.G. (2002). Brefeldin A: deciphering an enigmatic inhibitor of secretion. Plant Physiol. **130**: 1102–1108.

Nohe, A., Hassel, S., Ehrlich, M., Neubauer, F., Sebald, W., Henis, Y.I., and Knaus, P. (2002). The mode of bone morphogenetic protein (BMP) receptor oligomerization determines different BMP-2 signaling pathways. J. Biol. Chem. **277**: 5330–5338.

Ntoukakis, V., Schwessinger, B., Segonzac, C., and Zipfel, C. (2011). Cautionary notes on the use of C-terminal BAK1 fusion proteins for functional studies. Plant Cell **23**: 3871–3878.

Oh, M.-H., Wang, X., Kota, U., Goshe, M.B., Clouse, S.D., and Huber, S.C. (2009). Tyrosine phosphorylation of the BRI1 receptor kinase emerges as a component of brassinosteroid signaling in Arabidopsis. Proc. Natl. Acad. Sci. U.S.A. **106**: 658–663.

Oh, M.-H., Wang, X., Wu, X., Zhao, Y., Clouse, S.D., and Huber, S.C. (2010). Autophosphorylation of Tyr-610 in the receptor kinase BAK1 plays a role in brassinosteroid signaling and basal defense gene expression. Proc. Natl. Acad. Sci. U.S.A. **107**: 17827–17832.

Popescu, S.C. (2012). A model for the biosynthesis and transport of plasma membrane-associated signaling receptors to the cell surface. Front. Plant Sci. **3**: 71.

Reyes, F.C., Buono, R., and Otegui, M.S. (2011). Plant endosomal trafficking pathways. Curr. Opin. Plant Biol. **14**: 666–673.

Richter, S., Voss, U., and Jürgens, G. (2009). Post-Golgi traffic in plants. Traffic **10**: 819–828.

Roux, M., Schwessinger, B., Albrecht, C., Chinchilla, D., Jones, A., Holton, N., Malinovsky, F.G., Tör, M., de Vries, S., and Zipfel, C. (2011). The Arabidopsis leucine-rich repeat receptor-like kinases BAK1/SERK3 and BKK1/SERK4 are required for innate immunity to hemibiotrophic and biotrophic pathogens. Plant Cell **23**: 2440–2455.

Rozenfeld, R. and Devi, L.A. (2010). Functional Role(s) of Dimeric Complexes Formed from G-Protein-Coupled Receptors. Handbook of Cell Signaling, Three-Volume Set 2 ed, pp. 185–194.

Russinova, E., Borst, J.W., Kwaaitaal, M., Caño-Delgado, A., Yin, Y., Chory, J., and de Vries, S.C. (2004). Heterodimerization and endocytosis of Arabidopsis brassinosteroid receptors BRI1 and AtSERK3 (BAK1). Plant Cell **16**: 3216–3229.

Savaldi-Goldstein, S., Peto, C., and Chory, J. (2007). The epidermis both drives and restricts plant shoot growth. Nature **446**: 199–202.

Schmidt, E.D., Guzzo, F., Toonen, M.A., and de Vries, S.C. (1997). A leucine-rich repeat containing receptor-like kinase marks somatic plant cells competent to form embryos. Development **124**: 2049–2062.

Schrödinger, E. (1951). What is Life ? The Physical Aspect of the Living Cell.

Schwessinger, B., Roux, M., Kadota, Y., Ntoukakis, V., Sklenar, J., Jones, A., and Zipfel, C. (2011). Phosphorylation-Dependent Differential Regulation of Plant Growth, Cell Death, and Innate Immunity by the Regulatory Receptor-Like Kinase BAK1. PLoS Genet. **7**: e1002046.

Shah, K., Vervoort, J., and de Vries, S.C. (2001). Role of threonines in the Arabidopsis thaliana somatic embryogenesis receptor kinase 1 activation loop in phosphorylation. J. Biol. Chem. **276**: 41263–41269.

She, J., Han, Z., Kim, T.-W., Wang, J., Cheng, W., Chang, J., Shi, S., Wang, J., Yang, M., Wang, Z.-Y., and Chai, J. (2011). Structural insight into brassinosteroid perception by BRI1. Nature **474**: 472–476.

Shimizu, T., Nakano, T., Takamizawa, D., Desaki, Y., Ishii-Minami, N., Nishizawa, Y., Minami, E., Okada, K., Yamane, H., Kaku, H., and Shibuya, N. (2010). Two LysM receptor molecules, CEBiP and OsCERK1, cooperatively regulate chitin elicitor signaling in rice. Plant J. **64**: 204–214.

Shiu, S.H. and Bleecker, A.B. (2003). Expansion of the receptor-like kinase/Pelle gene family and receptor-like proteins in Arabidopsis. Plant Physiol. **132**: 530–543.

Shiu, S.H. and Bleecker, A.B. (2001a). Plant receptor-like kinase gene family: diversity, function, and signaling. Sci. STKE **2001**: re22.

Shiu, S.H. and Bleecker, A.B. (2001b). Receptor-like kinases from Arabidopsis form a monophyletic gene family related to animal receptor kinases. Proc. Natl. Acad. Sci. U.S.A. **98**: 10763–10768.

Sousa, L.P., Lax, I., Shen, H., Ferguson, S.M., De Camilli, P., and Schlessinger, J. (2012). Suppression of EGFR endocytosis by dynamin depletion reveals that EGFR signaling occurs primarily at the plasma membrane. Proc. Natl. Acad. Sci. U.S.A. **109**: 4419–4424.

Springael, J.-Y., Urizar, E., and Parmentier, M. (2005). Dimerization of chemokine receptors and its functional consequences. Cytokine Growth Factor Rev. **16**: 611–623.

Staehelin, L.A. and Kang, B.-H. (2008). Nanoscale architecture of endoplasmic reticulum export sites and of Golgi membranes as determined by electron tomography. Plant Physiol. **147**: 1454–1468.

Stahl, Y., Grabowski, S., Bleckmann, A., Kühnemuth, R., Weidtkamp-Peters, S., Pinto, K.G., Kirschner, G.K., Schmid, J.B., Wink, R.H., Hülsewede, A., Felekyan, S., Seidel, C.A.M., and Simon, R. (2013). Moderation of Arabidopsis Root Stemness by CLAVATA1 and ARABIDOPSIS CRINKLY4 Receptor Kinase Complexes. Curr. Biol. **23**: 362–371.

Sun, Y., Sun, Y., Fan, X.-Y., Fan, X.-Y., Cao, D.-M., Cao, D.-M., Tang, W., Tang, W., He, K., He, K., Zhu, J.-Y., Zhu, J.-Y., He, J.-X., He, J.-X., Bai, M.-Y., Bai, M.-Y., Zhu, S., Zhu, S., Oh, E., Oh, E., et al. (2010). Integration of brassinosteroid signal transduction with the transcription network for plant growth regulation in Arabidopsis. Dev. Cell **19**: 765–777.

Tang, W., Kim, T.-W., Oses-Prieto, J.A., Sun, Y., Deng, Z., Zhu, S., Wang, R., Burlingame, A.L., and Wang, Z.-Y. (2008). BSKs mediate signal transduction from the receptor kinase BRI1 in Arabidopsis. Science **321**: 557–560.

Tang, W., Yuan, M., Wang, R., Yang, Y., Wang, C., Oses-Prieto, J.A., Kim, T.-W., Zhou, H.-W., Deng, Z., Gampala, S.S., Gendron, J.M., Jonassen, E.M., Lillo, C., DeLong, A., Burlingame, A.L., Sun, Y., and Wang, Z.-Y. (2011). PP2A activates brassinosteroid-responsive gene expression and plant growth by dephosphorylating BZR1. Nat. Cell Biol. **13**: 124–131.

Van Craenenbroeck, K. (2012). GPCR Oligomerization: Contribution to Receptor Biogenesis. Subcell. Biochem. **63**: 43–65.

Van Craenenbroeck, K., Borroto-Escuela, D.O., Romero-Fernandez, W., Skieterska, K., Rondou, P., Lintermans, B., Vanhoenacker, P., Fuxe, K., Ciruela, F., and Haegeman, G. (2011). Dopamine D4 receptor oligomerization--contribution to receptor biogenesis. FEBS J. **278**: 1333–1344.

van Esse, G.W., van Mourik, S., Stigter, H., Hove, ten, C.A., Molenaar, J., and de Vries, S.C. (2012). A mathematical model for BRASSINOSTEROID INSENSITIVE1-mediated signaling in root growth and hypocotyl elongation. Plant Physiol. **160**: 523–532.

Vieira, A.V., Lamaze, C., and Schmid, S.L. (1996). Control of EGF receptor signaling by clathrin-mediated endocytosis. Science **274**: 2086–2089.

Vila-Coro, A.J., Mellado, M., Martin de Ana, A., Lucas, P., del Real, G., Martínez-A, C., and Rodríguez-Frade, J.M. (2000). HIV-1 infection through the CCR5 receptor is blocked by receptor dimerization. Proc. Natl. Acad. Sci. U.S.A. **97**: 3388–3393.

Viotti, C., Bubeck, J., Stierhof, Y.-D., Krebs, M., Langhans, M., van den Berg, W., van Dongen, W., Richter, S., Geldner, N., Takano, J., Jürgens, G., de Vries, S.C., Robinson, D.G., and Schumacher, K. (2010). Endocytic and secretory traffic in Arabidopsis merge in the trans-Golgi network/early endosome, an independent and highly dynamic organelle. Plant Cell **22**: 1344–1357.

Walker, J.C. (1994). Structure and function of the receptor-like protein kinases of higher plants. Plant Mol. Biol. **26**: 1599–1609.

Wang, J. and Norcross, M. (2008). Dimerization of chemokine receptors in living cells: key to receptor function and novel targets for therapy. Drug Discov. Today **13**: 625–632.

Wang, X., Kota, U., He, K., Blackburn, K., Li, J., Goshe, M.B., Huber, S.C., and Clouse, S.D. (2008). Sequential transphosphorylation of the BRI1/BAK1 receptor kinase complex impacts early events in brassinosteroid signaling. Dev. Cell **15**: 220–235.

Wang, X., Li, X., Meisenhelder, J., Hunter, T., Yoshida, S., Asami, T., and Chory, J. (2005). Autoregulation and homodimerization are involved in the activation of the plant steroid receptor BRI1. Dev. Cell **8**: 855–865.

Wang, Z.-Y., Bai, M.-Y., Oh, E., and Zhu, J.-Y. (2012). Brassinosteroid signaling network and regulation of photomorphogenesis. Annu. Rev. Genet. **46**: 701–724.

Wombacher, R. and Cornish, V.W. (2011). Chemical tags: applications in live cell fluorescence imaging. J. Biophotonics **4**: 391–402.

Wrana, J.L., Attisano, L., Wieser, R., Ventura, F., and Massague, J. (1994). Mechanism of activation of the TGF-beta receptor. Nature **370**: 341–347.

Yarden, Y. and Schlessinger, J. (1987). Epidermal growth factor induces rapid, reversible aggregation of the purified epidermal growth factor receptor. Biochemistry **26**: 1443–1451.

Yasuda, R. (2006). Imaging spatiotemporal dynamics of neuronal signaling using fluorescence resonance energy transfer and fluorescence lifetime imaging microscopy. Curr. Opin. Neurobiol. **16**: 551–561.

Yin, Y., Wang, Z.-Y., Mora-Garcia, S., Li, J., Yoshida, S., Asami, T., and Chory, J. (2002). BES1 accumulates in the nucleus in response to brassinosteroids to regulate gene expression and promote stem elongation. Cell **109**: 181–191.

Yu, X., Li, L., Zola, J., Aluru, M., Ye, H., Foudree, A., Guo, H., Anderson, S., Aluru, S., Liu, P., Rodermel, S., and Yin, Y. (2011). A brassinosteroid transcriptional network revealed by genome-wide identification of BESI target genes in Arabidopsis thaliana. Plant J. **65**: 634–646.

Zhao, D.-Z., Wang, G.-F., Speal, B., and Ma, H. (2002). The excess microsporocytes1 gene encodes a putative leucine-rich repeat receptor protein kinase that controls somatic and reproductive cell fates in the Arabidopsis anther. Genes Dev. **16**: 2021–2031.

Zhu, J.-Y., Sae-Seaw, J., and Wang, Z.-Y. (2013). Brassinosteroid signalling. Development **140**: 1615–1620.

Chapter 2

Probing Protein-Protein Interactions with FRET-FLIM

Christoph A. Bücherl, José Aker, Sacco C. de Vries, Jan Willem Borst

ABSTRACT

The quantification of molecular interactions or conformational changes can conveniently be studied by using Förster resonance energy transfer (FRET) as a spectroscopic ruler. The FRET phenomenon describes the transfer of energy from a donor to an acceptor molecule if they are in close proximity (<10 nm). The most straightforward method to measure FRET is fluorescence lifetime imaging microscopy (FLIM). In this chapter, we will describe an application of FRET using FLIM to monitor the hexamer formation of CrFP/eYFP-labeled Arabidopsis thaliana cell division cycle protein (AtCDC48) expressed in plant protoplasts.

This Chapter was published as:
Bücherl, C., Aker, J., de Vries, S., and Borst, J.W. (2010). Probing protein-protein Interactions with FRET-FLIM. Methods Mol. Biol. **655**: 389–399.

INTRODUCTION

The dimensions of proteins vary from 5 to 50 nm covering the experimental range of electron microscopy and, partly, optical microscopy. Although electron microscopy has the highest spatial resolution, it is not applicable in living tissue. In contrast, fluorescence microscopy including the genetically encoded visible protein (VFP) technology in particular has all non invasive capabilities for live cell imaging. However, the resolution of fluorescence microscopy is light-diffraction limited (~250 nm) and no information about protein interactions is obtained. In vivo detection of protein interactions has become feasible by combining fluorescence microscopy and FRET. FRET can be measured using a variety of fluorescence imaging approaches like FRET- or ratio imaging and acceptor photobleaching. The most reliable and quantitative method to spatially resolve FRET is Fluorescence Lifetime Imaging Microscopy (FLIM). In this chapter, an example of protein interactions will be shown by visualizing the hexamer formation of AtCDC48 proteins in plant protoplasts using a FRET-FLIM approach.

AtCDC48 belongs to the protein family of ATPases associated with various activities (AAA proteins). The characteristic function of AAA proteins is the coupling of ATP hydrolysis to processes like the disassembly or unfolding of protein substrates. Within the Arabidopsis thaliana genome five isoforms of AtCDC48 (A-E) are encoded. Best characterised is AtCDC48A, which shares 77% identity with the mammalian homologue vasolin containing protein (VCP) or p97. The crystal structure of this animal counterpart revealed a homo-hexameric mushroom-like shaped complex (Huyton et al., 2003; DeLaBarre and Brunger, 2003). Monomeric VCP comprises a N-domain important for cofactor and substrate binding, two AAA domains (D1 and D2) connected by a linker, the D1 domain and the linker region being crucial for hexamerisation and the D2 domain responsible for the major ATPase activity, as well as a C-terminal tail (Aker et al., 2006). After complex formation the N- and D1-domains are located at the top of the hexamer, the D2- and C-domains at the bottom. This domain architecture is also assumed for AtCDC48 despite the lack of crystallographic evidence. However, in vitro and in vivo studies showed a hexameric complex for the AtCDC48A isoform (Rancour et al., 2004; Aker et al., 2007). Using a FRET-FLIM approach Aker et al. (2007) additionally elucidated oligomerisation of AtCDC48C in Arabidopsis mesophyll protoplasts. Even though the two mentioned isoforms are predicted to share 95% amino acid identity their localization pattern is distinct. Whereas AtCDC48A is present at the plasma membrane, the ER, in the cytosol as well as the nucleus, AtCDC48C localizes solely to the nucleus (Aker et al., 2006). In this chapter we will focus on the complex formation of the fluorescently tagged AtCDC48 isoforms A and C expressed in Arabidopsis mesophyll protoplasts to highlight the potential of FRET- FLIM for investigating in vivo interactions.

MATERIALS

Transient transfection vectors

1. Plant expression vector: pMON999 (Monsanto, USA).
2. The cDNAs of AtCDC48A and AtCDC48C as well as Cerulean Fluorescent Protein (CrFP) and enhanced Yellow Fluorescent Protein (eYFP) were cloned into pMON999 vector.
3. DNA-Polymerase: PWO-DNA polymerase used in combination with the Mg^{2+} containing buffer solution provided by the manufacturer.
4. Nucleotides: 25 mM dNTP.
5. Restriction enzymes: depending on the cloning strategy chosen.
6. Ligase: T4 DNA ligase used in combination with the buffer solution provided by the manufacturer.

Protoplast isolation (adapted from Sheen, 2001)

1. Plant material: Rosette leaves of Arabidopsis thaliana plants (ecotype Columbia) grown for 4-5 weeks under long-day conditions (16 h light / 8 h dark) and 20-22°C (see **Note 1**).
2. Mannitol solution: 0.4 M mannitol, 20 mM KCl, 20 mM 2-(N-morpholino) ethanesulfonic acid (MES) pH 5.7 in Milli-Q water.
3. Calcium chloride solution: 1 M $CaCl_2$ in Milli-Q water.
4. Enzyme solution: 1% (w/v) cellulose R10 (Yakult Honsha Co. LTD, Japan) and 0.2% (w/v) pectinase from Rhizopus sp. (Biochemika/Fulka, Germany) dissolved in mannitol solution, subsequent addition of $CaCl_2$ to a final concentration of 10 mM.
5. Plastic round-bottom tubes (Sarstedt, Germany).

Protoplast transfection (adapted from Sheen, 2001)

1. PEG/Ca^{2+} solution: 40% (w/v) polyethylenglycol 4000 (PEG, Merck, Germany), 0.2 M mannitol, 100 mM $Ca(NO_3)_2$ in Milli-Q water (see **Note 2**).
2. W5 solution: 154 mM NaCl, 125 mM $CaCl_2$, 5 mM KCl, 2 mM MES pH 5.7.
3. W5/Glucose solution: W5 solution containing 1 mM glucose.
4. MMg solution: 0.2 M mannitol, 15 mM $MgCl_2$, 4 mM MES pH 5.7.
5. Plastic round-bottom tubes (Sarstedt, Germany).
6. Microscope 8-well slides, Lab-tek Nalge Nunc international (Rochester, NY, USA).

Methods

The question, whether a protein acts as an oligomer, can be addressed and answered by several approaches. Phage display and yeast two-hybrid assays are most commonly used (Causier and Davies, 2002; Burch et al., 2004). However, these methods lack spatial and physiological information, since the proteins expressed are not in their natural environment. The introduction of high-resolution confocal microscopy gave the opportunity to

investigate the co-expression of different proteins in their natural habitat. The optical resolution of a microscope allows detection of fluorescent molecules at sub-cellular level. At most, co-localization of two proteins equipped with two different fluorophores can be revealed, but physical interactions between proteins on nanometer scale cannot be determined. One possibility to go beyond the optical diffraction limit is using new advanced methods like PALM and STED microscopy but the resolution is still not at the molecular level (Betzig et al., 2006; Willig et al., 2006). However, Förster Resonance Energy Transfer (FRET) microscopy elucidates molecular interactions in living tissue.

The term FRET describes the non-radiative energy transfer from the electronically excited state of a donor fluorophore to an acceptor molecule. This photophysical process based

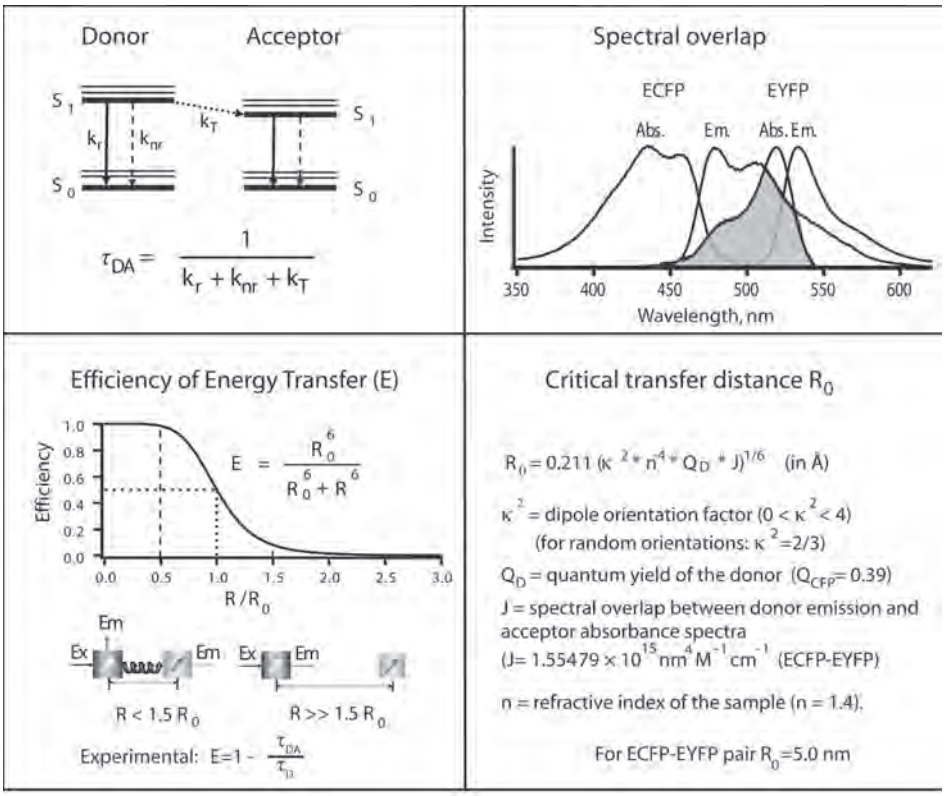

Figure 1: Summary of FRET principles.
When a donor and acceptor are in close proximity, energy transfer can take place leading to an additional relaxation pathway (k_T) (top left). Some prerequisites for FRET are spectral overlap between donor emission and acceptor absorption spectra (top right), small distance between donor and acceptor and adequate dipole orientation. These parameters determine the critical transfer distance (R0), which is characteristic for each FRET pair (bottom right). The efficiency of energy transfer can be related to relative distance and experimentally determined from fluorescence lifetime measurements (bottom left). (Taken from Borst et al., 2006)

on dipole-dipole coupling was first described by Theodor Förster (1948). Spectral overlap of donor emission and acceptor absorption, close proximity of the labeled specimen and adequate orientation of the donor and acceptor transition dipole moments are the requirements for FRET taking place. Exploiting the FRET phenomenon allows the investigation of protein-protein interactions with a distance range of approximately 1-10 nm – depending on the FRET couple used. The energy transfer efficiency is proportional to the reciprocal of the sixth power of the intermolecular fluorophore distance explaining the high distance sensitivity of FRET measurements. The so-called critical (or Förster) radius (R_0), a characteristic property of each FRET pair, is the distance between donor and acceptor, at which the energy transfer efficiency is 50%. The concepts of FRET and relevant equations are summarized in Figure 1.

For the quantification of protein interactions by means of FRET several methods are available. Intensity based methods such as FRET- or ratio imaging and acceptor photobleaching have severe disadvantages. The main drawbacks are: crosstalk of the emission spectra (donor detected in acceptor window), direct excitation of acceptor by donor laser light and dependence on differences in donor/acceptor concentrations. An alternative method to spatially resolve FRET is Fluorescence Lifetime Imaging Microscopy (FLIM), which measures the fluorescence lifetime pixel by pixel. FLIM overcomes problems of intensity-based methods by determining the fluorescence lifetime of the donor molecule only. Molecular interaction between donor and acceptor will result in both the quenching of donor fluorescence intensity and the consequent decrease of the donor fluorescence lifetime since energy transfer will introduce an additional relaxation path from the excited state to the ground state (see **Fig. 1**). The difference of the donor fluorescence lifetime in the absence or presence of acceptor is directly correlated with the FRET efficiency E via

$$E = 1 - \tau_{DA}/\tau_D$$

where τ_{DA} is the fluorescence lifetime of the donor in the presence of acceptor and τ_D is the fluorescence lifetime of the donor alone.

Transient expression vectors

1. Amplify AtCDC48C or AtCDC48A (or the cDNA of your protein-of-interest A) by PCR from an EST using appropriate primers and fuse to PCR amplified CrFP and eYFP into pMON999 vector.
2. Verify constructs by sequencing and the size of the fused proteins by Western-blotting using anti-GFP antibodies.

Protoplast isolation

1. All steps are carried out at room temperature unless otherwise noted.
2. A clean Petri dish (9 cm diameter) is covered with rosette leaves of 4-5 week old Arabidopsis thaliana (see **Note 1**) plants grown under long-day conditions. This will

result in a sufficient amount of protoplasts to perform approximately 6 independent transfections.

3. Slice leaves with a scalpel, add 15 mL of enzyme solution and swirl to dampen all plant material (see **Note 3**).
4. The sliced leave suspension is placed for 3 min in a vacuum desiccator with powered pump followed by 30 min incubation without pumping but under vacuum conditions.
5. The Petri dish is transferred on a platform shaker and incubated at 65-80 rpm and 27 °C for additional 2 h.
6. Protoplasts are released from the leaf matrix by carefully swirling the Petri dish for 1 min by hand. Subsequently, the suspension is filtered through a 35-100 µm nylon mesh into a clean plastic round-bottom tube.
7. Collect the protoplasts by centrifugation for 3 min at 50 x g using a tabletop centrifuge, wash once with 5 mL of W5 solution.
8. At this stage the isolated protoplasts can be kept on ice over night (see **Note 4**).

Protoplast transfection

1. All steps are carried out at room temperature, and the protocol is applicable for 6 independent transfections. Beside the double transfections with donor and acceptor constructs encoding the proteins of interest (interaction studies) at least one single transfection with the donor construct only has to be included next to positive and negative controls.
2. Prepare round-bottom tubes and plasmid DNAs. For single transfections 10-20 µg of the respective DNA is required. For double transfections 10-15 µg of each construct are combined in one Eppendorf tube. Single transfection is used to obtain protoplasts expressing the donor construct only whereas the transfections of two plasmids yield protoplasts for the interaction studies (see **Note 5**).
3. Collect the isolated and washed protoplasts by centrifugation for 3 min at 50 x g in a tabletop centrifuge and remove the supernatant carefully with a pipette.
4. The protoplasts are resuspended in 1.2 mL of MMg (see **Note 6**) and aliquots of 200 µL are transferred in round-bottom tubes (see **Note 7**).
5. Pipette the respective amount of plasmid DNA into the protoplast suspension, and then add 220 µL of PEG/Ca solution. Mix well but carefully and incubate for 5 min (see **Note 7**).
6. Add 800 µL of W5 solution to stop the transfection process and collect the protoplasts by centrifugation at 50 x g for 3 min in a tabletop centrifuge.
7. Remove the supernatant with a pipette and wash with 5 mL of W5 solution.
8. Collect protoplasts by centrifugation at 50 x g for 3 min. Remove the supernatant with a pipette and resuspend the protoplasts in 1 mL of W5 solution containing 1 mM glucose.

9. Transfer the protoplast suspension into a 24-well plate and incubate at 25 °C under long-day conditions. In general, measurements should be carried out about 16 h after transfection but depending on the used expression vectors and constructs early or later time points can be chosen. It is recommended to check the expression levels at several time points to figure out the optimal incubation period (see **Note 7**).

FRET-FLIM

1. FLIM is performed on a Biorad Radiance 2100 MP system in combination with a Nikon TE 300 inverted microscope (Tokyo, Japan) as described by Russinova et al. (2004). Two photon excitation pulses are generated by a Ti-Sapphire Mira Laser (Coherent), pumped by a 5 W Verdi laser, resulting in excitation pulses of 200 fs at a repetition of 76 Mhz. A 60x/1.2 water immersion objective is used.
2. CrFP emission is selected by a 480DF30 band pass filter and detected by a Hamamatsu R3809U MCP (Hamamatsu, Japan) photomultiplier with a time resolution of 50 ps.
3. Fluorescence images of 64×64 pixel size are acquired using the B&H SPC 830 module (Becker & Hickl, Germany) (see **Note 8**).
4. The average count rate is around 10^4 photons per second for an acquisition time of 90 s (Borst et al., 2003).
5. Measurements of single transfected protoplasts expressing N- or C-terminally CrFP-tagged AtCDC48A or AtCDC48C result in the donor fluorescence lifetime required as reference. To elucidate the hexamer formation of AtCDC48A/C monomers, protoplasts expressing donor and acceptor constructs are investigated (see **Note 9**). The protoplasts are transferred into an 8-well chamber for imaging (see **Note 10**).

Analysis of FLIM data with SPCImage 2.9.3

1. SPCImage is the software package included with the B&H acquisition card. The raw data can be imported and analyzed using an exponential model function. The fitted experimental data result in the output of fluorescence lifetime values per pixel depicted as a false-color code. During the fitting process the chi-square value between model function and data is minimised (Becker et al., 2003).
2. In general, FRET-FLIM experiments are based on the fluorescence lifetime of donor molecules in the absence and presence of acceptor. The data analysis involves first the determination of the fluorescence lifetime of single transfected protoplasts (donor only). Since one donor population is assumed (no FRET possible) a one-component analysis is carried out (see **Note 11**). The average donor fluorescence lifetime subsequently serves as reference value to judge if interactions occur when acceptor molecules are present. Energy transfer from the donor to the acceptor molecule will result in a reduction of the donor fluorescence lifetime and therefore a change in the color code.

3. The double transfected protoplasts (donor and acceptor) are analyzed based on a two-component model. Thereby the value of one fluorescence lifetime component can be fixed to the mean of the donor only analysis. This approach assumes two donor populations – one transferring energy to an adjacent acceptor molecule resulting in a reduce fluorescence lifetime, the second showing no FRET and hence exhibiting fluorescence decay kinetics as donor alone.
4. After loading the experimental data a fluorescence intensity image will be displayed. A blue crosshair allows the selection of single pixels to control the quality of the data set by surveying the corresponding fluorescence decay histograms. Areas showing high auto-fluorescence (identifiable by the steep fluorescence decay) or less than 200 photon counts for the maximum should be excluded from the fitting process (see **Notes 12 & 13**).
5. Before starting the analysis process, several settings have to be chosen. Using the "region of interest" (ROI) tool specific areas, e.g. plasma membrane or nucleus, of the intensity image can be selected. Additionally, the borders of the fluorescence decay histogram have to be set. Typical values are around 1 ns (before the rising edge) for the left and about 10.5 ns (to prevent TAC [time-to-amplitude converter] noise at long time scales) for the right border. Depending on the protoplast analyzed, the number of components for the underlying exponential fit function has to be defined (here one or two). In case of a two-component analysis for double-transfected protoplasts the τ_2 value is fixed to the mean fluorescence lifetime of the donor fluorophore. All other parameters should remain unfixed independent of the fit model.
6. After performing the calculations, the mean fluorescence lifetime, the distribution of the single pixel values as well as a false-color coded lifetime image will be displayed for the selected ROI (see **Fig. 2**).

NOTES

1. Wild type or transgenic lines possible.
2. Heat twice for 6 s at 300 Watt in a microwave to dissolve PEG.
3. Do not cut the leaves to small because this will lead to a higher ratio of dead protoplasts.
4. Nonetheless, it is recommended to proceed immediately - the quicker the transfection the better.
5. The total volume of plasmid DNA should not exceed 30 µL. Therefore, plasmid solutions with appropriate DNA concentrations of around 1 µg/µL plasmid DNA are recommended.
6. The amount of protoplasts can vary – so adapt the volume of MMg solution.

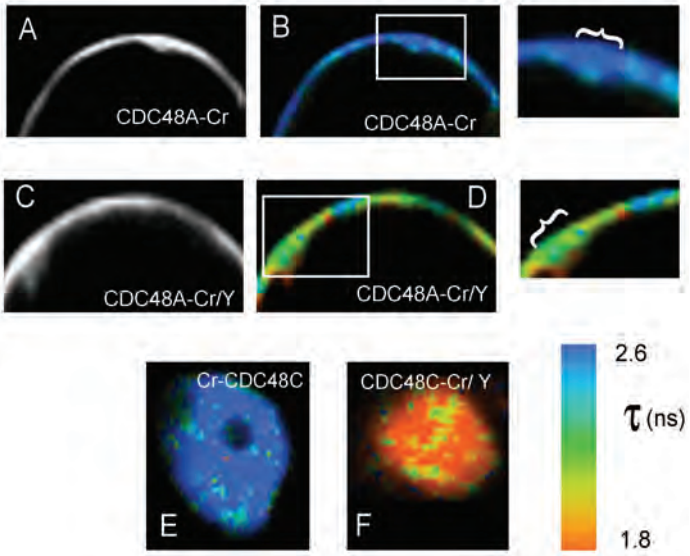

Figure 2. Interactions between AtCDC48A or AtCDC48C tagged protomers based on FRET measured by FLIM.
(**A, B**) Fluorescence intensity image of a section of the plasma membrane of a protoplast expressing the donor molecule AtCDC48A-CrFP alone (**A**) and the false-color or lifetime image (**B**). A long lifetime, giving a dark blue color, means no interaction; a reduction in donor lifetime generating a shift towards orange, means interaction.
(**C, D**) A combination of AtCDC48A-CrFP and AtCDC48A-eYFP proteins (**C**) shows a reduction of the fluorescence lifetime at the plasma membrane (**D**).
(**E, F**) Fluorescence lifetime images of the CrFP-AtCDC48C donor alone (**E**) and the combination of AtCDC48C-CrFP with AtCDC48C-eYFP (both C-terminal fusions) (**F**), showing a reduction in fluorescence lifetime being in line with the mushroom-like shape structure of p97/VCP (Aker et al., 2007). (Taken from Aker et al., 2007)

7. Use tips with enlarged openings to reduce shear forces.
8. Images are taken with 64×64 pixel size with a x,y pixel resolution of about 200 nm. Higher pixel resolution does not increase spatial information due to the light diffraction limitation. Instead using higher pixel resolution requires a prolonged data acquisition time to ensure the detection of a statistically relevant number of photons.
9. Living protoplasts can be selected by visual inspection. Using a long-pass filter (LP 520 nm) the red fluorescence of the chlorophyll is observed and a good indictor for a living cell.
10. Colocalisation has to be verified by confocal laser scanning microscopy.
11. CrFP shows also in absence of an acceptor bi-exponential decay kinetics but this effect is observed by applying the ADC (analog-digital converter) larger than 64. Therefore accurate data analysis should make use of two-component analysis even for donor only expressing protoplasts whereby one component is fixed.

12. In case the number of photons is too low for quantitative analysis, the binning factor can be increased. The binning is a procedure where the selected pixel is analyzed but the neighboring pixels are included for calculation the fluorescence lifetime. The binning factor can be calculated according to the following formula:

    Binning factor = $(2n+1)^2$, where n is number of pixels

    In Figure 2 FLIM images are shown where a binning factor of 1 has been applied. In other studies the effect of binning has been investigated and no significant change was observed.
13. Consider alternative FRET couples such as eGFP/mCherry. First, this FRET couple reduces crosstalk of eGFP fluorescence into the mCherry detection window in intensity based measurements. Second, eGFP can be excited optimal with a conventional confocal microscope, whereas CrFP is suboptimal excited. Third, direct excitation of mCherry is avoided at the donor excitation wavelength compared to the CrFP/eYFP situation. Fourth, the fluorescence lifetime of eGFP exhibits a mono-exponential decay profile and therefore quantitative analysis is improved in FRET-FLIM measurements. Fifth, using eGFP as a donor molecule in a FRET-FLIM experiment gives reduced background fluorescence.

REFERENCES

Aker, J., Borst, J.W., Karlova, R., and de Vries, S. (2006). The Arabidopsis thaliana AAA protein CDC48A interacts in vivo with the somatic embryogenesis receptor-like kinase 1 receptor at the plasma membrane. J. Struct. Biol. **156**: 62–71.

Aker, J., Hesselink, R., Engel, R., Karlova, R., Borst, J.W., Visser, A.J.W.G., and de Vries, S.C. (2007). In vivo hexamerization and characterization of the Arabidopsis AAA ATPase CDC48A complex using forster resonance energy transfer-fluorescence lifetime imaging microscopy and fluorescence correlation spectroscopy. Plant Physiol. **145**: 339–350.

Becker, W., Bergmann, A., and Hink, M.A. (2003). Fluorescence lifetime imaging by time-correlated single-photon counting. Microsc. Res. Tech. **63**: 58-66.

Betzig, E., PATTERSON, G.H., Sougrat, R., Lindwasser, O.W., Olenych, S., Bonifacino, J.S., Davidson, M.W., Lippincott-Schwartz, J., and Hess, H.F. (2006). Imaging Intracellular Fluorescent Proteins at Nanometer Resolution. Science **313**: 1642–1645.

Borst, J.W., Hink, M.A., van Hoek, A., and Visser, A. (2003). Multiphoton microspectroscopy in living plant cells. Proc. SPIE **4963**: 231-238.

Borst, J.W., Nougalli-Tonaco, I., Hink, M.A., Hoek, A., Immink, R.G.H., and Visser, A.J.W.G. (2006). Protein-Protein Interactions In Vivo: Use of Biosensors Based on FRET. Rev. Fluorescence 2006: 341–357.

Burch, L.R., Scott, M., Pohler, E., Meek, D., and Hupp, T. (2004). Phage-peptide Display Identifies the Interferon-responsive, Death-activated Protein Kinase Family as a Novel Modifier of MDM2 and p21WAF1. J. Mol. Biol. **337**: 115–128.

Causier, B. and Davies, B. (2002). Analysing protein-protein interactions with the yeast two-hybrid system. Plant Mol. Biol. **50**: 855–870.

DeLaBarre, B. and Brunger, A.T. (2003). Complete structure of p97/valosin-containing protein reveals communication between nucleotide domains. Nat. Struct. Biol. **10**: 856–863.

Förster, T. (1948). Zwischenmolekulare Energiewanderung und Fluoreszenz. Ann. Phys. **2**: 55-75.

Huyton, T., Pye, V.E., Briggs, L.C., Flynn, T.C., Beuron, F., Kondo, H., Ma, J., Zhang, X., and Freemont, P.S. (2003). The crystal structure of murine p97/VCP at 3.6Å. J. Struct. Biol. **144**: 337–348.

Rancour, D.M., Park, S., Knight, S.D., and Bednarek, S.Y. (2004). Plant UBX domain-containing protein 1, PUX1, regulates the oligomeric structure and activity of arabidopsis CDC48. J. Biol. Chem. **279**: 54264–54274.

Russinova, E., Borst, J.W., Kwaaitaal, M., Caño-Delgado, A., Yin, Y., Chory, J., and de Vries, S.C. (2004). Heterodimerization and endocytosis of Arabidopsis brassinosteroid receptors BRI1 and AtSERK3 (BAK1). Plant Cell **16**: 3216–3229.

Sheen, J. (2001). Signal transduction in maize and Arabidopsis mesophyll protoplasts. Plant Physiol. **127**: 1466–1475.

Willig, K.I., Rizzoli, S.O., Westphal, V., Jahn, R., and Hell, S.W. (2006). STED microscopy reveals that synaptotagmin remains clustered after synaptic vesicle exocytosis. Nature **440**: 935–939.

Chapter 3

Visualization of BRI1 and BAK1(SERK3) membrane receptor hetero-oligomers during brassinosteroid signaling

Christoph A. Bücherl[1], G. Wilma van Esse[1], Alex Kruis[1], Jeroen Luchtenberg[1], Adrie H. Westphal[1], José Aker[1], Arie van Hoek[2,3], Catherine Albrecht[1], Jan Willem Borst[1,3,4], Sacco C. de Vries[1]

[1] Laboratory of Biochemistry, [2] Laboratory of Biophysics and [3] Microspectroscopy Centre, Department of Agrotechnology and Food Sciences, Wageningen, The Netherlands

[4] Centre for BioSystems Genomics, 6708 PB Wageningen, The Netherlands

ABSTRACT

The LRR-RLK BRI1 is the main ligand perceiving receptor for brassinosteroids (BRs) in Arabidopsis thaliana. Binding of BRs to the ectodomain of plasma membrane (PM)-located BRI1 receptors initiates an intracellular signal transduction cascade that influences various aspects of plant growth and development. Even though the major components of BR signaling have been revealed and the PM was identified as the main site of BRI1 signaling activity, the very first steps of signal transmission are still elusive. Recently, it was shown that initiation of BR signal transduction requires the interaction of BRI1 with its SERK coreceptors. In addition, the resolved structure of the BRI1 ectodomain suggested that BAK1(SERK3) may constitute a component of the ligand perceiving receptor complex. We therefore investigated the spatial correlation between BRI1 and BAK1(SERK3) in the natural habitat of both LRR-RLKs using comparative colocalization analysis and fluorescence lifetime imaging microscopy (FLIM). We show that activation of BR signaling by exogenous ligand application resulted in both elevated colocalization between BRI1 and BAK1(SERK3) and an about 50% increase of receptor hetero-oligomerization in the PM of live Arabidopsis thaliana root epidermal cells. However, large populations of BRI1 and BAK1(SERK3) colocalized independently of BRs. Moreover, we could visualize that approximately 7% of the BRI1 PM pool constitutively hetero-oligomerizes with BAK1(SERK3) in live root cells. We propose that only small populations of PM-located BRI1 and BAK1(SERK3) receptors participate in active BR signaling and that initiation of downstream signal transduction involves preassembled BRI1-BAK1(SERK3) hetero-oligomers.

This Chapter was published as: **Bücherl CA, van Esse GW, Kruis A, Luchtenberg J, Westphal AH, Aker J, van Hoek A, Albrecht C, Borst JW, de Vries SC** (2013). Visualization of BRI1 and BAK1(SERK3) Membrane Receptor Heterooligomers during Brassinosteroid Signaling. Plant Physiol. 162(4):1911-25.

INTRODUCTION

Brassinosteroids (BRs) form a class of plant growth hormones that are structurally similar to animal steroids (Grove et al., 1979). Mutants unable to synthesize or unable to perceive BRs show dwarfed stature, impaired photomorphogenesis and fertility defects (Clouse and Sasse, 1998). Unlike animal steroid signaling, which employs intracellular steroid receptors, in Arabidopsis thaliana BR signaling is mainly mediated via the plasma membrane (PM)-located leucine-rich repeat receptor-like kinase (LRR-RLK) Brassinosteroid-insensitive 1 (BRI1) (Li and Chory, 1997). This receptor perceives BRs at the cell surface (He et al., 2000; Kinoshita et al., 2005) and initiates an intracellular signal transduction cascade, which controls various aspects of plant growth and development (Clouse, 2011; Kutschera and Wang, 2012; Wang et al., 2012).

Current models of BR signaling assume that in the absence of ligands BRI1 resides in a homodimeric configuration in the PM (Wang et al., 2008; Kim and Wang, 2010; Jaillais et al., 2011a) and that a double-lock mechanism prevents aberrant signaling activity (Jaillais et al., 2011a; Wang et al., 2012). This inhibitory mechanism involves the BRI1 kinase inhibitor 1 (BKI1), which binds to the kinase domain of unliganded BRI1 receptors and thereby keeps the LRR-RLK inactive (Jaillais et al., 2011b). In vitro, BKI1 precludes BRI1 from associating with BRI1-associated kinase 1 (BAK1; also known as SERK3 for Somatic embryogenesis receptor-like kinase 3) (Wang and Chory, 2006; Jaillais et al., 2011b), another LRR-RLK required for BR signal transduction (Li et al., 2002; Nam and Li, 2002; Gou et al., 2012). Binding of BRs to the extracellular LRR domain of BRI1 homodimers is thought to result in conformational changes, which trigger basal BRI1 kinase activity and auto-phosphorylation (Wang et al., 2008; Kim and Wang, 2010; Jaillais et al., 2011a). Subsequently, BRI1 can trans-phosphorylate BKI1 leading to the release of the kinase inhibitor into the cytosol (Jaillais et al., 2011b). The dissociation of BKI1 in turn may enable recruitment of BAK1(SERK3) into the BRI1 receptor complex (Wang et al., 2008; Kim and Wang, 2010; Jaillais et al., 2011a; Jaillais et al., 2011b). Via sequential trans-phosphorylation events within the BRI1-BAK1(SERK3) hetero-oligomers BRI1 eventually gains full kinase activity (Wang et al., 2008) and downstream BR signaling is initiated (Wang et al., 2008; Kim and Wang, 2010; Clouse, 2011; Jaillais et al., 2011a; Wang et al., 2012). A phosphorylation and dephosphorylation cascade relays the signal of BR binding through BR signaling kinases (BSKs) (Tang et al., 2008; Kim et al., 2009) or constitutive differential growth 1 (CDG1) and CDG1-like 1 (CDL1) (Kim et al., 2011) to downstream targets culminating in the transcriptional regulation of BR-responsive genes (Kim and Wang, 2010; Sun et al., 2010; Yu et al., 2011) mediated by the Brassinazole-resistent 1 (BZR1) and bri1-EMS suppressor 1 (BES1; also known as BZR2) transcription factors (He et al., 2002; Wang et al., 2002; Yin et al., 2002; He et al., 2005; Yin et al., 2005).

Even though genetic, biochemical and proteomic approaches have revealed the major components of BR signaling (Wang et al., 2012), two recent findings require modification of the model proposed for initial steps of BR signaling, the hetero-oligomerization of BRI1 and BAK1(SERK3) and the initiation of downstream signaling. The first is the observation by Gou et al. (2012) that BAK1(SERK3), SERK1 and SERK4 (also known as BKK1 for BAK1-like kinase 1) not only enhance BRI1 kinase activity but are essential for initiating downstream signal transduction. The second derives from the resolved crystal structure of the BRI1 ectodomain and opposes the hypothesis that BRI1 homodimers function as ligand perceiving receptor complexes. Instead, a hetero-oligomeric configuration was proposed (Hothorn et al., 2011; She et al., 2011). Because the ligand-binding site within the BRI1 ectodomain, designated island domain, is located about five LRR units away from the PM surface and therefore coincides with the tip of the BAK1(SERK3) 4.5 LRR units, this coreceptor was proposed as the ideal candidate for the hetero-oligomeric complex partner of BRI1 even in the absence of ligand (Hothorn et al., 2011; She et al., 2011). Thus, the coreceptor BAK1(SERK3) may already participate in BR perception rather than being recruited to hormone-bound BRI1 receptors, which would imply that the two RLKs can form constitutive hetero-oligomers.

To date, only one example of constitutive plant receptor oligomers has been reported, the chitin-sensing receptor system in rice (Shimizu et al., 2010). However, receptor complex preformation is a common phenomenon in animal signaling systems. For example, the insulin receptor is expressed as a constitutive dimer due to disulphide linkages between extracellular domains (Massague et al., 1980) and also epidermal growth factor receptors (EGFRs) reside as preformed complexes in the PM of mammalian cells (Gadella and Jovin, 1995; Bader et al., 2009). Preformation of receptor oligomers has also been reported for several families of animal receptors (Springael et al., 2005; Van Craenenbroeck, 2012). Some suggested functional consequences of constitutive receptor complexes are increased avidity for ligands (Ehrlich et al., 2012), enhanced signaling efficiency (Hsieh et al., 2010), and differential signaling specificity (Ehrlich et al., 2011).

Here, we employed confocal imaging and fluorescence lifetime imaging microcopy (FLIM) to study the spatial correlation between BRI1 and BAK1(SERK3), the main coreceptor of BR signaling (Albrecht et al., 2008). Fluorescently tagged BRI1 and BAK1(SERK3) receptor proteins expressed in root epidermal cells, a cell file shown to exhibit active BR signaling (Hacham et al., 2011), were used for investigating receptor colocalization and hetero-oligomerization in an intact plant organ. Our results show that only around 10% of BRI1 receptors form hetero-oligomers with BAK1(SERK3) during active BR signaling in the PM, the main site of BRI1 signaling activity (Irani et al., 2012), of root epidermal cells. Pretreatment of roots with the BR biosynthesis inhibitors brassinazole (BRZ) or propiconazole (PPC) clearly decreased the amount of BRI1-BAK1(SERK3) hetero-oligomers. Still, approximately 7% of the BRI1 PM pool showed physical interaction with BAK1(SERK3)

in heterogeneously distributed patches. Therefore we propose that BR signaling employs only a small population of both LRR-RLKs and that initiation of signal transduction involves constitutive BRI1-BAK1(SERK3) hetero-oligomers.

RESULTS

Colocalization of BRI1 and SERK3 is influenced by the BR signaling status

To investigate the BR dependent spatial correlation between BRI1 and BAK1(SERK3) receptors at subcellular level in Arabidopsis roots, first a comparative colocalization analysis of immuno-labeled tissue was performed. For simplicity, we will refer to SERK3 hereafter without reference to its BAK1 designation. In Figure 1, confocal images of a double transgenic Arabidopsis line expressing BRI1-GFP (hereafter referred to as BRI1-GFP 1; Geldner et al., 2007) and SERK3-HA using their native promoters are shown. Immuno-cytochemical labeling was performed with primary antibodies against the GFP and HA epitopes visualized with Alexa488- and Alexa568-conjugated secondary antibodies, respectively. Under regular growth conditions BRI1 and SERK3 mainly colocalized at the PM and to a lesser extent in endomembrane compartments (Figure 1A-C and Table 1). The observed endosomal structures for BRI1-GFP most likely represent Golgi stacks, trans-Golgi network/early endosome (TGN/EE) compartments and multivesicular bodies (MVBs) as reported previously using live-cell imaging (Geldner et al., 2007; Viotti et al., 2010; Irani et al., 2012) and electron microscopy (Viotti et al., 2010). In contrast, SERK3-HA showed a more diffuse localization pattern and additionally large endomembrane compartments, which could represent tonoplast membranes, were visible (Figure 1B and Figure S4). Colocalization analysis based on modified Manders' colocalizaton coefficients, which indicate the fractional overlap of fluorescence intensities in the separate imaging channels, revealed that approximately half of the PM BRI1-GFP and SERK3-HA receptor populations colocalize (Table 1). For the intracellular endomembrane compartments Manders' colocalization coefficients of about 50% and 30% for BRI1 and SERK3, respectively, were determined (Table 1).

To test whether ligand depletion reduces the spatial correlation of the two LRR-RLKs, seedlings were cultured for two days in the presence of 5 µM BRZ prior to imaging. BRZ is a BR biosynthesis inhibitor and reduces the amount of endogenous BRs by approximately 95% (Asami et al., 2001). BES1 phosphorylation was used as read-out to confirm that BRZ treatment indeed abolishes BR signaling (Figure S1). Depletion of endogenous BRs did not affect the localization pattern of BRI1 and SERK3 nor the fluorescence overlap at the PM. However, a minor decrease in colocalization of both receptors was revealed in the intracellular space (Figure 1D-F and Table 1).

Subsequently, BR signaling was restored by exogenous application of 24-epi-brassinolide (BL) to BRZ pretreated roots. In line with the findings of Geldner et al. (2007), no obvious

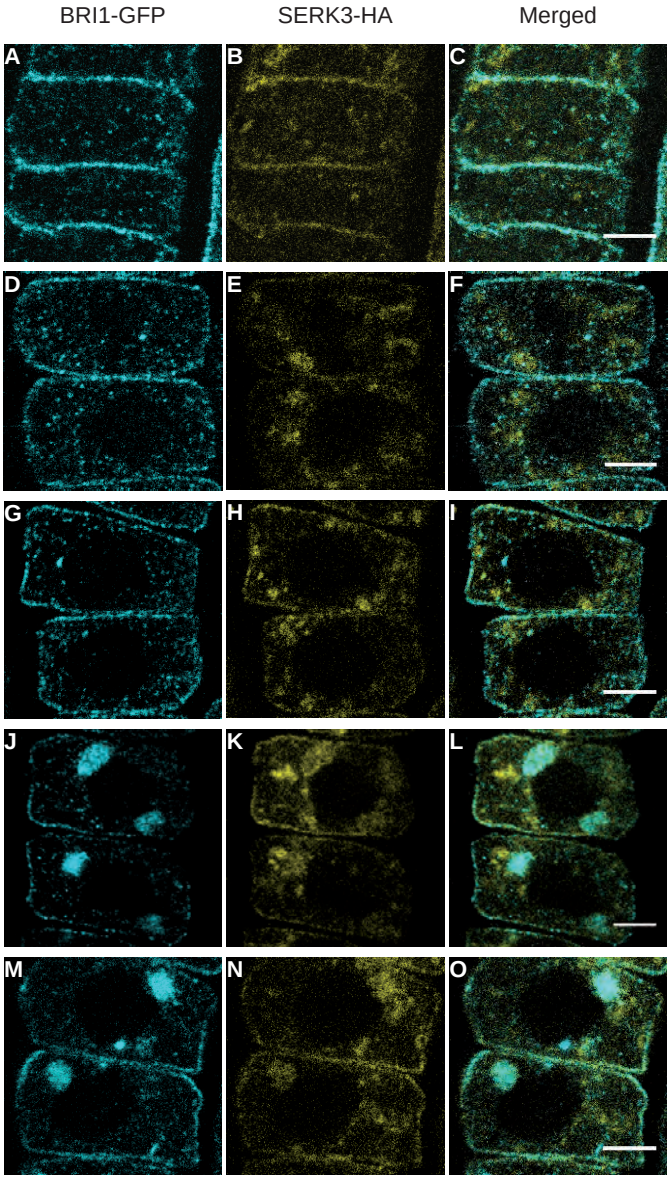

Figure 1: BRI1 and SERK3 colocalize in different compartments of Arabidopsis **meristematic root epidermal cells.**
(**A-C**) Localization of BRI1-GFP (**A**) and SERK3-HA (**B**) as well as the merged image **(C)** of both immuno-labeled proteins in untreated roots.
(**D-F**) Localization of BRI1-GFP (**D**) and SERK3-HA (**E**) as well as the merged image (**F**) after BRZ treatment.
(**G-I**) Localization of BRI1-GFP (**G**) and SERK3-HA (**H**) as well as the merged image (**I**) after BRZ treatment and BL application (1 µM, 1 h).
(**J-L**) Localization of BRI1-GFP (**J**) and SERK3-HA (**K**) as well as the merged image (**L**) after BRZ treatment and BFA application (50 µM, 1 h).

Table 1: Quantification of BRI1 and SERK3 colocalization after immuno-labeling.
Comparative colocalization analysis of immuno-labeled BRI1-GFP and SERK3-HA in roots of 5 day old Arabidopsis seedlings coexpressing BRI-GFP 1 and SERK3-HA. BRZ (5 µM) was added to the growth medium 3 days after germination. 24-epi-brassinolide (BL, 1 µM) and BFA (50 µM) were applied for 1 h. BRI1-GFP was visualized using rabbit-anti-YFP/goat-anti-rabbit-Alexa488 antibodies and SERK3-HA was labeled using mouse-anti-HA/goat-anti-mouse-Alexa568 antibodies. Colocalizing fractions are presented as modified Manders' colocalization coefficients ± S.E.M. Additionally, Pearson correlation coefficients ± S.E.M. are given as independent measure for colocaliztion. "N" represents the number of ROIs analyzed.

	Plasma membrane			
	BRI1-GFP	SERK3-HA	r(Pearson)	N
untreated	0.57 ± 0.01	0.48 ± 0.02	0.14 ± 0.01	67
BRZ	0.56 ± 0.01	0.49 ± 0.03	0.12 ± 0.01	68
BRZ+BL	0.63 ± 0.02[a,b]	0.60 ± 0.02[a,b]	0.14 ± 0.01	86
BRZ+BFA	0.69 ± 0.02[a,b]	0.65 ± 0.02[a,b]	0.20 ± 0.01[a,b]	82
BRZ+BFA/BL	0.74 ± 0.02[a,b]	0.73 ± 0.02[a,b]	0.24 ± 0.01[a,b]	84

	Intracellular			
	BRI1-GFP	SERK3-HA	r(Pearson)	N
untreated	0.48 ± 0.04	0.29 ± 0.03	0.07 ± 0.02	63
BRZ	0.35 ± 0.03	0.23 ± 0.03	0.06 ± 0.02	56
BRZ+BL	0.45 ± 0.04	0.37 ± 0.03[b]	0.12 ± 0.02	71
BRZ+BFA	0.49 ± 0.05[b]	0.41 ± 0.03[a,b]	0.04 ± 0.02	53
BRZ+BFA/BL	0.43 ± 0.04	0.37 ± 0.03[b]	0.07 ± 0.02	61

	BFA compartment			
	BRI1-GFP	SERK3-HA	r(Pearson)	N
BRZ+BFA	0.64 ± 0.02	0.64 ± 0.03	0.12 ± 0.02	73
BRZ+BFA/BL	0.68 ± 0.02	0.65 ± 0.03	0.13 ± 0.02	72

[a] The mean difference is significant at the $p < 0.05$ level compared to untreated samples (two-tailed Student's t-test for equal variance).
[b] The mean difference is significant at the $p < 0.05$ level compared to BRZ treated samples (two-tailed Student's t-test for equal variance).

(**M-O**) Localization of BRI1-GFP (**M**) and SERK3-HA (**N**) as well as the merged image (**O**) after BRZ treatment and simultaneous BFA/BL application (50 µM and 1 µM, respectively, 1 h).
Confocal images of immuno-labeled BRI1-GFP and SERK3-HA in roots of 5 day old Arabidopsis seedlings coexpressing BRI1-GFP 1 and SERK3-HA. BRI1-GFP was stained using rabbit-anti-YFP and goat-anti-rabbit-Alexa488 antibodies, whereas mouse-anti-HA and goat-anti-mouse-Alexa568 antibodies were used for labeling SERK3-HA. Except for (**A-C**), all seedlings were cultured for 2 days in medium containing 5 µM BRZ. The BRI1-GFP 1/SERK3-HA line used here is homozygous for both tagged receptors and has approximately twice the amount of endogenous BRI1 and SERK3 proteins (van Esse et al. 2011).
24-epi-brassinolide (BL) was used throughout the experiments. Scale bars correspond to a size of 5 µm.

effect on the localization of BRI1-GFP was observed (Figure 1G). As shown in Figure 1H, also the distribution of SERK3-HA seemed unaffected. However, colocalization analysis indicated increased fluorescence overlap for both PM and intracellular BRI1 and SERK3 populations. The Manders' colocalization coefficients for PM colocalization and intracellularly located SERK3 even exceeded the initial values obtained for untreated roots (Table 1). Thus, it seems that the BR signaling status influences the spatial correlation between BRI1 and SERK3.

This finding was further investigated by treatment of roots with the endosomal trafficking inhibitor brefeldin A (BFA), a compound reported to result in enhanced BR signaling in the absence of exogenously added ligand (Geldner et al., 2007; Irani et al., 2012). The results displayed in Figure 1L clearly show that BRI1-GFP and SERK3-HA were sequestered into the large BFA compartments. Significantly increased colocalization was observed at the PM (Figure 1J-L compared with Figure 1D-F), the presumed site of active BR signaling as suggested by Irani et al. (2012). In general, BRI1-GFP distribution was more drastically affected by BFA than that of SERK3-HA. Still, most of the BFA compartments contained colocalizing BRI1-GFP and SERK3-HA receptors (Figure 1L). Simultaneous application of BFA and BL additionally increased the amount of colocalizing BRI1-GFP and SERK3-HA receptors in BFA compartments as shown in Figures 1M-O and Table 1.

To answer whether the partial colocalization observed for BRI1-GFP and SERK3-HA in the same BFA compartments reflects a general phenomenon, a comparative analysis was performed. The results presented in Figure S2 revealed that BRI1-GFP, SERK1-YFP and SERK2-YFP are highly sensitive to BFA while SERK3-GFP was only weakly visible in BFA compartments. This suggests that receptors operative in different pathways can employ the same ARF-GEF mediated pathway, whereas receptors that act in the same pathway may be sorted differentially.

Taken together, our comparative colocalization analysis of immuno-labeled Arabidopsis roots indicates that a substantial amount of BRI1 and SERK3 receptors colocalizes independently of BR ligands. Activation of BR signaling resulted in significantly elevated colocalizing receptor populations, in accordance with the proposed recruitment models for BRI1-SERK3 hetero-oligomerization.

BRI1 and SERK3 interact in BFA compartments

Colocalization is a good indicator for the involvement of proteins in the same biological process. However, due to the limited spatial resolution of confocal imaging, colocalization analysis cannot answer whether two proteins of interest also physically interact, a requirement for many signaling events. Therefore fluorescence lifetime imaging microscopy (FLIM) was employed to detect Förster resonance energy transfer (FRET) between the Alexa dye-conjugated secondary antibodies used above. The results of the FRET-FLIM experiments are presented in Figure 2 and show that within BFA compartments BRI1-GFP and SERK3-HA were indeed in close physical proximity, as indicated by a reduction of the Alexa488

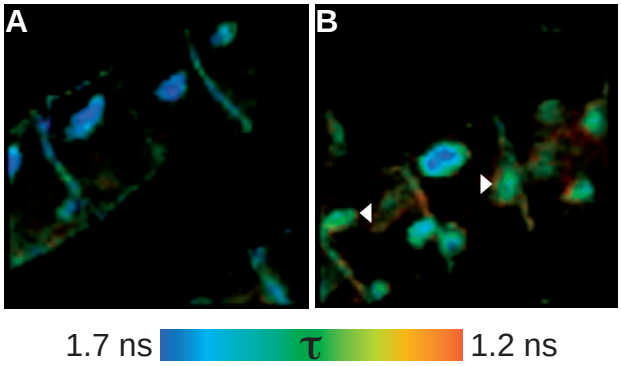

Figure 2: BFA compartments contain BRI1-SERK3 hetero-oligomers.
(**A**) Fluorescence lifetime image of BRI1-GFP labeled with rabbit-anti-YFP and goat-anti-rabbit-Alexa488.
(**B**) Fluorescence lifetime image of double labeled BRI1-GFP and SERK3-HA with rabbit-anti-YFP/goat-anti-rabbit-Alexa488 and mouse-anti-HA/goat-anti-mouse-Alexa568, respectively.
FRET-FLIM of immuno-labeled BRI1-GFP and SERK3-HA in roots of 5 day old Arabidopsis seedlings, coexpressing BRI-GFP 1 and SERK3-HA, in response to BFA (50 µM BFA, 1 h). The BRI1-GFP 1/SERK3-HA line used here is homozygous for both tagged receptors and has approximately twice the amount of endogenous BRI1 and SERK3 proteins (van Esse et al. 2011).
White arrowheads indicate BFA compartments with reduced Alexa488 fluorescence lifetimes. Color bar represents false color-code for Alexa488 fluorescence lifetimes (τ).

fluorescence lifetime from 1.7 ns to 1.3 ns. Interaction of both receptors was observed in a subset of the intracellular membrane compartments (arrowheads in Figure 2B), in line with the colocalization data (Figure 1L and 1O). Most likely these intracellular BRI1-SERK3 hetero-oligomers originate from endocytosed PM receptor complexes. Further validation of the FRET-FLIM data using antibody labeling is described in Figure S3. Unfortunately, the detection of FRET was restricted to BFA compartments that contained sufficient BRI1-GFP and SERK3-HA receptors. Using the immuno-cytochemical approach it was not possible to obtain reliable photon counts for statistical fluorescence lifetime analysis at the PM.

BR signaling activity affects colocalization between BRI1 and SERK3 also in live roots

To monitor the dynamic features of BRI1 and SERK3, also live-cell imaging was applied. In Figures 3A-C, confocal images of a double transgenic line expressing pSERK3::SERK3-mCherry and BRI1-GFP (hereafter referred to as BRI1-GFP 2; Friedrichsen et al., 2000) are shown. As expected, both receptors localized to the PM. For BRI1-GFP similar vesicular structures as seen in Figure 1 were observed (Figure 3A). SERK3-mCherry again showed a more diffuse intracellular localization pattern (Figure 3B compared with Figure 1B) and localization to the tonoplast was revealed (e.g. Figure 3E compared with Figure S4).

Similar to the findings obtained by immuno-labeling, BRI1 and SERK3 colocalized highly at the PM and less pronounced in endomembrane compartments (Figure 3C), as indicated

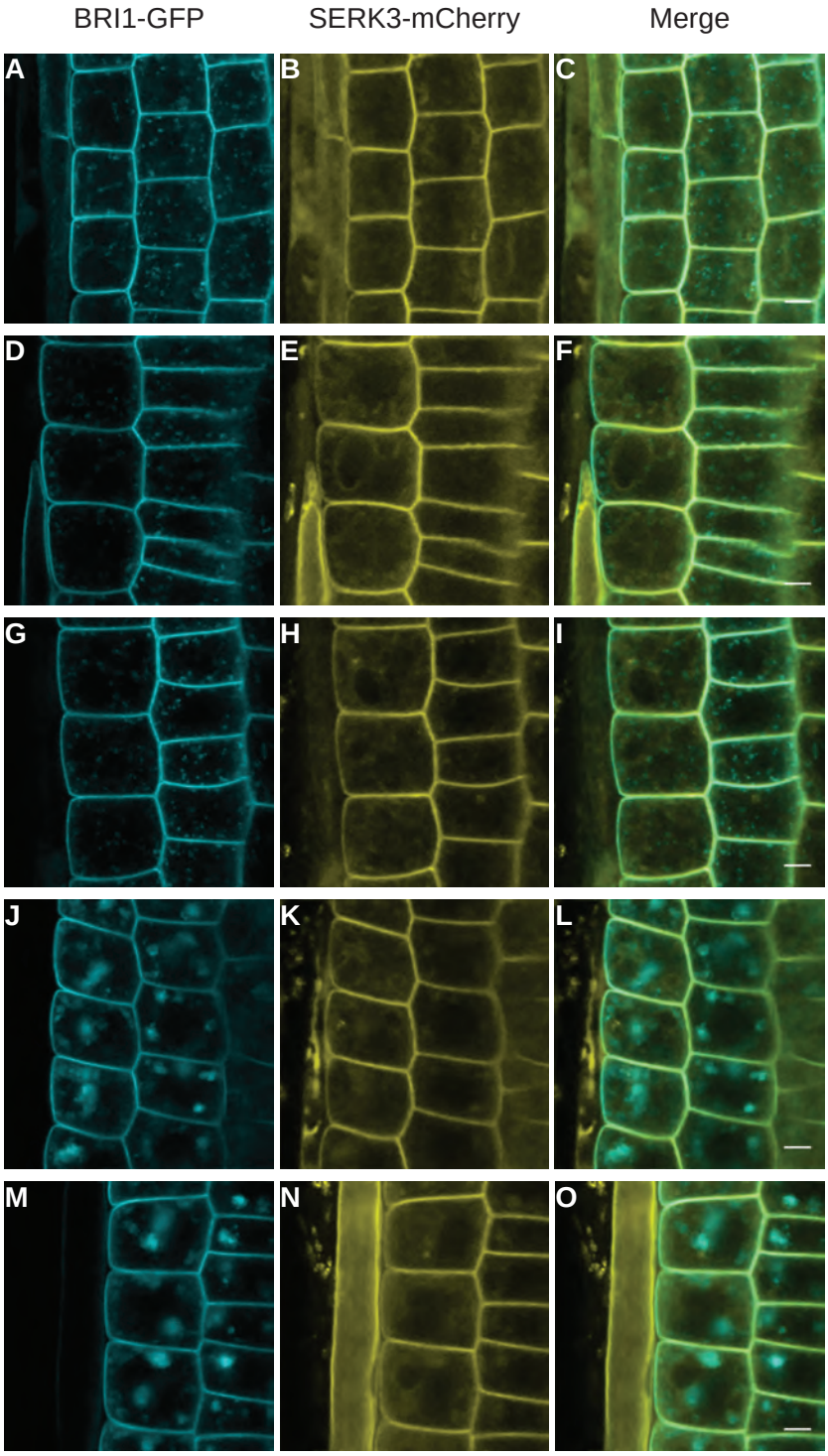
BRI1-GFP
SERK3-mCherry
Merge
A
B
C
D
E
F
G
H
I
J
K
L
M
N
O

Figure 3: Colocalization of BRI1 and SERK3 in different compartments of live Arabidopsis **root meristem epidermal cells.**
(**A-C**) Localization of BRI1-GFP (**A**) and SERK3-mCherry (**B**) as well as the merged image (**C**) of both fluorescently tagged proteins in untreated roots.
(**D-F**) Localization of BRI1-GFP (**D**) and SERK3-mCherry (**E**) as well as the merged image (**F**) after BRZ treatment.
(**G-I**) Localization of BRI1-GFP (**G**) and SERK3-mCherry (**H**) as well as the merged image (**I**) after BRZ treatment and BL application (1 µM, 1 h).
(**J-L**) Localization of BRI1-GFP (**J**) and SERK3-mCherry (**K**) as well as the merged image (**L**) after BRZ treatment and BFA application (50 µM, 1 h).
(**M-O**) Localization of BRI1-GFP (**M**) and SERK3-mCherry (**N**) as well as the merged image (**O**) after BRZ treatment and simultaneous BFA/BL application (50 µM and 1 µM, respectively, 1 h).
Confocal images of BRI1-GFP and SERK3-mCherry in live roots of 5 day old Arabidopsis seedlings coexpressing BRI1-GFP 2/SERK3-mCherry. Except for (**A-C**), all seedlings were cultured for 2 days in medium containing 5 µM BRZ. The BRI1-GFP 2/SERK3-mCherry line used here is homozygous for both tagged receptors (numerical analysis in Supplemental note S2).
24-epi-brassinolide (BL) was used throughout the experiments. Scale bars correspond to a size of 5 µm.

by the Manders' colocalization coefficients summarized in Table 2. In the presence of endogenous BRs, about 73% of BRI1-GFP and 75% of SERK3-mCherry receptors colocalized at the PM, whereas the intracellular colocalization comprised around 35% or 55% of BRI1-GFP and SERK3-mCherry molecules, respectively. Depletion of endogenous BRs using BRZ had no observable effect on the localization and hardly affected the colocalization of both receptors (Figures 3D-F and Table 2). Only the intracellular colocalization of BRI1-GFP with SERK3-mCherry slightly increased. Activation of BR signaling by incubating BRZ-treated seedlings in 1 µM BL prior to imaging resulted in significantly increased colocalization of the two LRR-RLKs both at the PM and intracellular (Figure 3G-I and Table 2), similar to the findings presented in Table 1.

Increased PM colocalization was also observed in response to BFA, known to stabilize BRI1 at the PM (Irani et al., 2012). As shown in Table 2, Manders' colocalization coefficients for BRI1 and SERK3 were elevated to 89% and 86%, respectively, and also an increased Pearson correlation coefficient was obtained. In contrast, intracellular colocalization of SERK3 with BRI1 decreased (Table 2). Colocalization of both receptors in BFA compartments showed similar values as obtained for immuno-labeled roots and was significantly increased by simultaneous application of BFA and BL (Table 2). In comparison to BFA-treated samples, additional BL application did not change PM and intracellular colocalization of BRI1 and SERK3.

To summarize, quantitative microscopic analysis in live cells confirmed that a large population of BRI1 and SERK3 receptors colocalizes independently of BR signaling activity. A smaller yet distinct minority of both receptors is affected by the BR signaling status indicated by increased colocalization upon BL and BFA application.

Table 2: Quantification of BRI1-SERK3 colocalization obtained by live root imaging. Comparative colocalization analysis in live roots of 5 day old Arabidopsis seedlings coexpressing BRI1-GFP 2 and SERK3-mCherry. BRZ (5 μM) was added to the growth medium 3 days after germination. For ligand-stimulation 1 μM 24-epi-brassinolide (BL) was applied for 1 h. Colocalizing fractions of BRI1-GFP and SERK3-mCherry are presented as modified Manders' colocalization coefficients ± S.E.M. Additionally, Pearson correlation coefficients ± S.E.M. are given. "N" represents the number of ROIs analyzed. For plasma membrane analysis one ROI included at least three plasma membrane sections.

	Plasma membrane			
	BRI1-GFP	SERK3-mCherry	r(Pearson)	N
untreated	0.73 ± 0.01	0.75 ± 0.01	0.24 ± 0.02	28
BRZ	0.74 ± 0.01	0.77 ± 0.01	0.22 ± 0.02	41
BRZ+BL	0.77 ± 0.0[a,b]	0.81 ± 0.0[a,b]	0.31 ± 0.01[a,b]	47
BRZ+BFA	0.89 ± 0.01[a,b]	0.86 ± 0.01[a,b]	0.48 ± 0.03[a,b]	36
BRZ+BFA/BL	0.90 ± 0.06[a,b]	0.86 ± 0.01[a,b]	0.59 ± 0.01[a,b]	38

	Intracellular			
	BRI1-GFP	SERK3-mCherry	r(Pearson)	N
untreated	0.35 ± 0.02	0.55 ± 0.02	-0.26 ± 0.01	184
BRZ	0.41 ± 0.02[a]	0.57 ± 0.02	-0.21 ± 0.01[a]	215
BRZ+BL	0.46 ± 0.02[a,b]	0.58 ± 0.02	-0.16 ± 0.02[a,b]	202
BRZ+BFA	0.39 ± 0.02	0.42 ± 0.02[a,b]	-0.13 ± 0.01[a,b]	112
BRZ+BFA/BL	0.39 ± 0.02	0.42 ± 0.02[a,b]	-0.09 ± 0.03[a,b]	102

	BFA compartment			
	BRI1-GFP	SERK3-mCherry	r(Pearson)	N
BRZ+BFA	0.60 ± 0.02	0.64 ± 0.01	-0.12 ± 0.02	112
BRZ+BFA/BL	0.78 ± 0.01[c]	0.71 ± 0.01[c]	0.08 ± 0.02[c]	107

[a] The mean difference is significant at the $p < 0.05$ level compared to untreated samples (two-tailed Student's t-test for equal variance).

[b] The mean difference is significant at the $p < 0.05$ level compared to BRZ treated samples (two-tailed Student's t-test for equal variance).

[c] The mean difference is significant at the $p < 0.05$ level compared to BRZ+BFA treated samples (two-tailed Student's t-test for equal variance).

BRI1 and SERK3 interact independently of ligand in root epidermal cells

To investigate whether and how BR signaling influences the hetero-oligomerization between BRI1 and SERK3, roots of the double transgenic BRI1-GFP 2/SERK3-mCherry line were examined using in planta FRET-FLIM (Figure 4). The images presented in Figure 4A-D were derived from seedlings heterozygous for BRI1-GFP to have a more physiological level of the tagged BRI1 receptor, while remaining homozygous for SERK3-mCherry. After BL stimulation of BRZ cultured seedlings the amount of BRI1-SERK3 hetero-oligomers found

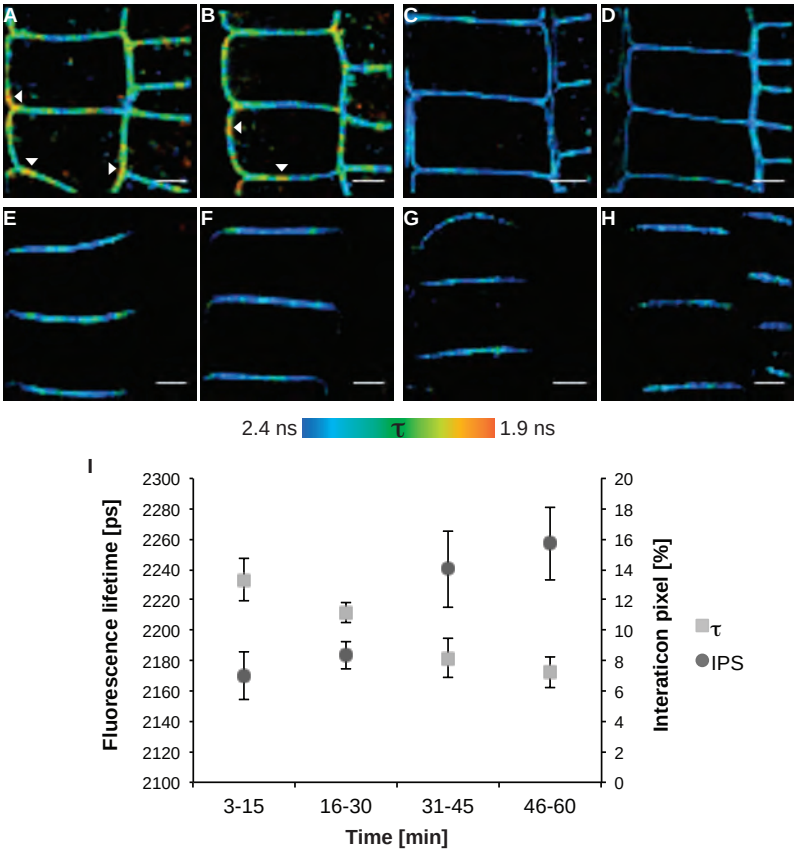

Figure 4: BRI1 and SERK3 interact independently of ligand.

(A) Fluorescence lifetime image of BRI1-GFP in the presence of SERK3-mCherry after BRZ treatment and BL stimulation (1 µM, 1 h).

(B) Fluorescence lifetime image of BRI1-GFP in the presence of SERK3-mCherry after BRZ treatment.

(C) Fluorescence lifetime image of BRI1-GFP after BRZ treatment and BL stimulation (1 µM, 1 h).

(D) Fluorescence lifetime image of BRI1-GFP after BRZ treatment.

(E) Fluorescence lifetime image of PIN2-GFP in the presence of SERK3-mCherry after BRZ treatment and BL stimulation (1 µM, 1 h).

(F) Fluorescence lifetime image of PIN2-GFP in the presence of SERK3-mCherry after BRZ treatment.

(G) Fluorescence lifetime image of PIN2-GFP after BRZ treatment and BL stimulation (1 µM, 1 h).

(H) Fluorescence lifetime image of PIN2-GFP after BRZ treatment.

(I) BRI1-GFP and SERK3-mCherry associate in a time-dependent manner after BL stimulation (1 µM). FRET-FLIM on roots of 5 day old Arabidopsis seedlings expressing BRI1-GFP 2 or coexpressing BRI1-GFP 2 and SERK3-mCherry, grown for 2 days in medium containing 5 µM BRZ. For time course measurements roots were embedded in BL containing medium and consecutive FLIM measurements were performed within a time frame of 1 h. PIN2-GFP in combination with SERK3-mCherry served as negative control. The BRI1-GFP 2/SERK3-mCherry line used in Figure 4 A-D and I is heterozygous for BRI1-GFP and homozygous for SERK3-mCherry proteins (numerical analysis in Supplemental note S2). 24-epi-brassinolide (BL) was used throughout the experiments. Color bar represents the false color-code for BRI1-GFP fluorescence lifetimes (τ). White arrowheads indicate areas with BRI1-GFP fluorescence lifetimes below 2 ns. Scale bars correspond to a size of 5 µm.

after coimmunoprecipitation is significantly increased (Wang et al., 2005; Wang et al., 2008) and amounts to about 5% of the total amount of BRI1 and about 10% of SERK3 receptors (Albrecht et al., 2012, Supplemental Note S2C). A fluorescence lifetime image of BRI1-GFP in the presence of SERK3-mCherry after BRZ and subsequent BL treatment is shown in Figure 4A. The color-code clearly indicates a non-uniform distribution of GFP fluorescence lifetimes. Remarkably, small and restricted areas in the PM with a strongly reduced donor fluorescence lifetime became visible (Figure 4A, white arrowheads). The observed strong heterogeneity in the distribution of interacting receptors indicates that a minority of PM-located BRI1-GFP and SERK3-mCherry receptors are in direct physical proximity. A numerical evaluation of the observed fluorescence lifetime values and interaction pixels (IPS) is presented in Table 3. Corrected IPS values represent the percentage of pixels with strongly reduced GFP fluorescence lifetimes and are taken as an estimate of the percentage of BRI1 interacting with SERK3. We estimate that about 10% of BRI1 can be seen as hetero-oligomers with SERK3 in the PM of BL stimulated epidermal root cells. This corresponds to an average of 263 BRI1-GFP receptors per confocal section (see Supplemental Note S2A and S2B for calculations). To determine whether depletion of endogenous BRs abolishes BRI1-SERK3 interactions, BRZ treated seedlings were imaged. The resulting fluorescence lifetime image is shown in Figure 4B. Unexpectedly, similar regions with a strong reduction in fluorescence lifetime were observed, suggesting that BRI1-SERK3 hetero-oligomers are preformed in the absence of ligand. Numerical analysis showed a reduction in corrected IPS of approximately one-third, suggesting that at strongly reduced ligand concentrations still about 6.7% of BRI1-GFP receptors or 176 per confocal section are in complex with SERK3. This is far more than the single BRI1-SERK3 hetero-oligomer that was expected based on possibly residual BL concentration after BRZ treatment (see Supplemental Note S2A). Consequently, the majority of BRI1-GFP/SERK3-mCherry hetero-oligomers observed in the BRZ treated roots is formed in the absence of ligand. Control experiments using BRI1-GFP donor fluorescence lifetime only (Figure 4C and 4D) revealed small local variations in lifetime of the fluorophore (Table 3). To provide an independent estimate of the amount of BRI1-SERK3 hetero-oligomers the more potent BR biosynthesis inhibitor propiconazole (PPC) (Hartwig et al., 2012) was employed. The results show that at a much lower concentration of PPC compared to BRZ seedling growth is more strongly affected (Figure S5). However, the amount of physically interacting BRI1-SERK3 hetero-oligomers remains the same (Table 3). To provide an independent biological control, PIN2-GFP (Abas et al., 2006) was employed alone or in combination with SERK3-mCherry using seedlings cultured in BRZ or treated with BRZ and BL (Figure 4E-H). In none of these images regions in the PM showing a strong reduction in fluorescence lifetime were observed. The IPS values obtained for the PIN2-GFP/SERK3-mCherry combination were used to calculate the corrected IPS values for the hetero-oligomerization of BRI1 and SERK3. To validate our observation that in planta FRET-FLIM faithfully reports the number of interacting receptors, a number of

Table 3: Numerical analysis of in planta **FRET-FLIM.**
Quantitative analysis of FLIM measurements performed in planta on roots of 5 day old BRI1-GFP 2 and BRI1-GFP 2/SERK3-mCherry expressing seedlings using PIN2-GFP in combination with SERK3-mCherry as negative control. Endogenous BRs were depleted either by PPC (100 nM) or BRZ treatment (5 µM). 24-epi-brassinolide (BL) was used throughout the experiments (1 µM, 1 h). The τ values given represent mean donor fluorescence lifetimes of the GFP moiety of BRI1-GFP or PIN2-GFP, respectively, in ps ± S.E.M. The values given for interaction pixels (IPS) represent the mean percentage of pixels with strongly reduced BRI-GFP fluorescence lifetimes ± S.E.M. The corrected IPS values were obtained by subtracting the IPS values of the negative control from the IPS values determined for BRZ+BL treated BRI1-GFP 2+SERK3-mCherry. "N" represents the number of analyzed fluorescence lifetime images.

	PPC				PPC+BL			
	τ [ps]	FRET [%]	IPS [%]	N	τ [ps]	FRET [%]	IPS [%]	N
BRI1-GFP	2422 ± 4			33	2385 ± 4			32
BRI1-GFP+SERK3-mCherry	2302 ± 6[a]	5.0 ± 0.3	7.4 ± 0.7	24	2238 ± 11[a]	6.1 ± 0.4[c]	15 ± 2[c]	25
	BRZ				BRZ+BL			
BRI1-GFP	2398 ± 4			69	2379 ± 4			72
BRI1-GFP+SERK3-mCherry	2272 ± 6[a]	5.2 ± 0.3[b]	7.6 ± 0.6[b]	57	2226 ± 6[a]	6.4 ± 0.2[b,c]	13 ± 1[b,c]	64
PIN2-GFP	2271 ± 20			24	2321 ± 54			20
PIN2-GFP+SERK3-mCherry	2253 ± 9[a]	0.8 ± 0.5	0.9 ± 0.2	22	2262 ± 45[a]	2.5 ± 0.3	2.5 ± 0.3	19
	corrected IPS [%]							
BRI1-GFP+SERK3-mCherry	6.7				10.5			

[a] The mean difference is significant at the $p < 0.05$ level compared to donor only (BRI1-GFP or PIN2-GFP) samples (two-tailed Student's t-test for unequal variance).
[b] The mean difference is significant at the $p < 0.05$ level compared to PIN2-GFP+SERK3-mCherry samples (two-tailed Student's t-test for equal variance).
[c] The mean difference is significant at the $p < 0.05$ level compared to PPC- or BRZ-treated BRI1-GFP+SERK3-mCherry samples (two-tailed Student's t-test for equal variance).

additional control experiments were performed. The first was to use BFA treated roots where inside the large BFA compartments a similar reduction in fluorescence lifetimes was observed as obtained for the immuno-labeling approach (Figure S6). In comparison with wild type SERK3, the SERK3 mutant elongated (elg; Halliday et al., 1996) showed an increased association with BRI1 (Jaillais et al. 2011a). Indeed, a slight increase in association between BRI1-sCFP and ELG-sYFP was observed using FLIM in a transient expression system (Figure S7 and Table S1).

Finally, the time-course of BRI1-SERK3 hetero-oligomerization was determined. Treatment of BRZ cultured double transgenic roots with exogenous BL led to a time-dependent rise of BRI1-SERK3 hetero-oligomers from an uncorrected IPS of about 7% to 16% after 1 h (Figure 4I). Surprisingly, a significant increase was only detected after a lag period (see

also Table S2), indicating that the amount of BRI1-SERK3 hetero-oligomers is almost stable during the first half hour of signaling.

In summary, we conclude that a significant subpopulation of BRI1 and SERK3 form heterogeneously distributed BR signaling units within the PM. We propose that these units carry out the initial signaling activity, later followed by an increase in BRI1-SERK3 hetero-oligomers employing a maximum of 10% of BRI1 present in root epidermal cells.

DISCUSSION

In this work we have for the first time visualized BRI1-SERK3 hetero-oligomers in PMs of live Arabidopsis root epidermal cells. Based on the FRET-FLIM results, the amount of receptor hetero-oligomers in the PM after application of exogenous ligand was estimated to include approximately 10% of the total amount of the BRI1 receptors. The observation that only small populations of BRI1 and SERK3 form hetero-oligomers is in line with those obtained by semi-quantitative coimmunoprecipitation experiments (Albrecht et al., 2012). In that work, the amount of SERK3 coprecipitating with BRI1 after activation of BR signaling in entire seedlings was estimated to be about 5%. Using mathematical modeling, we recently showed that at endogenous ligand concentration about 1% of active BRI1 is required with about 5% being sufficient for full inhibition of root growth (van Esse et al., 2012). We conclude that our microscopic approach to detect physical interaction between PM-localized receptors by FRET-FLIM is a novel read-out for visualizing signaling processes and is in agreement with other semi-quantitative approaches.

Nonetheless, a significant difference between FRET-FLIM and coimmunoprecipitation read-outs with respect to the BL-induced association of BRI1 and SERK3 was noted. Our FLIM analysis only revealed an approximately 50% increase of receptor hetero-oligomers, whereas coimmunoprecipitation usually results in a several fold increase upon ligand application (Wang et al., 2005; Wang et al., 2008; Albrecht et al., 2012). To explain this discrepancy, different aspects of the two methods need to be considered. FRET, observed by FLIM, is an orientation- and distance-dependent process. Energy transfer from donor to acceptor molecules requires a favorable angle between the transition dipole moments of GFP and mCherry and the distance between the interacting fluorophores is restricted to around 10 nm. This constraint implies a true physical interaction between the complex partners to be detected by FLIM. However, it also limits the position in which the fluorophores can be attached to the proteins under investigation while not affecting their functionality. The C-terminal fusions employed here are both functional. Attempts to locate the fluorophores elsewhere in the SERK protein or attach them to truncated receptors invariably led to unstable or non-fluorescent versions. In contrast to fluorescence microscopy, coimmunoprecipitation can also reveal indirect interactions mediated by additional complex constituents

such as ligands or other proteins. However, this approach requires the isolation of proteins from their natural habitat and therefore a stable interaction between complex partners to withstand the obligate membrane extraction procedures. This pitfall of coimmunoprecipitation was also noted during investigations of animal receptor signaling systems and as a consequence, receptor recruitment models as originally proposed for several signaling pathways often resulted in revised models including preformed receptor oligomers after application of imaging techniques (Springael et al., 2005; Wang and Norcross, 2008).

Previously, it was shown that BRI1 does not exhibit ligand-mediated endocytosis but maintains its distribution between the PM and intracellular compartments (Geldner et al., 2007). Our work is in agreement with that observation, but in addition we demonstrate that hetero-oligomerization of BRI1 and SERK3 is increased after ligand application. Furthermore, colocalization between BRI1 and SERK3 at the PM increased after BFA application and high colocalization values for BFA compartments were obtained. Because the PM is the major site of BRI1 signaling activity (Irani et al., 2012), collectively this offers an alternative explanation for the observed increase in BR signaling activity in presence of BFA, previously attributed to endosomal compartments mainly (Geldner et al., 2007).

Our results suggest that preformed BRI1-SERK3 hetero-oligomers are an essential element of BR-triggered BRI1-mediated signal transduction since even in root cells depleted of ligand using two different BR biosynthesis inhibitors, a significant amount of receptor complexes remained present in the PM. An alternative method, to employ BR biosynthesis mutants was considered but not deemed practical due to the severe reproductive and developmental defects such lines exhibit (Clouse and Sasse, 1998). The concept of receptor preassociation is in line with animal signaling systems. Preformed receptor complexes have been identified and proposed to increase affinity for the ligand, exhibit increased half-life of the complex, accelerate signal transduction and promote lateral signal propagation (Martin-Fernandez et al., 2002; Yu et al., 2002; Bader et al., 2009). Our observation that only a subset of BRI1-SERK3 hetero-oligomers is present after ligand depletion is comparable to findings for EGFR in mammalian cells as demonstrated by Bader et al. (2009). Notably, for bone morphogenic protein (BMP) receptors differential signaling responses (Nohe et al., 2002) and endocytic routes (Hartung et al., 2006) for preformed and ligand-induced receptor complexes were observed. This led to the hypothesis that low ligand concentrations predominantly activate signaling from preassembled receptor complexes, while increased ligand availability shifts the equilibrium towards signaling from complexes induced by ligand-dependent recruitment (Ehrlich et al., 2011). This hypothesis is intriguing with respect to our time-course measurements. Our data indicate that approximately the same total number of BRI1-GFP receptors is associated with SERK3 coreceptors within the first 30 mins after exogenous BL application. We conclude that the phosphorylation of SERK3 within 2 mins in response to BL (Schulze et al., 2010) can only be attributed to preformed BRI1-SERK3 hetero-oligomers.

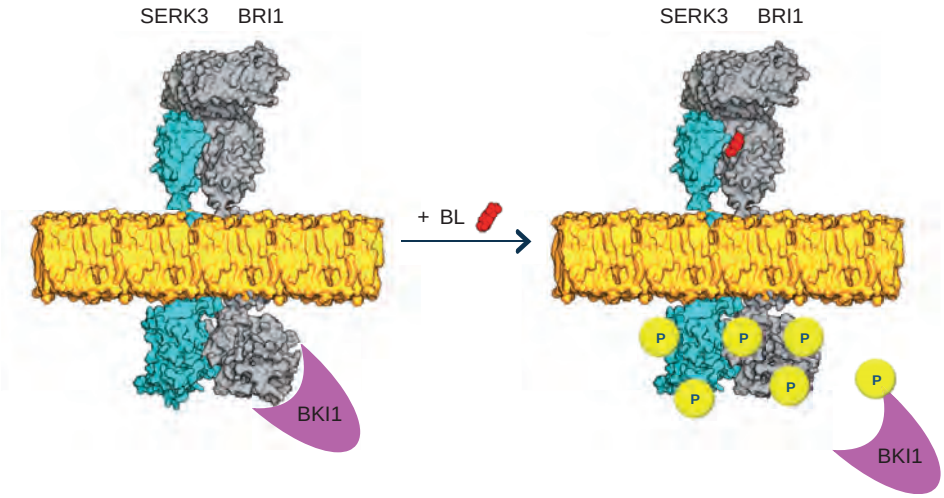

Figure 5: Model for BR signaling with preformed BRI1-SERK3 hetero-oligomers as functional units.
In the absence of ligand BRI1 and SERK3 reside in the plasma membrane of Arabidopsis meristematic epidermal root cells partially as hetero-oligomers. The kinase activity of BRI1 is inhibited by BKI1. Upon ligand-binding the BRI1 kinase is activated. This results in transphosphyorlation and release of BKI1 and transphosphorylation events within the preformed BRI1-SERK3 hetero-oligomers, enabling downstream signaling. Next to preformed hetero-oligomers, formation of new BRI1-SERK3 complexes is possible. In this illustration, the actual protein dimensions of BRI1 and SERK3 are taken into account. The extracellular domain of SERK3 was modeled using the crystal structure of the ligand-binding domain of BRI1 (PDB: 3rgz) as template, and the kinase domains of SERK3 and BRI1 were modeled using the crystal structure of Pto (PDB: 2qkw) as template (Modeller, version 9.10). The molecular surface representation of both molecules was generated using PyMOL (version 1.4).

Based on our study we propose to modify the present model of BRI1-SERK3 activation (Wang et al., 2008; Chinchilla et al., 2009; Kim and Wang, 2010) to include the presence of both receptors in a ligand-independent fashion as a functional unit that perceives BRs and initiates downstream signaling (Figure 5). Additionally, the results from this study and others (Albrecht et al., 2012) suggest that only a very limited number of BRI1 and BAK1(SERK3) receptors is required to serve the BL pathway. Upon binding of BL to BRI1 a structural change in the ligand-binding domain of BRI1 occurs (Hothorn et al., 2011; She et al., 2011). Since no further changes in the extracellular domain of BRI1 were noted after BL binding, possible rotational changes between BRI1 and SERK extracellular domains may reorient the kinase domains to trigger auto- and transphosphorylation events. Recent work on the transmission of conformational changes between two dimeric EGFR extracellular domains additionally points out that one single pass transmembrane helix alone cannot propagate sufficient structural change to initiate kinase activity (Abulrob et al., 2010). Hothorn et al. (2011) propose that the BRI1-ligand surface provides a platform for protein interaction, in line with this concept. After ligand binding, BRI1 is internalized in presumably an active form (Geldner et al., 2007) and was found in the TGN/EE and in MVBs (Viotti

et al., 2010; Irani et al., 2012), including the SERK coreceptor (this work), on their way to vacuolar degradation. Previously, we found BR-independent interaction between BRI1 and SERK3 in a heterologous cell system (Russinova et al., 2004), while coimmunoprecipitation of BRI1 and SERK3, even after prolonged BRZ treatment, was noted but not further investigated (Wang et al., 2005).

There appears to be a clear difference between the association of SERK3 with the BRI1 receptor, an RD kinase, and the immune receptors Flagellin Sensing 2 (FLS2) and EF-TU Receptor (EFR), which are both non-RD kinases (Gómez-Gómez and Boller, 2000; Zipfel et al., 2006). In contrast to the rapid association of SERK3 and FLS2 after flg22 stimulation in Arabidopsis cell culture (Schulze et al., 2010), our FRET-FLIM results show much slower kinetics for the physical interaction of BRI1 and SERK3. However, the assays differ largely and the kinetics observed here are comparable to the findings of Albrecht et al. (2012) using Arabidopsis seedlings and coimmunoprecipitation to identify time dependent BRI1-SERK3 association after BL application. Additionally, the association of SERK3 with FLS2 is strictly ligand-dependent and even cross-linking experiments do not allow extraction of ligand-independent receptor hetero-oligomers (Schulze et al., 2010). Similar observations account for EFR-SERK3 interactions (Roux et al., 2011). Whether the observed difference between FLS2-SERK3 and BRI1-SERK3 complexes can be generalized for immune and hormonal signaling or RD- and non-RD kinase activation in plants remains to be determined. However, mechanistic parallels exist in animal cell signaling employing EGFR and Toll-like receptor 4 (TLR4). The latter is a receptor involved in innate immune responses upon lipopolysaccharide (LPS) perception. EGFR constitutive dimer formation in absence of ligand was demonstrated in NIH 3T3 cells using anisotropy measurements, whereas dimerization of TLR4 is triggered upon LPS-binding (Saitoh et al., 2004; Bader et al., 2009).

In conclusion, based on the well-characterized receptor pair BRI1 and BAK1(SERK3) we have demonstrated the added value of low invasive and spatially resolved quantitative imaging methods to gain better insight into plant signaling mechanisms.

MATERIAL AND METHODS

Growth conditions

Arabidopsis (*Arabidopsis thaliana*) plants (ecotype Columbia [Col-0]) were used as wild type. Seeds were surface sterilized and germinated on ½ Murashige and Skoog medium (Duchefa) supplemented with 1% sucrose (Sigma) and 0.8% Daishin agar (Duchefa). Plants were grown at 22 °C under fluorescent light, with 16 h light/8 h dark photoperiods, unless otherwise specified. Transgenic seedlings were selected on ½ Murashige and Skoog medium containing either 50 mg/L kanamycin (KAN, Duchefa), 15 mg/L phosphinothricin (PPT, Duchefa), or 40 mg/L hygromycin (Sigma). Col-0 plants expressing BRI1 (AT4G39400)

fused to GFP under its native promoter, here referred to as BRI1-GFP 1, were provided by N. Geldner (Geldner et al., 2007). The BRI1-GFP line overexpressing the transgene about three-fold, here referred to as BRI1-GFP 2, was provided by J. Chory (Friedrichsen et al., 2000). Genotyping was performed by PCR using primer combinations (AGCACG-CAAAACTGCGGATTAGCGA)/BRI1-kdF and (TTTGATGCCGTTCTTTTGCTTGTC)/M5GFP-R (Geldner et al., 2007). The PIN2::PIN2-GFP (Abas et al., 2006) expressing line was provided by C. Schwechheimer and genotyping was performed by PCR using primer combinations (TGTATCCACCGACCCTAAAGTTTC)/PIN2-forward and (TTTGATGCCGTTCTTTTGCTTGTC)/M5GFP-R.

Plants that were subjected to fixation and immuno-labeling were grown on ½ Murashige and Skoog medium supplemented with 1% sucrose and 0.8% Daishin agar. After 3 days seedlings were transferred to 24-well plates (Greiner Bio One) into 1 mL ½ Murashige and Skoog medium supplemented with 1% sucrose containing 5 µM brassinazole (TCI Europe) or medium containing the same volume of 80% ethanol, which was used to dissolve brassinazole, and grown for 2 additional days.

Plant materials and Arabidopsis transformation

The entire open reading frames of SERK3 cDNA was amplified by RT-PCR from Arabidopsis Col-0. The forward and reverse primers were engineered with an NcoI site to replace the SERK3 stop codon and allow an in frame fusion with HA. The primers used were S3-NcoF CCATGGAACGAAGATTAATGATCCCTTGC and S3-NcoR CCATGGATCTTGGACCC-GAGGGGTATTCG.

To prepare the SERK3 promoter constructs, a 2kb region upstream of the start codons of the SERK3 gene was amplified from Col-0 genomic DNA and cloned in the pGEM-T vector (Promega, Madison, WI, USA). The primers used were P3F GTCGTCATATTGAGAAGTCG and P3-NcoR CCATGGTTTATCCTCAAGAGATTAAAAACAAACCC. The pGEM-T cloned promoters were inserted via SalI-NcoI in a modified pBluescript vector containing the HA gene inserted as NcoI-BamH1 fragment in front of the tNOS terminator. The entire open reading frame of SERK3 as described above was then inserted as NcoI fragment. The resulting full cassette was subsequently sub-cloned into the 1390 pCambia (Cambia) vector via SalI-SmaI.

This construct was verified by sequencing and was electroporated in Agrobacterium tumefaciens strain C58C1 containing a disarmed C58 Ti plasmid (Koncz et al., 1989). The construct was transformed into the BRI1-GFP 1 background by the floral dipping method (Clough and Bent, 1998). The transgenic lines were selected on hygromycin and genotyping for SERK3-HA was performed by PCR reactions using primer combinations SERK3-forward (AGCTGATGGTACTTTAGTGG) and tNOS (AAGACCGGCAACAGGATTC).

For generating the translational fusion of SERK3 and mCherry the SERK3 genomic DNA fragment was amplified by RT PCR from BAC clone F17M5, after which the fragment was

cloned into a pENTR-D-topo vector (Invitrogen). To ensure a fusion with the mCherry tag, the reversed primer did not contain the stop codon at the end of the SERK3 sequence. The 2 kb SERK3 promoter fragment was PCR amplified from BAC clone F17M5 and transferred to a pGEM-T easy vector. The cloned promoter fragment was inserted via XhoI-SACII into a modified gateway vector containing a pENTR p4p1 site. The pENTR-D-TOPO vector, containing the SERK3 promoter construct, the pENTRp4p1 vector containing SERK3 and the pENTRp2p3 vector containing the mCherry coding sequence were cloned into the destination vector containing a pENTRp4p1 site, using a multisite gateway reaction (Invitrogen). The entry clones and the destination vector were kindly provided by Dr. R. Geurts from the department of Molecular Biology, Wageningen UR. The destination vector contains PPT resistance for in planta selection.

The pSERK3::SERK3-mCherry construct was electroporated in Agrobacterium tumefaciens strain C58C1 containing a disarmed C58 Ti plasmid (Koncz et al., 1989). The construct was transformed into Col wild type background by the floral dipping method (Clough and Bent, 1998). Homozygous plants for SERK3-mCherry were crossed into the BRI1-GFP 2 background (Friedrichsen et al., 2000). The transgenic lines were selected on PPT and KAN and genotyping for SERK3-mCherry was performed by PCR reactions using primer combinations SERK3-forward (AGCTGATGGTACTTTAGTGG) and mCherry-reverse (CTTGTACAGCTCGTCCATG). To generate the heterozygous BRI1-GFP 2 and homozygous SERK3-mCherry expressing plants SERK3-mCherry was crossed with BRI1-GFP 2. Plants were selected on KAN and PPT and genotyping was performed by PCR using the primer combinations described above. Double transgenic PIN2-GFP/SERK3-mCherry plants were obtained by crossing homozygous PIN2-GFP (Abas et al., 2006) and SERK3-mCherry plants. Plants were selected on KAN and PPT and the presence of the transgenes was confirmed by PCR using the primer combinations described above. The double transgenic SERK3-mCherry/WAVE11-Cerulean line was generated by crossing and seedlings of the F1 generation were used for imaging.

Protein extraction and immunoprecipitation

For immunoprecipitation of BES1-GFP seedlings were grown vertically on MS medium containing 1.2% agar. BRZ was added to the growth medium 6 days after germination in a final concentration of 5 µM. For BL stimulation, 1 µM of BL was added to 7 day old seedlings 1 h before extraction. Seedlings were ground in liquid nitrogen. Proteins were extracted by adding 1 ml extraction buffer containing 50 mM Tris-HCl pH 7.5, 150 mM NaCl, 1% Triton X100, 1% protease inhibitor cocktail (Roche) per gram grounded roots. Samples were centrifuged 10 min at 4 °C and 13,000 rpm. The supernatants were adjusted to equal amounts of total protein and incubated 4 h at 4 °C with 10 μL GFP-Trap coupled to agarose beads (Miltenyi Biotec). After incubation, the beads were washed three times with the extraction buffer after which the samples were boiled for 5 min in SDS loading

buffer. Proteins were separated with a 10% SDS-polyacrylamide gel and transferred to a PVDF membrane (Millipore) by wet electro blotting (Mini-Protean II system; Bio-Rad). The BES1-GFP was probed using anti-GFP-HRP antibody (Miltenyi Biotec). The HRP was detected with the ECL plus detection kit (GeHealthcare).

Fixation and Immuno-cytochemical labeling

For the immuno-labeling experiments 5 day old seedlings were used. Treatments and fixation were performed in 24-well plates used for cultivation. Prior to treatments, seedlings were washed once with 1 mL ½ Murashige and Skoog medium (Duchefa) supplemented with 1% sucrose (Sigma). For stimulation experiments seedlings were incubated for 1 h in 1 mL ½ Murashige and Skoog medium supplemented with 1% sucrose containing 50 µM cycloheximide (Sigma) and the respective agents. Final concentrations used were 1 µM 24-epi-brassinolide and 50 µM brefeldin A (Sigma). The stock solutions were 4 mM brassinolide dissolved in 80% ethanol and 50 mM brefeldin A dissolved in dimethylsulfoxide (DMSO, Merck). After treatment, seedlings were washed once with PBS buffer pH 6.9. Subsequently, seedlings were fixed, placed on SuperFrost object slides (Menzel-Gläser) and immuno-labeled (Sauer et al., 2006). Antibodies used were rabbit-anti-GFP (generated by Eurogentec), mouse-anti-HA, goat-anti-rabbit-Alexa488 and goat-anti-mouse-Alexa568 (all Invitrogen).

Inhibitor treatments

Seedlings were incubated in 1 mL ½ Murashige and Skoog medium supplemented with 1% sucrose containing 1 µM 24-epi-brassinolide (BL, Sigma), 50 µM brefeldin A (BFA, Sigma), 5 µM brassinazole (BRZ, TCI Europe), and 100 nM propiconazole (PPC, Fluka). The seedlings were incubated with inhibitors under regular growth conditions as described above. The stock solutions used were 4 mM BL in 80% ethanol, 50 mM BFA in DMSO, 23 mM BRZ in 80% ethanol, and 1 mM PPC in DMSO.

Confocal Laser Scanning Microscopy

Optical sections of immuno-stained roots were acquired using a confocal laser scanning microscope (LSM510 Carl Zeiss, Jena, Germany). Alexa488 was excited using an argon laser (488 nm) and fluorescence was detected via a band-pass filter 505-530 nm. For double stained samples, excitation light of 488 nm was used for goat-anti-rabbit-Alexa488 and a He/Ne diode laser (543 nm) was used for goat-anti-mouse-Alexa568 and fluorescence was detected using band-pass-filters of 505-530 nm and 550-615 nm, respectively. A 40x water immersion objective with a numeric aperture of 1.2 was used for imaging. The pinhole setting was 1 Airy unit, which yielded a theoretical thickness (full width at half- maximum) of 1 µm. Images and data captures were analyzed with Zeiss LSM510 software (version 4.2).

Live root imaging was performed on a confocal laser scanning microscope (Leica TCS SP5 X system, Mannheim, Germany). GFP was excited using an argon laser (488 nm) and fluorescence emission was detected from 500-540 nm. mCherry was excited using a white light continuum laser selecting the 580 nm laser line. Fluorescence was detected from 590-640 nm. Images were captured using a 63x water immersion objective with a numeric aperture of 1.2 with a pinhole set to 1 Airy unit. Confocal images were analyzed with FIJI software (ImageJA 1.45j, Max Planck Society).

Colocalization analysis

Colocalization analysis of images acquired by confocal laser scanning microscopy was performed using the software FIJI (ImageJA 1.45j, Max Planck Society). The plugin "Coloc 2" allows the quantitative determination of colocalizing fluorescence intensities acquired in different channels using the methods of Manders and Costes (Manders et al., 1993; Costes et al., 2004). The obtained modified Manders coefficients were used as fraction of colocalization for both channels, i.e. colocalization of BRI1-GFP with SERK3-HA or SERK3-mCherry and vice versa. Next to modified Manders coefficients, Pearson correlation coefficients were obtained as a second measure for colocalization.

FRET-FLIM

FRET is a photo physical process in which the excited-state energy from a fluorescent donor molecule is transferred non-radiatively to an acceptor molecule. FRET is based on weak dipole–dipole coupling and therefore can only occur at molecular distances. There are several methods to quantify and visualize FRET, of which donor fluorescence lifetime imaging is the most straightforward, since a fluorescence lifetime is concentration-independent property. However, fluorescence lifetimes are sensitive to the environment, which is the basis for FRET-FLIM. FRET-FLIM experiments consist of measuring donor fluorescence lifetimes (here Alexa488) in the absence (τ_D) and presence (τ_{DA}) of acceptor molecules (here Alexa568) resulting in spatially resolved color-coded lifetime images. Observation of a decreased donor fluorescence lifetime is used as read-out for molecular interactions (Borst and Visser, 2010).

A Leica TCS SP5 X system equipped with a 63x/1.20 NA water-immersion objective lens was used for confocal/FLIM imaging. Confocal and FLIM images were acquired by exciting the respective fluorophores GFP/mCherry or Alexa488/568 using a white-light laser (WLL; or super continuum laser). This laser emits a continuous spectrum from 470 to 670 nm, within which any individual excitation wavelength in 1 nm increments can be selected. For excitation of sCFP3A and sYFP2 (Kremers et al., 2006), a diode laser (440 nm) or the 514 nm line of an Argon laser was used, respectively. Confocal imaging was performed using internal filter-free spectral photomultiplier tube (PMT) detectors. For GFP/Alexa488 detection a spectral window of 500-550 nm was selected, whereas mCherry/Alexa568

was detected using 590-640 nm. Detection of sCFP3A and sYFP2 was accomplished using a spectral window of 450-500/520-560 nm. Confocal images were acquired with 512 x 512 pixels.

For FRET- FLIM experiments, a pulsed diode laser (440 nm) or WLL (470 nm) at a pulsed frequency of 40 MHz was used. For recording of donor fluorescence, an external fiber output was connected to the Leica SP5 X scan head and coupled to a Hamamatsu HPM-100-40 Hybrid detector (Becker & Hickl), which has a time resolution of 120 ps. Selection of sCFP3A and GFP/Alexa488 fluorescence was performed using band pass filters 470-500 and 505-545 nm, respectively. Images with a frame size of 64 x 64 pixels were acquired with acquisition times of up to 90 sec.

From the fluorescence intensity images the decay curves were calculated per pixel and fitted with either a mono- or double-exponential decay model using the SPCImage software (Becker & Hickl, version 3.2.3.0). The mono-exponential model function was applied for donor samples with only GFP/Alexa488 or sCFP3A present. For samples containing two fluorophores, Alexa488/Alexa568, GFP/mCherry or sCFP3A/sYFP2, respectively, a double-exponential model function was used without fixing any parameter.

To calculate the fraction of "interaction pixels", fluorescence intensity and the corresponding fluorescence lifetime data for each pixel were exported from SPCImage and imported into an Excel spreadsheet (Microsoft® Excel® for Mac 2011, version 14.1.3). Quantification of interacting pixels was set according to the following criteria. The photon counts per pixel must be at least 1,200 counts in total using a binning factor of 1, ensuring a statistically required peak value (± 200 counts) in the respective photon histogram used for fluorescence lifetime calculation. To ensure a reliable fit, only pixels with $\chi^2 < 2.5$ were selected. Additionally, fluorescence lifetimes below 1.6 ns and above 2.6 ns respectively were excluded from the calculation of interacting fractions. The reason for setting these values was to avoid false positive or negative interactions. The total amount of pixels for each fluorescence intensity image was set after applying these above-mentioned criteria resulting almost exclusively in pixels representing PM or adjacent areas. Subsequently, the average donor fluorescence lifetimes were determined. The individual minimum of a set of measurements was used to calculate the interaction threshold, which usually corresponded to a FRET-efficiency of about 13%. Only pixels with fluorescence lifetimes below the interaction threshold were collected as interaction pixels. The ratio between interaction pixels and total amount of selected pixels represented the value of interaction pixels (IPS).

Transient Arabidopsis protoplast transfection

Arabidopsis mesophyll protoplasts were isolated and transfected according as described previously (Bücherl et al., 2010). Only the isolation procedure was adapted according to Wu et al. (2009).

Site-directed mutagenesis

To obtain the Asn(122) to Asp substitution in the coding sequence of SERK3 for generating an ELG coding sequence site-directed mutagenesis using PCR with primer combination elg-forward (GAATTGGTGAGCTTGAATCTTTACTTGAAC) and elg-reverse (GTTCAAG-TAAAGATTCAAGCTCACCAATTC) was performed. Introduction of the base change was confirmed by sequencing.

Statistical Analysis

Statistical analysis was performed using the Excel® sofware (Microsoft® Excel® for Mac 2011, version 14.1.3).

Accession Numbers

Sequence data from this article can be found in the Arabidopsis Genome Initiative or EMBL/GenBank data libraries under accession numbers: BRI1 (AT4G39400), PIN2 (AT5G57090), SERK3/BAK1 (AT4G22430).

SUPPLEMENTAL MATERIAL

Supplemental Figures and Tables

Figure S1: Brassinazole abolishes BES1-GFP dephosphorylation.
Figure S2: SERK family members respond differently towards BFA.
Figure S3: Immuno-cytochemical FRET-FLIM discriminates interacting and non-interacting proteins in BFA compartments.
Figure S4: SERK3 localizes to the tonoplast.
Figure S5: Phenotypical comparison of PPC and BRZ treatments.
Figure S6: BRI1 and SERK3 interact in BFA compartments in planta.
Figure S7: ELG shows a stronger decrease in overall fluorescence lifetime with BRI1 than SERK3.
Table S1: Fluorescence lifetime analysis of the BRI1-sCFP interaction with SERK3-sYFP and ELG-sYFP.
Table S2: Fluorescence lifetime analysis of time-course FLIM.

Supplemental Notes

Note S1: Approximation of the number of BRI1-GFP and SERK3-mCherry molecules per pixel in a FLIM image.
Note S2: Approximation of BRI1-GFP ligand-occupancy after brassinazole treatment and exogenous BL application as well as the amount of BAK1 receptor pulled down by BRI1

Supplemental References

ACKNOWLEDGEMENTS

We thank C. Schwechheimer for providing the PIN2-GFP line, J. Chory for providing the BRI1-GFP 2 and N. Geldner for providing the BRI1-GFP 1 line. Furthermore, we thank D. Weijers and all the members of the S.dV. laboratory for fruitful discussion and comments on the manuscript. This research was funded by the Marie Curie training ITN network BRAssinosteroid Venture Increasing StudentS' International MObility (BRAVISSIMO) grant number 215118 (C.A.B.), the IPOP Systems Biology project of Wageningen UR (G.W.vE.), the Netherlands Organization for Research NWO (J.A.) and the Department of Agrotechnology and Food Sciences, Wageningen University (S.C.d.V., A.v.H., J.W.B., A.H.W. and C.A.).

REFERENCES

Abas L, Benjamins R, Malenica N, Paciorek T, Wiśniewska J, Wirniewska J, Moulinier-Anzola JC, Sieberer T, Friml J, Luschnig C (2006) Intracellular trafficking and proteolysis of the Arabidopsis auxin-efflux facilitator PIN2 are involved in root gravitropism. Nat. Cell Biol. **8**: 249–256.

Abulrob A, Lu Z, Baumann E, Vobornik D, Taylor R, Stanimirovic D, Johnston LJ (2010) Nanoscale imaging of epidermal growth factor receptor clustering: effects of inhibitors. J. Biol. Chem. **285**: 3145–3156.

Albrecht C, Boutrot F, Segonzac C, Schwessinger B, Gimenez-Ibanez S, Chinchilla D, Rathjen JP, de Vries SC, Zipfel C (2012) Brassinosteroids inhibit pathogen-associated molecular pattern-triggered immune signaling independent of the receptor kinase BAK1. Proc. Natl. Acad. Sci. U.S.A. **109**: 303–308.

Albrecht C, Russinova E, Kemmerling B, Kwaaitaal M, de Vries SC (2008) Arabidopsis SOMATIC EMBRYOGENESIS RECEPTOR KINASE proteins serve brassinosteroid-dependent and -independent signaling pathways. Plant Physiol. **148**: 611–619.

Asami T, Mizutani M, Fujioka S, Goda H, Min YK, Shimada Y, Nakano T, Takatsuto S, Matsuyama T, Nagata N, et al (2001) Selective interaction of triazole derivatives with DWF4, a cytochrome P450 monooxygenase of the brassinosteroid biosynthetic pathway, correlates with brassinosteroid deficiency in planta. J. Biol. Chem. **276**: 25687–25691.

Bader AN, Hofman EG, Voortman J, en Henegouwen PMPVB, Gerritsen HC (2009) Homo-FRET imaging enables quantification of protein cluster sizes with subcellular resolution. Biophys. J. **97**: 2613–2622.

Borst JW, Visser AJWG (2010) Fluorescence lifetime imaging microscopy in life sciences. Meas. Sci. Technol. **21**: 102002.

Boyd G (2002) Assembly and Cell Surface Expression of Homomeric and Heteromeric 5-HT3 Receptors: The Role of Oligomerization and Chaperone Proteins. Mol. Cell. Neurosci. **21**: 38–50.

Bücherl C, Aker J, de Vries S, Borst JW (2010) Probing protein-protein Interactions with FRET-FLIM. Methods Mol. Biol. **655**: 389–399.

Chinchilla D, Shan L, He P, de Vries S, Kemmerling B (2009) One for all: the receptor-associated kinase BAK1. Trends Plant Sci. **14**: 535–541.

Clough SJ, Bent AF (1998) Floral dip: a simplified method for Agrobacterium-mediated transformation of Arabidopsis thaliana. Plant J. **16**: 735–743.

Clouse SD (2011) Brassinosteroid signal transduction: from receptor kinase activation to transcriptional networks regulating plant development. Plant Cell **23**: 1219–1230.

Clouse SD, Sasse JM (1998) BRASSINOSTEROIDS: Essential Regulators of Plant Growth and Development. Annu. Rev. Plant Physiol. Plant Mol. Biol. **49**: 427–451.

Costes SV, Daelemans D, Cho EH, Dobbin Z, Pavlakis G, Lockett S (2004) Automatic and quantitative measurement of protein-protein colocalization in live cells. Biophys. J. **86**: 3993–4003.

Ehrlich M, Gutman O, Knaus P, Henis YI (2012) Oligomeric interactions of TGF-β and BMP receptors. FEBS Lett. **586**: 1885–1896.

Ehrlich M, Horbelt D, Marom B, Knaus P, Henis YI (2011) Homomeric and heteromeric complexes among TGF-β and BMP receptors and their roles in signaling. Cell. Signal. **23**: 1424–1432.

Friedrichsen DM, Joazeiro CA, Li J, Hunter T, Chory J (2000) Brassinosteroid-insensitive-1 is a ubiquitously expressed leucine-rich repeat receptor serine/threonine kinase. Plant Physiol. **123**: 1247–1256.

Gadella TW, Jovin TM (1995) Oligomerization of epidermal growth factor receptors on A431 cells studied by time-resolved fluorescence imaging microscopy. A stereochemical model for tyrosine kinase receptor activation. J. Cell Biol. **129**: 1543–1558.

Geldner N, Hyman DL, Wang X, Schumacher K, Chory J (2007) Endosomal signaling of plant steroid receptor kinase BRI1. Genes Dev. **21**: 1598–1602.

Gou X, Yin H, He K, Du J, Yi J, Xu S, Lin H, Clouse SD, Li J (2012) Genetic evidence for an indispensable role of somatic embryogenesis receptor kinases in brassinosteroid signaling. PLoS Genet. **8**: e1002452.

Gómez-Gómez L, Boller T (2000) FLS2: an LRR receptor-like kinase involved in the perception of the bacterial elicitor flagellin in Arabidopsis. Mol. Cell **5**: 1003–1011.

Grove MD, Spencer GF, Rohwedder WK, Mandava N, Worley JF, Warthen JD, Steffens GL, Flippen-Anderson JL, Cook JC (1979) Brassinolide, a plant growth-promoting steroid isolated from Brassica napus pollen. Nature **281**: 216–217.

Hacham Y, Holland N, Butterfield C, Ubeda-Tomas S, Bennett MJ, Chory J, Savaldi-Goldstein S (2011) Brassinosteroid perception in the epidermis controls root meristem size. Development **138**: 839–848.

Halliday K, Devlin PF, Whitelam GC, Hanhart C, Koornneef M (1996) The ELONGATED gene of Arabidopsis acts independently of light and gibberellins in the control of elongation growth. Plant J. **9**: 305–312.

Hartung A, Bitton-Worms K, Rechtman MM, Wenzel V, Boergermann JH, Hassel S, Henis YI, Knaus P (2006) Different routes of bone morphogenic protein (BMP) receptor endocytosis influence BMP signaling. Mol. Cell. Biol. **26**: 7791–7805.

Hartwig T, Corvalan C, Best NB, Budka JS, Zhu J-Y, Choe S, Schulz B (2012) Propiconazole is a specific and accessible brassinosteroid (BR) biosynthesis inhibitor for Arabidopsis and maize. PLoS ONE **7**: e36625.

He J-X, Gendron JM, Sun Y, Gampala SSL, Gendron N, Sun CQ, Wang Z-Y (2005) BZR1 is a transcriptional repressor with dual roles in brassinosteroid homeostasis and growth responses. Science **307**: 1634–1638.

He J-X, Gendron JM, Yang Y, Li J, Wang Z-Y (2002) The GSK3-like kinase BIN2 phosphorylates and destabilizes BZR1, a positive regulator of the brassinosteroid signaling pathway in Arabidopsis. Proc. Natl. Acad. Sci. U.S.A. **99**: 10185–10190.

He Z, Wang ZY, Li J, Zhu Q, Lamb C, Ronald P, Chory J (2000) Perception of brassinosteroids by the extracellular domain of the receptor kinase BRI1. Science **288**: 2360–2363.

Hothorn M, Belkhadir Y, Dreux M, Dabi T, Noel JP, Wilson IA, Chory J (2011) Structural basis of steroid hormone perception by the receptor kinase BRI1. Nature **474**: 467–471.

Hsieh M-Y, Yang S, Raymond-Stinz MA, Edwards JS, Wilson BS (2010) Spatio-temporal modeling of signaling protein recruitment to EGFR. BMC Syst. Biol. **4**: 57.

Irani NG, Di Rubbo S, Mylle E, Van den Begin J, Schneider-Pizoń J, Hniliková J, Síša M, Buyst D, Vilarrasa-Blasi J, Szatmari A-M, et al (2012) Fluorescent castasterone reveals BRI1 signaling from the plasma membrane. Nat. Chem. Biol. **8**: 583–589.

Jaillais Y, Belkhadir Y, Balsemão-Pires E, Dangl JL, Chory J (2011a) Extracellular leucine-rich repeats as a platform for receptor/coreceptor complex formation. Proc. Natl. Acad. Sci. U.S.A. **108**: 8503–8507.

Jaillais Y, Hothorn M, Belkhadir Y, Dabi T, Nimchuk ZL, Meyerowitz EM, Chory J (2011b) Tyrosine phosphorylation controls brassinosteroid receptor activation by triggering membrane release of its kinase inhibitor. Genes Dev. **25**: 232–237.

Kim T-W, Guan S, Burlingame AL, Wang Z-Y (2011) The CDG1 kinase mediates brassinosteroid signal transduction from BRI1 receptor kinase to BSU1 phosphatase and GSK3-like kinase BIN2. Mol. Cell **43**: 561–571.

Kim T-W, Guan S, Sun Y, Deng Z, Tang W, Shang J-X, Sun Y, Burlingame AL, Wang Z-Y (2009) Brassinosteroid signal transduction from cell-surface receptor kinases to nuclear transcription factors. Nat. Cell Biol. **11**: 1254–1260.

Kim T-W, Wang Z-Y (2010) Brassinosteroid signal transduction from receptor kinases to transcription factors. Annu. Rev. Plant Biol. **61**: 681–704.

Kinoshita T, Caño-Delgado A, Seto H, Hiranuma S, Fujioka S, Yoshida S, Chory J (2005) Binding of brassinosteroids to the extracellular domain of plant receptor kinase BRI1. Nature **433**: 167–171.

Koncz C, Martini N, Mayerhofer R, Koncz-Kalman Z, Körber H, Redei GP, Schell J (1989) High-frequency T-DNA-mediated gene tagging in plants. Proc. Natl. Acad. Sci. U.S.A. **86**: 8467–8471.

Kremers G-J, Goedhart J, van Munster EB, Gadella TWJ (2006) Cyan and yellow super fluorescent proteins with improved brightness, protein folding, and FRET Förster radius. Biochemistry **45**: 6570–6580.

Kutschera UU, Wang Z-YZ (2012) Brassinosteroid action in flowering plants: a Darwinian perspective. J. Exp. Bot. **63**: 3511–3522.

Li J, Chory J (1997) A putative leucine-rich repeat receptor kinase involved in brassinosteroid signal transduction. Cell **90**: 929–938.

Li J, Wen J, Lease KA, Doke JT, Tax FE, Walker JC (2002) BAK1, an Arabidopsis LRR receptor-like protein kinase, interacts with BRI1 and modulates brassinosteroid signaling. Cell **110**: 213–222.

Manders E, Verbeek F, Aten J (1993) Measurement of Colocalization of Objects in Dual-Color Confocal Images. J. Microsc.**169**: 375–382.

Martin-Fernandez M, Clarke DT, Tobin MJ, Jones SV, Jones GR (2002) Preformed oligomeric epidermal growth factor receptors undergo an ectodomain structure change during signaling. Biophys. J. **82**: 2415–2427.

Massague J, Pilch PF, Czech MP (1980) Electrophoretic resolution of three major insulin receptor structures with unique subunit stoichiometries. Proc. Natl. Acad. Sci. U.S.A. **77**: 7137–7141.

Nam KH, Li J (2002) BRI1/BAK1, a receptor kinase pair mediating brassinosteroid signaling. Cell **110**: 203–212.

Nohe A, Hassel S, Ehrlich M, Neubauer F, Sebald W, Henis YI, Knaus P (2002) The mode of bone morphogenetic protein (BMP) receptor oligomerization determines different BMP-2 signaling pathways. J. Biol. Chem. **277**: 5330–5338.

Oh M-H, Wang X, Clouse SD, Huber SC (2012) Deactivation of the Arabidopsis BRASSINOSTEROID INSENSITIVE 1 (BRI1) receptor kinase by autophosphorylation within the glycine-rich loop. Proc. Natl. Acad. Sci. U.S.A. **109**: 327–332.

Roux M, Schwessinger B, Albrecht C, Chinchilla D, Jones A, Holton N, Malinovsky FG, Tör M, de Vries S, Zipfel C (2011) The Arabidopsis leucine-rich repeat receptor-like kinases BAK1/SERK3 and BKK1/SERK4 are required for innate immunity to hemibiotrophic and biotrophic pathogens. Plant Cell **23**: 2440–2455.

Russinova E, Borst JW, Kwaaitaal M, Caño-Delgado A, Yin Y, Chory J, de Vries SC (2004) Heterodimerization and endocytosis of Arabidopsis brassinosteroid receptors BRI1 and AtSERK3 (BAK1). Plant Cell **16**: 3216–3229.

Saitoh S-I, Akashi S, Yamada T, Tanimura N, Matsumoto F, Fukase K, Kusumoto S, Kosugi A, Miyake K (2004) Ligand-dependent Toll-like receptor 4 (TLR4)-oligomerization is directly linked with TLR4-signaling. J. Endotoxin Res. **10**: 257–260.

Sauer M, Paciorek T, Benková E, Friml J (2006) Immunocytochemical techniques for whole-mount in situ protein localization in plants. Nat. Protoc. **1**: 98–103.

Schulze B, Mentzel T, Jehle AK, Mueller K, Beeler S, Boller T, Felix G, Chinchilla D (2010) Rapid heteromerization and phosphorylation of ligand-activated plant transmembrane receptors and their associated kinase BAK1. J. Biol. Chem. **285**: 9444–9451.

She J, Han Z, Kim T-W, Wang J, Cheng W, Chang J, Shi S, Wang J, Yang M, Wang Z-Y, et al (2011) Structural insight into brassinosteroid perception by BRI1. Nature **474**: 472–476.

Shimizu T, Nakano T, Takamizawa D, Desaki Y, Ishii-Minami N, Nishizawa Y, Minami E, Okada K, Yamane H, Kaku H, et al (2010) Two LysM receptor molecules, CEBiP and OsCERK1, cooperatively regulate chitin elicitor signaling in rice. Plant J. **64**: 204–214.

Springael J-Y, Urizar E, Parmentier M (2005) Dimerization of chemokine receptors and its functional consequences. Cytokine Growth Factor Rev. **16**: 611–623.

Sun Y, Sun Y, Fan X-Y, Fan X-Y, Cao D-M, Cao D-M, Tang W, Tang W, He K, He K, et al (2010) Integration of brassinosteroid signal transduction with the transcription network for plant growth regulation in Arabidopsis. Dev. Cell **19**: 765–777.

Tang W, Kim T-W, Oses-Prieto JA, Sun Y, Deng Z, Zhu S, Wang R, Burlingame AL, Wang Z-Y (2008) BSKs mediate signal transduction from the receptor kinase BRI1 in Arabidopsis. Science **321**: 557–560.

Van Craenenbroeck K (2012) GPCR Oligomerization: Contribution to Receptor Biogenesis. Subcell. Biochem. **63**: 43–65.

Van Craenenbroeck K, Borroto-Escuela DO, Romero-Fernandez W, Skieterska K, Rondou P, Lintermans B, Vanhoenacker P, Fuxe K, Ciruela F, Haegeman G (2011) Dopamine D4 receptor oligomerization--contribution to receptor biogenesis. FEBS J. **278**: 1333–1344.

van Esse G, Westphal AH, Surendran RP, Albrecht C, van Veen B, Borst JW, de Vries SC (2011) Quantification of the brassinosteroid insensitive1 receptor in planta. Plant Physiol. **156**: 1691–1700.

van Esse GW, van Mourik S, Stigter H, Hove ten CA, Molenaar J, de Vries SC (2012) A mathematical model for BRASSINOSTEROID INSENSITIVE1-mediated signaling in root growth and hypocotyl elongation. Plant Physiol. **160**: 523–532.

Viotti C, Bubeck J, Stierhof Y-D, Krebs M, Langhans M, van den Berg W, van Dongen W, Richter S, Geldner N, Takano J, et al (2010) Endocytic and secretory traffic in Arabidopsis merge in the trans-Golgi network/early endosome, an independent and highly dynamic organelle. Plant Cell **22**: 1344–1357.

Wang J, Norcross M (2008) Dimerization of chemokine receptors in living cells: key to receptor function and novel targets for therapy. Drug Discov. Today **13**: 625–632.

Wang X, Chory J (2006) Brassinosteroids regulate dissociation of BKI1, a negative regulator of BRI1 signaling, from the plasma membrane. Science **313**: 1118–1122.

Wang X, Goshe MB, Soderblom EJ, Phinney BS, Kuchar JA, Li J, Asami T, Yoshida S, Huber SC, Clouse SD (2005) Identification and functional analysis of in vivo phosphorylation sites of the Arabidopsis BRASSINOSTEROID-INSENSITIVE1 receptor kinase. Plant Cell **17**: 1685–1703.

Wang X, Kota U, He K, Blackburn K, Li J, Goshe MB, Huber SC, Clouse SD (2008) Sequential transphosphorylation of the BRI1/BAK1 receptor kinase complex impacts early events in brassinosteroid signaling. Dev. Cell **15**: 220–235.

Wang Z-Y, Bai M-Y, Oh E, Zhu J-Y (2012) Brassinosteroid signaling network and regulation of photomorphogenesis. Annu. Rev. Genet. **46**: 701–724.

Wang Z-Y, Nakano T, Gendron J, He J, Chen M, Vafeados D, Yang Y, Fujioka S, Yoshida S, Asami T, et al (2002) Nuclear-localized BZR1 mediates brassinosteroid-induced growth and feedback suppression of brassinosteroid biosynthesis. Dev. Cell **2**: 505–513.

Wu F-H, Shen S-C, Lee L-Y, Lee S-H, Chan M-T, Lin C-S (2009) Tape-Arabidopsis Sandwich - a simpler Arabidopsis protoplast isolation method. Plant Methods **5**: 16.

Yin Y, Vafeados D, Tao Y, Yoshida S, Asami T, Chory J (2005) A new class of transcription factors mediates brassinosteroid-regulated gene expression in Arabidopsis. Cell **120**: 249–259.

Yin Y, Wang Z-Y, Mora-Garcia S, Li J, Yoshida S, Asami T, Chory J (2002) BES1 accumulates in the nucleus in response to brassinosteroids to regulate gene expression and promote stem elongation. Cell **109**: 181–191.

Yu X, Li L, Zola J, Aluru M, Ye H, Foudree A, Guo H, Anderson S, Aluru S, Liu P, et al (2011) A brassinosteroid transcriptional network revealed by genome-wide identification of BESI target genes in Arabidopsis thaliana. Plant J. **65**: 634–646.

Yu X, Sharma KD, Takahashi T, Iwamoto R, Mekada E (2002) Ligand-independent dimer formation of epidermal growth factor receptor (EGFR) is a step separable from ligand-induced EGFR signaling. Mol. Biol. Cell **13**: 2547–2557.

Zipfel C, Kunze G, Chinchilla D, Caniard A, Jones JDG, Boller T, Felix G (2006) Perception of the bacterial PAMP EF-Tu by the receptor EFR restricts Agrobacterium-mediated transformation. Cell **125**: 749–760.

SUPPLEMENTAL MATERIAL

Supplemental Notes

Note S1: Approximation of the number of BRI1-GFP and SERK3-mCherry molecules per pixel in a FLIM image.

Recently, the absolute numbers of BRI1 and SERK3 were determined in Arabidopsis roots by quantitative confocal fluorescence microscopy and receptor densities of 34 receptors/μm² for homozygous BRI1-GFP 2, 17 receptors/μm² for heterozygous BRI1-GFP 2 and 5 receptors/μm² for SERK3-GFP were obtained (van Esse et al., 2011). Based on these findings the number of BRI1-GFP and SERK3-mCherry molecules per pixel in a fluorescence lifetime image were estimated.

The FLIM images presented here were recorded on a confocal microscope using a water immersive objective (N.A. 1.2) with the pinhole set from 1.5 to 2.0 AU. BRI1-GFP (emission wavelength peak at 509 nm) was excited with laser light of 470 nm. The volume of a voxel is determined by the pixel size in x,y,z-dimensions. For calculation purposes the pixel size in x,y-dimensions is set to 250 nm x 250 nm. The z-dimension of a corresponding voxel can be obtained by calculating the Full Width Half Maximum (FWHM) in the axial direction:

$$FWHM_{det,axial} = \sqrt{\left(\frac{0.88 \bullet \lambda_{em}}{n - \sqrt{n^2 - NA^2}}\right)^2 + \left(\frac{\sqrt{2} \bullet n \bullet \left(AU \bullet \frac{1.22 \bullet \lambda_{ex}}{NA}\right)}{NA}\right)^2}$$

$$FWHM_{det,axial} = \sqrt{\left(\frac{0.88 \bullet 0.509}{1.33 - \sqrt{1.33^2 - 1.2^2}}\right)^2 + \left(\frac{\sqrt{2} \bullet 1.33 \bullet \left(1.5 \bullet \frac{1.22 \bullet 0.470}{1.2}\right)}{1.2}\right)^2} = 1.27\ \mu m$$

With:

λ_{em} = emission wavelength
λ_{ex} = excitation wavelength
n = refractive index of the immersion liquid
NA = numerical aperture of the objective
AU = pinhole diameter in airy units

Since plasma membrane localizing receptors were investigated the observation volume reduces to a 2-dimensional plane determined by the pixel size in x-direction and the FWHM in axial direction. This results in an observation plane of 0.32 μm². Assuming a homogenous receptor distribution throughout the plasma membrane one pixel of a fluorescence lifetime image contains approximately 11 or 5 BRI1-GFP, for homozygous and heterozygous line 2

respectively, and 2 SERK3-mCherry receptors. Considering a minimal pixel size and pinhole diameter used for this calculation, the obtained values represent the minimum of receptors to be expected in a single pixel during data acquisition.

Note S2: Approximation of BRI1-GFP ligand-occupancy after brassinazole treatment and exogenous BL application as well as the amount of BAK1(SERK3) receptor pulled down by BRI1

The two BRI1-GFP lines used here are routinely employed by many laboratories and are well described in literature (Friedrichsen et al., 2000; Geldner et al., 2007). This also applies to variants of the SERK3-mCherry lines developed in our laboratory and others (Jaillais et al., 2011). Because the lines were generated in wild type background they exhibit mild to moderate overexpression phenotypes as also observed previously. In particular, van Esse et al. (2012) showed that the BRI1-GFP 2 as used here is about ten-fold more sensitive to exogenous brassinolide (BL) due to an approximately three-fold overexpression of BRI1-GFP compared to wild type level (van Esse et al., 2011). This could lead to a situation where the use of brassinazole (BRZ) is not sufficient to reduce the endogenous level of brassinosteroids (BRs) below the activation threshold leaving a low level of BRI1 activation. To provide further insight into this potential caveat, we have calculated the amount of receptors that could be in active hetero-oligomeric conformation in the BRI1-GFP 2/SERK3-mCherry and segregating BRI1-GFP 2/SERK3-mCherry combination using literature data, the conditions applied here and our own previous observations.

(A) BRI1-GFP ligand-occupancy after brassinazole treatment

The concentration of BL is between 0.06 and 0.1 nM in root extracts, so about 1 nM when all active ligand is outside the cells (van Esse et al., 2012). BRZ reduces the ligand concentration to about 6% (Asami et al., 2001), or 0.06 nM. The wild type BRI1 concentration at the plasma membrane (PM) is 62 nM and the BRI1-GFP concentration in the homozygous and heterozygous line 2 is about 176 nM or 88 nM, respectively. Assuming a 1 to 1 ratio between ligand and receptor this would mean that out of the total 64,400 (46,800 from homozygous BRI1-GFP 2 + 17,600 wild-type BRI1) or 41,000 (23,400 heterozygous BRI1-GFP 2 + 17,600 wild-type BRI1) BRI1 receptors (adapted from van Esse et al., 2011) per cell in the PM, only 16 BRI1 receptors, representing 0.03% (homozygous line 2) or 0.04% (heterozygous line 2) (either BRI1 or BRI1-GFP) can be in complex with BL and BAK1(SERK3) in the presence of BRZ.

To determine the number of BRI1 receptors that are theoretically in a ligand-bound configuration in a FLIM image, we have to take the dimensions of meristematic epidermal root cells (van Esse et al., 2011) and the FRET-FLIM imaging parameters (see Note S1) into account. This results for a single cell in a PM area of 45.5 μm^2. Since we are not able to resolve two adjacent PMs the observation area doubles to 91 μm^2. With a total BRI1 (BRI1 and BRI1-GFP) density of 82 receptors/μm^2 (homozygous line 2) or 53 receptors/μm^2

(heterozygous line 2) the average number of BRI1 receptors is determined to be 7,462 or 4,823 (5,278 or 2,639 BRI1-GFP for homozygous and heterozygous line 2, respectively). Using the assumed ligand-occupancy of 0.03% or 0.04% after BRZ treatment, the theoretical number of ligand-bound BRI1 receptors in the PM of a single cell in a FLIM images is estimated to be 2 for homozygous BRI1-GFP 2 or 1 for heterozygous BRI1-GFP 2.

However, we observe 6.7% corrected IPS (Table 3) along the PM in a FLIM image representing approximately 176 BRI1-GFP receptors for the heterozygous line 2 in a hetero-oligomeric configuration with SERK3.

(B) BRI1-GFP ligand-occupancy after BL treatment

Upon activation with 1 μM of BL, full saturation could be expected of all 64,400 BRI1 receptors. This clearly does not take place in live roots, since only about 2,340 BRI1-GFP receptors per cell (10% of 23,400 for heterozygous line 2) or about 263 (heterozygous line 2) per confocal section are seen to be in complex with SERK3. This suggests that the active configuration of BRI1-SERK3 complexes is relatively independent from the ambient ligand concentration.

(C) Amount of BAK1 receptor pulled down by BRI1

An independent method of estimating the amount of BAK1(SERK3) in complex with BRI1 was recently published (Albrecht et al., 2012). In that work the distribution of BAK1(SERK3) between BRI1 and FLS2 was estimated under conditions where both pathways were fully activated. The results suggested that the amount of SERK3 coimmunoprecipitated by BRI1 was not more than 5% of the total SERK3 pool upon full activation. Since in the present study wild type and fluorescently tagged SERK3 proteins are expressed the amount of SERK3 has to be doubled to around 10%. However, SERK3 is about half of the amount of BRI1, and assuming a one to one stoichiometry, the amount of BRI1 employed is approximately 5%, which is about half of the estimated value based on FRET-FLIM.

Table S1: Fluorescence lifetime analysis of the BRI1-sCFP interaction with SERK3-sYFP and ELG-sYFP.

Arabidopsis mesophyll protoplasts were transiently transfected with BRI1-sCFP or BRI1-sCFP in combination with either SERK3-sYFP or ELG-sYFP.

	τ [ps]	FRET [%]	IPS [%]	N
BRI1-sCFP	2804 ± 14			26
BRI1-sCFP+SERK3-sYFP	2410 ± 41[a]	14 ± 1	48 ± 6	26
BRI1-sCFP+ELG-sYFP	2332 ± 39[a]	17 ± 1	62 ± 5[b]	39

[a] The mean difference is significant at the $p < 0.05$ level compared to BRI1-sCFP samples (two-tailed Student's t-test for unequal variance).

[b] The mean difference is significant at the $p < 0.05$ level compared to BRI1-sCFP+SERK3-sYFP samples (two-tailed Student's t-test for equal variance).

FLIM of transiently transfected Arabidopsis mesophyll protoplasts revealed an increased interaction of BRI1 with ELG compared to BRI1 and SERK3. Therefore we conclude that the FRET-FLIM setup is sufficiently sensitive to discriminate between interacting proteins with slightly different affinity.

Table S2: Fluorescence lifetime analysis of time-course FLIM.

Quantitative FRET-FLIM analysis of time-course FRET-FLIM measurements performed in planta using 5 day old Arabidopsis roots expressing heterozygous BRI1-GFP 2 and homozygous SERK3-mCherry in response to 24-epi-brassinolide (BL, 1 µM). Seedlings were precultured in the presence of 5 µM BRZ for 2 days. The τ values given represent GFP fluorescence lifetimes ± S.E.M. Interaction pixels (IPS) correspond to the percentage of pixels in a fluorescence lifetime image with strongly reduced BRI1-GFP fluorescence lifetimes and are presented ± S.E.M. "N" represents the number of analyzed fluorescence lifetime images.

	Time after BL addition [min]			
	3 - 15	16 – 30	31 – 45	46 – 60
τ [ps]	2233 ± 14	2212 ± 7	2182 ± 13[a,b]	2173 ± 10[a,b]
IPS [%]	7.0 ± 1.6	8.4 ± 0.9	14 ± 2.5[a,b]	16 ± 2.4[a,b]
N	10	7	10	10

[a] The mean difference is significant at the $p < 0.05$ level compared to "3 – 15 min" samples (two-tailed Student's t-test for equal variance).

[b] The mean difference is significant at the $p < 0.05$ level compared to "16 – 30 min" samples (two-tailed Student's t-test for equal variance).

During a time frame of 1 h after BL application fluorescence lifetime images were recorded and a reduction of BRI1-GFP fluorescence was observed. The reduced donor fluorescence lifetime is also reflected by the increasing IPS values in this time period. A significant change in fluorescence lifetime or IPS occurred after 30 min.

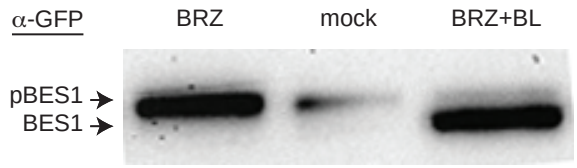

Figure S1: Brassinazole abolishes BES1-GFP dephosphorylation.
Western blot analysis of BES1-GFP phosphorylation in response to brassinazole (BRZ) and 24-epi-brassinolide (BL) using anti-GFP antibodies. BES1-GFP in wild type background was isolated from 8 day old seedlings cultured for 2 days in medium containing 5 µM BRZ. A final BL concentration of 1 µM and an incubation time of 1 h were applied.
In the presence of BRZ only a phosphorylated BES1-GFP band was detected. Activation of BR signaling by exogenous application of BL led to a band shift towards unphosphorylated BES1-GFP, similar to results obtained by Yin et al. (2002). Therefore we conclude that the BRZ conditions applied throughout the experiments were sufficient to strongly reduce or abolish BR signaling.

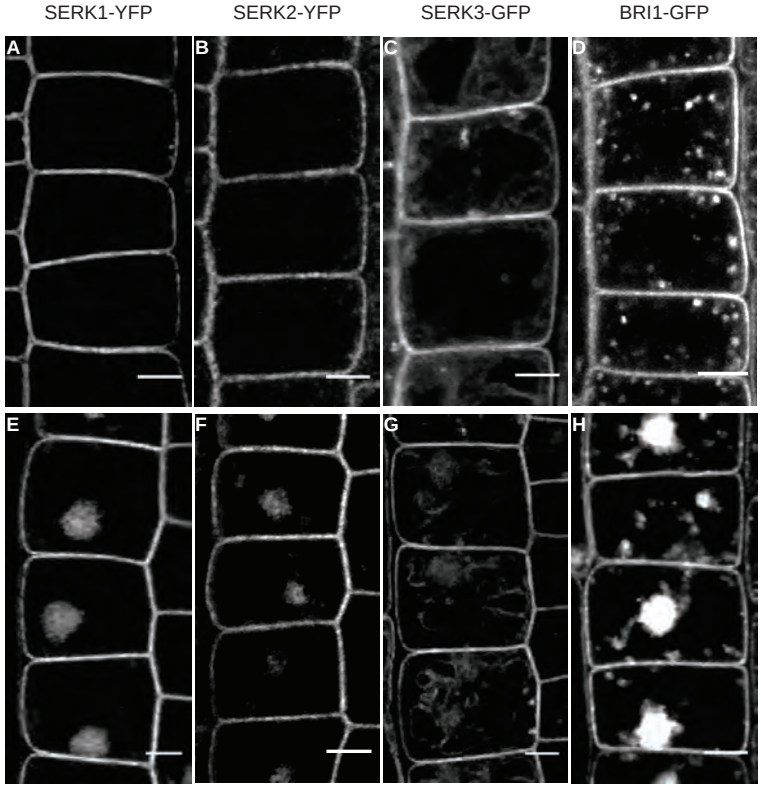

Figure S2: SERK family members respond differently towards BFA.
(**A-D**) Confocal images of Arabidopsis epidermal root cells expressing SERK1-YFP (**A**), SERK2-YFP (**B**), SERK3-GFP (**C**), and BRI1-GFP (**D**), respectively.
(**E-H**) Confocal images of Arabidopsis epidermal root cells expressing SERK1-YFP (**E**), SERK2-YFP (**F**), SERK3-GFP (**G**), and BRI1-GFP (**H**), respectively, in response to brefeldin A (BFA) (50 µM, 1 h).
Scale bars correspond to a size of 5 µm.
In transgenic lines expressing BRI1-GFP, SERK1-YFP or SERK2-YFP a clear induction of BFA compartments was observed. However, SERK3-GFP only showed weak BFA sensitivity.

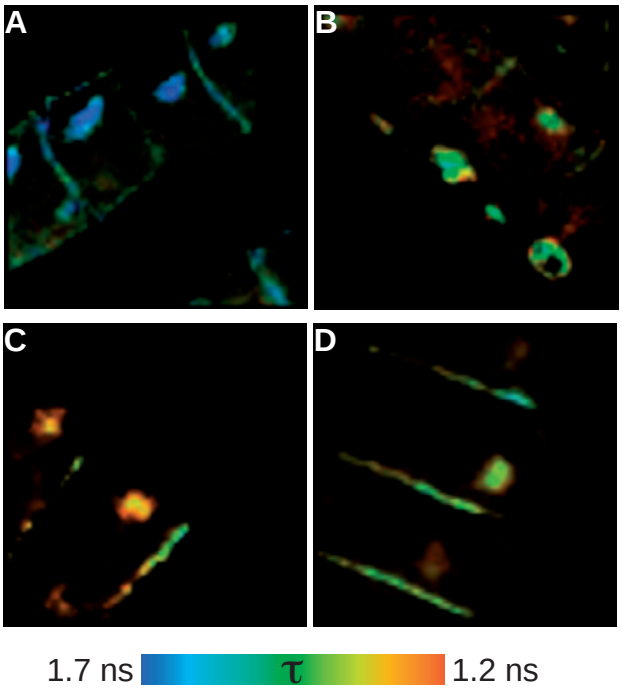

Figure S3: Immuno-cytochemical FRET-FLIM discriminates interacting and non-interacting proteins in BFA compartments.

(A) Fluorescence lifetime image of BRI1-GFP labeled with rabbit-anti-GFP and goat-anti-rabbit-Alexa488.

(B) Fluorescence lifetime image of double-labeled BRI1-GFP with rabbit-anti-YFP/goat-anti-rabbit-Alexa488 and rabbit-anti-YFP/goat-anti-mouse-Alexa568, respectively, used as positive control.

(C) Fluorescence lifetime image of PIN2-GFP labeled with rabbit-anti-GFP and goat-anti-rabbit-Alexa488.

(**D**) Fluorescence lifetime image of PIN2-GFP/SERK3-mCherry double-labeled with rabbit-anti-GFP/goat-anti-rabbit-Alexa488 and mouse-anti-mCherry/goat-anti-mouse-Alexa568, respectively, used as negative control.

FLIM of immuno-labeled BRI1-GFP 1 as well as PIN2-GFP/SERK3-mCherry in 5 day old Arabidopsis seedlings in response to BFA (50 µM BFA, 1 h). Color bar represents false color-code for Alexa488 fluorescence lifetimes (τ).

The homotypic interaction of BFA-sensitive BRI1 receptors served as positive control for the immuno-cytochemical FRET-FLIM assay. Indeed, a drastic decrease in donor fluorescence lifetime (Alexa488) in BFA compartments was observed when BRI1-GFP was double-labeled (Alexa488-Alexa568). PIN2 and SERK3 were chosen as negative control since PIN2 also shows BFA-sensitivity, but no interaction with SERK3 has been reported. As expected, BFA application led to the induction of PIN2 containing BFA compartments, but the donor fluorescence lifetime was unaffected. This confirms the ability of the immuno-cytochemical FRET-FLIM approach for revealing interacting and non-interacting protein populations in BFA compartments.

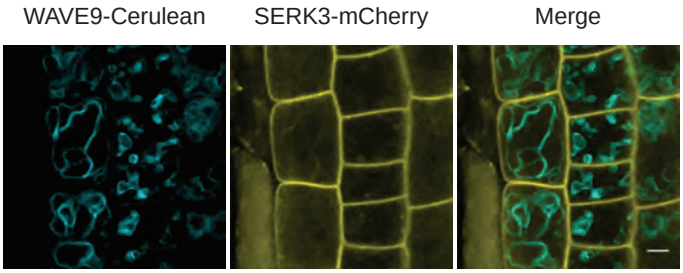

Figure S4: SERK3 localizes to the tonoplast.
Confocal images were acquired from 5 day old Arabidopsis seedlings coexpressing WAVE9 (VAMP711)-Cerulean (Geldner et al., 2009) and SERK3-mCherry. The individual images of WAVE9-Cerulean and SERK3-mCherry localization in live root epidermal cells as well as the merged image are shown. The SERK3-mCherry line used here is heterozygous for the tagged receptor as well as the WAVE9 marker. White arrowheads indicate localization of SERK3-mCherry to the tonoplast. The scale bar corresponds to a distance of 5 µm.
Since WAVE9 labels the tonoplast and we observed colocalization of both fluorescently tagged proteins, we conclude that SERK3 localizes to vacuole-limiting membrane entities.

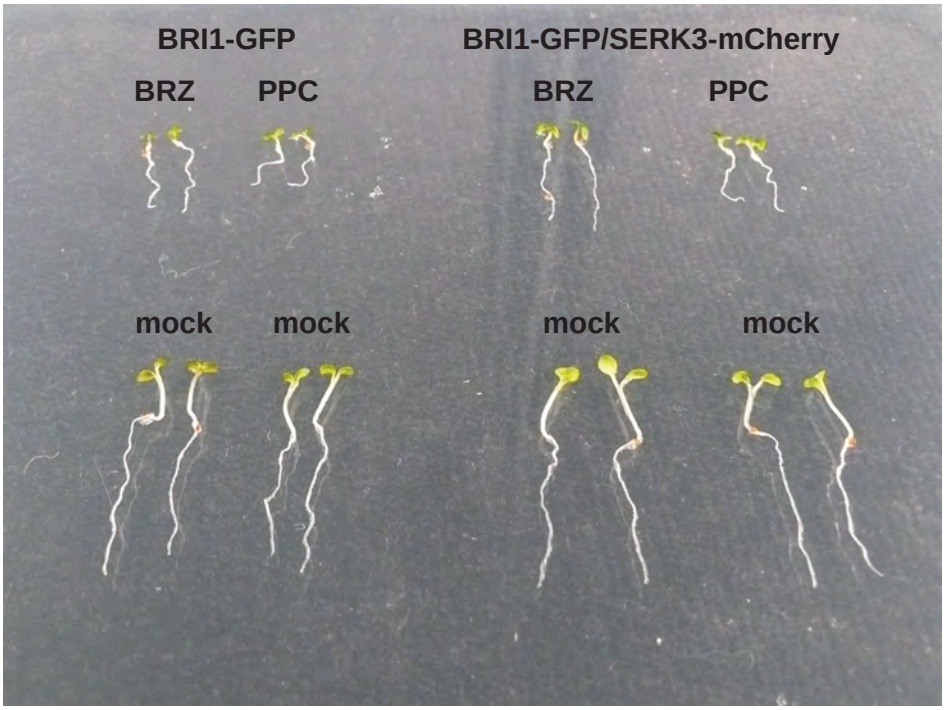

Figure S5: Phenotypical comparison of PPC and BRZ treatments.
Seedlings expressing BRI1-GFP 2 or coexpressing BRI1-GFP 2 and SERK3-mCherry were cultured for 2 days in liquid growth medium containing 5 µM BRZ or 100 nM PPC. The image was taken 5 days after germination. The BRI1-GFP 2/SERK3-mCherry line used here is heterozygous for BRI1-GFP and homozygous for SERK3-mCherry (numerical analysis in Supplemental note S2).
PPC, even though applied in a significantly lower concentration, more strongly inhibited the root growth of Arabidopsis seedlings than BRZ.

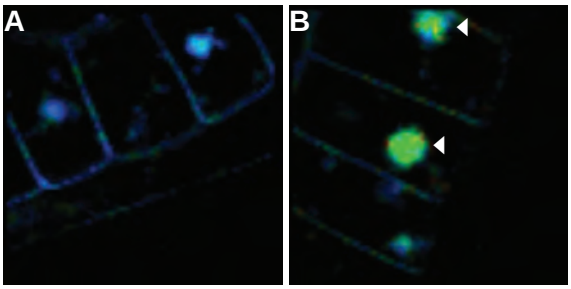

Figure S6: BRI1 and SERK3 interact in BFA compartments in planta.
(A) Fluorescence lifetime image of BRI1-GFP in live Arabidopsis root meristem epidermal cells.
(B) Fluorescence lifetime image of live Arabidopsis root meristem epidermal cells coexpressing BRI1-GFP and SERK3-mCherry.
FLIM performed on live roots of 5 day old Arabidopsis seedlings expressing BRI1-GFP 2 or coexpressing BRI1-GFP 2 and SERK3-mCherry in response to BFA (50 µM BFA, 1 h). The BRI1-GFP 2/SERK3-mCherry line used here is homozygous for both tagged receptors (numerical analysis in Supplemental note S2). White arrowheads indicate BFA compartments with reduced BRI1-GFP fluorescence lifetimes. Color bar represents false color-code for BRI1-GFP fluorescence lifetimes (τ).

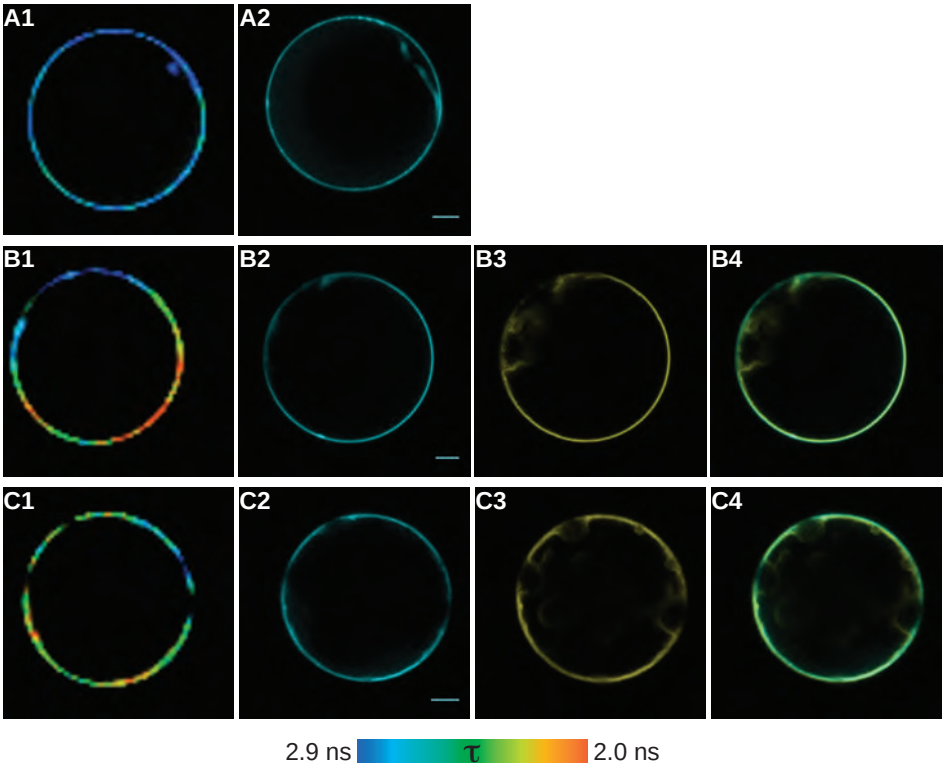

Figure S7: ELG shows a stronger decrease in overall fluorescence lifetime with BRI1 than SERK3.

(**A1, A2**) Fluorescence lifetime (**A1**) and confocal (**A2**) image of BRI1-sCFP.
(**B1-B4**) Fluorescence lifetime (**B1**) and confocal images of BRI1-sCFP (**B2**) and SERK3-sYFP (**B3**) as well as the merged confocal image (**B4**).
(**C1-C4**) Fluorescence lifetime (**C1**) and confocal images of BRI1-sCFP (**C2**) and ELG-sYFP (**C3**) as well as the merged confocal image (**C4**).
FLIM was performed on transiently transfected Arabidopsis mesophyll protoplasts expressing BRI1-sCFP or BRI1-sCFP in combination with either SERK3-sYFP or ELG-sYFP. Scale bars correspond to a size of 5 µm.
Color bar represents false color-code for BRI1-GFP fluorescence lifetimes (τ).
Quantitative FRET-FLIM analysis revealed a slightly increased interaction between BRI1-sCFP and ELG-sYFP in comparison to BRI1-sCFP and SERK3-sYFP (see Table S1).

SUPPLEMENTAL REFERENCES

Albrecht C, Boutrot F, Segonzac C, Schwessinger B, Gimenez-Ibanez S, Chinchilla D, Rathjen JP, de Vries SC, Zipfel C (2012) Brassinosteroids inhibit pathogen-associated molecular pattern-triggered immune signaling independent of the receptor kinase BAK1. Proc. Natl. Acad. Sci. U.S.A. **109**: 303–308.

Asami T, Mizutani M, Fujioka S, Goda H, Min YK, Shimada Y, Nakano T, Takatsuto S, Matsuyama T, Nagata N, et al (2001) Selective interaction of triazole derivatives with DWF4, a cytochrome P450 monooxygenase of the brassinosteroid biosynthetic pathway, correlates with brassinosteroid deficiency in planta. J. Biol. Chem. **276**: 25687–25691.

Friedrichsen DM, Joazeiro CA, Li J, Hunter T, Chory J (2000) Brassinosteroid-insensitive-1 is a ubiquitously expressed leucine-rich repeat receptor serine/threonine kinase. Plant Physiol. **123**: 1247–1256.

Geldner N, Dénervaud-Tendon V, Hyman DL, Mayer U, Stierhof Y-D, Chory J (2009) Rapid, combinatorial analysis of membrane compartments in intact plants with a multicolor marker set. Plant J. **59**: 169–178.

Geldner N, Hyman DL, Wang X, Schumacher K, Chory J (2007) Endosomal signaling of plant steroid receptor kinase BRI1. Genes Dev. **21**: 1598–1602.

Jaillais Y, Hothorn M, Belkhadir Y, Dabi T, Nimchuk ZL, Meyerowitz EM, Chory J (2011) Tyrosine phosphorylation controls brassinosteroid receptor activation by triggering membrane release of its kinase inhibitor. Genes Dev. **25**: 232–237.

van Esse GW, van Mourik S, Stigter H, Hove ten CA, Molenaar J, de Vries SC (2012) A mathematical model for BRASSINOSTEROID INSENSITIVE1-mediated signaling in root growth and hypocotyl elongation. Plant Physiol. **160**: 523–532.

van Esse G, Westphal AH, Surendran RP, Albrecht C, van Veen B, Borst JW, de Vries SC (2011) Quantification of the brassinosteroid insensitive1 receptor in planta. Plant Physiol. **156**: 1691–1700.

Yin Y, Wang Z-Y, Mora-Garcia S, Li J, Yoshida S, Asami T, Chory J (2002) BES1 accumulates in the nucleus in response to brassinosteroids to regulate gene expression and promote stem elongation. Cell **109**: 181–191.

Chapter 4

Comparative colocalization and FRET-FLIM analysis in plants – a case study for the plasma membrane receptors BRI1 and SERK3

Christoph A. Bücherl, Sacco C. de Vries, Jan Willem Borst

ABSTRACT

Fluorescence microscopy offers various tools for investigating the spatiotemporal dynamics of signaling events. However, many of these techniques provide solely qualitative read-outs, which can hamper the biological interpretation of light microscopic experiments. In this chapter we introduced a novel FRET-FLIM analysis procedure to quantitatively assess interacting protein populations and we described the different steps of quantitative colocalization analysis. Two colocalization analysis approaches were applied for discriminating colocalizing protein fractions in live Arabidopsis roots under varying physiological conditions or with respect to endosomal compartments. The comparative analysis revealed a predominante localization of BRI1-GFP to ARA7-positive endosomal compartments when compared to ARA6-labeled endomembrane structures. In addition, drug-induced PM-stabilization of BRI1-GFP resulted in increased colocalization with SERK3-mCherry. Our pixel-based FRET-FLIM analysis approach moreover enabled us to estimate the number of BRI1-SERK3 hetero-oligomers in the PM of live root epidermal cells and to conclude that approximately 70% of these receptor complexes are preformed.

INTRODUCTION

Signal transduction processes comprise the translation of extracellular signals into physiological responses. All steps along signaling pathways that lead to modulations of cellular functions rely on spatiotemporal regulation of protein localization and molecular interactions. These molecular interactions result in the assembly and disassembly of biomolecular "machines", often accompanied by physical repositioning of regulatory proteins into or away from specific subcellular compartments (Day et al., 2005). Unraveling protein localization and interaction patterns is therefore a key step for elucidating cellular processes (Visser et al., 2010). Many molecular components of signal transduction pathways have been identified and characterized by traditional biochemical approaches. These methods usually require cell disruption and isolation of proteins from their natural habitat for further analysis. Fluorescence microscopy techniques offer alternative and complementary methods to study signaling processes in intact cells or organisms under low invasive conditions (Visser et al., 2010). In Chapter 3, fluorescence microspectroscopy was applied to investigate the colocalization and molecular interactions between two plant receptor-like kinases in living tissue. Due to the subtle changes of receptor dynamics, we realized that much more extended image analysis procedures were required. These procedures are described in this chapter.

Colocalization Analysis

Since the introduction of confocal microscopy in the mid 1990's, it has enabled the visualization of biological processes in living systems with high spatial resolution. This made confocal imaging the most widespread fluorescence microscopic method for investigating protein localization. Dual color imaging moreover allows investigating subcellular colocalization patterns. However, mostly the final images are only qualitatively interpreted. Therefore quantitative colocalization analysis tools have been developed, which offer the possibility to extract far more information from the recorded images than the qualitative description of localization patterns and overlap of two fluorescence signals (Zinchuk and Grossenbacher-Zinchuk, 2009).

Colocalization is a measure for the relative distribution of fluorophores (Manders et al., 1993) and actually covers two different circumstances (Adler and Parmryd, 2010). Proteins or fluorophores can be described to colocalize either because they occupy the same place, which represents co-occurrence, or because there is a relationship between their intensities, which corresponds to correlation (Adler and Parmryd, 2010). Based on these two concepts various methods have been developed to quantify the fraction of colocalization in confocal images.

Co-occurrence is quantified by determining the fraction of pixels or objects that contain fluorescence intensities of two or more probes (Manders et al., 1993; Fletcher et al., 2010).

Often co-occurrence is described by a single overlap coefficient or separate overlap or colocalization coefficients for each fluorophore recorded. Depending on the mathematical model used these coefficients can be independent of fluorescence intensity or intensity-weighted. Commonly used overlap metrics are the Manders colocalization coefficients (MANDERS et al., 1993). These coefficients range from 0 to 1 and strictly represent co-occurrence independent of signal proportionality (Dunn et al., 2011).

The most common measure for correlation between fluorescence intensities is the Pearson product-moment coefficient, also known as Pearson correlation coefficient. It has a range from +1 for perfect correlation to -1 for perfect anti-correlation. The Pearson correlation coefficient assumes normal distribution of and a linear relationship between two variables, here the fluorescence intensities, and is a measure for the strength of the linear dependence between these variables (Zou et al., 2003). However, since in many biological samples neither the criterion of linearity nor of normality is fulfilled, an additional coefficient is frequently used, the Spearman rank coefficient (Fletcher et al., 2010). The Spearman rank coefficient is a derivative of the Pearson correlation coefficient, applied to ranked data. It is based on a non-parametric rank statistic and only assumes a monotonic relationship between the variables, i.e. the fluorescence intensities (Adler and Parmryd, 2010). That means, instead of using absolute values, the fluorescence intensities are ranked according to their absolute values before the Spearman rank coefficient is calculated. Like the Pearson correlation coefficient, the Spearman rank coefficient ranges from +1 to -1.

Besides the numerical description of colocalization between two proteins using one or more of the above-mentioned coefficients also a visual representation is recommended (Adler and Parmryd, 2010). Usually confocal images of the separate channels and merged images are used for this purpose. However, it is difficult to judge the degree of overlap or correlation from this type of images. A more informative way is the representation of scatter grams or scatter plots, which display the intensities of the pairs of homologous pixels (Adler and Parmryd, 2010). The two axis of a scatter plot represent the fluorescence intensities for the separate channels and the frequencies of occurrence of each pair of intensities are displayed (Adler and Parmryd, 2010). This representation can reveal any correlation between the imaged fluorophores or proteins of interest (Adler and Parmryd, 2010).

Prior to the visual representation of colocalization and calculation of colocalization coefficients appropriate confocal images are required. Therefore this analysis requires four subsequent steps: image acquisition, data pre-processing, calculation of colocalization coefficients, and interpretation of the obtained results (Bolte and Cordelières, 2006; Zinchuk and Grossenbacher-Zinchuk, 2009). Accurate acquisition of confocal images is essential to avoid spectral bleed-through, chromatic shifts and background intensities, which can cause both false-positive and false-negative colocalization results (Zinchuk et al., 2007). Extensive protocols describing all requirements for optimizing imaging setups to obtain accurate

confocal images are available in literature (French et al., 2008; Zinchuk and Grossenbacher-Zinchuk, 2009; Zinchuk and Zinchuk, 2008; Zinchuk and Grossenbacher-Zinchuk, 2011; Zinchuk et al., 2007; Adler and Parmryd, 2013; 2010; Bolte and Cordelières, 2006).

Even though imaging may be performed under optimal conditions, pre-processing of digital images is essential, since any image is an imperfect representation of biological systems (Bolte and Cordelières, 2006). Also a perfect imaging setup cannot compensate for background from intrinsic sample fluorescence and noise (Bolte and Cordelières, 2006). Background in fluorescence microscopic images can stem from endogenous fluorophores that are present in the sample next to the specifically labeled proteins of interest or may result from sample preparation, especially if exogenous dyes are used for staining. Also detector noise, which follows a Poisson distribution, cannot be omitted in fluorescence microscopy (Bolte and Cordelières, 2006). Therefore background and/or noise correction for the recorded confocal images is required to avoid misinterpretation of the obtained results (Zinchuk and Zinchuk, 2008). Several image-processing methods are available to compensate for both effects, whereby most of them rely on setting an intensity threshold for the acquired fluorescence channels. An intensity threshold can either be set manually or can be determined via automated algorithms (Costes et al., 2004).

The last step of image pre-processing comprises the segmentation of acquired confocal images (French et al., 2008). In principle, quantitative colocalization analysis can be performed for whole images, but many biological processes are restricted to specific cell types or cellular compartments (French et al., 2008). Therefore image segmentation should be applied to limit the colocalization analysis to regions of interest (ROIs) only. This allows omitting image areas that are biologically irrelevant or that may contain saturated pixels (French et al., 2008). Similar to thresholding, segmentation can be carried out manually, semi-automatically or fully automatically with trade-offs in terms of accuracy and speed (French et al., 2008). After having carried out all steps of confocal image pre-processing the calculation of colocalization coefficients can be performed, followed by the last step of quantitative colocalization analysis, the data interpretation.

FRET-FLIM analysis

To quantitatively define localization and colocalization profiles is a major step in elucidating biological functions of proteins. Though, many physiological processes not only require colocalization, but inevitably dependent on the physical interaction of proteins. Due to the diffraction limit of light the spatial resolution of conventional microscopy is restricted to about 200-300 nm (Day et al., 2005), which makes it impossible to deduce protein-protein interactions from confocal images. Recent developments in fluorescence microscopy have been able to break this physical barrier leading to the so-called super-resolution imaging methods like structured illumination microscopy (SIM), photo-activated localization microscopy (PALM), or stimulated emission depletion (STED). Under standard

conditions superresolution imaging can improve the spatial resolution approximately by a factor of two. However, optimized setups are able to achieve a lateral resolution of about 20 nm in biological samples (Leung and Chou, 2011) and therefore allow describing biological processes at the molecular scale (Patterson et al., 2013). Although progress is made rapidly, to reach optimal resolution many applications of superresolution microscopy still rely on fixed samples. To overcome this limitation and to gain access to dynamic protein interactomes, confocal and multi-photon excitation microscopy have been combined with the Förster resonance energy transfer (FRET) methodology. FRET is a photo-physical process that describes the exited-state energy transfer from a donor fluorophore to an adjacent acceptor fluoro- or chromophore. This process requires an overlap of donor emission and acceptor excitation spectra as well as a favorable orientation of donor and acceptor transition dipole moments. Additionally, FRET is limited to low nanometer distances, the dimension of protein structures, since the energy transfer occurs non-radiatively via dipole-dipole coupling of the transition dipole moments. Therefore FRET offers a tool to investigate protein-protein interactions using light microscopy and can be applied to living systems.

There exist several methods for monitoring FRET in live cells. These methods are either fluorescence intensity-based like sensitized emission, ratio imaging or acceptor photo bleaching, based on fluorescence anisotropy or require fluorescence lifetime measurements (Yasuda, 2006; Borst and Visser, 2010). The fluorescence lifetime represents the average time an electron resides in the excited state before relaxing to the ground state of the fluorophore. In contrast to fluorescence intensity, the fluorescence lifetime is an intrinsic property of the fluorophore and is concentration-independent (Peter and Ameer-Beg, 2004). However, it is sensitive to changes in the microenvironment of fluorophores, which makes fluorescence lifetime measurements a suitable read-out for FRET (Breusegem et al., 2006). The presence of an acceptor molecule in the close proximity of an excited donor fluorophore creates an additional relaxation pathway via FRET and therefore results in a decreased donor fluorescence lifetime. Since fluorophore concentrations are hard to control and to determine in living cells and since only donor fluorescence lifetimes need to be recorded, fluorescence lifetime imaging microscopy (FLIM) is among the most robust and efficient methods to detect FRET (Nair et al., 2006). FRET-FLIM produces spatially resolved fluorescence lifetime images and enables the visualization of protein-protein interactions on subcellular level (Chang et al., 2007).

Experimentally, FLIM can be carry out in the time or frequency domain. The physical principles that underlie both methods are essentially identical, as they are finite Fourier transforms of each other (Sun et al., 2011). For frequency domain measurements the phase and amplitude modulations of the fluorescence emission with respect to the modulated excitation light are used to deduce the fluorescence lifetime. To determine fluorescence lifetimes in time domain experiments, high-speed detectors are synchronized with pulsed excitation light sources and the fluorescence decay profile at different time windows are

measured after each excitation pulse (Sun et al., 2011). Photons emitted from the donor fluorophore can either be detected in time bins generated by time-gated detection or by time-correlated single photon counting (TCSPC) (Morton and Parsons, 2011). In TCSPC the correlation between the photon arrival time at the detector and the time point of the excitation pulse are determined (Kemnitz et al., 1996). Repetitive sample excitation by the pulsed light source generates photon histograms that represent the fluorescence decay profile of the donor fluorophore (Morton and Parsons, 2011). Subsequently, fluorescence lifetimes are estimated by fitting exponential model functions to the fluorescence decay profiles (Sun et al., 2011). The most general and reliable method for analyzing time-resolved FLIM data is the nonlinear least square method (Lakowicz, 1999). The goal of this method is to minimize goodness of fit (χ^2) by varying the values of model parameters.

Traditionally, TCSPC-FLIM data are analyzed pixel by pixel. This means that for each pixel and fluorescence decay profile an individual fitting process is carried out to obtain the respective fluorescence lifetime. However, to obtain reliable and statistically relevant fluorescence lifetime values a sufficient photon count and signal-to-noise ratio is required. For distinguishing two fluorescence lifetimes, which are expected in a FRET experiment due to FRETting and non-FRETting donor populations, at least 1,000 photons are needed (Gratton et al., 2003). This can be problematic, in particular for live-cell imaging, since expression levels of fluorophores may be low and mild excitation light intensities are applied to avoid bleaching of fluorophores and photo-toxicity. Therefore often pixel binning is applied. However, this leads to a decrease in spatial resolution. To avoid lose of spatial resolution new analysis methods that significantly improve the signal-to-noise ratio have been developed in recent years (Grecco et al., 2009; Laptenok et al., 2010; Visser et al., 2010). These global analysis methods analyze the fluorescence decay profiles of all (selected) pixels in a time-resolved fluorescence intensity image simultaneously (Grecco et al., 2009). Therefore lower photon counts per pixel are acceptable, though, under the assumption that the fluorescence relaxation parameters are constant throughout the grouped pixels, which may not be valid for many experimental systems (Sun et al., 2011).

In this chapter, the different steps of quantitative colocalization analysis are described, followed by the comparison of two quantitative colocalization analysis methods with respect to their ability to discriminate variations in protein colocalization. The ImageJ plugins Coloc2 and PSC Colocalization were applied on two biological examples imaged in live Arabidopsis roots. Our comparative analysis indicated that both approaches are suitable for analyzing the colocalization of plasma membrane (PM)-located proteins as well as for revealing colocalizing populations located in small and dispersed endomembrane compartments.

In addition, a novel FRET-FLIM analysis procedure is introduced based on TCSPC-FLIM data and single pixel analysis performed with SPCImage (Becker & Hickl). It was especially designed to reveal small populations of interacting molecules as observed for the biological

example used here, the BRI1-SERK3 hetero-oligomerization in the PM of live Arabidopsis root cells. BRI1 and SERK3 are leucine-rich repeat receptor-like kinases (LRR-RLKs) that initiate as a protein complex brassinosteroid signal transduction upon ligand binding to BRI1 (Wang et al., 2008; Gou et al., 2012). Using our analysis approach allowed the identification of preformed receptor hetero-oligomers and induction of BRI1-GFP/SERK3-mCherry complexes in response to exogenously applied ligand. Due to the pixel-based analysis procedure also estimates of absolute receptor populations were obtained by coupling the FRET-FLIM results to available quantitative confocal imaging data.

RESULTS

Image pre-processing for quantitative colocalization analysis

Nowadays, various commercially or freely distributed software packages allow the estimation of colocalizing fractions in dual-color confocal images. In the following, we use the freely available ImageJ plugins Coloc2 and PSC Colocalization to perform quantitative and comparative colocalization analysis. These two plugins provide three major measures of colocalization as read-outs, the Manders colocalization coefficients (Coloc2) as well as Pearson correlation and Spearman rank coefficients (PSC Colocalization) (Dunn et al., 2011).

In general, quantification of colocalization between two fluorescently labeled proteins comprises four steps (Zinchuk et al., 2001). First, recorded confocal images need to be pre-processed in order to obtain images suitable for subsequent colocalization analysis. This step involves correction for background and/or noise as well as segmentation of images according to specific cellular structures. In this study, confocal images of Arabidopsis epidermal root cells, expressing either BRI1-GFP in combination with SERK3-mCherry or BRI1-GFP with two endosomal markers, were used to illustrate the different procedures essential for the calculation of colocalization coefficients. Next to the processed images the corresponding scatter plots, Pearson correlation and Spearman rank coefficients are given as indicators of the resulting image modifications.

Thresholding and denoising

To compensate for background and noise in digital images, mainly intensity thresholds for the recorded fluorescence channels are applied. In Figure 1 a comparison of three different thresholding approaches is shown. The first method applied was the PSC Colocalization plugin, which uses by default an intensity threshold of 40 gray levels for both image channels (Figure 1E-G) (French et al., 2008). This thresholding procedure affected mainly the low and more diffuse fluorescence signals derived from intracellular areas and led to a relatively strong decrease in Pearson correlation and Spearman rank coefficients compared

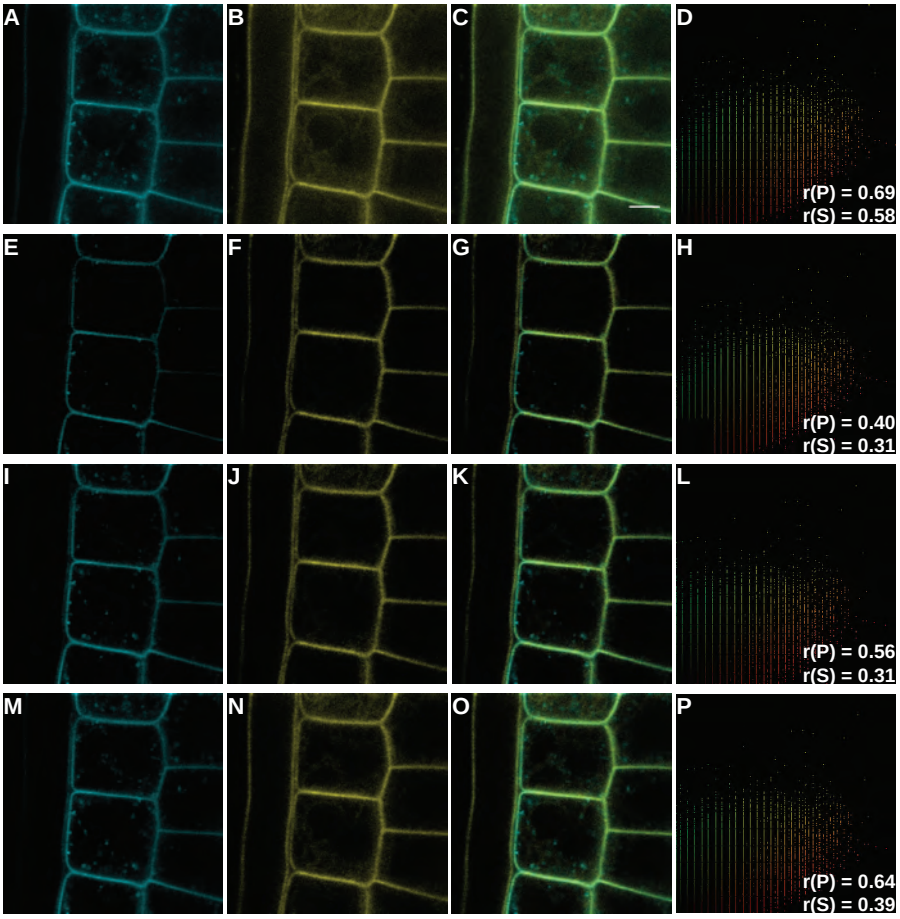

Figure 1: Different methods can be applied to correct for background in confocal images.
(**A-D**) Confocal images of BRI1-GFP (**A**) and SERK3-mCherry (**B**) fluorescence intensities as well as the merged image (**C**) and the corresponding scatter plot (**D**) without background correction.
(**E-H**) Confocal images of BRI1-GFP (**E**) and SERK3-mCherry (**F**) fluorescence intensities as well as the merged image (**G**) and the corresponding scatter plot (**H**) using a single intensity threshold of 40 for both fluorescence channels.
(**I-L**) Confocal images of BRI1-GFP (**I**) and SERK3-mCherry (**J**) fluorescence intensities as well as the merged image (**K**) and the corresponding scatter plot (**L**) using intensity thresholds of 21 and 30 for BRI1-GFP and SERK3-mCherry, respectively.
(**M-P**) Confocal images of BRI1-GFP (**M**) and SERK3-mCherry (**N**) fluorescence intensities as well as the merged image (**O**) and the corresponding scatter plot (**P**) using intensity thresholds of 12 and 17 for BRI1-GFP and SERK3-mCherry, respectively.
Confocal images were obtained from 5 day old Arabidopsis roots expressing BRI1-GFP and SERK3-mCherry under their native promoters. The scale bar represents a distance of 5 µm. The fluorescence intensity thresholds were set by applying the default settings of the PSC Colocalization plugin (E-H), by reference measurements using Col-0 wild type roots (I-L), or by applying the Coloc2 plugin based on the Costes approach (M-P). As indicators of colocalization Pearson correlation r(P) and Spearman rank coefficients r(S) calculated from whole images are given together with the scatter plots of the processed confocal images.

to the raw data (Figure 1H). In case of SERK3-mCherry, most of the information for intracellular localization was lost, whereas for BRI1-GFP still some intracellular endomembrane compartments were observed.

For the second approach the fluorescence intensity threshold was determined from confocal images of Col-0 wild type plants recorded under the same settings used for BRI1-GFP/SERK3-mCherry roots. The maximum fluorescence intensities for both channels were measured and set as background level for the corresponding BRI1-GFP/SERK3-mCherry images presented in Figure 1I-K. This resulted in intensity thresholds of 21 and 30 grey levels for the GFP and mCherry channels, respectively, and in comparison to the original images in reduced correlation and rank coefficients (Figure 1L). However, the Spearman coefficient was more drastically affected than the Pearson product moment. Application of these intensity thresholds still enabled to visualize intracellular SERK3-mCherry localization as well as BRI1-GFP containing endomembrane structures.

The third background correction procedure tested was the Costes approach (Costes et al., 2004). Here, an automated algorithm based on Pearson correlation determines the intensity thresholds for the separate fluorescence intensity channels. The individual thresholds are set to fluorescence intensity values, for which pixels with low intensities do not show any correlation, i.e. for which the Pearson correlation coefficient is close zero. This approach led to intensity threshold values of 12 for the GFP channel and 17 for the mCherry channel (Figure 1M-O). For both BRI1-GFP and SERK3-mCherry intracellular localization was preserved and the Pearson correlation coefficient was only mildly affected (Figure 1P). Similar to the two thresholding methods described above the Spearman coefficient was reduced more strongly compared to the value obtained from the original confocal images. Considering the information content of the images displayed in Figure 1 the Costes thresholding procedure resulted in the highest quality of processed images. The major advantage of this thresholding procedure is the independency of investigator bias. Additionally, the automation increases the speed of data processing. However, a drawback is that, like for the other thresholding approaches described above, a single intensity threshold is applied to the whole image. This may be inappropriate, in particular for studies of dispersed objects (Dunn et al., 2011).

To circumvent this drawback of a single threshold another method, called PureDenoise, was developed (Luisier et al., 2011). Assuming a mixed Poisson-Gaussian noise model, this algorithm performs data-adaptive thresholding by taking fluorescence intensities of neighboring pixels into account (Luisier et al., 2011). As shown in Figure 2, this denoising procedure is often accompanied by a loss of sharpness in the processed confocal images, but clearly improves the visibility of intracellular structures. Whereas the localization of SERK3-mCherry to the tonoplast is only weakly visible in the original confocal image (Figure 2B), it became more evident after image denoising (Figure 2F). Similar observations were also made for ARA6-mRFP, which labels late endosomes (LE) (see Figure 2J and 2N).

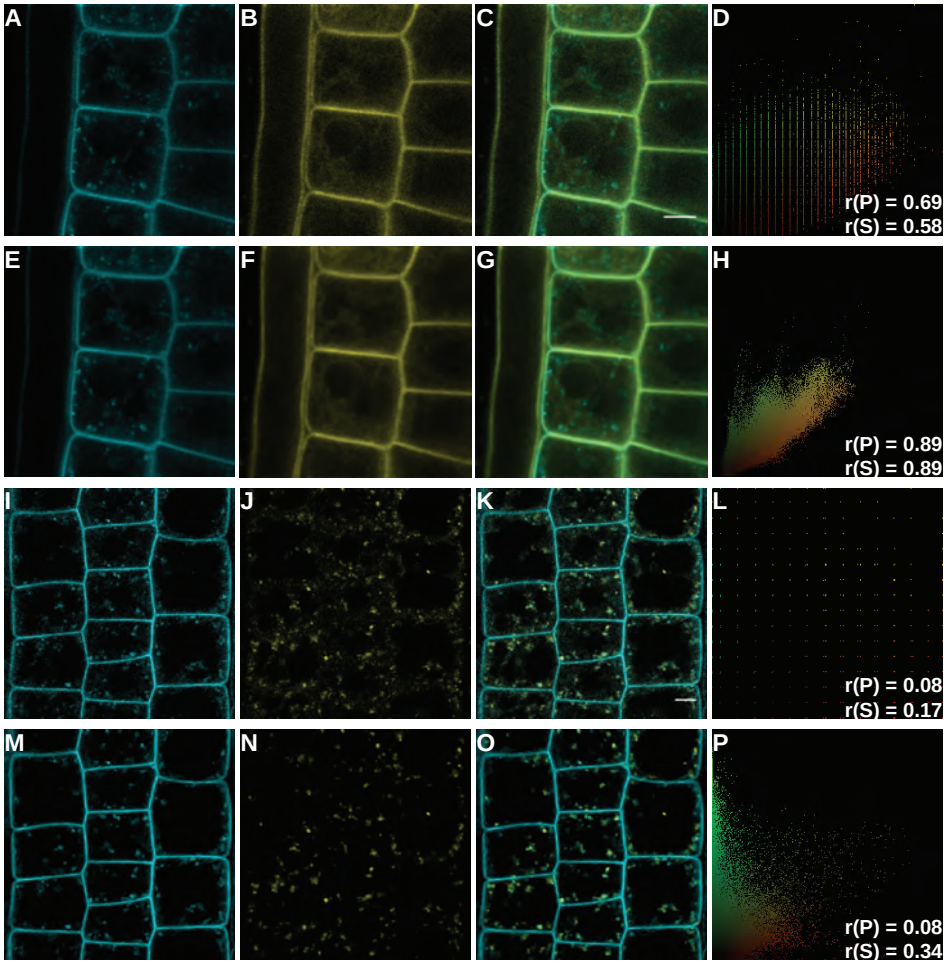

Figure 2: Denoising of confocal images result in increased colocalization.
(**A-D**) Original confocal images showing BRI1-GFP (**A**) and SERK3-mCherry (**B**) fluorescence intensities as well as the merged image (**C**) and the corresponding scatter plot (**D**).
(**E-H**) Denoised confocal images showing BRI1-GFP (**E**) and SERK3-mCherry (**F**) fluorescence intensities as well as the merged image (**G**) and the corresponding scatter plot (**H**).
(**I-L**) Original confocal images showing BRI1-GFP (**I**) and ARA6-mRFP (**J**) fluorescence intensities as well as the merged image (**K**) and the corresponding scatter plot (**L**).
(**M-P**) Denoised confocal images showing BRI1-GFP (**M**) and SERK3-mCherry (**N**) fluorescence intensities as well as the merged image (**O**) and the corresponding scatter plot (**P**).
Confocal images were obtained from 5 day old Arabidopsis roots expressing either BRI1-GFP and SERK3-mCherry or BRI1-GFP and ARA6-mRFP. Scale bars represent a distance of 5 µm. For denoising of the confocal images the ImageJ plugin PureDenoise was applied. As indicators of colocalization Pearson correlation r(P) and Spearman rank coefficients r(S) calculated from whole images are given together with the scatter plots of the processed confocal images.

After image denoising these endomembrane compartments were clearly distinguishable from background fluorescence.

In addition to the improved visual effect on intracellular structures, this procedure also led to increased correlation coefficients for colocalization. For whole image analysis a Pearson correlation values of 0.89 was obtained for BRI1-GFP and SERK3-mCherry (Figure 2H). For the colocalization of BRI1-GFP with ARA6-mRFP image processing did not improve the Pearson correlation, but a much higher Spearman correlation coefficient was obtained (Figure 2P). This discrepancy between Pearson correlation and Spearman rank coefficients may be attributed to the different mathematical concepts underlying the calculation of the two coefficients. Due to the reduced background the rank statistic for determining the Spearman coefficient changes resulting in an elevated rank coefficient. It also indicates that the relationship between the fluorescence intensities derived from the endosomal marker and BRI1-GFP is not linear. Taken together, image denoising can clearly help to visualize small and lower intensity structures, but may result in loss of sharpness of the processed images.

Image segmentation

Next to background and noise correction, image pre-processing usually also comprises image segmentation (Adler and Parmryd, 2013). Independent of the method used, a segmented confocal image may contain one or more regions of interest (ROIs) for which the colocalization is determined. In the case of BRI1 and SERK3 it was of particular interest to reveal colocalization at the PM, the main site of BRI1 signaling activity (Irani et al., 2012). The segmented confocal images and the obtained colocalization results are displayed in Figure 3, whereby only manual segmentation was applied. The colocalization analysis of the whole confocal image with intensity thresholds derived by the Costes approach (Figure 3A) served as a control and resulted in Pearson correlation and Spearman rank coefficients of 0.64 and 0.39, respectively (Figure 3B). First, three PM ROIs were selected and analyzed (Figure 3C and 3D). This led to a clear improvement of Spearman correlation, whereas the Pearson coefficient remained almost constant. A dramatic change of correlation was observed by selecting intracellular ROIs. Both correlation coefficients strongly decreased indicating only low correlation between BRI1-GFP and SERK3-mCherry intracellularly. This clearly shows the need of image segmentation. Subcellular colocalization patterns can be revealed and different colocalizing populations can be quantified as illustrated by the two LRR-RLKs BRI1-GFP and SERK3-mCherry. While these two receptors colocalize to a high degree at the PM, their intracellular pools show only little correlation. This observation was to expect, since BRI1 and SERK3 are both type I transmembrane proteins, but show distinct endomembrane localization patterns.

In Figure 3G - 3J the colocalization of BRI1-GFP with an endosomal marker protein was investigated demonstrating how image segmentation can improve colocalization analy-

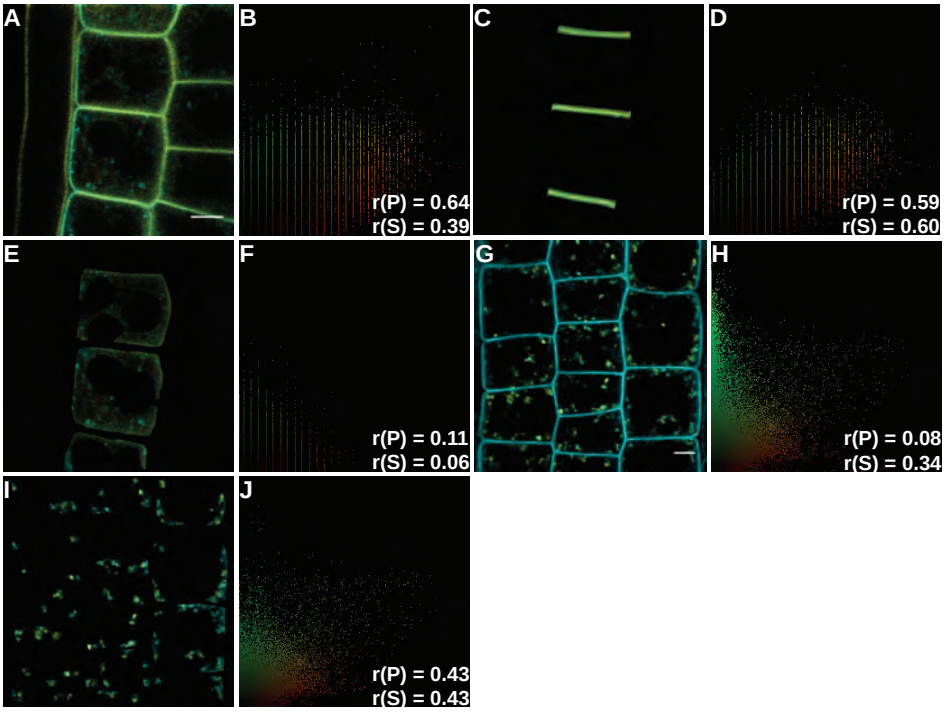

Figure 3: Segmentation of confocal images can reveal colocalization patterns.
(**A, B**) Merged confocal image showing BRI1-GFP and SERK3-mCherry fluorescence intensities after Costes thresholding (**A**) and the corresponding scatter plot (**B**).
(**C, D**) Segmentation mask (**C**) for selecting three plasma membrane areas of the merged confocal image shown in (**A**) and the corresponding scatter plot (**D**).
(**E, F**) Segmentation mask (**E**) for selecting cytosolic regions of the merged confocal image shown in (**A**) and the corresponding scatter plot (**F**).
(**G, H**) Merged confocal image showing BRI1-GFP and ARA6-mRFP fluorescence intensities after denoising (**G**) and the corresponding scatter plot (**H**).
(**I, J**) Segmentation mask (**I**) for selecting cytosolic regions of the merged confocal image shown in (**G**) and the corresponding scatter plot (**J**).
Confocal images were obtained from 5 day old Arabidopsis roots expressing either BRI1-GFP and SERK3-mCherry or BRI1-GFP and ARA6-mRFP. Scale bars represent a distance of 5 µm. As indicators of colocalization Pearson correlation r(P) and Spearman rank coefficients r(S) calculated from whole images or the indicated regions of interest are given together with the scatter plots of the processed confocal images.

sis. Analysis of intracellular ROIs only resulted in a clear colocalization of both proteins (Figure 3J). However, based on whole image analysis BRI1-GFP showed only a relatively moderate colocalization with ARA6-mRFP, reflected by a Pearson correlation coefficient of 0.08 and a Spearman coefficient of 0.34 (Figure 3H). The drastic change due to segmentation can be explained by the predominant localization of BRI1-GFP at the PM, where ARA6-mRFP is absent. Thus by analyzing the unsegmented image most of the BRI1-GFP fluorescence is uncorrelated to the intracellular fluorescence of the endomembrane marker.

Calculating colocalization coefficients

Based on the findings of image pre-processing, two complete colocalization analysis procedures are described in the following section. First the colocalization coefficients of BRI1-GFP with ARA6-mRFP and ARA7-mRFP were determined. ARA6 (Rab F1) and ARA7 (Rab F2b) are commonly used as markers for endosomal compartments. Whereas ARA7 labels both early and late endosomes (EE and LE), ARA6 mainly localizes to LE (Ueda et al.,

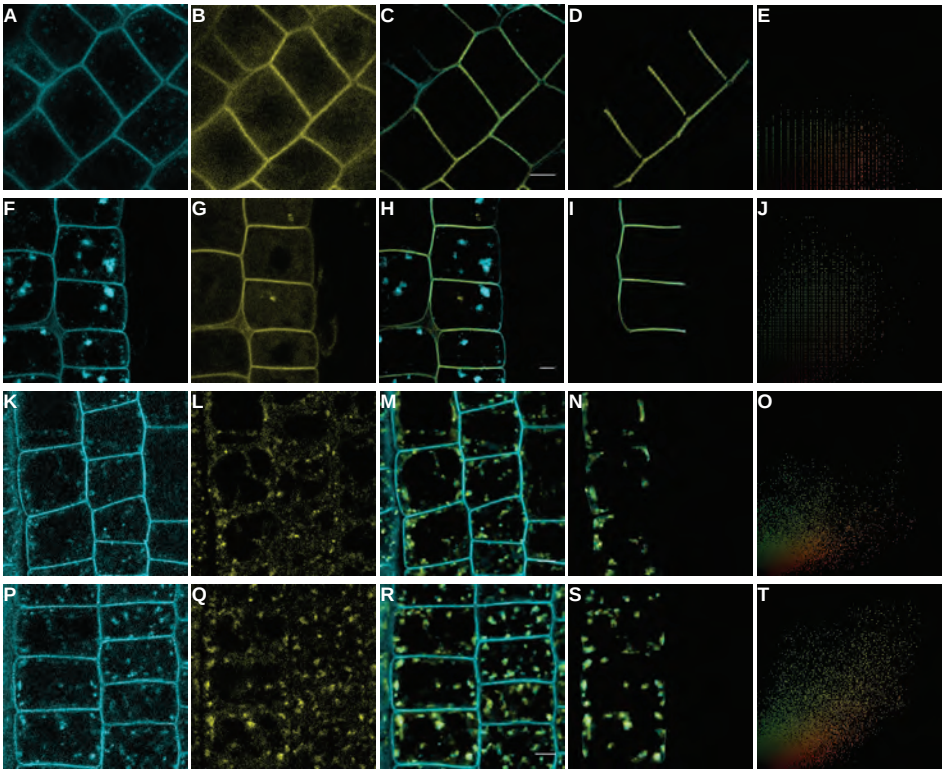

Figure 4: Quantitative colocalization analysis reveals increased BRI1/SERK3 PM colocalization in response to BFA and preferential localization of BRI1 to ARA7-labeled endomembrane compartments.

(**A-E**) Original confocal images of BRI1-GFP (**A**) and SERK3-mCherry (**B**) after BRZ treatment (5 µM, 2 days) as well as the merged image after Costes thresholding (**C**), the selection mask for PM regions (**D**), and the corresponding scatter plot (**E**).

(**F-J**) Original confocal images of BRI1-GFP (**F**) and SERK3-mCherry (**G**) after BRZ+BFA treatment (5 µM, 2 days; 50 µM, 1 h) as well as the merged image after Costes thresholding (**H**), the selection mask for PM regions (**I**), and the corresponding scatter plot (**J**).

(**K-O**) Original confocal images of BRI1-GFP (**K**) and ARA6-mRFP (**L**) as well as the denoised merged image (**M**), the selection mask for cytosolic regions (**N**), and the corresponding scatter plot (**O**).

(**P-T**) Original confocal images of BRI1-GFP (**P**) and ARA7-mRFP (**Q**) as well as the denoised merged image (**R**), the selection mask for cytosolic regions (**S**), and the corresponding scatter plot (**T**).

Confocal images were obtained from 5 day old Arabidopsis roots expressing either BRI1-GFP/SERK3-mCherry, BRI1-GFP/ARA6-mRFP or BRI1-GFP/ARA7-mRFP. The scale bars represent a distance of 5 µm.

2004; Ebine et al., 2011). As shown in Figure 5K-T, the fluorescence intensities of BRI1-GFP and the both endosomal markers clearly overlapped.

Initially, the confocal images were manually assessed, to obtain reference values for the subsequent computational colocalization analysis. The endosomal structures for both image channels were counted individually and the overlap ratio with respect to the total amount of marker labeled endomembrane compartments was calculated. The manual analysis indicated predominate localization of BRI1-GFP with ARA7-mRFP (Table 1A). Approximately 55% of ARA7-positive endosomes contained BRI1-GFP receptors, whereas this receptor colocalized to only 40% to ARA6-mRFP labeled structures.

Computational colocalization analysis between BRI1-GFP and ARA6-mRFP or ARA7-mRFP, respectively, was performed using the two ImageJ plugins Coloc2 and PSC Colocalization. The analysis was restricted to the endomembrane compartments labeled by the two marker proteins. Using the Coloc2 plugin, which is based on Costes thresholding, revealed the same trend as observed for our manual analysis (Table 1A and 1B). Both read-outs, the Manders colocalization coefficients and the corresponding Pearson correlation coefficient, reflected the preferential colocalization of BRI1-GFP and ARA7-mRFP. Low correlation coefficients were obtained for both combinations, which made the interpretation of these results difficult. Therefore the same data sets were also analyzed using the PSC Colocalization plugin. Prior to the calculation of colocalization coefficients the separate fluorescence intensity channels were denoised. Subsequently, a threshold of 10 was applied and the same ROIs as selected for the Coloc2 approach were analyzed. As shown in Table 1C, also this method led to the conclusion that BRI1-GFP preferentially colocalized to ARA7-positive endosomal structures. Moreover, the analysis performed with PSC Colocalization revealed a positive correlation between BRI1-GFP and the two fluorescently tagged marker proteins. It yielded Pearson correlation and Spearman rank coefficients of 0.49 and 0.44, respectively, for BRI1-GFP with ARA6-mRFP. In contrast, analysis of BRI1-GFP/ARA7-mRFP images resulted in 30% increased colocalization coefficients, clearly indicating that BRI1-GFP localizes predominantly to endomembrane compartments characterized by the marker protein ARA7-mRFP.

Besides for establishing subcellular colocalization patterns, quantitative colocalization analysis can also be applied to investigate the overlap or correlation between two proteins of interested, which may for example function in the same signal transduction pathway. Here, the colocalization of BRI1-GFP and SERK3-mCherry at the PM of root epidermal cells was determined before and after BFA treatment. BFA is a fungal toxin known to inhibit the secretory pathway. Recently, Irani et al. (2012) reported an additional feature of BFA by showing the stabilization of BRI1 at the PM in response to this drug. To address whether this effect of BFA can translate in changes of colocalization between BRI1 and SERK3 comparative colocalization analysis was performed. First the Coloc2 analysis was applied using ROIs along the PM. The colocalization analysis indeed revealed elevated overlap

Table 1: Quantitative colocalization analysis for the localization of BRI1-GFP to different endomembrane compartments.

Confocal images of 5 day Arabidopsis roots expressing either BRI1-GFP and ARA6-mRFP or BRI1-GFP and ARA7-mRFP were analyzed either manually or using the ImageJ plugins Coloc2 and PSC Colocalization. Only selected cytosolic areas were subjected to colocalization analysis. The average colocalization coefficients are represented ± standard deviations. "N" represents the number of roots analyzed.

(**A**) Confocal images were manually analyzed by counting the endosomal compartments for the separate image channels. The overlap was calculated as ratio between colocalizing endosomes and total number of marker endomembrane compartments.

(**B**) Original confocal images were analyzed using the Coloc2 analysis tool. "M" represents the Manders colocalization coefficients without a threshold, "tM" represents the Manders colocalization coefficients after intensity thresholds were set according to the Costes approach, and "r(Pearson)" represents the corresponding Pearson correlation coefficient. Pearson correlation coefficients are given for confocal images without threshold, for image contents below threshold, and for the image content above threshold. Thus the r(Pearson) values for above threshold fluorescence intensities correspond to the obtained tM values.

(**C**) The presented values were obtained using the PSC Colocalization analysis tool. "r(Pearson)" and "r(Spearman)" represent the Pearson correlation and Spearman rank coefficients, respectively. The colocalization coefficients were calculated either based on Costes thresholds, a single threshold of 40 for both fluorescence intensity channels, or after image denoising was performed.

A	Overlap [%]	
	ARA6-mRFP	ARA7-mRFP
BRI1-GFP	35 ± 12	55 ± 7[a]

B	M [%]		tM [%]		r(Pearson)			
	BRI1-GFP	Marker-mRFP	BRI1-GFP	Marker-mRFP	without	below	above	N
BRI1-GFP/ ARA6-mRFP	0.92 ± 0.01	0.86 ± 0.06	0.46 ± 0.06	0.42 ± 0.06	0.41 ± 0.23	0.04 ± 0.03	-0.12 ± 0.10	4
BRI1-GFP/ ARA7-mRFP	0.95 ± 0.02	0.90 ± 0.04	0.60 ± 0.07[a]	0.62 ± 0.04[a]	0.44 ± 0.06	0.01 ± 0.06	0.13 ± 0.04	5

C	Costes Thresholds		40 Thresholds		Denoised		
	r(Pearson	r(Spearman)	r(Pearson	r(Spearman)	r(Pearson	r(Spearman)	N
BRI1-GFP/ARA6-mRFP	0.01 ± 0.12	-0.22 ± 0.11	-0.11 ± 0.12	0.02 ± 0.32	0.50 ± 0.12	0.42 ± 0.14	4
BRI1-GFP/ARA7-mRFP	0.23 ± 0.09[a]	0.03 ± 0.09[a]	0.12 ± 0.13[a]	-0.03 ± 0.10	0.69 ± 0.09[a]	0.66 ± 0.09[a]	5

[a] The mean difference is significant at the $p < 0.05$ level compared to BRI1-GFP/ARA6-mRFP (one-tailed Student's t-test for equal variance).

of BRI1-GFP and SERK3-mCherry fluorescence in response to BFA (Table 2A). The initial Manders colocalization coefficients of 0.71 and 0.77 for BRI1-GFP and SERK3-mCherry, respectively, obtained for the control measurements increased in the presence of BFA to 0.89 and 0.87, accordingly. The elevated colocalization of the two receptors after drug

treatment was also reflected by the increase of the corresponding Pearson correlation coefficient from 0.23 to 0.52.

PSC Colocalization in combination with denoised confocal images revealed a similar trend (Table 2B). Though, the differences of Pearson correlation and Spearman rank coefficients were only minor and no significant difference in response to changed physiological conditions were obtained. In contrast, applying the default settings of PSC Colocalization or the fluorescence intensity thresholds revealed by the Costes approach resulted in similar findings as observed using Coloc2 (Table 2B). It seems that denoising of the PMs resulted in an adaptation of the high and continuous fluorescence intensities and thus a loss of local intensity fluctuations. Therefore we conclude that both analysis procedures are applicable for the analysis of highly intense and continuously labeled fluorescent structures but that image denoising should be omitted in this case.

Taken together, colocalization analysis enabled us to quantitatively assess subcellular localization patterns and monitor changes in colocalization with respect to altered physi-

Table 2: Quantitative colocalization analysis of BRI1/SERK3 PM colocalization.
Confocal images of 5 day Arabidopsis roots expressing BRI1-GFP and SERK3-mCherry were analyzed using the ImageJ plugins Coloc2 and PSC Colocalization. Only selected PM areas were subjected to colocalization analysis. The average colocalization coefficients are represented ± standard deviations. "N" represents the number of roots analyzed.
(**A**) The presented values were obtained using the Coloc2 analysis tool. "M" represents the Manders colocalization coefficients without a threshold, "tM" represents the Manders colocalization coefficients after intensity thresholds were set according to the Costes approach, and "r(Pearson)" represents the corresponding Pearson correlation coefficient. Pearson correlation coefficients are given for confocal images without threshold, for image contents below threshold, and for the image content above threshold. Thus the r(Pearson) values for above threshold fluorescence intensities corresponds to the obtained tM values.
(**B**) The presented values were obtained using the PSC Colocalization analysis tool. "r(Pearson)" and "r(Spearman)" represent the Pearson correlation and Spearman rank coefficients, respectively. The colocalization coefficients were calculated either based on Costes thresholds, a single threshold of 40 for both fluorescence intensity channels, or after image denoising was performed.

A	M [%]		tM [%]		r(Pearson)			
	BRI1-GFP	SERK3-mCherry	BRI1-GFP	SERK3-mCherry	without	below	above	N
BRZ+mock	1.0 ± 0.00	1.0 ± 0.00	0.71 ± 0.06	0.77 ± 0.06	0.51 ± 0.10	-0.01 ± 0.01	0.23 ± 0.18	5
BRZ+BFA	1.0 ± 0.00	1.0 ± 0.00	0.89 ± 0.02[a]	0.87 ± 0.05[a]	0.67 ± 0.11	-0.01 ± 0.01	0.52 ± 0.19	5

B	Costes Thresholds		40 Thresholds		Denoised		
	r(Pearson	r(Spearman)	r(Pearson	r(Spearman)	r(Pearson	r(Spearman)	N
BRZ+mock	0.27 ± 0.16	0.21 ± 0.19	0.47 ± 0.10	0.48 ± 0.09	0.77 ± 0.15	0.80 ± 0.15	5
BRZ+BFA	0.54 ± 0.18[a]	0.54 ± 0.18[a]	0.54 ± 0.14	0.55 ± 0.15	0.78 ± 0.11	0.82 ± 0.08	5

[a] The mean difference is significant at the $p < 0.05$ level compared to BRI1-GFP/ARA6-mRFP (one-tailed Student's t-test for equal variance).

ological conditions as illustrated in our study. Although the biological interpretation of individual colocalization coefficients may be difficult, a comparative analysis allows quantitative conclusions.

FRET analysis based on fluorescence lifetimes

Confocal microscopy allows defining spatiotemporal protein (co)localization patterns based on fluorescence intensities as shown above. However, for fulfilling their biological functions proteins often require the direct interaction with other cellular components. Colocalization is a good indicator for the spatial association of proteins in the same subcellular compartment but cannot reveal if proteins physically interact. FRET is a well-established read-out for detecting protein interactions and the most quantitative and reliable fluorescence parameter for visual investigation of interactions in live cells is fluorescence lifetime microscopy (FLIM). This additional parameter of fluorescence microscopy allows sensing the immediate environment of a fluorophore and reduction of donor fluorescence indicates the physical association of the fluorescently labeled proteins. Therefore the hetero-oligomerization of BRI1-GFP and SERK3-mCherry in the PM of live Arabidopsis epidermal cells was studied using FRET-FLIM. The experimental setup and the regular data analysis procedure based on the SPCImage software (Becker & Hickl) have already been described in Bücherl et al. (2010). For that reason only the final results of the FRET-FLIM analysis are presented here. The fluorescence lifetime of the GFP moiety of BRI1-GFP along the PM of epidermal cells in BRZ-treated roots, thus under conditions of abolishes BR signaling (Yin et al., 2002), was determined to approximately 2.40 ns (Table 3). As can be seen in Figure 5A, the GFP fluorescence lifetime was not completely homogenous but showed local variations most likely due to changes in the immediate environment of BRI1-GFP located in different areas of the PM. In the presence of SERK3-mCherry, the FRET acceptor, these donor fluorescence lifetime variations remained but additionally restricted areas within the PM with strongly reduced GFP fluorescence lifetimes became visible (Figure 5B). In these areas GFP fluorescence lifetimes of 2.0 ns and lower were obtained, indicating FRET between the GFP and mCherry moieties linked to BRI1 and SERK3, respectively. Estimation of the average GFP fluorescence lifetime along the PM resulted in a value of about 2.27 ns, equivalent to a FRET efficiency of approximately 5% (Table 3).

Subsequently, fluorescence lifetime analysis was performed on samples treated with brassinolide (BL), an agonist for BRI1. Stimulation of BR signaling activity by exogenous application of BRI1 ligand resulted in a donor fluorescence lifetime of around 2.38 ns along the PM (Table 3). A color-coded FLIM image is presented in Figure 5C and shows local variations of the GFP fluorescence lifetime similar to the BRZ-treated situation. Also for the donor/acceptor samples, i.e. expression of SERK3-mCherry in the BRI1-GFP background, similar results as for BRZ only treated samples were obtained. However, the areas of strongly reduced GFP fluorescence lifetimes increased, whereby the reduction of donor

Table 3: Quantitative FRET-FLIM analysis for BRI1/SERK3 hetero-oligomerization.
FLIM was performed on 5 day old Arabidopsis roots expressing either BRI1-GFP or BRI1-GFP in combination with SERK3-mCherry. Seedlings were grown for 3 days on solid half-strength MS medium and were subsequently transferred to liquid half-strength MS containing 5 µM BRZ to deplete endogenous BRs. For activation of BR signaling 24-epi-brassinolide (BL) was applied in a concentration of 1 µM for 1 h prior to imaging. For imaging roots were imbedded in liquid half-strength MS containing 5 µM BRZ or additionally 1 µM BL. The τ values given represent donor fluorescence lifetimes of the GFP moiety of BRI1-GFP or PIN2-GFP, respectively, in ps ± S.E.M. The values given for interaction pixels (IPS) represent the percentage of pixels with strongly reduced BRI-GFP fluorescence lifetimes ± S.E.M. The corrected IPS values were obtained by subtracting the IPS values of the negative control from the initially determined BRI1-GFP/SERK3-mCherry IPS values. "N" represents the number of analyzed fluorescence lifetime images.

	BRZ				BRZ+BL			
	τ [ps]	FRET [%]	IPS [%]	N	τ [ps]	FRET [%]	IPS [%]	N
BRI1-GFP	2398 ± 4			69	2379 ± 4			72
BRI1-GFP+SERK3-mCherry	2272 ± 6[a]	5.2 ± 0.3[b]	7.6 ± 0.6[b]	57	2226 ± 6[a]	6.4 ± 0.2[b,c]	13.0 ± 1[b,c]	64
PIN2-GFP	2271 ± 20			24	2321 ± 54			20
PIN2-GFP+SERK3-mCherry	2253 ± 9[a]	0.8 ± 0.5	0.9 ± 0.2	22	2262 ± 45[a]	2.5 ± 0.3	2.5 ± 0.3	19
	corrected IPS [%]							
BRI1-GFP+SERK3-mCherry	6.7				10.5			

[a] The mean difference is significant at the $p < 0.05$ level compared to donor only (PIN2-GFP or BRI1-GFP) samples (two-tailed Student's t-test for unequal variance).
[b] The mean difference is significant at the $p < 0.05$ level compared to PIN2-GFP+SERK3-mCherry samples (two-tailed Student's t-test for equal variance).
[c] The mean difference is significant at the $p < 0.05$ level compared to BRZ-treated BRI1-GFP 2+SERK3-mCherry samples (two-tailed Student's t-test for equal variance).

fluorescence lifetime remained constant (Figure 5D). An average GFP fluorescence lifetime of about 2.23 ns was estimated at the PM (Table 3). Thus the FRET efficiency was elevated from approximately 5% for BRZ-treated samples to roughly 6% after activating the BR signaling system. To verify that these low values of FRET efficiencies indeed represent physical interaction between BRI1-GFP and SERK3-mCherry the results were compared to a negative control. PIN2-GFP was used as FRET donor and mCherry linked to SERK3 was kept as acceptor. The resulting fluorescence lifetimes and corresponding FRET efficiencies are presented in Table 3. Due to the statistical significant difference between the FRET efficiencies of the BRI1-GFP/SERK3-mCherry combination with respect to the negative control, we conclude a true interaction for our proteins of interest confirming the results obtained by coimmunoprecipitation (Wang et al., 2005; Albrecht et al., 2012).

Taken together, conventional analysis of time-resolved fluorescence intensity images revealed the interaction of BRI1-GFP and SERK3-mCherry in planta. Additionally, it was possible to monitor a slight increase of BRI1-SERK3 hetero-oligomers in response to ex-

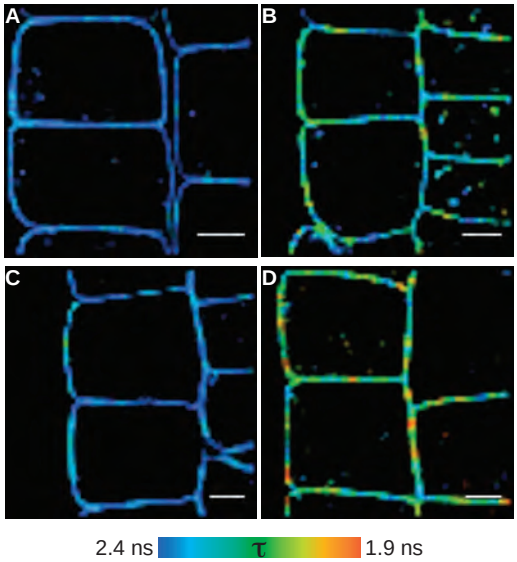

Figure 5: Fluorescence lifetime based FRET-FLIM analysis reveals ligand-independent and ligand-dependent BRI1-SERK3 hetero-oligomers.
(**A, B**) Color-coded fluorescence lifetime images of BRI1-GFP (**A**) and BRI1-GFP in the presence of SERK3-mCherry (**B**) after BRZ treatment.
(**C, D**) Color-coded fluorescence lifetime images of BRI1-GFP (**C**) and BRI1-GFP in the presence of SERK3-mCherry (**D**) after BRZ+BL treatment (1 µM, 1 h).
FLIM was performed on 5 day old Arabidopsis roots expressing either BRI1-GFP or BRI1-GFP/SERK3-mCherry. Seedlings were grown for 3 days on solid half-strength MS medium and were subsequently transferred to liquid half-strength MS medium containing 5 µM BRZ. 24-epi-brassinolide was used for activating BR signaling. The scale bars represent a distance of 5 µm and the color bar indicates the color code for the fluorescence lifetime images.

ogenous ligand application and to localize the interacting receptors within the PM of live epidermal root cells. However, the results are qualitative and show only a minor variation of FRET efficiency upon full stimulation of the biological system, which hampers the biological interpretation.

Revealing interacting populations based on pixel analysis

To gain a more detailed view on the hetero-oligomerization of BRI1-GFP and SERK3-mCherry a novel analysis procedure for time-resolved fluorescence intensity images was established, which allowed linking the obtained FRET-FLIM results to quantitative confocal microscopy data (Wilma van Esse et al., 2011). Combining the results of FLIM with absolute numbers of BRI1 and SERK3 receptor molecules present in the PM of epidermal root cells enabled revealing the interacting populations of the two LRR-RLKs.

The extended analysis procedure started with the regular analysis of FLIM data as described in Bücherl et al. (2010). Samples containing donor only, here BRI1-GFP, were ana-

lyzed with a mono-exponential decay model using the SPCImage software (Becker & Hickl). The GFP fluorescence lifetime in the presence of SERK3-mCherry was estimated using a bi-exponential decay function assuming FRETting and non-FRETting donor populations. Due to modest photon counts per pixel a binning factor of one was applied, which means that also the surrounding pixels were taken into account for the fluorescence lifetime calculation. For further analysis the obtained data sets for photon counts, fluorescence lifetimes and goodness-of-fit (χ^2) were exported to Excel (Windows Office) data sheets. Each pixel in the time-resolved fluorescence intensity images was therefore characterized by the three parameters binned photon counts, fluorescence lifetime and goodness-of-fit. Based on these parameters pixels were selected to ensure reliable and statistical relevant results. Only pixels with binned photon counts above 1,200, fluorescence lifetimes ranging from 1.6 to 2.9 ns, and goodness-of-fit values below 2.5 were taken into account for further analysis. Using these criteria mainly pixels resembling the PM of the imaged epidermal root cells were selected (Figure 6). From the respective pixel ensembles the average donor fluorescence lifetimes were obtained (Table 3).

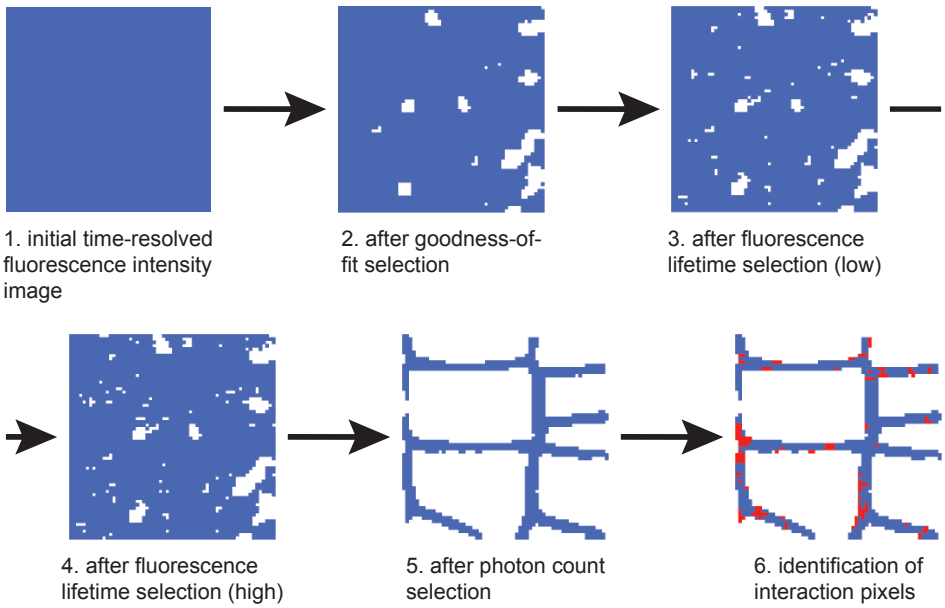

Figure 6: Schematic workflow of the introduced quantitative FRET-FLIM analysis procedure. The scheme shows the sequential steps that lead to the identification of interaction pixels (IPS) from a time-resolved fluorescence intensity image derived by TCSPC data acquisition. By setting selection criteria for goodness-of-fit, fluorescence lifetimes and photon counts only pixels representing the PM of Arabidopsis epidermial root cells are maintained. The identification of IPS in donor/acceptor images is based on fluorescence lifetime interaction thresholds obtained by donor reference measurements. Pixels shown in blue fulfilled the respective selection criteria, whereas pixels shown in red resemble the identified IPS.

To establish a fluorescence lifetime threshold for pixels that contain interacting or FRETting receptor molecules the analysis proceeded firstly with donor samples only. For each BRI1-GFP fluorescence image the apparent maximal FRET efficiency [E_{app}(max)] was determined using the minimal and average fluorescence lifetime of the selected pixel ensemble. The average fluorescence lifetime and maximal E_{app}(max) of each donor data set in turn enabled the calculation of the fluorescence lifetime interaction threshold for the corresponding donor/acceptor data set.

Subsequently, the established interaction threshold was applied as a further selection criterion for donor and acceptor containing samples and allowed to determine the number of interaction pixels (IPS), pixels showing strongly reduced donor fluorescence lifetimes, from the already pre-selected pixel ensemble. By forming the ratio between IPS and the total number of pre-selected pixels the percentage of IPS per FLIM image was calculated.

Using this analysis procedure an IPS value of about 7.6% for BRZ-treated BRI1-GFP/SERK3-mCherry samples was determined (Table 3). Application of exogenous BL resulted in an increase of IPS to approximately 13% (Table 3). However, these initial values still had to be corrected for background, which was estimated using the PIN2-GFP/SERK3-mCherry control measurements, leading to approximately 6.7% of IPS in a BRZ-treated situation and roughly 10% upon activation of BRI1-mediated BR signaling (Table 3). Hence, by applying the refined analysis procedure the dynamic range of the FRET-FLIM measurements was improved. Furthermore, since the calculation was pixel-based coupling to quantitative confocal microscopy data was possible.

Recently, the absolute numbers of fluorescently tagged BRI1 and SERK3 receptors in Arabidopsis roots have been revealed (van Esse et al., 2011). Using the imaging parameters applied for FLIM enabled an estimation of interacting receptor populations and revealed that in a confocal section around 176 or 263 BRI1-GFP were in complex with SERK3-mCherry after BRZ-treatment or upon BL stimulation, respectively. Thus the combination of semi-quantitative FRET-FLIM analysis and quantitative confocal imaging allows an approximation of absolute interacting receptor molecules, instead of a qualitative description of interaction only.

Collectively, we showed that numerical analysis of fluorescence microscopic images can reveal (co)localization and interaction patterns if suitable approaches are applied. By quantitatively assessing colocalization and hetero-oligomerization of the BR signaling components BRI1 and SERK3 even minor variations in response to changed physiological conditions could be extracted. These features are inevitable for elucidating the mode of action of any cellular component.

DISCUSSION

In the current investigation, we introduced a novel FRET-FLIM analysis procedure and compared two quantitative colocalization analysis approaches in their ability to discriminate different colocalizing protein populations. Using these low-invasive light-microscopic methods enabled us to reveal mechanistic details about BRI1-SERK3 hetero-oligomerization and the colocalization patterns of BRI1 in respect to two endosomal marker proteins as well as changes in BRI1/SERK3 colocalization upon drug treatment. Importantly, both FRET-FLIM and colocalization analyses were performed on fluorescence images obtained from live Arabidopsis epidermal root cells, expressing BRI1 and SERK3 under control of their native promoters and in their natural habitat.

Analysis of time-resolved fluorescence images

The current models of BR signal transduction and BRI1-SERK3 association have mainly been based on coimmunoprecipitation studies performed on whole seedlings (Wang et al., 2005; 2008; Albrecht et al., 2012). These models propose strictly ligand-dependent recruitment of SERK3 to basally activated BRI1 receptors (Wang et al., 2008; Chinchilla et al., 2009; Kim and Wang, 2010; Jaillais et al., 2011). Using FRET-FLIM allowed us to visualize this oligomer formation in live Arabidopsis root epidermal cells, the proposed sites of active BR signaling (Hacham et al., 2011). In line with these models, our data showed the induction of BRI1-SERK3 hetero-oligomers upon BL application. The added value of investigating the oligomerization of the two LRR-RLKs using an imaging approach was the possibility to spatially resolve the location of these receptor complexes within 2-dimensional fluorescence lifetime images. That way we revealed that BRI1-SERK3 hetero-oligomers are present in heterogeneously distributed and spatially restricted PM areas of root epidermal cells. Similar findings were reported for the mammalian receptor tyrosine kinase (RTK) epidermal growth factor receptor (EGFR). Application of live cell imaging (Bader et al., 2009; Abulrob et al., 2010) and electron microscopy (Hsieh et al., 2010; Rong and Reinhard, 2011) showed the clustering of EGFRs in the PM of mammalian cells.

Notably, Bader et al. (2009) could additionally observed that around 40% of PM-residing EGFR receptors form ligand-independent dimers, a phenomenon reported for several mammalian PM receptor families (Ehrlich et al., 2011; Van Craenenbroeck et al., 2011). Constitutive receptor oligomerization was recently also reported in plants (Shimizu et al., 2010). This study showed preformation of the chitin-sensing receptors in rice (Shimizu et al., 2010). Interestingly, preformation of receptor hetero-oligomers was proposed for the BR signaling unit BRI1-SERK3 as well (Wang et al., 2005), however it was not further investigated at that time. Our FRET-FLIM data provide evidence that BRI1 and SERK3 exhibit similar interaction patterns as observed for mammalian and the rice PM receptors. After

BRZ treatment dispersed BRI1-SERK3 hetero-oligomers were maintained in the PM of the imaged epidermal root cells.

Using the conventional FRET-FLIM analysis procedure we speculated that ligand depletion may lead to a slight reduction in receptor complexes, indicated by the decrease of the average FRET efficiency from around 6% in the presence of BL to approximately 5% after strongly reduced ligand availability. However, due to the minor differences in FRET efficiencies interpretation of the obtained results was difficult. To obtain quantitative measures for BRI1-SERK3 hetero-oligomers under the different physiological conditions we established a novel analysis procedure. This approach determines the number of interaction pixels (IPS) within a fluorescence lifetime image and revealed that approximately 70% of BRI1-SERK3 PM receptor complexes were preformed. Stimulation of BR signaling by exogenous ligand application resulted in an increase of IPS to approximately 10%, compared to about 6.7% under BRZ-cultured conditions. These findings are in line with recently reported in silico modeling data (van Esse et al., 2012) and semi-quantitative coimmunoprecipitation experiments (Albrecht et al., 2012) suggesting that only a low percentage of BRI1 receptors are participating in active BR signal transduction.

Since our FRET-FLIM analysis procedure is pixel-based it also allowed coupling the protein interaction results to available quantitative confocal microscopy data (van Esse et al., 2011). By combining the results of both imaging approaches we estimated that around 263 of the PM-located BRI1 receptors are in physical contact with SERK3 coreceptors after BL addition. Being able to approximate absolute interacting protein populations and to discriminate quantitatively between different phyisiological conditions clearly shows the advantages of applying imaging techniques in particular FRET-FLIM for investigating signaling events.

Recent developments in FLIM methodologies like acceptor rise time measurements in combination with global analysis (Grecco et al., 2009; Laptenok et al., 2010; Visser et al., 2010) in principle offer similar read-outs. Global analysis assumes discrete fluorescence lifetimes for the interacting and non-interacting populations. Using this analysis procedure results in amplitudes for donor fluorescence lifetimes representing FRETting and non-FRETting populations. These amplitudes in turn correspond to certain pixel or molecule fractions and thus the amount of oligomers can be approximated. This situation can be easily achieved in cuvette experiments. Though, for measurements in live cells it may be a too harsh assumption (Sun et al., 2011).

A very promising alternative for in vivo measurements is the acceptor rise time method. Here, the fluorescence rise time of the FRET acceptor fluorophore can be simultaneously recorded along the fluorescence lifetime decrease of the donor molecule. This provides a direct measure for energy absorbing acceptor populations. Even though this approach allows quantitative read-outs and provides an excellent internal control, the technical feasibility still needs progress. Thus the introduced approach, which can be applied to

conventional FLIM setups and data processing software, offers an easy applicable alternative for obtaining quantitative FRET-FLIM measures.

However, our refined analysis procedure also has its limitations. The selection criteria applied to extract IPS cannot be generalized and need to be considered for each application. Setting a fluorescence lifetime interaction threshold for determining IPS may result in an underestimation of interacting species. Only pixels with strongly reduced donor fluorescence lifetimes are taken into account, whereas weak interactions remain unconsidered. To damp this effect no absolute fluorescence lifetime limit was used, but instead the interaction threshold was determined for each data set analyzed. Similar considerations apply for the low and high fluorescence lifetime borders. Taking too small or too large fluorescence lifetime intervals can result in over- and underestimations of oligomer containing pixels. A careful manual assessment of the recorded time-resolved fluorescence intensity images is required and individual decay profiles have to be inspected. Depending on the pixel resolution used for FLIM also the goodness-of-fit limit may be adjusted. Since in the present example a pixel resolution of 64 x 64 was used the goodness-of-fit value was set to 2.5. However, when using higher pixel resolutions lower values may be applicable. Even though individual selection criteria need to be reconsidered for different FRET-FLIM data sets, the principles of our analysis procedure can be universally applied to fluorescence lifetime measurements.

Analysis of confocal images

Next to the quantitative analysis of protein-protein interactions in fluorescence microscopic images, also quantitative colocalization analysis was performed during this study. Colocalization of BRI1-GFP with ARA6-mRFP and ARA7-mRFP labeled endosomal compartments enabled us to discriminate different endocytotic BRI1 popluations. Furthermore, we demonstrated increased BRI1-GFP/SERK3-mCherry colocalization at the PM of live epidermal root cells upon BFA treatment. Due to the PM-stabilizing effect of BFA on BRI1 receptors (Irani et al., 2012) this increased colocalization between the two BR signaling components was not unexpected. But the finding that both Manders colocalization coefficients increased after drug treatment additionally suggests PM stabilization of SERK3 in response to BFA. Thus retention of receptors or proteins at the PM may be a general effect of the fungal toxin BFA, similar as observed for the protein translational inhibitor cyclohexamide (Geldner, 2011).

The observation that BRI1-GFP preferentially colocalized with ARA7-mRFP positive endosomal structures most likely reflects the ligand-independent recycling of BRI1, as previously demonstrated (Geldner et al., 2007). However, Geldner et al. (2007) did not support their findings by colocalization analysis of BRI1 with endosomal marker proteins like ARA6 and ARA7. Recently, constitutive recycling was also reported for the plant immune receptor Flagellin sensing 2 (FLS2) (Beck et al., 2012). In line with our findings, also this LRR-RLK

predominately localizes to ARA7-mRFP endosomal structures while exhibiting recycling (Beck et al., 2012). A biological explanation for these observations may be given by the identity of the ARA6- and ARA7-containing endomembrane compartments. ARA6 localizes mainly to LE (Ueda et al., 2004; Ebine et al., 2011), which are determined for vacuolar fusion and subsequent protein degradation. In contrast, ARA7 resides in LE as well as EE (Ueda et al., 2004; Ebine et al., 2011). The latter are part of the cellular recycling machinery (Reyes et al., 2011). Since ARA7 labels compartments both for recycling and degradation it is reasonable to find an increased amount of BRI1 receptors in the respective endosomal structures.

To verify that the obtained colocalization coefficients indeed originate from a true co-localization between the fluorescently labeled proteins, one of the image channels was rotated by 90 ° prior to image analysis. Under this condition only random colocalization is observed and therefore such images can be used as a negative control (Dunn et al., 2011). This analysis setup abolished the colocalization for BRI1-GFP and the two marker proteins completely, independent of the applied analysis approach (data not shown).

Colocalization analysis can be a powerful tool to quantitatively assess the information present in confocal images. Though, a common difficulty of this type of analysis is the interpretation of the acquired colocalization coefficients. This accounts especially for intermediate Pearson correlation and Spearman rank coefficients (Dunn et al., 2011). Even though the Pearson correlation coefficient is considered as the most quantitative measure for colocalization, Manders colocalization coefficients are sometimes seen as the biological more meaningful read-outs (Costes et al., 2004). One of the reasons is the assumption of a linear relationship between the analyzed fluorescence intensities, which forms the basis of Pearson correlation coefficients, but is often not fulfilled in biological samples (Adler and Parmryd, 2010; Dunn et al., 2011). Moreover, Manders colocalization coefficients provide two separate measures for the two images, which is of particular value if the two proteins of interest differ largely in their expression levels (Manders et al., 1993). However, Manders colocalization coefficients are largely independent of the fluorescence intensities and only represent overlapping pixel fractions. Here, the Pearson correlation coefficient is superior, which determines correlation between fluorescence intensities and thereby considers signal strengths (Dunn et al., 2011). Another advantage of the Pearson correlation coefficient is the low sensitivity for background and noise (Adler and Parmryd, 2010; Dunn et al., 2011). To circumvent misinterpretations of Pearson-based colocalization analysis due to the assumption of linearity a modified version of the Pearson correlation coefficient can be applied, the Spearman rank coefficient. Thus, in summary neither the Manders colocalization coefficients nor the Pearson correlation and Spearman rank coefficients are superior to the other (Dunn et al., 2011).

This indeed was observed during our comparative colocalization analysis. Both applied analysis approaches resulted in similar colocalization read-outs demonstrating the

reliability of the two applied methods. However, an influence of image pre-processing on the resulting colocalization coefficients was noted. Image denoising led to dramatically increased Pearson correlation and Spearman rank coefficients for the analysis of endosomal compartments. On the contrary, this processing procedure resulted in a loss of colocalization sensitivity for the analyzed PM fragments. Both effects can most likely be attributed to the underlying processing algorithm. In the case of the dispersed and intense endomembrane compartments the consideration of neighboring pixel intensities during thresholding enhances the signal-to-noise ratio (Luisier et al., 2011). Hence, by suppressing the low and uncorrelated background signals, the correlation between intense endosomal compartments is enhanced. For the intense and continuously fluorescently labeled PMs, in turn, denoising leads to an equalization of fluorescence intensities and thereby a loss of local intensity fluctuations. Thus denoising is a suitable thresholding procedure for dispersed cellular structures and can clearly improve the colocalization analysis. But this procedure should be omitted in conjunction with bright and continuous fluorescent entities.

Based on our comparative colocalization analyses, we conclude that both tools are applicable to investigate localization and colocalization patterns in living plant tissues. Even though the interpretation of individual colocalization coefficients may be difficult, a comparative analysis of image data sets, recorded under the same imaging conditions, offers the possibility of reliable and quantitative colocalization read-outs (Dunn et al., 2011). Which approach to choose, depends on the spatial profile of the fluorescently labeled cellular structures and the colocalization read-outs aimed for.

Collectively, we could show that the choice of appropriate quantitative image analysis methods enables identifying even minor variations in colocalization and interaction patterns. Using our novel FRET-FLIM analysis procedure moreover allowed the approximation of absolute interacting protein species. This clearly demonstrates how quantitative fluorescence microscopy can improve our understanding of molecular processes by illuminating proteins in their natural habitat.

MATERIALS AND METHODS

Growth conditions and plant lines

Arabidopsis (Arabidopsis thaliana) plants (ecotype Columbia [Col-0]) were used as wild type. Seeds were surface sterilized and germinated on ½ Murashige and Skoog medium (Duchefa) supplemented with 1% sucrose (Sigma) and 0.8% Daishin agar (Duchefa). Plants were grown at 22 °C under fluorescent light, with 16 h light/8 h dark photoperiods, unless otherwise specified. Transgenic seedlings were selected on ½ Murashige and Skoog medium containing either 50 mg/L kanamycin (Duchefa), 15 mg/L phosphinothricin (PPT, Duchefa) or both. Col-0 plants expressing BRI1 fused to GFP under its native promoter re-

sulting in an about three-fold overexpression were provided by J. Chory (Friedrichsen et al., 2000). The double-transgenic BRI1-GFP/SERK3-mCherry line was generated as described previously (Chapter 3). ARA6-mRFP and ARA7-mRFP lines were obtained from K. Schumacher (Heidelberg, Germany). Double-transgenic BRI1-GFP lines coexpressing ARA6-mRFP or ARA7-mRFP were generated by crossing and F1 generations were used for imaging.

Confocal imaging

Live root imaging was performed on five day old seedlings using a confocal laser scanning microscope (Leica TCS SP5 X system, Mannheim, Germany). Confocal imaging was performed using internal filter-free spectral photomultiplier tube (PMT) detectors. GFP was excited using an argon laser (488 nm) and fluorescence emission was detected from 500-540 nm. mCherry and mRFP were excited using a white light continuum laser selecting the 580 nm laser line. Fluorescence was detected from 590-640 nm. Images were captured using a 63x water immersion objective with a numeric aperture of 1.2 with a pinhole set to 1 Airy unit. Confocal images were analyzed with FIJI software (ImageJA 1.45j, Max Planck Society).

Brassinazole (BRZ, TCI Europe) was applied in a final concentration of 5 µM (25 mM stock solution in 80% ethanol) dissolved in liquid ½ Murashige and Skoog medium (Duchefa) and supplemented with 1% sucrose (Sigma). For BRZ treatment seedlings were transferred 3 days after germination to 24-well plates containing 1 mL of liquid ½ Murashige and Skoog medium (Duchefa) and supplemented with 1% sucrose (Sigma) containing 5 µM BRZ per well and seedlings were cultured for two additional days.

Brefeldin A (BFA) was applied in a final concentration of 50 µM (50 mM stock solution in DMSO) dissolved in liquid ½ Murashige and Skoog medium (Duchefa) and supplemented with 1% sucrose (Sigma). The incubation time was 1 h.

For live root imaging roots were embedded in liquid ½ Murashige and Skoog medium (Duchefa) supplemented with 1% sucrose (Sigma) and the respective agents.

FRET-FLIM

A Leica TCS SP5 X system equipped with a 63x 1.20 NA water-immersion objective lens was used for confocal/FLIM imaging. Confocal and FLIM images were acquired by exciting the respective fluorophores GFP/mCherry using a white-light laser (WLL; or super continuum laser). This laser emits a continuous spectrum from 470 to 670 nm, within which any individual excitation wavelength in 1 nm increments can be selected.

For FRET- FLIM experiments, the WLL (470 nm) at a pulsed frequency of 40 MHz was used. For recording of donor fluorescence, an external fiber output was connected to the Leica SP5 X scan head and coupled to a Hamamatsu HPM-100-40 Hybrid detector (Becker & Hickl), which has a time resolution of 120 ps. Selection of GFP fluorescence was performed using a band pass filter 505-545 nm. Images with a frame size of 64 x 64 pixels were acquired with acquisition times of up to 90 sec.

From the fluorescence intensity images the decay curves were calculated per pixel and fitted with either a mono- or double-exponential decay model using the SPCImage software (Becker & Hickl, version 3.2.3.0). The mono-exponential model function was applied for donor samples with only GFP present. For samples containing two fluorophores, GFP and mCherry, respectively, a double-exponential model function was used without fixing any parameter.

To calculate the fraction of interaction pixels (IPS), fluorescence intensity and the corresponding fluorescence lifetime data for each pixel were exported from SPCImage and imported into an Excel spreadsheet (Microsoft® Excel® for Mac 2011, version 14.1.3). Quantification of interacting pixels was set according to the following criteria. The photon counts per pixel must be at least 1,200 counts in total using a binning factor of 1, ensuring a statistically required peak value (± 200 counts) in the respective photon histogram used for fluorescence lifetime calculation. To ensure a reliable fit, only pixels with $\chi^2 < 2.5$ were selected. Additionally, fluorescence lifetimes below 1.6 ns and above 2.6 ns respectively were excluded from the calculation of interacting fractions. The reason for setting these values was to avoid false positive or negative interactions. The total amount of pixels for each fluorescence intensity image was set after applying these above-mentioned criteria resulting almost exclusively in pixels representing PM or adjacent areas. Subsequently, the average donor fluorescence lifetimes were determined. The individual minimum of a set of measurements was used to calculate the interaction threshold, which usually corresponded to a FRET-efficiency of about 13%. Only pixels with fluorescence lifetimes below the interaction threshold were collected as interaction pixels. The ratio between interaction pixels and total amount of selected pixels represented the value of interaction pixels (IPS).

Colocalization analysis

Colocalization analysis of images acquired by confocal laser scanning microscopy was performed using the software FIJI (ImageJA 1.45j, Max Planck Society). The plugin "Coloc 2" allows the quantitative determination of colocalizing fluorescence intensities acquired in different channels using the methods of Manders and Costes (Manders et al., 1993; Costes et al., 2004). The obtained modified Manders coefficients were used as fraction of colocalization for both channels, i.e. colocalization of BRI1-GFP with SERK3-mCherry or the endosomal markers ARA6-mRFP and ARA7-mRFP and vice versa. Next to modified Manders coefficients, Pearson correlation coefficients were obtained as a second measure for colocalization.

Additionally, the FIJI plugin "PSC Colocalization" (French et al., 2008) was applied. Using this method Pearson correlation and Spearman rank coefficients are obtained as colocalization read-outs. Confocal images were either denoised and an intensity threshold of 10 grey levels was applied prior to the calculation of colocalization coefficients or raw images and the intensity thresholds as mentioned were applied.

Statistical Analysis

Statistical analysis was performed using the Excel® sofware (Microsoft® Excel® for Mac 2011, version 14.1.3).

Accession Numbers

Sequence data from this chapter can be found in the Arabidopsis Genome Initiative or EMBL/GenBank data libraries under accession numbers: BRI1 (AT4G39400), SERK3/BAK1 (AT4G22430), ARA6/RABF1 (AT3G54840) and ARA7/RABF2B (AT4G19640).

REFERENCES

Abulrob, A., Lu, Z., Baumann, E., Vobornik, D., Taylor, R., Stanimirovic, D., and Johnston, L.J. (2010). Nanoscale imaging of epidermal growth factor receptor clustering: effects of inhibitors. J. Biol. Chem. **285**: 3145–3156.

Adler, J. and Parmryd, I. (2013). Colocalization analysis in fluorescence microscopy. Methods Mol. Biol. **931**: 97–109.

Adler, J. and Parmryd, I. (2010). Quantifying colocalization by correlation: The Pearson correlation coefficient is superior to the Mander's overlap coefficient. Plant J. **77A**: 733–742.

Albrecht, C., Boutrot, F., Segonzac, C., Schwessinger, B., Gimenez-Ibanez, S., Chinchilla, D., Rathjen, J.P., de Vries, S.C., and Zipfel, C. (2012). Brassinosteroids inhibit pathogen-associated molecular pattern-triggered immune signaling independent of the receptor kinase BAK1. Proc. Natl. Acad. Sci. U.S.A. **109**: 303–308.

Bader, A.N., Hofman, E.G., Voortman, J., en Henegouwen, P.M.P.V.B., and Gerritsen, H.C. (2009). Homo-FRET imaging enables quantification of protein cluster sizes with subcellular resolution. Biophys. J. **97**: 2613–2622.

Beck, M., Zhou, J., Faulkner, C., Maclean, D., and Robatzek, S. (2012). Spatio-Temporal Cellular Dynamics of the Arabidopsis Flagellin Receptor Reveal Activation Status-Dependent Endosomal Sorting. Plant Cell. doi: 10.1105/tpc.112.100263

Bolte, S. and Cordelières, F.P. (2006). A guided tour into subcellular colocalization analysis in light microscopy. J. Microsc. **224**: 213–232.

Borst, J.W. and Visser, A.J.W.G. (2010). Fluorescence lifetime imaging microscopy in life sciences. Meas. Sci. Technol. **21**: 102002.

Breusegem, S.Y., Levi, M., and Barry, N.P. (2006). Fluorescence correlation spectroscopy and fluorescence lifetime imaging microscopy. Nephron Exp. Nephrol. **103**: e41–9.

Chang, C.-W., Sud, D., and Mycek, M.-A. (2007). Fluorescence lifetime imaging microscopy. Methods Cell Biol. **81**: 495–524.

Chinchilla, D., Shan, L., He, P., de Vries, S., and Kemmerling, B. (2009). One for all: the receptor-associated kinase BAK1. Trends Plant Sci. **14**: 535–541.

Costes, S.V., Daelemans, D., Cho, E.H., Dobbin, Z., Pavlakis, G., and Lockett, S. (2004). Automatic and quantitative measurement of protein-protein colocalization in live cells. Biophys. J. **86**: 3993–4003.

Day, R.N., Day, R.N., Schaufele, F., and Schaufele, F. (2005). Imaging molecular interactions in living cells. Mol. Endocrinol. **19**: 1675–1686.

Dunn, K.W., Kamocka, M.M., and McDonald, J.H. (2011). A practical guide to evaluating colocalization in biological microscopy. AJP: Cell Physiol. **300**: C723–C742.

Ebine, K., Fujimoto, M., Okatani, Y., Nishiyama, T., Goh, T., Ito, E., Dainobu, T., Nishitani, A., Uemura, T., Sato, M.H., Thordal-Christensen, H., Tsutsumi, N., Nakano, A., and Ueda, T. (2011). A membrane trafficking pathway regulated by the plant-specific RAB GTPase ARA6. Nat. Cell Biol. **13**: 853–859.

Ehrlich, M., Horbelt, D., Marom, B., Knaus, P., and Henis, Y.I. (2011). Homomeric and heteromeric complexes among TGF-β and BMP receptors and their roles in signaling. Cell. Signal. **23**: 1424–1432.

Fletcher, P.A., Scriven, D.R.L., Schulson, M.N., and Moore, E.D.W. (2010). Multi-image colocalization and its statistical significance. Biophys. J. **99**: 1996–2005.

French, A.P., Mills, S., Swarup, R., Bennett, M.J., and Pridmore, T.P. (2008). Colocalization of fluorescent markers in confocal microscope images of plant cells. Nat. Protoc. **3**: 619–628.

Geldner, N. (2011). Quantifying degradation rates of transmembrane receptor kinases. Methods Mol. Biol. **779**: 217–224.

Geldner, N., Hyman, D.L., Wang, X., Schumacher, K., and Chory, J. (2007). Endosomal signaling of plant steroid receptor kinase BRI1. Genes Dev. **21**: 1598–1602.

Gou, X., Yin, H., He, K., Du, J., Yi, J., Xu, S., Lin, H., Clouse, S.D., and Li, J. (2012). Genetic evidence for an indispensable role of somatic embryogenesis receptor kinases in brassinosteroid signaling. PLoS Genet. **8**: e1002452.

Gratton, E., Breusegem, S., Sutin, J., Ruan, Q., and Barry, N. (2003). Fluorescence lifetime imaging for the two-photon microscope: time-domain and frequency-domain methods. J. Biomed. Opt. **8**: 381–390.

Grecco, H.E., Roda-Navarro, P., and Verveer, P.J. (2009). Global analysis of time correlated single photon counting FRET-FLIM data. Opt. Express **17**: 6493–6508.

Hacham, Y., Holland, N., Butterfield, C., Ubeda-Tomas, S., Bennett, M.J., Chory, J., and Savaldi-Goldstein, S. (2011). Brassinosteroid perception in the epidermis controls root meristem size. Development **138**: 839–848.

Hsieh, M.-Y., Yang, S., Raymond-Stinz, M.A., Edwards, J.S., and Wilson, B.S. (2010). Spatio-temporal modeling of signaling protein recruitment to EGFR. BMC Syst. Biol. **4**: 57.

Irani, N.G., Di Rubbo, S., Mylle, E., Van den Begin, J., Schneider-Pizoń, J., Hniliková, J., Síša, M., Buyst, D., Vilarrasa-Blasi, J., Szatmari, A.-M., Van Damme, D., Mishev, K., Codreanu, M.-C., Kohout, L., Strnad, M., Caño-Delgado, A.I., Friml, J., Madder, A., and Russinova, E. (2012). Fluorescent castasterone reveals BRI1 signaling from the plasma membrane. Nat. Chem. Biol. **8**: 583–589.

Jaillais, Y., Belkhadir, Y., Balsemão-Pires, E., Dangl, J.L., and Chory, J. (2011). Extracellular leucine-rich repeats as a platform for receptor/coreceptor complex formation. Proc. Natl. Acad. Sci. U.S.A. **108**: 8503–8507.

Kemnitz, K., Pfeifer, L., Paul, R., Fink, F., and Bergmann, A. (1996). Time- and space-correlated single-photon-counting spectroscopy. In H.-J. Foth, R. Marchesini, H. Podbielska, M. Robert-Nicoud, and H. Schneckenburger, eds (SPIE), pp. 2–11.

Kim, T.-W. and Wang, Z.-Y. (2010). Brassinosteroid signal transduction from receptor kinases to transcription factors. Annu. Rev. Plant Biol. **61**: 681–704.

Laptenok, S.P., Borst, J.W., Mullen, K.M., van Stokkum, I.H.M., Visser, A.J.W.G., and van Amerongen, H. (2010). Global analysis of Förster resonance energy transfer in live cells measured by fluorescence lifetime imaging microscopy exploiting the rise time of acceptor fluorescence. Phys. Chem. Chem. Phys. **12**: 7593–7602.

Leung, B.O. and Chou, K.C. (2011). Review of super-resolution fluorescence microscopy for biology. Appl. Spectrosc. **65**: 967–980.

Luisier, F., Blu, T., and Unser, M. (2011). Image denoising in mixed Poisson-Gaussian noise. IEEE Trans. Image. Process. **20**: 696–708.

Manders, E., Verbeek, F., and Aten, J. (1993). Measurement of Colocalization of Objects in Dual-Color Confocal Images. J. Microsc. **169**: 375–382.

Morton, P.E. and Parsons, M. (2011). Measuring FRET using time-resolved FLIM. Methods Mol. Biol. **769**: 403–413.

Nair, D.K., Jose, M., Kuner, T., Zuschratter, W., and Hartig, R. (2006). FRET-FLIM at nanometer spectral resolution from living cells. Opt. Express **14**: 12217–12229.

Patterson, G., Davidson, M., Manley, S., and Lippincott-Schwartz, J. (2013). Superresolution Imaging using Single-Molecule Localization. Annu. Rev. Phys. Chem. **61**: 345–367.

Peter, M. and Ameer-Beg, S.M. (2004). Imaging molecular interactions by multiphoton FLIM. Biol. Cell **96**: 231–236.

Reyes, F.C., Buono, R., and Otegui, M.S. (2011). Plant endosomal trafficking pathways. Curr. Opin. Plant Biol. **14**: 666–673.

Rong, G.G. and Reinhard, B.M.B. (2011). Monitoring the size and lateral dynamics of ErbB1 enriched membrane domains through live cell plasmon coupling microscopy. PLoS ONE **7**: e34175–e34175.

Shimizu, T., Nakano, T., Takamizawa, D., Desaki, Y., Ishii-Minami, N., Nishizawa, Y., Minami, E., Okada, K., Yamane, H., Kaku, H., and Shibuya, N. (2010). Two LysM receptor molecules, CEBiP and OsCERK1, cooperatively regulate chitin elicitor signaling in rice. Plant J. **64**: 204–214.

Sun, Y., Day, R.N., and Periasamy, A. (2011). Investigating protein-protein interactions in living cells using fluorescence lifetime imaging microscopy. Nat. Protoc. **6**: 1324–1340.

Ueda, T., Uemura, T., Sato, M.H., and Nakano, A. (2004). Functional differentiation of endosomes in Arabidopsis cells. Plant J. **40**: 783–789.

Van Craenenbroeck, K., Borroto-Escuela, D.O., Romero-Fernandez, W., Skieterska, K., Rondou, P., Lintermans, B., Vanhoenacker, P., Fuxe, K., Ciruela, F., and Haegeman, G. (2011). Dopamine D4 receptor oligomerization--contribution to receptor biogenesis. FEBS J. **278**: 1333–1344.

van Esse, G.W., van Mourik, S., Stigter, H., Hove, ten, C.A., Molenaar, J., and de Vries, S.C. (2012). A mathematical model for BRASSINOSTEROID INSENSITIVE1-mediated signaling in root growth and hypocotyl elongation. Plant Physiol. **160**: 523–532.

van Esse, G., Westphal, A.H., Surendran, R.P., Albrecht, C., van Veen, B., Borst, J.W., and de Vries, S.C. (2011). Quantification of the brassinosteroid insensitive1 receptor in planta. Plant Physiol. **156**: 1691–1700.

Visser, A.J.W.G., Laptenok, S.P., Visser, N.V., van Hoek, A., Birch, D.J.S., Brochon, J.-C., and Borst, J.W. (2010). Time-resolved FRET fluorescence spectroscopy of visible fluorescent protein pairs. Eur. Biophys. J. **39**: 241–253.

Wang, X., Goshe, M.B., Soderblom, E.J., Phinney, B.S., Kuchar, J.A., Li, J., Asami, T., Yoshida, S., Huber, S.C., and Clouse, S.D. (2005). Identification and functional analysis of in vivo phosphorylation sites of the Arabidopsis BRASSINOSTEROID-INSENSITIVE1 receptor kinase. Plant Cell **17**: 1685–1703.

Wang, X., Kota, U., He, K., Blackburn, K., Li, J., Goshe, M.B., Huber, S.C., and Clouse, S.D. (2008). Sequential transphosphorylation of the BRI1/BAK1 receptor kinase complex impacts early events in brassinosteroid signaling. Dev. Cell **15**: 220–235.

Yasuda, R. (2006). Imaging spatiotemporal dynamics of neuronal signaling using fluorescence resonance energy transfer and fluorescence lifetime imaging microscopy. Curr. Opin. Neurobiol. **16**: 551–561.

Yin, Y., Wang, Z.-Y., Mora-Garcia, S., Li, J., Yoshida, S., Asami, T., and Chory, J. (2002). BES1 accumulates in the nucleus in response to brassinosteroids to regulate gene expression and promote stem elongation. Cell **109**: 181–191.

Zinchuk, V. and Grossenbacher-Zinchuk, O. (2011). Quantitative colocalization analysis of confocal fluorescence microscopy images. Curr. Protoc. Cell Biol. **Chapter 4**: Unit4.19.

Zinchuk, V. and Grossenbacher-Zinchuk, O. (2009). Recent advances in quantitative colocalization analysis: focus on neuroscience. Prog. Histochem. Cytochem. **44**: 125–172.

Zinchuk, V. and Zinchuk, O. (2008). Quantitative colocalization analysis of confocal fluorescence microscopy images. Curr. Protoc. Cell Biol. **Chapter 4**: Unit 4.19.

Zinchuk, V., Zinchuk, O., and Okada, T. (2007). Quantitative Colocalization Analysis of Multicolor Confocal Immunofluorescence Microscopy Images: Pushing Pixels to Explore Biological Phenomena. Acta Histochem. Cytochem. **40**: 101–111.

Zou, K.H., Tuncali, K., and Silverman, S.G. (2003). Correlation and Simple Linear Regression. Radiology **227**: 617–628.

Chapter 5

Illuminating BRI1 and BAK1(SERK3) endosomal trafficking

Christoph A. Bücherl[1], Lingzi Li[1], Corrado Viotti[4,5], Sacco C. de Vries[1], Jan Willem Borst[1,2,3]

[1] Laboratory of Biochemistry and [2] Microspectroscopy Centre, Department of Agrotechnology and Food Sciences, Wageningen, The Netherlands

[3] Centre for BioSystems Genomics, Wageningen, The Netherlands

[4]Centre for Organismal Studies, Heidelberg, Germany

[5]present: Department of Plant Physiology, Umeå, Sweden

ABSTRACT

Brassinosteroid (BR) signaling in Arabidopsis requires the hetero-oligomerization of the ligand-perceiving receptor BRI1 and its SERK coreceptors. Recently, it was shown that BRI1 and SERK3 reside as constitutive receptor complexes in the plasma membrane (PM) of root epidermal cells. However, it is still unknown where or when receptor hetero-oligomers are established. Here, we performed a comparative colocalization analysis for the two LRR-RLKs and revealed that both receptors colocalized during anterograde and retrograde trafficking. In addition, application of FRET-FLIM enabled us to identify BRI1-SERK3 hetero-oligomers early after biogenesis in restricted areas of the endoplasmic reticulum membrane system and on the secretory pathway. We conclude that SERK3 and BRI1 hetero-oligomers are established shortly after biosynthesis and that these preformed BR signaling units are inserted into the PM of root epidermal cells.

INTRODUCTION

Steroid hormone signaling plays an essential role in growth and development of animals and plants (Bishop and Koncz, 2002). In contrast to animal cells, which perceive steroids by cytosolic receptors (Jensen and DeSombre, 1973), ligand binding in plant cells occurs at the plasma membrane (PM) (Kinoshita et al., 2005). Brassinosteroids (BRs) bind to the extracellular island domain of the leucine-rich repeat (LRR) receptor-like kinase (RLK) Brassinosteroid Insensitive 1 (BRI1) resulting in partial activation of the cytosolic BRI1 kinase domain by auto-phosphorylation (Wang et al., 2008). Auto-phosphorylated BRI1 kinase subsequently trans-phosphorylates the BRI1-Kinase Inhibitor 1 (BKI1), which causes dissociation of BKI1 from the ligand bound receptor (Jaillais et al., 2011b). Successively, BRI1 can associate with another LRR-RLK, BRI1-associated kinase 1 (BAK1, Li et al., 2002; also known as SERK3 for Somatic Embroygenesis Receptor-like Kinase 3) (Wang et al., 2008; Jaillais et al., 2011a). Through trans-phosphorylation events within this receptor complex BRI1 gains its full kinase and signaling activity. This way, extracellular perception of BRs by BRI1 at the PM can be transduced intracellularly via phosphorylation-dependent cascades and eventually regulates gene transcription via the action of BZR1 and BES1/BZR2 in a BR-dependent fashion (Wang et al., 2002; Yin et al., 2002; Yin et al., 2005; Kim et al., 2009).

However, recent findings have led to modifications of the BR signaling model, in particular concerning the early steps of BRI1-mediated signal transduction, the BRI1-BAK1(SERK3) hetero-oligomerization and the origin of signal propagation. Geldner et al. (2007) proposed BRI1 to signal predominantly from endosomal compartments, whereas Irani et al. (2012) showed that the main signaling activity originates from PM-localized BRI1 receptors. Gou et al. (2012) provided further details for BRI1-mediated signal transduction by demonstrating the essential role of the SERK1 (Shah et al., 2001), BAK1(SERK3), and BAK1-like 1 (BKK1, He et al., 2007; also known as SERK4) coreceptors for initiating downstream BR signaling, instead of only enhancing basal BRI1 activity (Wang et al., 2008). This implies that hetero-oligomerization of BRI1 and SERK coreceptors is a prerequisite for BR signal transduction and that BRI1-coreceptor complexes form a BR signaling unit. Additionally, our recent work (Bücherl et al., submitted) showed that BRI1-BAK1(SERK3) hetero-oligomers reside in the PM independent of ligand, and are internalized in complex. The biological consequences of receptor complex preformation are however not fully understood.

Assembly of receptor complexes or subunits prior to localization at the site of signal perception has so far only been shown in mammalian systems. Subunits of the kainate receptor (KAR), for example, oligomerize early after biogenesis in the endoplasmic reticulum (ER) followed by their targeted transport through the Golgi apparatus to the PM (Ma-Högemeier et al., 2010). Similar observations were made for the PM-localizing type I and II transforming growth factor beta (TGFβ) receptors. Both types form homodimers already in the ER and persist at the PM (Gilboa et al., 1998). A possible explanation for

such early receptor complex formation may be additional quality control in the ER. Besides correct folding also initial functionality of the receptor oligomers could be verified before entering the secretory pathway to the PM (Fleck, 2006; Achour et al., 2008).

Popescu (2012) has recently proposed a model for the anterograde or secretory transport of PM receptors in plants. The biogenesis of PM-localized receptors starts with the translation in the ER. After maturation, including polypeptide folding and addition of post-translational modifications (Jürgens, 2004), the nascent receptors undergo ER quality control, followed by targeted transport from ER exit sites (ERES) (daSilva et al., 2004; Langhans et al., 2012) to the Golgi apparatus. In contrast to mammalian cells, the higher plant Golgi apparatus is polydisperse and made up of rapidly moving individual Golgi stacks (Boevink et al., 1998; Nebenführ et al., 1999). Here, post-translational modifications are further processed and additional quality control of the maturing receptors takes place. Successfully processed receptors leave the Golgi and are sorted in the trans-Golgi network (TGN) for PM secretion (Richter et al., 2009). Signaling competent receptors reach their destination through fusion of TGN-derived vesicles with the PM.

Inactive PM receptors often undergo constitutive recycling as described for BRI1 and FLS2 (Geldner et al., 2007; Beck et al., 2012). This endosomal pathway overlaps with but is distinct from the degradative route, which leads to proteasomal or vacuolar breakdown of endocytosed PM receptors. Together, these pathways form the retrograde transport route. Sorting of receptors for recycling or degradation commonly takes place at the TGN, an interface between anterograde and retrograde trafficking and therefore also called the early endosome (EE) compartment. However, sorting can also occur later, at the stage of multivesicular bodies (MVBs), which are matured forms of EEs also known as late endosomes (LEs) (Reyes et al., 2011).

The identification of anterograde and retrograde compartments that harbor both receptors simultaneously is of particular interest, since hetero-oligomerization of BRI1 and BAK1(SERK3) is required for BR signal transduction. For BRI1, localizations to various endosomal compartments of the two pathways has been documented, whereas little is known about the cellular distribution of BAK1(SERK3). Besides PM and tonoplast localization (Bücherl et al., submitted), BAK1(SERK3) was only observed in EEs (Russinova et al., 2004). In contrast, BRI1 was identified at the PM, Golgi, TGN/EE and MVBs using electron microscopy (Viotti et al., 2010) and live-cell imaging (Friedrichsen et al., 2000; Geldner et al., 2007; Viotti et al., 2010; Irani et al., 2012). However, neither a comparative colocalization analysis for the individual receptors nor for both receptors together has been performed to date. Colocalization and physical interaction of both receptors has only been described for the PM and brefeldin A (BFA) bodies (Bücherl et al., submitted), which contain Golgi and TGN/EE moieties (Nebenführ et al., 2002).

In this study, we investigated the spatial distribution of BRI1 and BAK1(SERK3) using live-cell confocal imaging. Colocalization analysis of double transgenic plant lines expressing

fluorescently tagged organelle markers and either BRI1-GFP or BAK1(SERK3)-GFP led to the identification of different anterograde and retrograde compartments, to which the two LRR-RLKs localize during their endosomal trafficking. Subsequently, we defined the cellular compartments harboring both receptors simultaneously in Arabidopsis protoplasts expressing both LRR-RLKs and the respective markers. The ER was identified as the first organelle, where BRI1 and BAK1(SERK3) colocalize. To test whether the two PM receptors also physically interact at the site of their biogenesis we performed FRET-FLIM on Arabidopsis protoplasts expressing BRI1 and BAK1(SERK3) in the presence of an ER marker and hetero-oligomerization of the two receptors at the ER membrane was revealed. In addition, short-term heat-shock induction of BRI1 was used to confirm hetero-oligomerization of BRI1 and BAK1(SERK3) on the anterograde transport route to the PM. Thus, the BRI1-BAK1(SERK3) signaling unit is established shortly after synthesis of its two main components.

RESULTS

BRI1 and SERK3 follow the traditional anterograde transport route

To investigate the localization of BRI1 and BAK1(SERK3) at subcellular level, double transgenic plants harboring BRI1-GFP (Friedrichsen et al., 2000) or BAK1(SERK3)-GFP (Li et al., 2002) and the corresponding markers tagged with either mCherry or mRFP were generated. For convenience we will only refer to SERK3 in the following sections, without its BAK1 designation. The first cellular compartment, where BRI1 and SERK3 were expected to localize to, was the ER. WAVE6-mCherry was used (NIP1;1, Geldner et al., 2009) as ER-marker and confocal live-cell imaging revealed BRI1-GFP and SERK3-GFP fluorescence at their site of biogenesis in Arabidopsis root epidermal cells. As shown in Figure 1C and 1L, BRI1-GFP- and SERK3-GFP-positive vesicular structures located closely to the ER network. Only a few of these ER-associated endomembrane compartments were visible in each image for both of the receptors. However, colocalization analysis using Pearson and Spearman correlation coefficients as read-out showed clear positive correlation between WAVE6-mCherry and either BRI1-GFP or SERK3-GFP fluorescence signals (Table 1), whereby higher correlation coefficients were obtained for BRI1-GFP.

After translation in the ER, proteins are usually targeted to the Golgi apparatus. WAVE18-mCherry (Got1p homolog, Geldner et al., 2009), which is a marker for Golgi stacks, was coexpressed with either BRI1-GFP or SERK3-GFP in Arabidopsis roots. Due to the mobile nature of the Golgi apparatus (Boevink et al., 1998; Nebenführ et al., 1999) confocal time-lapse imaging was performed to determine whether BRI1 and SERK3 associate with this organelle. As reported previously, BRI1-GFP was present in numerous vesicular structures (Friedrichsen et al., 2000; Geldner et al., 2007; Viotti et al., 2010; Irani et al., 2012), similar to the appearance of WAVE18-mCherry-labeled Golgi stacks. Many BRI1-GFP-positive en-

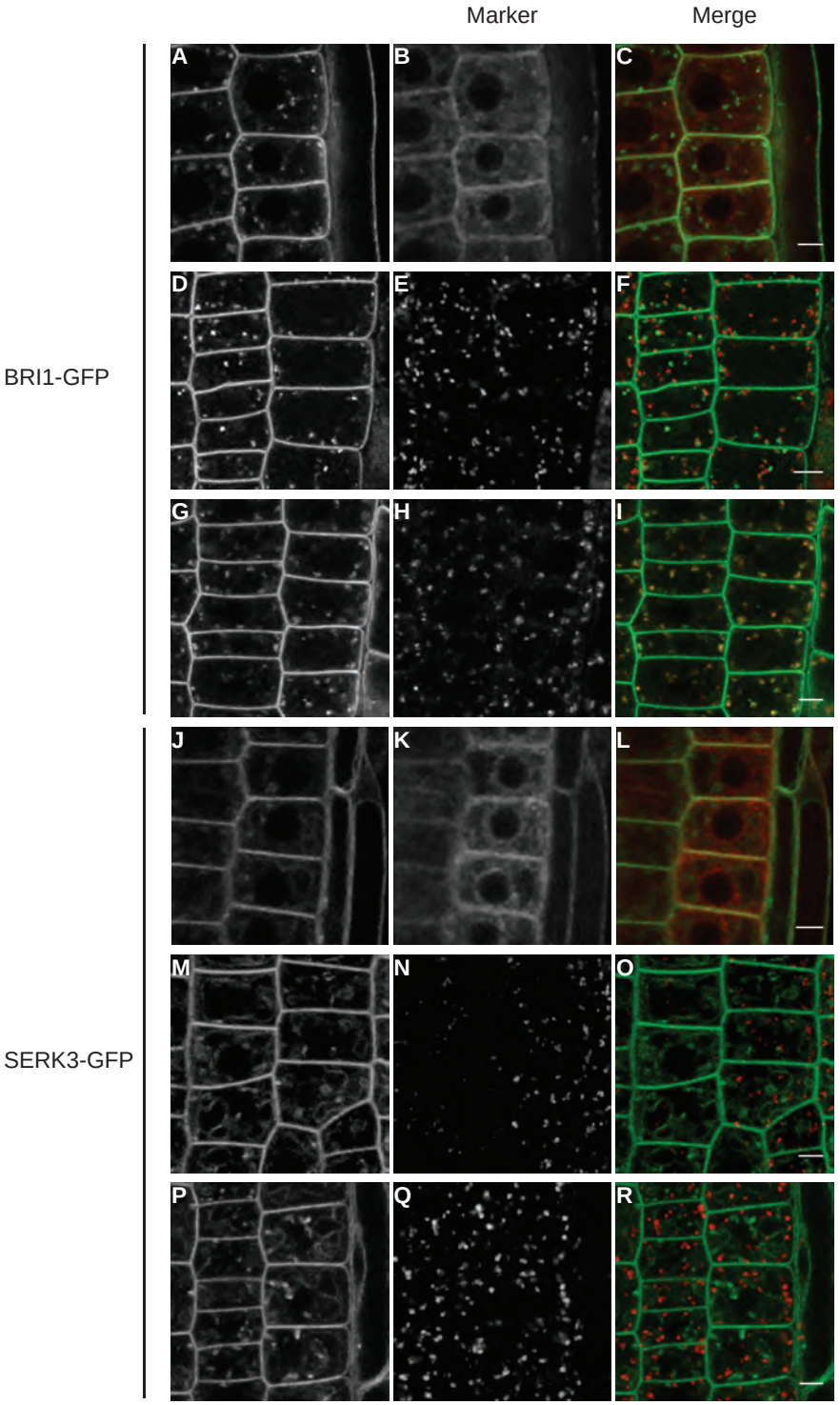
Marker
Merge
A
B
C
D
E
F
G
H
I
BRI1-GFP
J
K
L
M
N
O
P
Q
R
SERK3-GFP

Figure 1: BRI1 and SERK3 follow the traditional anterograde transport route from ER to PM.
Live-cell confocal imaging was performed on 5 day old Arabidopsis seedling roots harboring either BRI1-GFP or SERK3-GFP and the respective markers tagged with mCherry or mRFP. For labeling of the ER WAVE6-mCherry was used, Golgi stacks were marked using WAVE18-mCherry and the TGN/EE was visualized with mRFP tagged VHAa1. Scale bars represent a distance of 5 µm.
(**A-C**) Confocal images of BRI1-GFP (**A**) and the ER marker WAVE6-mCherry (**B**) as well as the corresponding merged image (**C**).
(**D-F**) Confocal images of BRI1-GFP (**D**) and Golgi stacks labeled with WAVE18-mCherry (**E**) as well as the corresponding merged image (**F**).
(**G-I**) Confocal images of BRI1-GFP (**G**) and VHAa1-mRFP marked TGN/EE (**H**) as well as the corresponding merged image (**I**).
(**J-L**) Confocal images of SERK3-GFP (**J**) and WAVE6-mCherry labeled ER (**K**) as well as the corresponding merged image (**L**).
(**M-O**) Confocal images of SERK3-GFP (**M**) and WAVE18-mCherry as Golgi marker (**N**) as well as the corresponding merged image (**O**).
(**P-R**) Confocal images of SERK3-GFP (**P**) and TGN/EE labeled with VHAa1-mRFP (**Q**) as well as the corresponding merged image (**R**).

domembrane compartments were closely associated with Golgi structures, however, only a few compartments showed a true overlap in fluorescence (Figure 1F), which is in line with the findings of Viotti et al. (2012) using electron microscopy. The colocalization quantification using Pearson and Spearman correlation coefficients also reflected this observation. Both coefficients were lower compared to the ER colocalization analysis (Table 1), but the positive values clearly indicate interdependency of fluorescence intensities derived from the Golgi-marker and BRI1-GFP. Similar results were obtained when SERK3-GFP was coexpressed with WAVE18-mCherry. Both correlation coefficients decreased in respect to the colocalization analysis performed on the ER compartment as shown in Table 1. Comparable to the findings for BRI1-GFP, SERK3-GFP-positive vesicular structures were found to associate with Golgi stacks, but only a minority showed direct fluorescence overlap (Figure 1O). This hints towards a short residence time and only transient localization of both receptors in the Golgi apparatus. In contrast to BRI1-GFP, the total number of vesicular structures harboring SERK3-GFP was low (Figure 1).

The limited number of SERK3-GFP-positive endomembrane structures also resulted in low correlation coefficients for the next compartment during the secretory transport, the TGN. Analysis of confocal time-lapse images obtained from Arabidopsis root epidermal cells expressing SERK3-GFP and the TGN-marker VHAa1-mRFP (Dettmer et al., 2006) revealed only a low number of endosomal compartments harboring fluorescently tagged SERK3 and TGN-marker simultaneously, as shown in Figure 1R. This observation was also reflected by Pearson and Spearman correlation coefficients of 0.02 ± 0.03 and 0.16 ± 0.05, respectively (Table 1). The situation changed completely when BRI1-GFP and VHAa1-mRFP were coexpressed. BRI1 clearly localized to the TGN, as also shown by Viotti et al. (2010) and Irani et al. (2012), and a high overlap of GFP and mRFP fluorescence was observed (Figure 1I & Table 1). A large number of endomembrane compartments was doubly labeled

Table 1: Quantification of colocalization between BRI1-GFP or SERK3-GFP with different organelle markers of the anterograde transport route.
Confocal images or time-lapse series of epidermal cells in 5 old Arabidopsis roots coexpressing BRI1-GFP or SERK3-GFP with the respective subcellular markers tagged with mCherry or mRFP were analyzed for colocalization using ImageJ 1.47g and the plugin "PSC Colocalization". Given are the Pearson correlation and Spearman rank coefficients ± S.E.M.. "N" represents the number of images or time-lapse series analyzed.

	WAVE6-mCherry			WAVE18-mCherry			VHAa1-mRFP		
	r(Pearson)	r(Spearman)	N	r(Pearson)	r(Spearman)	N	r(Pearson)	r(Spearman)	N
BRI1-GFP	0.43 ± 0.04	0.56 ± 0.05	15	0.24 ± 0.03[a]	0.37 ± 0.05[a]	23	0.71 ± 0.02[a,b]	0.62 ± 0.03[b]	22
SERK3-GFP	0.33 ± 0.03	0.43 ± 0.03	27	-0.13 ± 0.04[a]	0.06 ± 0.06[a]	24	0.02 ± 0.03[a,b]	0.16 ± 0.05[a]	22

[a] The mean difference is significant at the $p < 0.05$ level compared to WAVE6-mCherry (two-tailed Student's t-test for equal variance).
[b] The mean difference is significant at the $p < 0.05$ level compared to WAVE18-mCherry (two-tailed Student's t-test for equal variance).

with BRI1-GFP and VHAa1-mRFP and were maintained during a time course of 2.5 min used for time-lapse imaging.

Taken together, the colocalization analysis of BRI1-GFP and SERK3-GFP with the corresponding markers for ER, Golgi and TGN revealed that both LRR-RLKs follow the traditional anterograde transport route, whereby high colocalization values for both receptors were obtained for the ER, the site of their biogenesis.

BRI1 and SERK3 localize to MVBs

After localization of BRI1 and SERK3 in different secretory compartments was identified, also colocalization of both receptors with specific markers for the retrograde transport was investigated. The TGN/EE as bifunctional organelle involved in exo- and endocytosis represents the first endocytic compartment. However, localization of both receptors to TGN/ EE was already visualized using VHAa1-mRFP (Figure 1 and Table 1). Therefore ARA7/Rab F2b, which labels both EE and LE/MVBs (Ueda et al., 2004; Ebine et al., 2011), was selected as suitable marker to study the subsequent retrograde trafficking route of BRI1 and SERK3. As shown in Figure 2A, for BRI1-GFP and ARA7-mRFP high fluorescence overlap was observed during confocal time-lapse imaging, which resulted in Pearson and Spearman correlation coefficients of 0.73 ± 0.01 and 0.68 ± 0.01 (Table 2), respectively. In contrast, SERK3-GFP localized only marginally to ARA7/Rab F2b-mRFP-positive endosomal compartments. Only for a small number of vesicular structures direct GFP and mRFP fluorescence overlap was observed (Figure 2I), which is also indicated by the low values of Pearson and Spearman correlation coefficients given in Table 2.

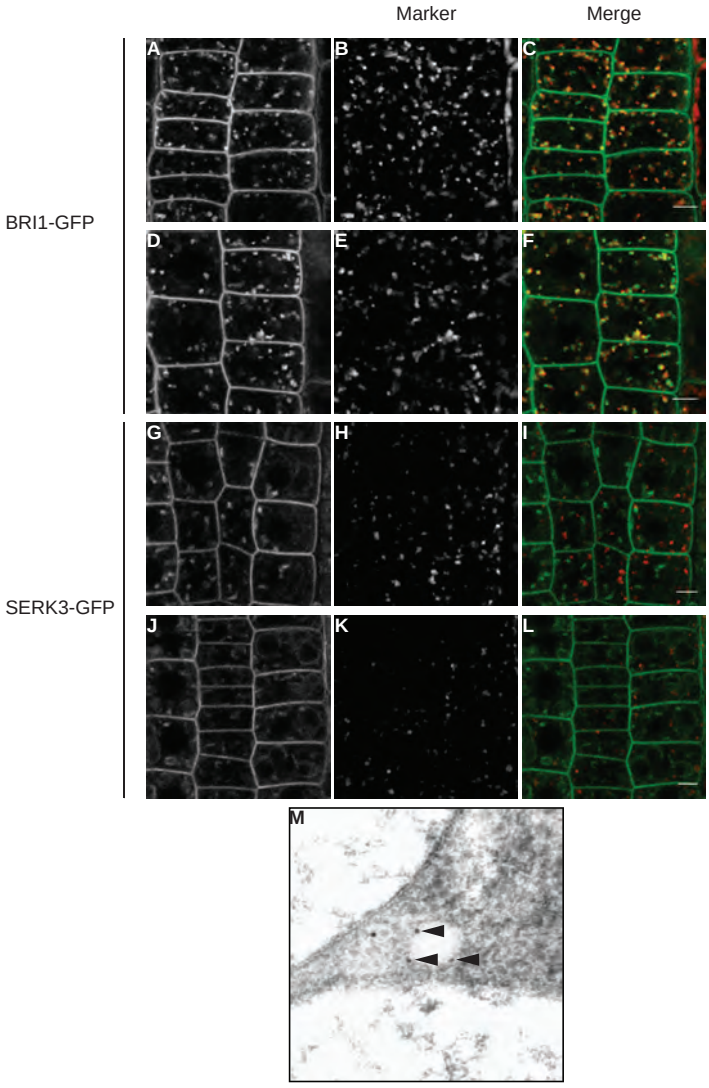

Figure 2: BRI1 and SERK3 localize to EE and LE/MVBs during their retrograde trafficking.
Confocal live-cell imaging was performed on 5 day old Arabidopsis seedling roots expressing either BRI1-GFP or SERK3-GFP in combination with ARA7/Rab F2b-mRFP or ARA6/Rab F1-mRFP for labeling EE and LE or LE/MVBs, respectively. Scale bars represent a distance of 5 µm.
(**A-C**) Confocal images of BRI1-GFP (**A**) and ARA7/Rab F2b-mRFP labeled EE and LE (**B**) as well as the corresponding merged image (**C**).
(**D-F**) Confocal images of BRI1-GFP (**D**) and LE/MVBs labeled with ARA6/Rab F1-mRFP (**E**) as well as the corresponding merged image (**F**).
(**G-I**) Confocal images of SERK3-GFP (**G**) and the EE/LE marker ARA7/Rab F2b-mRFP (**H**) as well as the corresponding merged image (**I**).
(**J-L**) Confocal images of SERK3-GFP (**J**) and ARA6/Rab F1-mRFP labeled LE/MVBs (**K**) as well as the corresponding merged image (**L**).
(**M**) Electron microscopic image showing the localization of SERK3-GFP to the limiting membrane of a PVC.

Table 2: Quantitative colocalization between BRI1-GFP or SERK3-GFP with markers for retrograde trafficking compartments.
Confocal time-lapse series of epidermal cells in 5 old Arabidopsis roots coexpressing BRI1-GFP or SERK3-GFP with either ARA6-mRFP labeling MVBs or ARA7-mRFP labeling EEs and MVBs were analyzed for colocalization using ImageJ 1.47g and the plugin "PSC Colocalization". Given are the Pearson correlation and Spearman rank coefficients ± S.E.M.. "N" represents the number of time-lapse series analyzed.

	ARA6-mRFP			ARA7-mRFP		
	r(Pearson)	r(Spearman)	N	r(Pearson)	r(Spearman)	N
BRI1-GFP	0.66 ± 0.03	0.60 ± 0.04	22	0.73 ± 0.01[a]	0.68 ± 0.01[b]	20
SERK3-GFP	0.08 ± 0.04	0.18 ± 0.07	23	0.03 ± 0.05	0.15 ± 0.07	18

[a] The mean difference is significant at the $p < 0.05$ level compared to ARA6-mRFP (two-tailed Student's t-test for equal variance).
[b] The mean difference is significant at the $p < 0.05$ level compared to ARA6-mRFP (one-tailed Student's t-test for equal variance).

A homolog of ARA7/Rab F2b, ARA6/Rab F1, was used to label the next step of endosomal trafficking. ARA6/Rab F1 localizes mainly to LE/MVBs, which mature from EEs (Ebine et al., 2011). Colocalization analysis of Arabidopsis roots coexpressing SERK3-GFP and ARA6/Rab F1-mRFP resulted in a trend towards elevated correlation coefficients compared to the results obtained with ARA7/Rab F2b (Table 2). Still, the majority of ARA6/Rab F1-labeled MVBs did not show direct fluorescence overlap with SERK3-GFP-positive endosomal compartments (Figure 2I). Again, for BRI1-GFP a much higher colocalization with this MVB marker was observed (Figure 2F and Table 2). However, in contrast to SERK3-GFP the Pearson and Spearman correlation coefficients decreased slightly compared to the ARA7/Rab F2b colocalization analysis, in accordance with the constitutive recycling of BRI1-GFP (Geldner et al., 2007).

Using electron microscopy Viotti et al. (2010) also showed that BRI1-GFP localizes to MVBs. In particular, localization of BRI1 to the inner vesicles of MVBs was observed. The same experimental setup in addition revealed that SERK3-GFP localizes to the limiting membrane of prevacuolar compartments (PVCs), which may be derived from TGN/EE or Golgi vesicles (Wolfenstetter et al., 2012) after endocytosis (Figure 2M).

Thus, we conclude that both BRI1 and SERK3 localize to MVBs during retrograde trafficking, however, both receptors may also follow different routes after endocytosis from the PM.

BRI1 and SERK3 colocalize during their antero- and retrograde transport

To address where BRI1-SERK3 hetero-oligomers reside or are established, the subsets of cellular compartments that harbor both receptors needed to be identified. For this purpose BRI1 and SERK3 were transiently expressed in Arabidopsis mesophyll protoplasts in the presence of the respective organelle markers. Subsequently, the number of endomem-

brane compartments for both receptors and the corresponding marker as well as the amount of vesicular structures harboring all three proteins simultaneously was determined. An endomembrane compartment was defined as circular, fluorescently intense structure of approximately the size of an individual TGN/EE (Figure 3). First, protoplasts expressing ARA6/Rab F1-mRFP were transfected with SERK3-sCFP and BRI1-sYFP. BRI1-sYFP was present in a larger number of endomembrane compartments than SERK3-sCFP, similar to the observations in planta (Figure 3). The ratio between BRI1- and SERK3-positive vesicular structures was approximately two and stayed constant throughout the protoplast experiments, independent of the marker background (Table 3). BRI1-sYFP and SERK3-sCFP were found together in about 38% of ARA6/Rab F1-mRFP labeled MVBs, the highest value observed for any of the organelle markers (Table 3). Finding a high degree of BRI1-SERK3 colocalization in LE/MVBs suggests that a considerable amount of endocytosed receptor hetero-oligomers is subject to vacuolar degradation. The total number of endomembrane structures that were positively labeled by the two LRR-RLKs and the marker protein was almost identical for ARA6/Rab F1 and ARA7/Rab F2b, as shown in Table 3. However, the higher amount of ARA7/Rab F2b-mRFP vesicular structures compared to ARA6/Rab F1-mRFP (Figure 3O & 3S) led to reduction in colocalization of BRI1 and SERK3 with ARA7/Rab F2b to around 25% (Table 3).

SERK3-sCFP and BRI1-sYFP also colocalized in VHAa1-mRFP labeled TGN/EE and WAVE18-mCherry labeled Golgi compartments in protoplasts (Figure 3H & 3L). The percentage of colocalization was determined to approximately 14% and 11% for TGN/EE and Golgi, respectively (Table 3). The total numbers of colocalizing endomembrane compartments containing both LRR-RLKs and the respective fluorescently labeled marker protein were reduced as well in respect to the results obtained for the retrograde markers ARA7/Rab F2b and ARA6/Rab F1, as shown in Table 3. Whereas around two TGN/EE compartments per confocal section contained BRI1-sYFP and SERK3-sCFP simultaneously, the value decreased to below one for the colocalization of both LRR-RLKs with Golgi stacks (Table 3).

Since the ER is a continuous endomembrane compartment, colocalization of BRI1 and SERK3 with the ER-marker AtVMA21 (Neubert et al., 2008) was determined analogous to the in planta analysis. BRI1-sYFP and SERK3-sCFP showed a clear fluorescence overlap in AtVMA21-mRFP labeled endomembranes, as shown in Figure 3A. Similar as observed for the individual receptors (Figure 1 & Table 1), high Pearson and Spearman correlation coefficients were obtained for the colocalization of both proteins in the ER.

Taken together, BRI1 and SERK3 not only localize individually to different stages of the retrograde and secretory pathways, but also colocalize in the respective endomembrane compartments. Colocalization of the BR signaling unit forming LRR-RLKs was most prominent at late stages of their lifespan and at the site of their biogenesis.

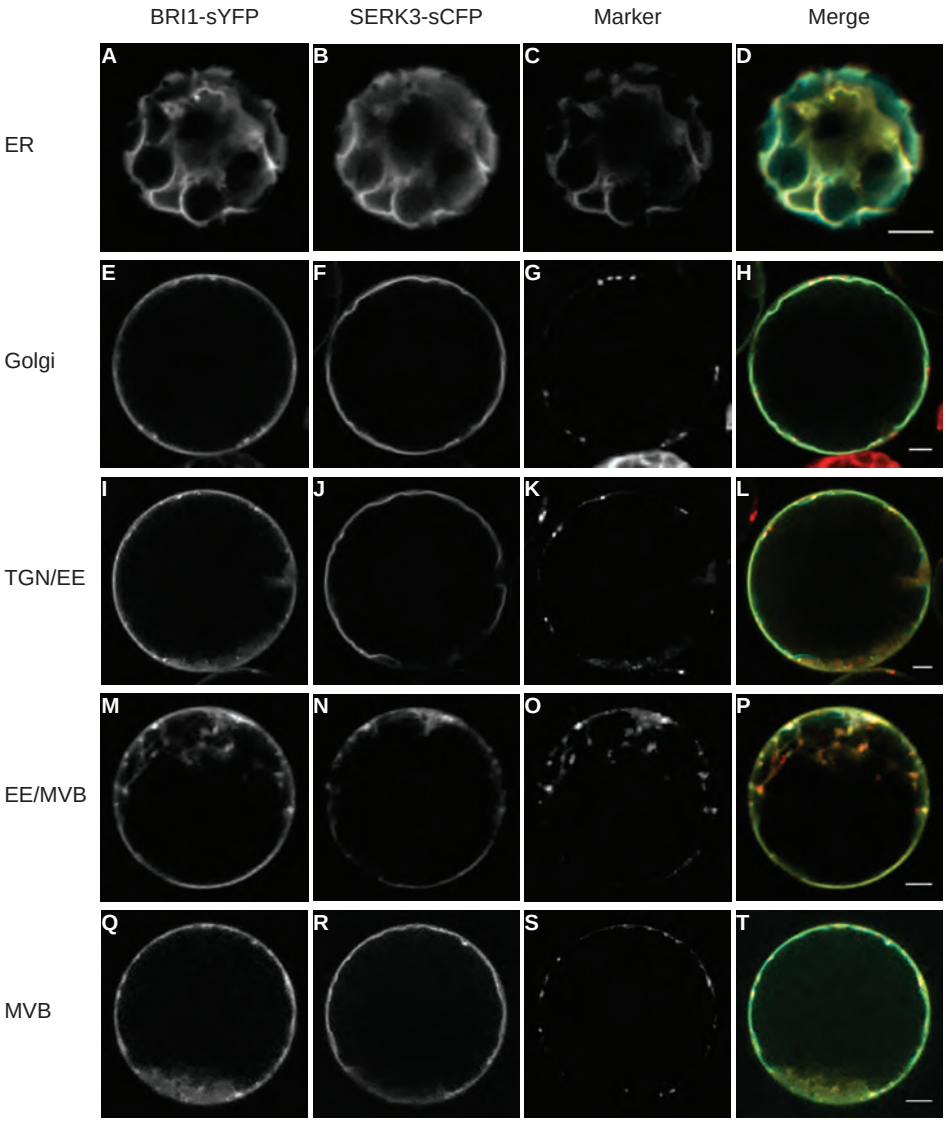

Figure 3: BRI1 and SERK3 colocalize during secretory and endocytic endosomal trafficking.
BRI1-sYFP and SERK3-sCFP were coexpressed in Arabidopsis mesophyll protoplasts with markers for antero- and retrograde trafficking. Confocal imaging of the protoplasts was performed 16-24 h after transfection. For labeling the ER AtVMA21-mRFP was additionally cotransfected. For all other compartments protoplasts were isolated from the respective transgenic lines and cotransfected with the BRI1 and SERK3 constructs. For Golgi stack-labeling WAVE18-mCherry was used. TGN/EE was labeled using VHAa1-mRFP and EE/LE or LE/MVBs were marked using ARA7/Rab F2b-mRFP or ARA6/Rab F1-mRFP, respectively.
(**A-D**) Confocal images of BRI1-sYFP (**A**), SERK3-sCFP (**B**), AtVMA21-mRFP labeled ER (**C**), and the corresponding merged image (**D**).
(**E-H**) Confocal images of BRI1-sYFP (**E**), SERK3-sCFP (**F**), Golgi stacks labeled with WAVE18-mCherry (**G**), and the corresponding merged image (**H**).

(**I-L**) Confocal images of BRI1-sYFP (**I**), SERK3-sCFP (**J**), VHAa1-mRFP labeled TGN/EE (**K**), and the corresponding merged image (**L**).
(**M-P**) Confocal images of BRI1-sYFP (**M**), SERK3-sCFP (**N**), EE and LE labeled with ARA7/Rab F2b-mRFP (**O**), and the corresponding merged image (**P**).
(**Q-T**) Confocal images of BRI1-sYFP (**Q**), SERK3-sCFP (**R**), ARA6/Rab F1-mRFP labeled LE/MVBs (**S**), and the corresponding merged image (**T**).
Scale bars represent a distance of 5 µm.

Table 3: Quantification of endosomal compartments harboring BRI1-sYFP2 and SERK3-sCFP3A during the anterograde and retrograde transport.
The number of endosomal compartments labeled by the respective marker as well as BRI1-sYFP and SERK3-sCFP was counted and colocalization was quantified based on confocal images obtained from protoplasts transiently transfected with the corresponding vector constructs. For quantification of ER colocalization (AtVMA21-mRFP) colocalization was determined analog to Table 1 and 2. "EMCs" represents the number of endomembrane compartments and the "Overlap" is given as absolute number or as percentage of "Marker EMCs". "N" represents the number of images analyzed. "r(P)" and "r(S)" represent the Pearson and Spearman correlation coefficients, respectively.

AtVMA21-mRFP				WAVE18-mCherry			VHAa1-mRFP			ARA6-mRFP			ARA6-mRFP		
r(P)	r(S)	N		BRI1	SERK3	N	BRI1	SERK3	N	BRI1	SERK3	N	BRI1	SERK3	N
0.72 ± 0.02	0.75 ± 0.02	22	EMCs	9.84 ± 0.79	5.47 ± 0.65	38	11.24 ± 0.73	6.11 ± 0.53	37	11.03 ± 0.90	6.72± 0.56	32	11.49 ± 0.95	6.49 ± 0.40	35
			Marker EMCs	5.32 ± 0.66			15.65 ± 1.19			9.28 ± 0.76			13.69 ± 1.13		
			Overlap [#]	0.68 ± 0.17			1.92 ± 0.19[a]			2.94 ± 0.26[a,b]			2.71 ± 0.18[a,b]		
			Overlap [%]	11.3 ± 3.14			14.37 ± 1.52			37.58 ± 4.57[a,b]			24.69 ± 2.64[a,b,c]		

[a] The mean difference is significant at the $p < 0.05$ level compared to WAVE18-mCherry (two-tailed Student's t-test for equal variance).
[b] The mean difference is significant at the $p < 0.05$ level compared to VHAa1-mRFP (two-tailed Student's t-test for equal variance).
[c] The mean difference is significant at the $p < 0.05$ level compared to ARA6-mRFP (two-tailed Student's t-test for equal variance).

BRI1 and SERK3 hetero-oligomerize soon after biogenesis in the ER

Based on the high degree of colocalization of both receptors especially in the ER, direct physical interaction between BRI1 and SERK3 was probed first in this particular organelle. Therefore FRET-FLIM was performed on double transfected Arabidopsis protoplasts expressing BRI1-sCFP and the ER-marker AtVMA21-mRFP or triple transfected protoplasts expressing additionally SERK3-sYFP. A donor fluorescence lifetime of BRI1-sCFP of approximately 2740 ps was found along the AtVMA21-mRFP labeled ER membranes (Table 4). This fluorescence lifetime served as control and was compared to the donor fluorescence lifetime of BRI1-sCFP in the presence of the FRET acceptor SERK3-sYFP. As shown in Table 4, for triple transfected protoplasts an average donor fluorescence lifetime at the

Table 4: Numerical FRET-FLIM analysis performed on ER compartments of transiently transfected Arabidopsis **protoplasts.**
Physical interaction between BRI1 and SERK3 in the ER was determined by FRET-FLIM analysis 16-24 h after transient transfection of Arabidopsis mesophyll protoplasts expressing BRI1 or/ and SERK3 with the corresponding tags and AtVMA21-mRFP as ER marker. CERK1-sCFP in combination with SERK3-sYFP served as negative control. "τ" represents the average donor fluorescence lifetime determined from sCFP fluorescence ± S.E.M., "FRET" represents the FRET-efficiency and "N" represents the number of ROIs analyzed.

	τ [ps]	FRET [%]	N
CERK1-sCFP	2908 ± 14		33
CERK1-sCFP/SERK3-sYFP	2781 ± 17	4.19 ± 0.56	35
BRI1-sCFP	2744 ± 18		17
BRI1-sCFP/SERK3-sYFP	2505 ± 25	8.69 ± 0.90[a]	34
SERK3-sCFP	2292 ± 30		30
SERK3-sCFP/BRI1-sYFP	2039 ± 33	11.07 ± 1.42[a]	31

[a] The mean difference is significant at the $p < 0.05$ level compared to the negative control (two-tailed Student's t-test for equal variance).

ER membrane of around 2510 ps was observed. This reduction in BRI1-sCFP fluorescence lifetime corresponds to a FRET efficiency of about 9% and indicates that BRI1 and SERK3 hetero-oligomerize already at the ER, the very beginning of the secretory pathway. In Figure 4 the corresponding fluorescence intensity and color-coded fluorescence lifetime images are presented and show that the reduction in donor fluorescence lifetime was not uniform. Large parts along the ER membrane did not show a significant FRET efficiency, even though BRI1-sCFP and SERK3-sYFP colocalized. Only in few spatially restricted areas a drastic reduction in donor fluorescence became evident, resulting in FRET efficiencies up to about 20% (Figure 4). This interaction pattern is in accord with our recent observations of BRI1-SERK3 hetero-oligomers *in planta*, which showed a non-uniform distribution along the PM (Bücherl et al., 2013). The obtained results for ER oligomerization of the two LRR-RLKs were confirmed by swapping the fluorescence tags between BRI1 and SERK3, which led to similar FRET efficiencies, and by comparison to a negative control, for which SERK3 was coexpressed with CERK1, a plant immunity receptor most likely not interacting with the SERK coreceptor (Gimenez-Ibanez et al., 2009) (Figure 4 and Table 4).

Thus, in contrast to the relative homogenous distribution and colocalization of BRI1 and SERK3 along the ER membrane of Arabidopsis mesophyll protoplasts, hetero-oligomerization of both receptors soon after biogenesis is restricted to distinct ER membrane areas.

Hetero-oligomers of newly synthesized BRI1 and SERK3 receptors are maintained during anterograde transport in Arabidopsis roots

To verify that the observed complexes are indeed composed of newly synthesized receptor molecules and to address whether hetero-oligomers are maintained during anterograde

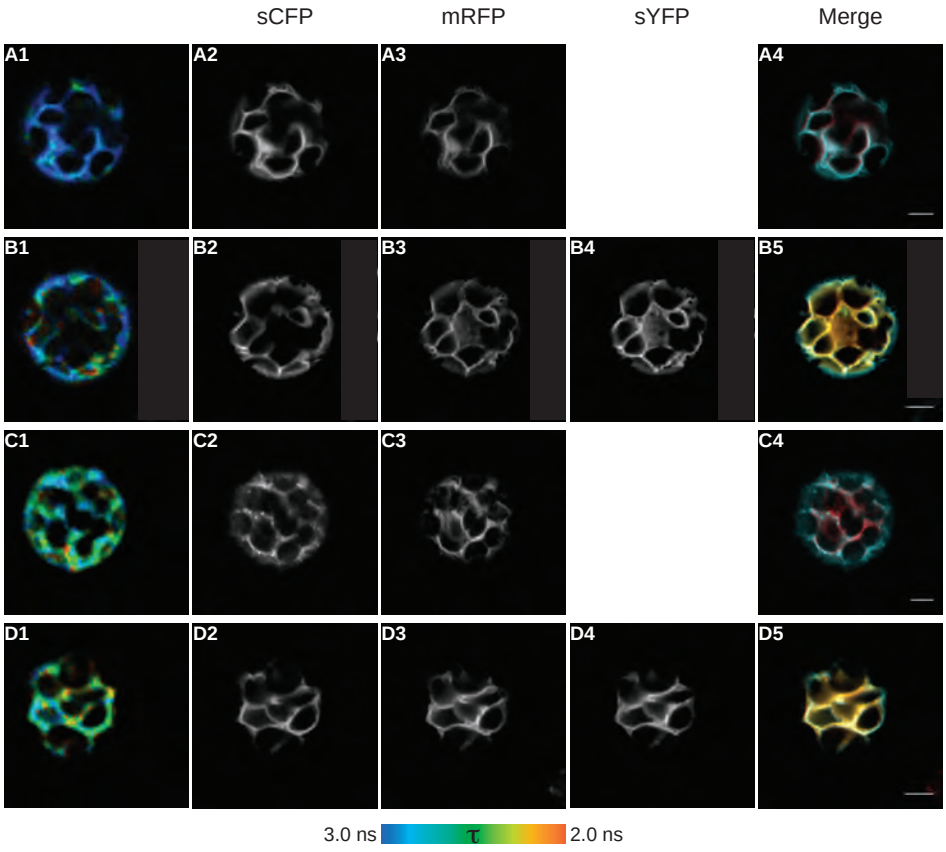

Figure 4: BRI1 and SERK3 hetero-oligomerize during their biogenesis in the ER.
In vivo confocal imaging and FRET-FLIM was performed on Arabidopsis mesophyll protoplasts 16-24 h after transfection. The ER marker AtVMA21-mRFP was used to label ER membranes. FRET-donors were tagged with sCFP and sYFP-labeling was used for the respective FRET-acceptor constructs.
(**A1-A4**) Fluorescence lifetime image (**A1**) and confocal fluorescence intensity images of CERK1-sCFP (**A2**) and AtVMA21-mRFP labeled ER (**A3**) as well as the corresponding merged image (**A4**).
(**B1-B5**) Fluorescence lifetime image (**B1**) and confocal fluorescence intensity images of CERK1-sCFP (**B2**), AtVMA21-mRFP labeled ER (**B3**), and SERK3-sYFP (**B4**) as well as the corresponding merged image (**B5**).
(**C1-C4**) Fluorescence lifetime image (**C1**) and confocal fluorescence intensity images of BRI1-sCFP (**C2**) and AtVMA21-mRFP labeled ER (**C3**) as well as the corresponding merged image (**C4**).
(**D1-D5**) Fluorescence lifetime image (**D1**) and confocal fluorescence intensity images of BRI1-sCFP (**D2**), AtVMA21-mRFP labeled ER (**D3**), and SERK3-sYFP (**D4**) as well as the corresponding merged image (**D5**).
Scale bars indicate a distance of 5 µm and the color bar represents the false-color code for the fluorescence lifetime images.

trafficking a stable transgenic Arabidopsis line expressing heat-shock inducible BRI1-YFP (Geldner et al., 2007) and pSERK3::SERK3-mCherry was examined shortly after heat-shock induction. BRI1-YFP requires more than 1 h after heat-shocking to reach a detectable

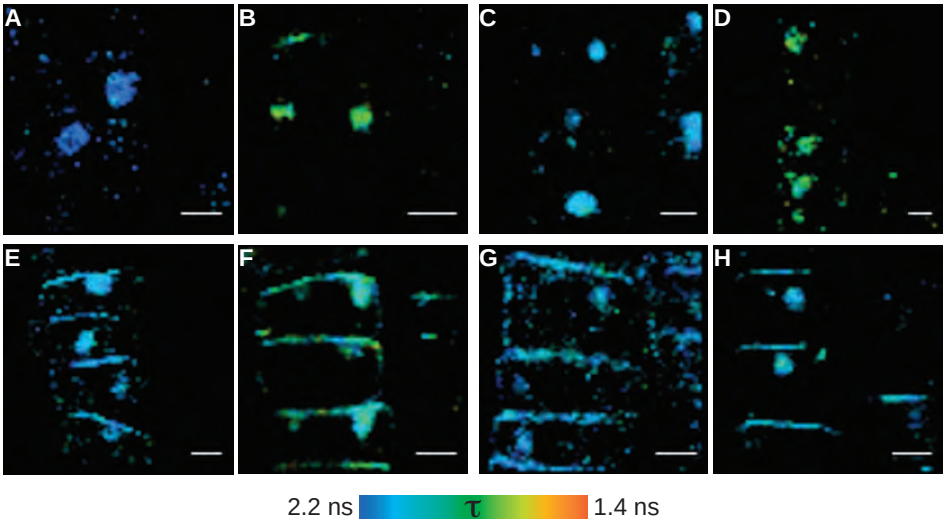

Figure 5: Newly synthesized BRI1 and SERK3 receptors hetero-oligomerize during the anterograde transport in Arabidopsis **roots.**
FRET-FLIM on roots of 5 day old Arabidopsis seedlings expressing heat-shock inducible BRI1-YFP or coexpressing BRI1-YFP and SERK3-mCherry, grown for 2 days in medium containing 5 µM BRZ. PIN2-GFP in combination with SERK3-mCherry served as negative control.
(**A**) Fluorescence lifetime image of heat-shock inducible BRI1-YFP after BFA treatment (50 µM, 1 h) and heat-shock induction (30 min).
(**B**) Fluorescence lifetime image of heat-shock inducible BRI1-YFP in the presence of SERK3-mCherry after BFA treatment (50 µM, 1 h) and heat-shock induction (30 min).
(**C**) Fluorescence lifetime image of heat-shock inducible BRI1-YFP after simultaneous BFA and Tyr23 application (50 µM each, 1 h) and heat-shock induction (30 min).
(**D**) Fluorescence lifetime image of heat-shock inducible BRI1-YFP in the presence of SERK3-mCherry after simultaneous BFA and Tyr23 treatment (1 µM, 1 h) and heat-shock induction (30 min).
(**E**) Fluorescence lifetime image of PIN2-GFP after BFA application (50 µM, 1 h).
(**F**) Fluorescence lifetime image of PIN2-GFP in the presence of SERK3-mCherry after BFA treatment (50 µM, 1 h).
(**G**) Fluorescence lifetime image of PIN2-GFP after simultaneous BFA and Tyr23 application (50 µM each, 1 h).
(**H**) Fluorescence lifetime image of PIN2-GFP in the presence of SERK3-mCherry after simultaneous BFA and Tyr23 treatment (50 µM each, 1 h).
Heat-shock induction was performed at 37°C in liquid half-strength MS for 30 min in the presence of BFA or BFA/Tyr23. To avoid heat-shock artifacts the negative controls were also subjected to the same heat-shock conditions. 24-epi-brassinolide (BL) was used throughout the experiments. Color bar represents a false color-code for BRI1-GFP fluorescence lifetimes (τ). Scale bars correspond to a size of 5 µm.

fluorescence signal at the PM (Viotti et al., 2010). Within that time frame, we could not obtain sufficient signal for reliable FRET analysis in the internal membrane compartments. Therefore the secretory inhibitor brefeldin A (BFA) was employed to obtain a higher local concentration of fluorescent proteins. Using immuno-gold labeling, Viotti et al. (2010) showed the accumulation of BRI1-YFP prior to detectable fluorescence at the PM in Golgi

Table 5: Fluorescence lifetime analysis of immuno-labeled BRI1-YFP.
Quantitative FRET-FLIM analysis of measurements performed on immuno-labeled roots of 5 day old heat-shock inducible BRI1-YFP and BRI1-YFP/SERK3-mCherry expressing seedlings using PIN2-GFP in combination with SERK3-mCherry as negative control. Endogenous BRs were depleted by BRZ treatment (5 µM). Heat-shock induction of BRI1-YFP was carried out at 37°C in liquid half-strength MS in the presence of BFA or BFA/Tyr23. BFA and Tyr23 were applied in concentrations of 50 µM. The τ values given represent Alexa488 donor fluorescence lifetimes of the immuno-labeled YFP and GFP moieties of BRI1-YFP or PIN2-GFP, respectively, in ps ± S.E.M.. "N" represents the number of analyzed fluorescence lifetime images.

	BFA			BFA+Tyr23		
	τ [ps]	FRET [%]	N	τ [ps]	FRET [%]	N
PIN2-GFP	2031 ± 12		31	2091 ± 21		29
PIN2-GFP/SERK3-mCherry	1917 ± 17[a]	5.6 ± 0.8	34	1994 ± 17[a]	4.6 ± 0.8	30
BRI1-YFP	2237 ± 19		24	2019 ± 12		28
BRI1-YFP/SERK3-mCherry	1965 ± 20[a]	12.2 ± 0.9[b]	33	1870 ± 11[a]	7.4 ± 0.6[b]	32

[a] The mean difference is significant at the $p < 0.05$ level compared to donor only (PIN2-GFP or BRI1-YFP) samples (two-tailed Student's t-test for unequal variance).
[b] The mean difference is significant at the $p < 0.05$ level compared to PIN2-GFP/SERK3-mCherry samples (two-tailed Student's t-test for equal variance).

and TGN, compartments sensitive to BFA (Nebenführ et al., 2002). Therefore BRZ-cultured BRI1-YFP and BRI1-YFP/SERK3-mCherry seedlings were heat-shocked in the presence of BFA and fixed 30 min after induction. Subsequently, roots were immuno-labeled with primary antibodies against the YFP and mCherry epitopes and visualized using Alexa488- and Alexa568-conjugated secondary antibodies. As shown in Figure 5A and 5B, heat-shock induced BRI1-YFP accumulated in BFA compartments of epidermal Arabidopsis root cells but was absent at the PM, in contrast to constitutively expressed PIN2-GFP, which in combination with SERK3-mCherry was used as a negative control (Figure 5E and 5F). To reveal whether in the observed BFA compartments BRI1-YFP and SERK3-mCherry are already in close physical proximity, FRET-FLIM was performed. The color-coded fluorescence lifetime images of Alexa488-labeled BRI1-YFP or Alexa488-/Alexa568-labeled BRI1-YFP/SERK3-mCherry expressing roots are presented in Figure 5. For BFA compartments containing BRI1-YFP only a Alexa488 fluorescence lifetime of about 2200 ps was determined (Figure 5A and Table 5), while in the presence of Alexa568-labeled SERK3-mCherry a significant reduction in donor fluorescence lifetime of approximately 300 ps was observed (Figure 5B and Table 5). This indicates the existence of BRI1-SERK3 hetero-oligomers on the antero-grade transport route.

To confirm that the observed BRI1-SERK3 hetero-oligomers are indeed formed by newly translated BRI1-YFP and SERK3-mCherry moieties, these experiments were also conducted under simultaneous application of BFA and Tyrphostin A23 (Tyr23), an inhibitor of clathrin-mediated endocytosis. BRI1-YFP and SERK3-mCherry also associated under these conditions in BFA compartments, though to a smaller extent, as shown in Figure 5D and Table 5.

In conclusion, we could show that BRI1 and SERK3 individually follow the traditional secretory pathway and also localize to EE and LE after endocytosis from the PM. However, we observed only subpopulations of both receptors trafficking together through the cellular endomembrane system. Most importantly, we identified that the first endomembrane compartment, in which BRI1 and SERK3 colocalize, the ER, is also the site where BRI1-SERK3 hetero-oligomers are established to form a BR signaling unit. These BR signaling units are maintained during the anterograde transport to the PM, the compartment of ligand perception and exhibition of signaling activity.

DISCUSSION

In the present study, live-cell and immuno-fluorescence imaging was employed to illuminate the endosomal trafficking of the BR signaling unit forming LRR-RLKs BRI1 and SERK3. We showed that these RLKs individually follow the traditional secretory pathway, via ER, Golgi, TGN/EE to the PM, that they reside in LE/MVBs, and that the two receptors also colocalize in the respective endsomal compartments. Additionally, we revealed that the ER is the organelle, where BRI1-SERK3 hetero-oligomers are established, and that complexes of newly synthesized receptor molecules are maintained during the anterograde transport.

Homo- and hetero-oligomerization of plant PM receptors in the ER has not been reported so far, in contrast to mammalian systems. Ma-Högemeier et al. (2010) showed the association of glutamate receptor subunits in the ER and additionally the target transport to the PM, similar to our observations of newly synthesized BRI1-SERK3 hetero-oligomers on the anterograde transport route. Receptor complex assembly at an early stage of biogenesis was also demonstrated for other classes of PM-localizing proteins like TGFβ receptors (Gilboa et al., 1998) or G-protein coupled receptors (GPCRs) (Boyd, 2002; Herrick-Davis et al., 2006; Canals et al., 2009; Van Craenenbroeck et al., 2011), for which ER hetero-oligomerization has been studied most extensively. Van Craenenbroeck et al. (2011) reported the functional significance of GPCR complex preformation in the ER by demonstrating enhanced folding efficiency, ER export and cell surface trafficking. Co- and post-translational interaction of nascent polypeptide chains is thought to mimic chaperone functions and thereby accelerating the folding process. Receptor oligomerization thus increases the probability of passing the ER quality control and of entering the secretory pathway (Van Craenenbroeck, 2012). A similar explanation could account for the observation of reduced amounts of BRI1-GFP in serk1serk3 coreceptor loss-of-function mutant backgrounds (Supplemental Figure S1). The lack of BRI1-coreceptor interactions may increase ER residence time of newly synthesized BRI1-GFP and lead to enhanced ER-associated degradation (ERAD) (Van Craenenbroeck, 2012). The essential role of ERAD for BRI1 biogenesis has been shown by several studies that revealed mechanistic details of

bri1-5 and bri1-9 ER retention (Hong et al., 2008; Hong et al., 2009; Su et al., 2011; Hong et al., 2012; Hüttner et al., 2012).

Besides assisting receptor biogenesis and cell surface trafficking, ligand-independent receptor oligomerization was shown to directly affect the signaling of PM-localized receptors. Receptor complex preformation can enhance ligand binding by reducing the dimensionality due to elevated local receptor density and increased avidity for the ligand (Ehrlich et al., 2012). Ligand availability can also lead to enhanced oligomer formation of PM receptors as shown for epidermal growth factor receptor (EGFR) (Hofman et al., 2010), TGFβ receptor (Rechtman et al., 2009), bone morphogenetic protein (BMP) receptor (Nohe et al., 2002), and also the receptor combination investigated here, BRI1 and SERK3 (Wang et al., 2005; Bücherl et al., submitted). Notably, for BMP receptors differential signaling responses (Nohe et al., 2002) and endocytotic routes (Hartung et al., 2006) for preformed and ligand-induced receptor complexes were observed. This led to the hypothesis that low ligand concentrations predominantly activate signaling from preassembled receptor complexes, while increased ligand availability shifts the equilibrium towards signaling from complexes induced by ligand-dependent recruitment. Such a mechanism could have important implications, for example, for morphogenic gradients in development (Ehrlich et al., 2011). This hypothesis for animal systems could also be addressed by a comparative receptor complex analysis in respect to BRI1-SERK mediated BR signaling, since especially young and developing tissues show high BR contents (Shimada et al., 2003).

Next to the identification of the ER as an important assembly line for ligand-independent BRI1-SERK3 hetero-oligomers, the present study also revealed other cellular compartments for BRI1 and SERK3 endosomal trafficking. This was of particular interest, since BRI1 was reported to signal from PM (Irani et al., 2012) as well as endosomes (Geldner et al., 2007) and requires hetero-oligomerization with SERK coreceptors for initiating downstream responses (Gou et al., 2012). BRI1 localizes to Golgi and TGN/EE during the anterograde transport, as observed by Viotti et al. (2010) using electron microscopy, which was extended in this study by observing BRI1 at the ER. Additionally, colocalization of BRI1 with SERK3 along the secretory pathway was shown, suggesting that BRI1-SERK3 receptor complexes, which are established in the ER, remain associated and are inserted in the PM in a hetero-oligomerized form. Similar observations were found in mammalian systems for KAR (Ma-Högemeier et al., 2010) and TGFβ receptors (Gilboa et al., 1998). The marginal colocalization of fluorescently tagged BRI1 and SERK3 with WAVE18-mCherry-labeled Golgi stacks indicates a short transit time for the individual receptors as well as for the BRI1-SERK3 hetero-oligomers (Figure 1 and 3, Table 1 and 3). A possible explanation could be the specific biochemical processes occurring in the individual biosynthetic compartments. In the Golgi apparatus only post-translational modifications take place, whereas in the ER processes like translation, folding, hetero-oligomerization and quality control occur. These processes most likely require a longer turnover time than enzymatic reactions carried

out in the Golgi. The TGN/EE represents the main sorting machinery for endosomal trafficking and is moreover part of the retrograde pathway. Thus, BRI1 and SERK3 receptors colocalizing with the TGN/EE marker VHAa1-mRFP are most likely combined populations of the secretory and endocytic transport. This accounts in particular for BRI1, which was shown to undergo ligand-independent constitutive recycling (Geldner et al., 2007).

Constitutive recycling was recently also reported for another plant LRR-RLK (Beck et al., 2012), Flagellin Sensing 2 (FLS2). This RLK is a PM receptor involved in bacterial immunity (Gómez-Gómez and Boller, 2000) and forms strictly ligand-dependent hetero-oligomers SERK3 (Chinchilla et al., 2007; Schulze et al., 2010). In contrast to BRI1, FLS2 showed enhanced internalization upon exogenous activation with flg22, the minimal epitope of bacterial flagellin recognize by this LRR-RLK. Live-cell imaging additionally revealed activation- and time-dependent colocalization of FLS2 with ARA7/Rab F2b and ARA6/Rab F1, both markers for the retrograde transport route. In general, a higher colocalization of FLS2 with ARA7/Rab F2b was observed, which is a Rab GTPase that labels EE and LE/MVBs simultaneously (Ueda et al., 2004; Ebine et al., 2011). This is in line with our observations for BRI1, whereas individual SERK3 receptors and SERK3 in combination with BRI1 colocalized preferentially with ARA6/Rab F1 (Table 2), which is a marker for LE/MVBs (Ueda et al., 2004; Ebine et al., 2011) and labels more specifically endosomal compartments directed for vacuolar degradation. A reason for finding higher colocalization of BRI1 and FLS2 with ARA7/Rab F2b may be the overlapping populations of labeled vesicular structures composed of EE and LE/MVB, which therefore harbor receptors determined for both recycling and degradation. That SERK3 was predominately associated with ARA6/Rab F1-labeled LE/MVBs suggests a differential endocytic route compared to the ligand binding receptors FLS2 and BRI1, in agreement with the different BFA sensitivities reported for SERK3 and BRI1 (Bücherl et al., 2013). The observation of elevated colocalization between BRI1 and SERK3 with ARA6/Rab F1 in respect to ARA7/Rab F2b also shows a certain degree of overlap in retrograde trafficking. A possible scenario is that activated endocytosed BRI1-SERK3 hetero-oligomers remain intact and are subject to vacuolar degradation, whereas the non-interacting receptor pool follows a separate trafficking pathway. However, based on the electron microscopic details provided by Viotti et al. (2010) and here, this has to be seen with caution. The observation of BRI1 in luminal MVB vesicles (Viotti et al., 2010) indeed would lead to vacuolar degradation. SERK3 instead was found at the limiting membrane of PVCs. Fusion of PVCs with the vacuole therefore would result in localization of SERK3 to the tonoplast, as observed by Bücherl et al. (submitted). These PVCs may originate from TGN/EE- or Golgi-derived vesicles after the endocytosis of SERK3 from the PM (Wolfenstetter et al., 2012). To find SERK3 at this particular membrane entity supports the hypothesis that BRI1 and SERK3 may indeed follow distinct endoytic routes. But it also means endocytosed SERK3 may undergo recycling independent of BRI1.

Another scenario is therefore the disassembly of BRI1-SERK3 hetero-oligomers at the transition from TGN/EE to LE/MVB, followed by vacuolar degradation of activated BRI1 receptors and reinsertion of SERK3 into the PM to establish de novo receptor complexes with ligand bound BRI1 at the cell surface as also discussed by Beck et al. (2012). This possibility is very tempting, especially since SERK3 protein is less abundant than BRI1 (van Esse et al., 2011) and only a small fraction of this coreceptor participates in BR response (Albrecht et al., 2012), whereas the majority is involved in various other signaling pathways (Chinchilla et al., 2009). Differences in protein abundance were still visible in this study, even though overexpression systems were employed that may give rise to aberrant protein levels compared to endogenous expression. However, these systems are of great value, especially for investigating endosomal trafficking, and produce reliable data (Denecke et al., 2012).

In summary, live-cell confocal imaging was conducted for visualizing endosomal trafficking of the BR signaling components BRI1 and SERK3. Our study showed that subpopulations of BRI1 and SERK3 shuttle together through the endomembrane system of Arabidopsis during antero- and retrograde transport. A possible compartment of BRI1-SERK3 BR signaling unit disassembly may be the TGN/EE, whereas the ER was defined as the compartment of receptor complex assembly. Biogenesis of both receptors in the ER is accompanied by hetero-oligomerization, which emphasizes functional importance and the notion that protein oligomers or supramolecular structures instead of sole linear signal transduction pathways are an inevitable component of PM receptor signaling.

MATERIALS AND METHODS

Growth conditions

Arabidopsis (Arabidopsis thaliana) plants (ecotype Columbia [Col-0]) were used as wild type. Seeds were surface sterilized and germinated on ½ Murashige and Skoog medium (Duchefa) supplemented with 1% sucrose (Sigma) and 0.8% Daishin agar (Duchefa). Plants were grown at 22 °C under fluorescent light, with 16 h light/8 h dark photoperiods, unless otherwise specified. Transgenic seedlings were selected on ½ Murashige and Skoog medium (Duchefa) supplemented with 1% sucrose (Sigma) and 0.8% Daishin agar (Duchefa) containing 50 mg/L kanamycin (Duchefa), 15 mg/L phosphinothricin (PPT, Duchefa) or both.

Col-0 plants expressing BRI1 fused to GFP under its native promoter resulting in an about three-fold overexpression were provided by J. Chory (Friedrichsen et al., 2000). Col-0 plants expressing BRI1-YFP under control of a heat-shock promoter were obtained from N. Geldner (Geldner et al., 2007). SERK3-mCherry was generated as described previously (Chapter 3). The PIN2::PIN2-GFP (Abas et al., 2006) expressing line was provided by C. Schwechheimer.

Dual-color fluorescently tagged plant lines were generated by crossing either BRI1-GFP (Friedrichsen et al., 2000), BRI1-YFP (Geldner et al., 2007), PIN2-GFP (Abas et al., 2006) or SERK3-GFP (BAK1-GFP, Li et al., 2002) with SERK3-mCherry (Chapter 3), WAVE6-mCherry (Geldner et al., 2009), WAVE18-mCherry (Geldner et al., 2009), VHAa1-mRFP (Dettmer et al., 2006), ARA7/Rab F2B-mRFP (provided by K. Schumacher, Heidelberg, Germany), and ARA6/Rab F1-mRFP (provided by K. Schumacher, Heidelberg). F1 lines were used for marker colocalization imaging experiments. For FRET-FLIM using the heat-shock inducible BRI1-YFP line homozygous BRI1-YFP/SERK3-mCherry seedlings were used.

Fixation and Immuno-cytochemical labeling

For the immuno-labeling experiments 5 day old seedlings were used. Treatments and fixation were performed in 24-well plates used for cultivation. Prior to treatments, seedlings were washed once with 1 mL ½ Murashige and Skoog medium (Duchefa) supplemented with 1% sucrose (Sigma). For stimulation experiments seedlings were incubated for 1 h in 1 mL ½ Murashige and Skoog medium supplemented with 1% sucrose and the respective agents. Final concentrations used were 50 µM brefeldin A (Sigma) and 50 µM tyrphostin A23 (Sigma). The stock solutions were 50 mM brefeldin A and 50 mM tyrphostin A23, both dissolved in dimethylsulfoxide (Merck). After treatment, seedlings were washed once with PBS buffer pH 6.9. Subsequently, seedlings were fixed, placed on SuperFrost object slides (Menzel-Gläser) and immuno-labeled (Sauer et al., 2006). Antibodies used were rabbit-anti-GFP (generated by Eurogentec), mouse-anti-mCherry, goat-anti-rabbit-Alexa488 and goat-anti-mouse-Alexa568 (all Invitrogen).

Heat-shock induction

To induce BRI1-YFP expression and translation seedlings were transferred to preheated liquid half-strength MS medium containing either 50 µM brefeldin A or 50 µM brefeldin A and 50 µM tyrphostin A23. Seedlings were incubated for 30 min at 37 °C. After heat-shock application seedlings were transferred back to liquid half-strength MS medium containing the respective agents, followed by incubation under the regular growth conditions. Fixation of brefeldin A treated samples occurred after 30 min of recovery time, whereas brefeldin A/ tyrphostin A23 treated samples were fixed 1.5 h after heat-shock induction due to the delay of BRI1-YFP translation in the presence of tyrphostin A23.

Confocal imaging

Live root imaging was performed on a confocal laser scanning microscope (Leica TCS SP5 X system, Mannheim, Germany). GFP was excited using an argon laser (488 nm) and fluorescence emission was detected from 500-540 nm. mCherry and mRFP were excited using a white light continuum laser selecting the 580 nm laser line. Fluorescence was detected from 590-640 nm. Images were captured using a 63x water immersion objective

with a numeric aperture of 1.2 with a pinhole set to 1 Airy unit. Confocal images were analyzed with FIJI software (ImageJA 1.45j, Max Planck Society).

Transmission Electron Microscopy

Four- to five-day-old Arabidopsis root tips were cut from the seedling, submerged in freezing media composed by 140 mM sucrose, 7 mM trehalose and 7 mM Tris buffer (pH 6.6), transferred into planchettes (Wohlwend GmbH, Sennwald, Switzerland; type 241 and 242) and frozen in a high-pressure freezer (HPM010; Bal-Tec). Freeze substitution was performed in a Leica EM AFS2 freeze substitution unit (Leica; Germany) in dry acetone supplemented with 0.4% uranyl acetate at –85°C for 16 h before gradually warming up to –50 °C over an 5-h period. After washing with 100% ethanol for 60 min, the roots were infiltrated and embedded in Lowicryl HM20 at –50 °C (intermediate steps of 30, 50, 75% HM20 in ethanol, 1 h each), and polymerized for 3 days with ultraviolet (UV) light in the freeze substitution apparatus. To increase sectioning quality, the blocks were then hardened with UV light for another 4 h at room temperature. Ultrathin sections were cut on a Leica Ultracut S (Leica) and incubated with antibodies against GFF at a dilution of 1:150, followed by incubation with 10-nm gold-coupled secondary antibodies (BioCell GAR10; BioCell) at a dilution of 1:50 in PBS supplemented with 1% BSA. Sections were post-stained with aqueous uranyl acetate/lead citrate and examined in a JEM1400 transmission electron microscope (JEOL, Japan) operating at 80 kV. Micrographs were recorded with a FastScan F214 digital camera (TVIPS, Germany). This procedure was also previously applied in Viotti et al. (2010).

Colocalization Analysis

Colocalization analysis was performed using the "PSC colocalization" plugin for ImageJ (version 1.47g). Prior to colocalization analysis confocal images or time-lapse series were processed using the ImageJ plugin "Pure Denoise". Subsequently, regions of interest (ROIs) were selected and colocalization analysis was carried out using a threshold of 10. For z-stack or time-lapse series all images were analyzed in one set. For colocalization analysis of confocal images obtained from Arabidopsis protoplasts denoising was performed as well, prior to manual counting of endosomal compartments.

FRET-FLIM

FRET is a photo physical process in which the excited-state energy from a fluorescent donor molecule is transferred non-radiatively to an acceptor molecule. FRET is based on weak dipole–dipole coupling and therefore can only occur at molecular distances. There are several methods to quantify and visualize FRET, of which donor fluorescence lifetime imaging is the most straightforward, since a fluorescence lifetime is concentration-independent property. However, fluorescence lifetimes are sensitive to the environment, which is the basis

for FRET-FLIM. FRET-FLIM experiments consist of measuring donor fluorescence lifetimes in the absence (τD) and presence (τ_{DA}) of acceptor molecules resulting in spatially resolved color-coded lifetime images. Observation of a decreased donor fluorescence lifetime is used as read-out for molecular interactions (Borst and Visser, 2010).

A Leica TCS SP5 X system equipped with a 63x 1.20 NA water-immersion objective lens was used for confocal/FLIM imaging. Confocal and FLIM images were acquired by exciting the respective fluorophores GFP/mCherry/mRFP using a white-light laser (WLL; or super continuum laser). This laser emits a continuous spectrum from 470 to 670 nm, within which any individual excitation wavelength in 1 nm increments can be selected. For excitation of sCFP3A and sYFP2 (Kremers et al., 2006), a diode laser (440 nm) or the 514 nm line of an Argon laser was used, respectively. Confocal imaging was performed using internal filter-free spectral photomultiplier tube (PMT) detectors. For GFP detection a spectral window of 500-550 was selected, whereas mCherry/mRFP was detected using 590-640 nm. Detection of sCFP3A and sYFP2 was accomplished using a spectral window of 450-500 or 520-560 nm, respectively. Confocal images were acquired with 512 x 512 pixels.

For FRET- FLIM experiments, a pulsed diode laser (440 nm) or WLL (470 nm) at a pulsed frequency of 40 MHz was used. For recording of donor fluorescence, an external fiber output was connected to the Leica SP5 X scan head and coupled to a Hamamatsu HPM-100-40 Hybrid detector (Becker & Hickl), which has a time resolution of 120 ps. Selection of sCFP3A fluorescence was performed using band pass filters 470-500. Images with a frame size of 64 x 64 pixels were acquired with acquisition times of up to 90 sec.

From the fluorescence intensity images the decay curves were calculated per pixel and fitted with either a double- or triple-exponential decay model using the SPCImage software (Becker & Hickl, version 3.2.3.0). The double-exponential model function was applied for donor samples with only sCFP3A and mRFP present. For samples containing three fluorophores, sCFP3A, sYFP2, and mRFP respectively, a triple-exponential model function was used without fixing any parameter.

Statistical Analysis

Statistical analysis was performed using the Excel® sofware (Microsoft® Excel® for Mac 2011, version 14.1.3).

Accession Numbers

Sequence data from this article can be found in the Arabidopsis Genome Initiative or EMBL/GenBank data libraries under accession numbers: BRI1 (AT4G39400), PIN2 (AT5G57090), SERK3/BAK1 (AT4G22430), WAV6/NIP1;1 (AT4G19030), WAVE18/Got1p homolog (AT3G03180), ARA6/RABF1 (AT3G54840), ARA7/RABF2B (AT4G19640) and VHA-A1 (AT2G28520).

SUPPLEMENTAL MATERIAL

Figure S1: The BRI1-GFP level is reduced in absence of the SERK1 and SERK3 coreceptors.

REFERENCES

Achour L, Labbé-Jullié C, Scott MGH, Marullo S (2008) An escort for GPCRs: implications for regulation of receptor density at the cell surface. Trends Pharmacol. Sci. **29**: 528–535.

Albrecht C, Boutrot F, Segonzac C, Schwessinger B, Gimenez-Ibanez S, Chinchilla D, Rathjen JP, de Vries SC, Zipfel C (2012) Brassinosteroids inhibit pathogen-associated molecular pattern-triggered immune signaling independent of the receptor kinase BAK1. Proc. Natl. Acad. Sci. U.S.A. **109**: 303–308.

Beck M, Zhou J, Faulkner C, Maclean D, Robatzek S (2012) Spatio-Temporal Cellular Dynamics of the Arabidopsis Flagellin Receptor Reveal Activation Status-Dependent Endosomal Sorting. Plant Cell. doi: 10.1105/tpc.112.100263.

Bishop GJ, Koncz C (2002) Brassinosteroids and plant steroid hormone signaling. Plant Cell **14 Suppl**: S97–110.

Boevink P, Oparka K, Santa Cruz S, Martin B, Betteridge A, Hawes C (1998) Stacks on tracks: the plant Golgi apparatus traffics on an actin/ER network. Plant J. **15**: 441–447.

Boyd G (2002) Assembly and Cell Surface Expression of Homomeric and Heteromeric 5-HT3 Receptors: The Role of Oligomerization and Chaperone Proteins. Mol. Cell. Neurosci. **21**: 38–50.

Bücherl CA, van Esse GW, Kruis A, Luchtenberg J, Westphal AH, Aker J, van Hoek A, Albrecht C, Borst JW, de Vries SC (2013). Visualization of BRI1 and BAK1(SERK3) Membrane Receptor Heterooligomers during Brassinosteroid Signaling. Plant Physiol. **162**(4):1911-25.

Canals M, Lopez-Gimenez JF, Milligan G (2009) Cell surface delivery and structural re-organization by pharmacological chaperones of an oligomerization-defective alpha(1b)-adrenoceptor mutant demonstrates membrane targeting of GPCR oligomers. Biochem. J. **417**: 161–172.

Chinchilla D, Shan L, He P, de Vries S, Kemmerling B (2009) One for all: the receptor-associated kinase BAK1. Trends Plant Sci. **14**: 535–541.

Chinchilla D, Zipfel C, Robatzek S, Kemmerling B, Nürnberger T, Jones JDG, Felix G, Boller T (2007) A flagellin-induced complex of the receptor FLS2 and BAK1 initiates plant defence. Nature **448**: 497–500.

daSilva LLP, Snapp EL, Denecke J, Lippincott-Schwartz J, Hawes C, Brandizzi F (2004) Endoplasmic reticulum export sites and Golgi bodies behave as single mobile secretory units in plant cells. Plant Cell **16**: 1753–1771.

Denecke J, Aniento F, Frigerio L, Hawes C, Hwang I, Mathur J, Neuhaus J-M, Robinson DG (2012) Secretory pathway research: the more experimental systems the better. Plant Cell **24**: 1316–1326.

Dettmer J, Hong-Hermesdorf A, Stierhof Y-D, Schumacher K (2006) Vacuolar H+-ATPase activity is required for endocytic and secretory trafficking in Arabidopsis. Plant Cell **18**: 715–730.

Ebine K, Fujimoto M, Okatani Y, Nishiyama T, Goh T, Ito E, Dainobu T, Nishitani A, Uemura T, Sato MH, et al (2011) A membrane trafficking pathway regulated by the plant-specific RAB GTPase ARA6. Nat. Cell Biol. **13**: 853–859.

Ehrlich M, Gutman O, Knaus P, Henis YI (2012) Oligomeric interactions of TGF-β and BMP receptors. FEBS Letters **586**: 1885–1896.

Ehrlich M, Horbelt D, Marom B, Knaus P, Henis YI (2011) Homomeric and heteromeric complexes among TGF-β and BMP receptors and their roles in signaling. Cell. Signal. **23**: 1424–1432.

Fleck MW (2006) Glutamate receptors and endoplasmic reticulum quality control: looking beneath the surface. Neuroscientist **12**: 232–244.

Friedrichsen DM, Joazeiro CA, Li J, Hunter T, Chory J (2000) Brassinosteroid-insensitive-1 is a ubiquitously expressed leucine-rich repeat receptor serine/threonine kinase. Plant Physiol. **123**: 1247–1256.

Geldner N, Dénervaud-Tendon V, Hyman DL, Mayer U, Stierhof Y-D, Chory J (2009) Rapid, combinatorial analysis of membrane compartments in intact plants with a multicolor marker set. Plant J. **59**: 169–178.

Geldner N, Hyman DL, Wang X, Schumacher K, Chory J (2007) Endosomal signaling of plant steroid receptor kinase BRI1. Genes Dev. **21**: 1598–1602.

Gilboa L, Nohe A, Geissendörfer T, Sebald W, Henis YI, Knaus P (2000) Bone morphogenetic protein receptor complexes on the surface of live cells: a new oligomerization mode for serine/threonine kinase receptors. Mol. Biol. Cell **11**: 1023–1035.

Gilboa L, Wells RG, Lodish HF, Henis YI (1998) Oligomeric structure of type I and type II transforming growth factor beta receptors: homodimers form in the ER and persist at the plasma membrane. J. Cell Biol. **140**: 767–777.

Gimenez-Ibanez S, Hann DR, Ntoukakis V, Petutschnig E, Lipka V, Rathjen JP (2009) AvrPtoB Targets the LysM Receptor Kinase CERK1 to Promote Bacterial Virulence on Plants. Curr. Biol. 1–7.

Gou X, Yin H, He K, Du J, Yi J, Xu S, Lin H, Clouse SD, Li J (2012) Genetic evidence for an indispensable role of somatic embryogenesis receptor kinases in brassinosteroid signaling. PLoS Genet. **8**: e1002452.

Gómez-Gómez L, Boller T (2000) FLS2: an LRR receptor-like kinase involved in the perception of the bacterial elicitor flagellin in Arabidopsis. Mol. Cell **5**: 1003–1011.

Hartung A, Bitton-Worms K, Rechtman MM, Wenzel V, Boergermann JH, Hassel S, Henis YI, Knaus P (2006) Different routes of bone morphogenic protein (BMP) receptor endocytosis influence BMP signaling. Mol. Cell. Biol. **26**: 7791–7805.

He K, Gou X, Yuan T, Lin H, Asami T, Yoshida S, Russell SD, Li J (2007) BAK1 and BKK1 regulate brassinosteroid-dependent growth and brassinosteroid-independent cell-death pathways. Curr. Biol. **17**: 1109–1115.

Herrick-Davis K, Weaver BA, Grinde E, Mazurkiewicz JE (2006) Serotonin 5-HT2C receptor homodimer biogenesis in the endoplasmic reticulum: real-time visualization with confocal fluorescence resonance energy transfer. J. Biol. Chem. **281**: 27109–27116.

Hofman EG, Bader AN, Voortman J, van den Heuvel DJ, Sigismund S, Verkleij AJ, Gerritsen HC, van Bergen en Henegouwen PMP (2010) Ligand-induced EGF receptor oligomerization is kinase-dependent and enhances internalization. J. Biol. Chem. **285**: 39481–39489.

Hong Z, Jin H, Fitchette A-C, Xia Y, Monk AM, Faye L, Li J (2009) Mutations of an alpha1,6 mannosyltransferase inhibit endoplasmic reticulum-associated degradation of defective brassinosteroid receptors in Arabidopsis. Plant Cell **21**: 3792–3802.

Hong Z, Jin H, Tzfira T, Li J (2008) Multiple mechanism-mediated retention of a defective brassinosteroid receptor in the endoplasmic reticulum of Arabidopsis. Plant Cell **20**: 3418–3429.

Hong Z, Kajiura H, Su W, Jin H, Kimura A, Fujiyama K, Li J (2012) Evolutionarily conserved glycan signal to degrade aberrant brassinosteroid receptors in Arabidopsis. Proc. Natl. Acad. Sci. U.S.A. **109**: 11437–11442.

Hüttner S, Veit C, Schoberer J, Grass J, Strasser R (2012) Unraveling the function of Arabidopsis thaliana OS9 in the endoplasmic reticulum-associated degradation of glycoproteins. Plant Mol. Biol. doi: 10.1007/s11103-012-9891-4.

Irani NG, Di Rubbo S, Mylle E, Van den Begin J, Schneider-Pizoń J, Hniliková J, Síša M, Buyst D, Vilarrasa-Blasi J, Szatmari A-M, et al (2012) Fluorescent castasterone reveals BRI1 signaling from the plasma membrane. Nat. Chem. Biol. **8**: 583–589.

Jaillais Y, Belkhadir Y, Balsemão-Pires E, Dangl JL, Chory J (2011a) Extracellular leucine-rich repeats as a platform for receptor/coreceptor complex formation. Proc. Natl. Acad. Sci. U.S.A. **108**: 8503–8507.

Jaillais Y, Hothorn M, Belkhadir Y, Dabi T, Nimchuk ZL, Meyerowitz EM, Chory J (2011b) Tyrosine phosphorylation controls brassinosteroid receptor activation by triggering membrane release of its kinase inhibitor. Genes Dev. **25**: 232–237.

Jensen EV, DeSombre ER (1973) Estrogen-Receptor Interaction: Estrogenic hormones effect transformation of specific receptor proteins to a biochemically functional form. Science **182**: 126–134.

Jürgens G (2004) Membrane trafficking in plants. Annu. Rev. Cell. Dev. Biol. **20**: 481–504.

Kim T-W, Guan S, Sun Y, Deng Z, Tang W, Shang J-X, Sun Y, Burlingame AL, Wang Z-Y (2009) Brassinosteroid signal transduction from cell-surface receptor kinases to nuclear transcription factors. Nat. Cell Biol. **11**: 1254–1260.

Kinoshita T, Caño-Delgado A, Seto H, Hiranuma S, Fujioka S, Yoshida S, Chory J (2005) Binding of brassinosteroids to the extracellular domain of plant receptor kinase BRI1. Nature **433**: 167–171.

Langhans M, MECKEL T, KRESS A, LERICH A, Robinson DG (2012) ERES (ER exit sites) and the "secretory unit concept". J. Microsc. **247**: 48–59.

Li J, Wen J, Lease KA, Doke JT, Tax FE, Walker JC (2002) BAK1, an Arabidopsis LRR receptor-like protein kinase, interacts with BRI1 and modulates brassinosteroid signaling. Cell **110**: 213–222.

Ma-Högemeier Z-L, Körber C, Werner M, Racine D, Muth-Köhne E, Tapken D, Hollmann M (2010) Oligomerization in the endoplasmic reticulum and intracellular trafficking of kainate receptors are subunit-dependent but not editing-dependent. J. Neurochem. doi: 10.1111/j.1471-4159.2009.06559.x.

Nebenführ A, Gallagher LA, Dunahay TG, Frohlick JA, Mazurkiewicz AM, Meehl JB, Staehelin LA (1999) Stop-and-go movements of plant Golgi stacks are mediated by the acto-myosin system. Plant Physiol. **121**: 1127–1142.

Nebenführ A, Ritzenthaler C, Robinson DG (2002) Brefeldin A: deciphering an enigmatic inhibitor of secretion. Plant Physiol. **130**: 1102–1108.

Neubert C, Graham LA, Black-Maier EW, Coonrod EM, Liu T-Y, Stierhof Y-D, Seidel T, Stevens TH, Schumacher K (2008) Arabidopsis has two functional orthologs of the yeast V-ATPase assembly factor Vma21p. Traffic **9**: 1618–1628.

Nohe A, Hassel S, Ehrlich M, Neubauer F, Sebald W, Henis YI, Knaus P (2002) The mode of bone morphogenetic protein (BMP) receptor oligomerization determines different BMP-2 signaling pathways. J. Biol. Chem. **277**: 5330–5338.

Popescu SC (2012) A model for the biosynthesis and transport of plasma membrane-associated signaling receptors to the cell surface. Front. Plant Sci. **3**: 71.

Rechtman MM, Nakaryakov A, Shapira KE, Ehrlich M, Henis YI (2009) Different domains regulate homomeric and heteromeric complex formation among type I and type II transforming growth factor-beta receptors. J. Biol. Chem. **284**: 7843–7852.

Reyes FC, Buono R, Otegui MS (2011) Plant endosomal trafficking pathways. Curr. Opin. Plant Biol. **14**: 666–673.

Richter S, Voss U, Jürgens G (2009) Post-Golgi traffic in plants. Traffic **10**: 819–828.

Russinova E, Borst JW, Kwaaitaal M, Caño-Delgado A, Yin Y, Chory J, de Vries SC (2004) Heterodimerization and endocytosis of Arabidopsis brassinosteroid receptors BRI1 and AtSERK3 (BAK1). Plant Cell **16**: 3216–3229.

Schulze B, Mentzel T, Jehle AK, Mueller K, Beeler S, Boller T, Felix G, Chinchilla D (2010) Rapid heteromerization and phosphorylation of ligand-activated plant transmembrane receptors and their associated kinase BAK1. J. Biol. Chem. **285**: 9444–9451.

Shah K, Vervoort J, de Vries SC (2001) Role of threonines in the Arabidopsis thaliana somatic embryogenesis receptor kinase 1 activation loop in phosphorylation. J. Biol. Chem. **276**: 41263–41269.

Shimada Y, Goda H, Nakamura A, Takatsuto S, Fujioka S, Yoshida S (2003) Organ-specific expression of brassinosteroid-biosynthetic genes and distribution of endogenous brassinosteroids in Arabidopsis. Plant Physiol. **131**: 287–297.

Su W, Liu Y, Xia Y, Hong Z, Li J (2011) Conserved endoplasmic reticulum-associated degradation system to eliminate mutated receptor-like kinases in Arabidopsis. Proc. Natl. Acad. Sci. U.S.A. **108**: 870–875.

Ueda T, Uemura T, Sato MH, Nakano A (2004) Functional differentiation of endosomes in Arabidopsis cells. Plant J. **40**: 783–789.

Van Craenenbroeck K (2012) GPCR Oligomerization: Contribution to Receptor Biogenesis. Subcell. Biochem. **63**: 43–65.

Van Craenenbroeck K, Borroto-Escuela DO, Romero-Fernandez W, Skieterska K, Rondou P, Lintermans B, Vanhoenacker P, Fuxe K, Ciruela F, Haegeman G (2011) Dopamine D4 receptor oligomerization--contribution to receptor biogenesis. FEBS J. **278**: 1333–1344.

van Esse G, Westphal AH, Surendran RP, Albrecht C, van Veen B, Borst JW, de Vries SC (2011) Quantification of the brassinosteroid insensitive1 receptor in planta. Plant Physiol. **156**: 1691–1700.

Viotti C, Bubeck J, Stierhof Y-D, Krebs M, Langhans M, van den Berg W, van Dongen W, Richter S, Geldner N, Takano J, et al (2010) Endocytic and secretory traffic in Arabidopsis merge in the trans-Golgi network/early endosome, an independent and highly dynamic organelle. Plant Cell **22**: 1344–1357.

Wang X, Goshe MB, Soderblom EJ, Phinney BS, Kuchar JA, Li J, Asami T, Yoshida S, Huber SC, Clouse SD (2005) Identification and functional analysis of in vivo phosphorylation sites of the Arabidopsis BRASSINOSTEROID-INSENSITIVE1 receptor kinase. Plant Cell **17**: 1685–1703.

Wang X, Kota U, He K, Blackburn K, Li J, Goshe MB, Huber SC, Clouse SD (2008) Sequential transphosphorylation of the BRI1/BAK1 receptor kinase complex impacts early events in brassinosteroid signaling. Dev. Cell **15**: 220–235.

Wang Z-Y, Nakano T, Gendron J, He J, Chen M, Vafeados D, Yang Y, Fujioka S, Yoshida S, Asami T, et al (2002) Nuclear-localized BZR1 mediates brassinosteroid-induced growth and feedback suppression of brassinosteroid biosynthesis. Dev. Cell **2**: 505–513.

Wolfenstetter, S., Wirsching, P., Dotzauer, D., Schneider, S., and Sauer, N. (2012). Routes to the Tonoplast: The Sorting of Tonoplast Transporters in Arabidopsis Mesophyll Protoplasts. Plant Cell **24**: 215–232.

Yin Y, Vafeados D, Tao Y, Yoshida S, Asami T, Chory J (2005) A new class of transcription factors mediates brassinosteroid-regulated gene expression in Arabidopsis. Cell **120**: 249–259.

Yin Y, Wang Z-Y, Mora-Garcia S, Li J, Yoshida S, Asami T, Chory J (2002) BES1 accumulates in the nucleus in response to brassinosteroids to regulate gene expression and promote stem elongation. Cell **10.9**: 181–191.

SUPPLEMENTAL MATERIAL

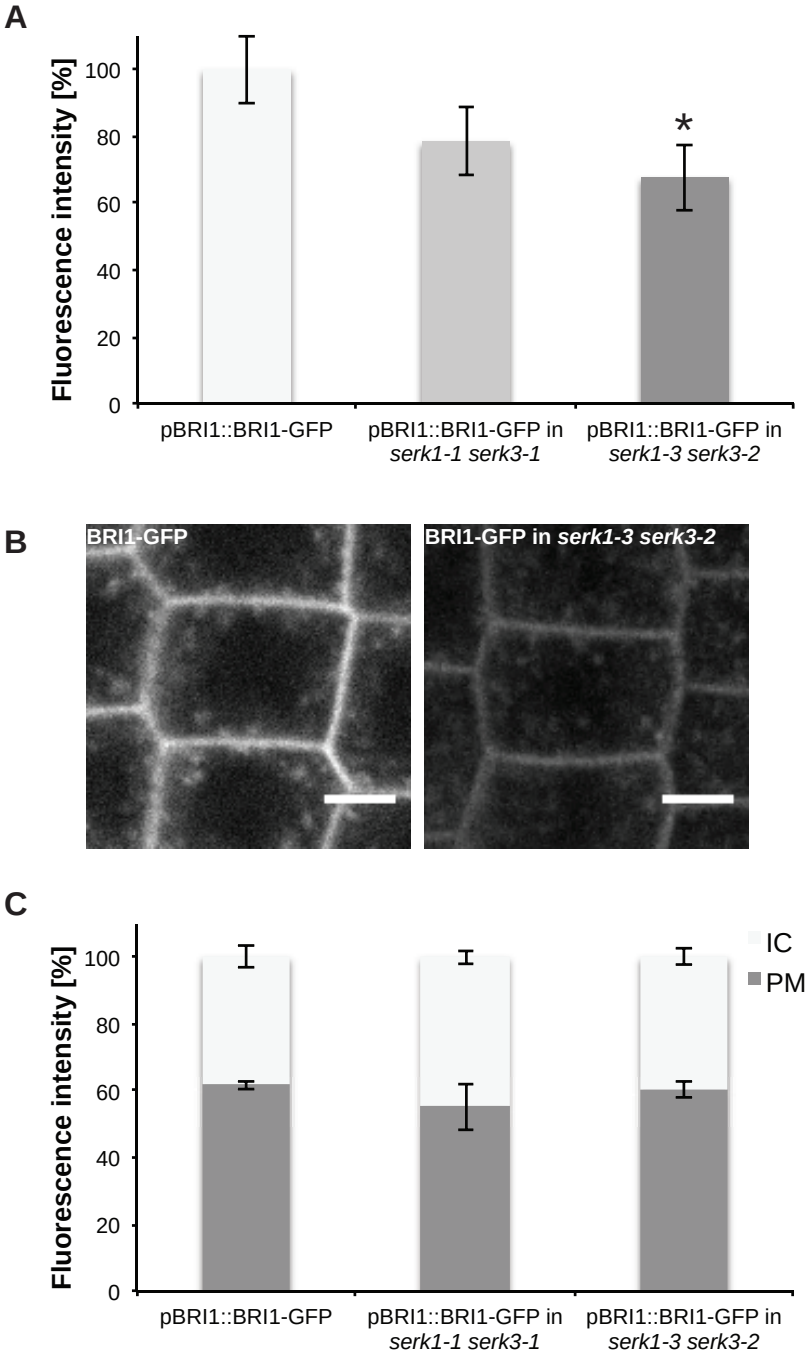

Figure S1: The BRI1-GFP level is reduced in absence of the SERK1 and SERK3 coreceptors.

Confocal imaging was performed on 5 day old live Arabidopsis seedling roots expressing BRI1-GFP in wild type or the indicated *serk1 serk3* loss-of-function mutant backgrounds. Meristematic epidermal root cells were imaged. Subsequently, fluorescence intensities were quantified for whole cells or separate for PM and cytosol. Scale bars indicate a distance of 5 µm.
(**A**) Quantification of total BRI1-GFP fluorescence intensities in wild type, *serk1-1 serk3-1*, and *serk1-3 serk3-2* double mutant backgrounds.
(**B**) Confocal images of BRI1-GFP in wild type and *serk1-3 serk3-2* loss-of-function mutant backgrounds.
(**C**) Quantification of the subcellular BRI1-GFP distribution.
Quantification of BRI1-GFP fluorescence intensities derived from wild type and mutant backgrounds showed a reduction of BRI1-GFP protein abundance in absence of the SERK1 and SERK3 coreceptors. Still, the subcellular distribution remained constant.
The reduced amount of BRI1-GFP may result from enhanced ERAD of newly translated BRI1-GFP due to the loss of interaction with the coreceptors in the ER during receptor biogenesis.

Chapter 6

Summarizing Discussion

Christoph A. Bücherl

SUMMARY

Living matter is continuously challenged by the dynamics of its environment and intrinsic fluctuations. In the course of evolution, cells have developed mechanisms to detect and adapt to environmental and endogenous cues by the use of a wide array of receptors (Afzal et al., 2008). These receptors perceive specific signals, which, in turn, initiate a sequence of molecular events within the cells that convert signal perception into an adequate physiological response. Collectively, these processes of signal perception, signal transmission and cell adaptation represent so-called signal transduction pathways.

For the perception of signals such as hormones or pathogens cells are equipped with receptors that are often located at the cell surface. In plants, many of these receptors belong to the class of leucine-rich repeat receptor-like kinases (LRR-RLKs) (Shiu and Bleecker, 2001). They comprise an extracellular LRR domain for ligand binding, a transmembrane domain, which anchors them within the plasma membrane (PM) of their host cells, and an intracellular kinase domain for transducing the event of ligand binding into the cell interior. One of the best-described plant LRR-RLKs is the Brassinosteroid insensitive 1 (BRI1) receptor. Since the discovery in 1997 (Li and Chory, 1997) its mode of action has been studied extensively and has resulted in the elucidation of a complete set of molecular components constituting the brassinoteroid (BR) signal transduction pathway (Clouse, 2011). BRs, the ligands of BRI1, are a group of polyhydroxy lactones that are structurally similar to animal steroid hormones (Grove et al., 1979). This class of phytohormones regulates several aspects of plant growth and development (Kutschera and Wang, 2012). During the last decade it has been shown that BRI1 indeed perceives BRs at the PM (Kinoshita et al., 2005), however, initiation of BR signal transduction requires interaction of BRI1 with other, non-ligand binding receptors (Nam and Li, 2002; Wang et al., 2008; Gou et al., 2012). These coreceptors belong to the family of Somatic embryogenesis receptor-like kinases (SERKs) and have a related structural architecture to BRI1, but with a smaller extracellular domain. Three members of this protein family are involved in BR signaling: SERK1, SERK3 (also known as BAK1 for BRI1-associated kinase 1), and SERK4 (also known as BKK1 for BAK1-like kinase 1). Besides their role as coreceptors of BRI1, the SERKs have also been implicated in various other signaling processes like somatic embryogenesis, male fertility, cell death regulation and plant immunity (Chinchilla et al., 2009).

In the **first Chapter** of this thesis, the BR signaling pathway was introduced in further detail and it was highlighted how genetic and biochemical approaches attributed to the identification of cellular components that link signal perception of BRs at the PM to BR-dependent transcriptional regulation in the nucleus. Based on these findings a model for BRI1-mediated signal transduction was established, which often serves as a paradigm for plant PM receptor signaling. Even though the molecular determinants of BR signaling have been revealed, full mechanistic detail is still missing. The aim of this thesis was to

describe BRI1-mediated signal transduction and the respective role of SERK3, the main coreceptor of BR signaling (Albrecht et al., 2008), at (sub)cellular level in Arabidopsis roots. For this purpose different fluorescence imaging techniques were applied, which allowed investigating the spatiotemporal localization and interaction dynamics of BRI1 and SERK3 in their natural environment.

One of the main microscopic methods applied throughout this thesis was fluorescence lifetime imaging microscopy (FLIM). Most imaging approaches, like confocal microscopy, only rely on fluorescence intensities as read-outs. However, the fluorescence lifetime τ is an additional parameter of fluorescence microscopy. This parameter is sensitive to the local environment of fluorescent probes and therefore can be exploited to illuminate cellular processes in live cells and tissues. In **Chapter 2**, the theoretical background of FLIM was introduced and it was illustrated how this technique can be used to reveal protein-protein interactions in Arabidopsis mesophyll protoplasts based on Förster resonance energy transfer (FRET). Next to a protocol for protoplast isolation and transient transfection, we provided a tutorial for analyzing time-resolved fluorescence intensity images using the software package SPCImage (Becker & Hickl). By determining the fluorescence lifetimes of a FRET donor fluorophore in the absence and the presence of a FRET acceptor chromophore physical interaction between the fluorescently tagged proteins of interest can be deduced. If the two proteins of interest, and thus the conjugated fluorophores, reside in close proximity FRET can occur and will result in a decrease of donor fluorescence lifetime. Besides the applicability to live cells and organisms, another important advantage of FRET-FLIM is the possibility to spatially resolve protein interactions within the two-dimensional imaging plane.

In **Chapter 3**, this technique was applied to live Arabidopsis roots. In our attempt to visualize the molecular events upon initiation of BR signaling, we performed FRET-FLIM on a double transgenic plant line expressing BRI1-GFP (Friedrichsen et al., 2000) and SERK3-mCherry. In accord with the current model of BR signal transduction (Jaillais et al., 2011a), a time-dependent and ligand-induced hetero-oligomerization between BRI1 and SERK3 was observed, similar to previous reports using coimmunoprecipitation (Wang et al., 2005; 2008; Albrecht et al., 2012). In addition, the spatially resolved FLIM images enabled us to localize these BRI1-SERK3 receptor complexes to restricted areas within the PM of live epidermal root cells, a cell file known to exhibit active BR signaling (Hacham et al., 2011). Application of brefeldin A (BFA), a fungal toxin reported to inhibit recycling (Nebenführ et al., 2002), allowed the visualization of intracellular receptor oligomers, which were most likely endocytosed from the PM. In contrast to the established BRI1 signaling model, FRET-FLIM revealed that a substantial amount of the BRI1-SERK3 hetero-oligomers was preformed. Constitutive receptor oligomerization is a well-established concept in animal signaling research (Gadella and Jovin, 1995; Martin-Fernandez et al., 2002; Issafras et al., 2002; Van Craenenbroeck et al., 2011), however in the plant field only a single study reported similar findings (Shimizu et al., 2010).

Besides the physical interaction between BRI1 and SERK3, also their localization and colocalization patterns were investigated (**Chapter 3**). As expected, most of the fluorescently tagged receptors localized to the PM. The intracellular fraction of BRI1-GFP mainly resided in punctate endosomal structures as documented previously (Geldner et al., 2007; Viotti et al., 2010; Irani et al., 2012). Similar endomembrane compartments were also observed for SERK3-mCherry, though to a lesser extent. In contrast to BRI1, for SERK3 an additional intracellular compartment was elucidated, the tonoplast. A further difference in the localization patterns of BRI1 and SERK3 was revealed when BFA was applied. Whereas BRI1-GFP strongly accumulated in BFA bodies, SERK3-GFP was only marginally affected, which hints at a differential endocytic pathway for both receptors. Although BRI1 and SERK3 showed distinct localization patterns, the two fluorescently tagged proteins also overlapped to some degree. Comparative colocalization analysis revealed that both the PM and the intracellular overlap between both LRR-RLKs is responsive to the BR signaling status. Application of brassinolide (BL), an endogenous BRI1 ligand, as well as BFA, which was demonstrated to elevate BR signaling activity (Geldner et al., 2007; Irani et al., 2012), resulted in an increased number of colocalizing BRI1 and SERK3 proteins. Thus FRET-FLIM and confocal imaging based colocalization analysis indicated that activation of the BR signaling system is accompanied by spatially distinct association of the two signal transduction inducing receptors BRI1 and SERK3.

As just illustrated, fluorescence microscopy is a valuable tool for investigating signal transduction processes in the natural environment of the executing molecular components. Unfortunately, a major drawback of the various techniques is that often only qualitative read-outs are obtained. Therefore we examined (**Chapter 4)** two different quantitative colocalization approaches in their ability to discriminate varying colocalizing protein populations. First, the cytosolic colocalization of BRI1-GFP with the endosomal marker proteins ARA6 and ARA7 was investigated. Both tested and freely available ImageJ plugins Coloc2 and PSC Colocalization (French et al., 2008) revealed that BRI1-GFP preferentially localized to ARA7-mRFP labeled endosomal compartments. This finding was confirmed by manual counting of the respective endosomal structures and verified the reliability of the two quantitative colocalization methods. A biological explanation of the obtained result is given by the identity of the labeled endomembrane compartments. ARA7 localizes to both early endosomes (EEs), which enable recycling to the PM, and late endosomes (LEs; also known as multivesicular bodies [MVBs]), which are determined for vacuolar fusion. In contrast, ARA6 labels mainly LEs/MVBs. Thus both markers overlap to a certain degree during the maturation of LE but still have distinct localization patterns (Ueda et al., 2004; Ebine et al., 2011). Since BRI1 undergoes constitutive recycling (Geldner et al., 2007), our finding of preferential colocalization between BRI1 and ARA7 is plausible. In addition, similar observations were recently also reported for Flagellin sensing 2 (FLS2), an LRR-RLK involved in plant immunity, which also exhibits constitutive recycling (Beck et al., 2012).

After establishing the applicability of both colocalization approaches, we also intended to confirm our previous observation of increased BRI1 and SERK3 colocalization in response to BFA obtained with the Coloc2 plugin (Chapter 3). The application of PSC Colocalization indeed confirmed our initial colocalization results. The elevated colocalization of BRI1 and SERK3 upon drug treatment mostly like reflects the PM-stabilizing effect of BFA (Irani et al., 2012), which may also account for SERK3, since both Manders' colocalization coefficients were increased. Nonetheless, a difficulty of quantitative colocalization analysis is the interpretation of colocalization coefficients obtained for individual images. However, they enable to assess image data sets, recorded under the same imaging conditions, in a comparative manner and that way allow to draw quantitative conclusions (Dunn et al., 2011).

Colocalization analysis is not the only approach that suffers from qualitative read-outs and interpretations. The same accounts for FRET-FLIM studies. In particular the observation of preformed BRI1-SERK3 hetero-oligomers triggered our interest in developing a quantitative FLIM analysis procedure, which would be able to resolve ligand-independent and ligand-induced receptor complex populations. The details of our approach, which is based on time-correlated single photon count (TCSPC) measurements, were described in Chapter 4. Using this novel FLIM analysis procedure enabled us to estimate the different populations of BRI1 and SERK3 complexes. Upon BL stimulation around 10% of PM-located BRI1-GFP receptors were in complex with SERK3-mCherry. This finding is in line with recently reported data based on an in silico modeling approach (van Esse et al., 2012) and semi-quantitative coimmunoprecipitation (Albrecht et al., 2012), which suggested that active BR signal transduction involves between 1-10% of BRI1 receptors. Unfortunately, there are no quantitative data available for constitutive BRI1-SERK3 hetero-oligomers, even though their existence was proposed (Wang et al., 2005). Based on our imaging approach and analysis procedure we estimate that approximately 70% of PM BRI1-SERK3 hetero-oligomers are preformed.

Finding such a considerable amount of preformed BRI1-SERK3 receptor complexes in the PM of root epidermal cells was intriguing since it contradicts the current view on BR signaling, which assumes a strictly ligand-dependent association of the two LRR-RLKs (Jaillais et al., 2011a). This posed the question when or where these preformed complexes are established. To address this point we investigated in **Chapter 5** which cellular compartments harbor individual BRI1 and SERK3 receptors, and in which organelles these two receptors colocalize. Comparative colocalization analysis in live Arabidopsis roots revealed that both LRR-RLKs follow the traditional secretory and retrograde transport routes. These observations confirmed and extended previous findings for BRI1 using live cell (Friedrichsen et al., 2000; Geldner et al., 2007; Viotti et al., 2010; Irani et al., 2012) and electron microscopy (Viotti et al., 2010). For SERK3, to date only localization to EEs was suggested (Russinova et al., 2004).

Using the transient expression system of Arabidopsis protoplasts we could moreover show that both receptors also colocalize in the various endomembrane compartments of anterograde and retrograde trafficking. However, using electron microscopy a striking difference between their localization in retrograde endosomal compartments was elucidated. Whereas BRI1 was previously shown to reside at the membranes of the enclosed vesicles (Viotti et al., 2010), SERK3 was visualized at the limiting membrane of prevacuolar compartments (PVCs). This finding also explains, why SERK3, but not BRI1, was observed at the tonoplast (Chapter 3). Fusion of MVBs with the vacuole results in the release of BRI1 along with the inner MVB vesicles into the vacuolar lumen. PVC-localized SERK3 instead is incorporated into the tonoplast after membrane fusion.

Collectively, the colocalization analysis of BRI1 and SERK3 with respect to endomembrane compartments revealed that subpopulations of both LRR-RLKs probably follow the same route to the PM, but that after endocytosis from the PM, possibly during the maturation of TGN/EEs to LEs/MVBs, a separation occurs. Still, these findings do not answer where or when BRI1-SERK3 hetero-oligomers are established. For that reason we applied FRET-FLIM on the subcellular compartment, in which BRI1 and SERK3 colocalized for the first time, the endoplasmic reticulum (ER). Similar to our observations at the PM of root epidermal cells (Chapter 3), most of the ER membrane did not show BRI1-SERK3 receptor complexes. Still, in restricted ER membrane regions strongly reduced donor fluorescence lifetimes were observed, indicating that BRI1-SERK3 hetero-oligomers are established already in the ER before entering the anterograde trafficking pathway. Finally, using a heat-shock inducible plant system we could confirm the establishment of BRI1-SERK3 hetero-oligomers shortly after biogenesis on their way to the PM. Thus, the observed preformed receptor complexes in the PM of root epidermal cells (Chapter 3) mostly likely originated from the ER and were inserted via targeted transport into the PM, the site where they fulfill their function as BR signaling units.

GENERAL DISCUSSION

Growing evidence emphasizes the interplay between the spatiotemporal dynamics of signaling components and the downstream signaling outputs (Dehmelt and Bastiaens, 2010). Therefore in this thesis different fluorescence microscopic techniques were employed to illuminate the subcellular fluctuations of BRI1 and SERK3, the basic components of the main BR signaling unit (Nam and Li, 2002; Albrecht et al., 2008; Gou et al., 2012).

SERK3's autonomy at the tonoplast

The comparative localization analysis revealed that BRI1 and SERK3 colocalize to a varying degree in all of the investigated cellular compartments. Only for one organelle, the tonoplast, a difference was found. At first glance, the tonoplast localization of SERK3 may not seem of significant importance. However, it actually could point to one of the SERK3 functions, to transmit the primary BR signal to downstream targets of the BR signaling pathway.

The vacuole of plant cells has many different functions besides its role as the cellular waste bin, such as the enormous storage capacity for ions, like K^+, Mg^{2+}, NO^{3-}, or Ca^{2+} (Peiter, 2011; Etxeberria et al., 2012). The release of ions from the vacuole is regulated via tonoplast-resident ion channels (Peiter, 2011; Etxeberria et al., 2012). Interestingly, a recent report suggests a possible link between BR and calcium signaling (Oh et al., 2012a). Thus, to find SERK3 at this particular endomembrane compartment may indicate an additional tie between these two signaling pathways.

Besides a possible role for tonoplast-localized SERK3 in regulating cytosolic Ca^{2+} levels, it could also be involved in the vacuolar release of additional classes of ions. An early cellular response of BR signaling is the hyperpolarization of the PM (Caesar et al., 2011). Caesar et al. (2011) could link this change of the electro-chemical potential to PM-bound H^+-ATPase (P-ATPase) activity. However, it cannot be ruled out that different ion sources, like the vacuole, are involved in the observed PM hyperpolarization. A role of SERK3 in regulating cellular ion concentrations, released from the vacuole or generated by other means, is a tempting hypothesis since the heterologous expression of BRI1 alone in Nicotina benthamiana failed to alter the cellular electro-chemical potential, even though P-ATPase homologs are present in the PM of this plant species (Caesar et al., 2011).

The same study revealed a P-ATPase-dependent cell wall expansion in response to brassinolide (BL), which required the physical interaction of P-ATPase and BRI1 (Caesar et al., 2011). But biosynthesis and modifications of cell walls not only involve P-ATPases, also vacuolar H^+-ATPases (V-ATPases) contribute to these processes in a BR-dependent fashion (Kutschera et al., 2010). Therefore a possible scenario is that PM-residing H^+-ATPases underlie the control of BRI1, and that tonoplast-localized SERK3 regulates the activity of their vacuolar counterparts. Hence, next to a regulative role of SERK3 in BRI1 trafficking

(Russinova et al., 2004) and BRI1 kinase activation (Wang et al., 2008) this RLK could also exhibit autonomous functions by controlling elements of cell wall biosynthesis and ion transport.

This hypothesis is of particular interest in the light of the plentiful pathways this coreceptor participates in. In addition to its role in BRI1-mediated signal transduction, SERK3 is also an essential component of plant immunity and cell death regulation (Chinchilla et al., 2009). One of the first reactions of plants in response to pathogenic invaders is calcium spiking (Nürnberger et al., 2004). At latter stages, defense responses can include the fortification of cell walls and the hypersensitive response, the locally restricted cell death of attacked plant cells (Jones and Dangl, 2006). For both plant immunity and cell death the vacuole plays an important role by providing a reservoir of defense proteins and lytic enzymes (Hara-Nishimura and Hatsugai, 2011). To observe the multifaceted SERK3 coreceptor at the tonoplast is therefore an intriguing finding and may help to understand why this particular LRR-RLK has been hijacked by various functionally diverse ligand-binding receptors.

BR versus immune signaling

The participation of the SERK3 as a coreceptor in distinct physiological pathways, like BR and immune signaling, also opens up the possibility to unravel different regulatory principles of PM receptor signaling by studying a single protein. Here, I want to focus on the hetero-oligomerization profile of SERK3 and the ligand-binding receptors BRI1 and FLS2. Our FRET-FLIM analysis showed that activation of BR signaling results in the induction of BRI1-SERK3 hetero-oligomers, although with slow kinetics, since a significant increase was only observed 30 min after BL stimulation. Similar results were obtained by Albrecht et al. (2012) using coimmunoprecipition and also the phosphorylation kinetics of BRI1 are in line with our observations (Oh et al., 2012b). But these findings are in stark contrast to the rapid association and trans-phosphorylation between SERK3 and FLS2, which occur almost instantaneously upon ligand application (Schulze et al., 2010). This suggests fundamental differences in the activation mechanisms of BR and immune signaling.

Activation of the first layer of plant immunity, to which FLS2 belongs (Monaghan and Zipfel, 2012), is elicited by so-called danger-associated molecular patterns (DAMPs). These elicitors are mainly derived from microbes and can indicate the onset of pathogen invasion. This also accounts for the ligand of FLS2, which is derived from the bacterial flagellin protein. Thus a rapid activation of immune signaling is desirable to restrict and fight colonization of the plant by pathogenic invaders. In contrast, BRs are endogenous phytohormones regulating many aspects of plant growth and development. Moreover, they result in concentration-dependent opposing physiological responses (van Esse et al., 2012). To avoid adverse effects of fluctuating hormone concentrations and to ensure robustness of the signaling system, BR signaling may be subject to an activation threshold or fold-change regulation (Hart and Alon, 2013). As a consequence, only changes in ligand

availability over an extended time frame or above certain concentrations would result in adjustments of signaling output.

An alternative, but not independent, explanation for the differences in immune and hormone signaling could be given by another striking difference we observed for the hetero-oligomerization profile of SERK3 with the two ligand-binding receptors BRI1 and FLS2. Whereas coimmunoprecipitation experiments indicate that FLS2 and SERK3 only associate upon ligand binding (Schulze et al., 2010), we observed a substantial amount of preformed BRI1-SERK3 receptor complexes using FRET-FLIM. These constitutive receptor complexes may represent the perception system for endogenous and very low amounts of ligand (Shimada et al., 2003). In response to further increasing ligand concentrations the de novo formation of BRI1-SERK3 hetero-oligomers may follow.

That preformed receptor complexes indeed could make a difference for signaling regulation is in line with observations for animal signaling systems. The dimerization of Toll-like receptor 4 (TLR4), an innate immune receptor, is regulated by ligand binding (Saitoh et al., 2004), whereas receptors that perceive endogenous ligands, like the epidermal growth factor receptor (EGFR) (Martin-Fernandez et al., 2002; Bader et al., 2009), the insulin receptor (Massague et al., 1980), or chemokine receptors (Issafras et al., 2002), form constitutive oligomers. For EGFR and other receptor classes, an additional increase of de novo oligomers in response to exogenously applied ligand has been shown as well (Martin-Fernandez et al., 2002; Ehrlich et al., 2012), similar to our findings.

Functional significance of preformed receptor oligomers

The observation of preformed BRI1-SERK3 hetero-oligomers was intriguing, even though we could not elucidate biological consequences for these constitutive receptor units to date. However, their early establishment shortly after biosynthesis in the ER hints towards a functional significance. Receptor biogenesis accompanied receptor oligomerization has not been described for other plant signaling systems, but was observed for several classes of animal receptors (Issafras et al., 2002; Ehrlich et al., 2011; Van Craenenbroeck et al., 2011).

Studies of these mammalian receptor systems revealed that constitutive receptor oligomerization affects receptor biogenesis itself as well as the trafficking and signaling of the involved receptor protomers (Bai, 2004; Wang and Norcross, 2008; Springael et al., 2005; Ehrlich et al., 2012; Van Craenenbroeck, 2012).

In particular for G-protein coupled receptors (GPCRs), increasing evidence has accumulated that the interactions of newly translated polypeptide chains may mimic chaperone functions and accelerate protein folding (Van Craenenbroeck, 2012). This in turn reduces the residence time of maturing receptor molecules in the ER, avoids recognition by the ER-associated protein degradation (ERAD) system, and thus increases the probability of receptor oligomers to reach the cell surface. Experimentally this was shown by rescuing the PM expression of a folding mutant in response to coexpression with a wild type protomer

variant (Van Craenenbroeck et al., 2011). The importance of ER processing and ERAD components during the biogenesis of BRI1 has been revealed by several studies (Hong et al., 2012; 2008; 2009; Su et al., 2011; Cui et al., 2012). In addition, our imaging data showed reduced BRI1 protein abundance in serk1serk3 mutant backgrounds (Chapter 5). Therefore it is tempting to speculate that the observed hetero-oligomerization of BRI1 and SERK3 in the ER facilitates the cell surface translocation.

Besides the possibly intrinsic chaperone function of ER receptor oligomerization, it was also shown that dimerization of nascent receptors can mask ER-retention signals within the polypeptide chains, which is required to enter the anterograde transport route. An example is the hetero-oligomerization of γ-aminobutyric acid B ($GABA_B$) receptors. These receptors form obligate heterodimers. Oligomerization, thus the full assembly of functional signaling units, is required for their ER exit and trafficking to the PM (Margeta-Mitrovic et al., 2000). Similar findings were obtained for the heterodimerization of α- and β-adrenergic receptors (Uberti et al., 2005; Canals et al., 2009). But are the various influences of receptor oligomerization on biogenesis and trafficking as described above also applied in our biological system? A possible experimental setup to test this hypothesis could be the overexpression of SERK coreceptors in ER-retained bri1 mutant backgrounds (Hong et al., 2008), which should elevate the PM abundance of the mutant BRI1 protein.

That coexpression of SERK3 indeed affects the trafficking of BRI1 was noted by Russinova et al. (2004), yet, with respect to endocytosis. Upon coexpression of both LRR-RLKs increased endosomal BRI1 populations were observed. Unfortunately, it is unknown if preformation of BRI1-SERK3 hetero-oligomers played a role in this finding. Interestingly, for mammalian bone morphogenic protein (BMP) receptors differential retrograde trafficking of preformed and ligand-induced receptor oligomers was observed (Hartung et al., 2006). Constitutive receptor complexes followed a clathrin-depedent endocytic pathway, whereas induced oligomers were subjected to caveolar-mediated uptake (Hartung et al., 2006). The same study also elucidated differential signaling of the two receptor complex populations. This is a fascinating finding in the light of BRI1-mediated BR signaling. As mentioned earlier, BRs elicit opposing physiological responses depending on their concentrations. For example, low, endogeneous levels of BRs result in root growth stimulation; on the contrary a high exogenous BR dosage inhibits root growth. Taken together with the time-course of BRI1-SERK3 hetero-oligomerization, a plausible hypothesis is that preformed BRI1-SERK3 hetero-oligomers account for signaling under low BR concentrations. Instead, signaling under elevated ligand availability may involve de novo induced receptor complexes. In other words, the stimulatory effect of low BR concentrations could be exhibited by preformed BRI1-SERK3 oligomers and the inhibitory effect may be executed by the ligand-dependent oligomerization of the two LRR-RLKs.

Commonly, receptor complex preformation is suggested to elevate the signaling efficiency. Constitutive receptor oligomers are thought to increase the avidity for ligands (Ehrlich et

al., 2012), lateral signal propagation (Martin-Fernandez et al., 2002), as well as acceleration of signal transduction (Yu et al., 2002). Furthermore, it was reported that receptor clustering enhances the recruitment efficiency of intracellular adapter proteins (Hsieh et al., 2010). These likely effects of preformed receptor complexes are actually in contradiction to the observed time course for BRI1-SERK3 hetero-oligomerization after application of exogeneous ligand at concentrations inhibitory to root growth. This again favors a model for differential signaling of preformed and ligand-induced BRI1-SERK3 hetero-oligomers, especially since the de novo formation of receptor complexes was substantially delayed. At the same time, it questions whether BRI1-coreceptor hetero-oligomerization is an appropriate read-out for BR signaling. As shown by Yu et al. (2002), receptor oligomerization is a distinct step from ligand-induced receptor activation. Therefore alternative experimental read-outs like the interaction or phosphorylation of downstream regulators of BR signaling should be considered as well.

It was previously demonstrated that receptor hetero-oligomerization is required for efficient BR signaling (Wang et al., 2008; Gou et al., 2012). But receptor hetero-oligomers not only impact signaling efficiency, additionally alternative receptor combinations can also influence signaling specificity. This phenomenon has been observed for many classes of animal PM receptors, like the EGF family (Pines et al., 2010), transforming growth factor (TGF) and BMP receptors (Ehrlich et al., 2011), as well as several families of GPCRs (Wang and Norcross, 2008). Hetero-oligomerization with different complexes partners can result in altered ligand specificities, differential signaling routes and distinct trafficking patterns (Ehrlich et al., 2011; Rozenfeld and Devi, 2010). Thus receptor hetero-oligomers allow a high degree of plasticity in response to similar ligands (Rozenfeld and Devi, 2010). Even though in most BR-related studies BL (24-epi-brassinolide) is used as the activating ligand, the class of BR hormones comprises many more endogenous compounds (Shimada et al., 2003). It is not known if there exists any specificity between them in addition to their varying capacities of inducing downstream signaling. Furthermore, not only BRI1 but also its homologs the BRI1-like (BRL) proteins BRL1 and BRL3 can perceive BRs (Caño-Delgado and Wang, 2009). Besides SERK3, also the SERK family members SERK1 and SERK4 are involved in BR signal transduction (He et al., 2007; Gou et al., 2012). This offers a plethora of combinatorial ligand and hetero-oligomer combinations that may participate and differentially regulate BR signal transduction. Support for this hypothesis was obtained from preliminary data, which suggest a different oligomerization profile of BRI1 and SERK1 as revealed for BRI1-SERK3 hetero-oligomers. In principle, not only heterodimer combinations are possible, but also higher-order receptor oligomers, as observed for BR signaling components (Karlova et al., 2006) and animal receptor systems (Rozenfeld and Devi, 2010). Consequently, even more combinatorial possibilities would arise. However, usually receptor dimers are considered as the basic functional unit (Rozenfeld and Devi, 2010).

FRET-FLIM versus coimmunoprecipitation

If receptors in general function in at least a dimeric configuration, why are not all receptor complexes preassembled? This would allow the cellular quality control systems to verify their functional integrity before risking the delivery of possibly oligomerization incompetent receptors to the PM. In this respect, it is interesting to discuss the techniques used to reveal protein oligomers.

In this thesis FRET-FLIM was applied to investigate the hetero-oligomerization of the BR signaling unit composed of BRI1 and SERK3. In principle, this approach resulted in the same trend as previously observed using coimmunopreciptiation (Wang et al., 2005; 2008; Albrecht et al., 2012). Both approaches showed the existence of preformed and ligand-induced receptor complexes. The two major differences were the fold changes upon activation of BR signaling and the detection of in general lower amounts of receptor complexes using the biochemical approach. In comparison to the approximately 50% induction of BRI1-SERK3 hetero-oligomers suggested by FRET-FLIM experiments, coimmunoprecipitation usually revealed an increase of several folds. Also the amount of BRI1 receptors in complex with SERK3 after BL application was different. Whereas semi-quantitative coimmunoprecipitiation suggests that approximately 5% of BRI1 receptors hetero-oligomerize with the coreceptor (Albrecht et al., 2012), based on FRET-FLIM an amount of around 10% was estimated. The discrepancy between the two methods most likely stems from different sensitivities for detecting ligand-independent receptor complexes and the dissociation of receptor oligomers during the protein isolation steps required for coimmunoprecipitation.

Identification of protein-protein interactions using FRET read-outs, like the decrease of donor fluorescence lifetime, is mainly dependent on the distance between the fluorophores conjugated to the proteins of interest. An additional factor influencing the FRET efficiency is the orientation between the transition dipole moments of the fluorophores. Thus FRET approaches can reveal even weak and transient interactions between proteins, as long as the interaction is maintained during the time window of acquisition and the prerequisites of favorable orientation and close proximity between the fluorescent labels are fulfilled. In contrast to the low invasive imaging technique, coimmunoprecipitation requires a stable association between complex partners that can withstand the different steps of protein extraction from their natural environment. Therefore this technique is prone to underestimate protein interactions, in particular weak or transient ones. This phenomenon was not only encountered during our investigation, but also during the studies of other receptor proteins (Springael et al., 2005; Wang and Norcross, 2008). As a consequence, initial receptor recruitment models were established that afterwards have been modified by including ligand-independent receptor oligomers into the signaling schemes.

However, it has to be noted, coimmunoprecipitation is still the method of choice for revealing higher-order receptor complexes. FRET-FLIM is based on a 1:1 ratio of donor and acceptor and consequently reveals the physical interaction of proteins of interest, which

represents a protein oligomer in the narrow sense. Instead, coimmunoprecipitation enables to reveal also indirect interactions, mediated by additional protein complex components. This emphasizes the need of combined biochemical and biophysical approaches. By unfolding their synergistic effects they allow us to take a step closer to the true nature of the molecular events during signaling activity.

BRI1 on its own

The combined findings presented here obtained using an imaging approach and independent investigations based on modeling (van Esse et al., 2012) and coimmunoprecipitation (Albrecht et al., 2012) still leave a puzzling question – what is the role of the vast excess of BRI1 receptors?

A seemingly straightforward explanation is that the remaining BRI1 receptors, which do not associate with SERK3, undergo hetero-oligomerization with the two additional SERK family members involved in BR signaling SERK1 and SERK4 (Gou et al., 2012). This could give rise to signaling specificity by differential hetero-oligomerization as discussed earlier. If the amount of BRI1-SERK1 and BRI1-SERK4 receptor complexes were in a comparable magnitude as estimated for SERK3 this would also be in line with the observation that 50% of total BRI1 protein is sufficient for wild type-like growth (van Esse et al., 2012). Similar reasoning is also possible with respect to the many endogenous brassinosteroids (Shimada et al., 2003). Different ligands could result in the formation of specific receptor complexes, which were simply not revealed during this study since only BL was applied. However, this point of view contradicts the in silico studies of van Esse et al. (2012), who showed that only a very limited amount of BRI1 is required for proper plant growth.

Alternatively, BRI1 could hetero-oligomerize with so far undiscovered RLKs. The Arabidopsis genome harbors more than 600 RLKs and more than 240 LRR-RLKs (Shiu and Bleecker, 2003). Most of them are still unassigned and some of them may represent further BRI1-interacting receptors. A possible function of these hypothetical BRI1 hetero-oligomers could be the regulation of pathway crosstalk since BR signaling coregulates many other hormonal and stress-related signal transduction cascades (Wang et al., 2012).

Similarly, association of BRI1 with other ligand-binding receptors like FLS2 or EFR is conceivable. This could create direct crosstalk circuits within the PM. That different ligand-binding receptors hetero-oligomerize and influence each other's signaling activity was shown for mammalian PM receptors (Borroto-Escuela et al., 2011; Fuxe et al., 2007; Flajolet et al., 2008). An example is the constitutive interaction of EGFR with KISS1R, a receptor of the GPCR family, which resulted in EGFR transactivation by KISS1R ligand (Zajac et al., 2011).

Another hypothesis is based on the finding that not the amount of BRI1 but the BRI1 receptor density is maintained in Arabidopsis roots (Wilma van Esse et al., 2011). Taken together with the limited transport of BRs within the plant organism (Symons et al., 2008)

it seems that cells create an optimal spatial distribution of BRI1 receptors in their PMs to sense hormone availability and fluctuations. Since most of the PM-residing BRI1 receptors are most likely not associated with coreceptors required for downstream signaling a possible scenario is that ligand binding induces by an yet unknown mechanism the propagation of lateral activation waves that initiate BR signaling by BRI1-coreceptor hetero-oligomers. Lateral signal propagation was shown for EGFR (Reynolds et al., 2003), however, in that case it represented an early step of signal amplification.

Thus, even though BRI1 represents one of the best characterized plant receptors (Kemmerling et al., 2011), still many aspects remain purely speculative. Nonetheless, by combining the current view on BR signal transduction with the results presented in this thesis an adapted model of BR signaling is proposed in the following.

A refined BR signaling model

Collectively, the results presented and discussed in this thesis lead to a refined model for BR signaling (Figure 1). A subset of BRI1 and SERK3 hetero-oligomerize shortly after biosynthesis in the ER. Targeted transport of the receptor complexes through the Golgi apparatus and TGN culminates in the PM insertion of preformed BRI1-SERK3 hetero-oligomers, where the two LRR-RLKs reside as a signaling-competent receptor unit. Transport of receptor monomers probably follows the same route, but is not specifically portrayed in the model. Ligand binding to BRI1 most likely results in conformational changes and subsequently in activation of the cytoplasmic kinase domains. After release of the BRI1-kinase inhibitor 1 (BKI1) (Jaillais et al., 2011b) the BR signaling unit gains full signaling competence (not shown in Figure 1). The initiation of BR signaling at the PM is followed by the endocytosis of BRI1-SERK3 hetero-oligomers. Disassembly of the BR signaling unit may occur during the maturation of TGN/EE to LE/MVB. Whereas ligand-bound BRI1 receptors are targeted for protein degradation in the vacuole lumen, activated SERK3 receptors are incorporated into the tonoplast to exhibit further BRI1-autonomous functions. After fulfilling their signaling activities also the SERK3 receptors are taken up into the vacuolar lumen for protein degradation.

This scenario is thought to represent a possible mechanism for stimulatory BR actions. The model can be expanded to include high BR concentrations, which result in inhibitory signaling outputs possibly transduced by ligand-induced BRI1-SERK3 hetero-oligomers. In addition, other hetero-oligomeric configurations including BRLs and other SERK family members may extend the described BR signaling model. For simplicity other downstream regulators of BR signal transduction are omitted. Still, it should be discussed that preformed BRI1-SERK3 hetero-oligomers could comprise more components than only the two LRR-RLKs. In principle, interacting BRI1 and SERK3 receptors represent a signaling competent configuration. Thus they have to be kept inactive until BR binding to BRI1 elicits signaling. The most likely candidate to inhibit accidental kinase activation is BKI1.

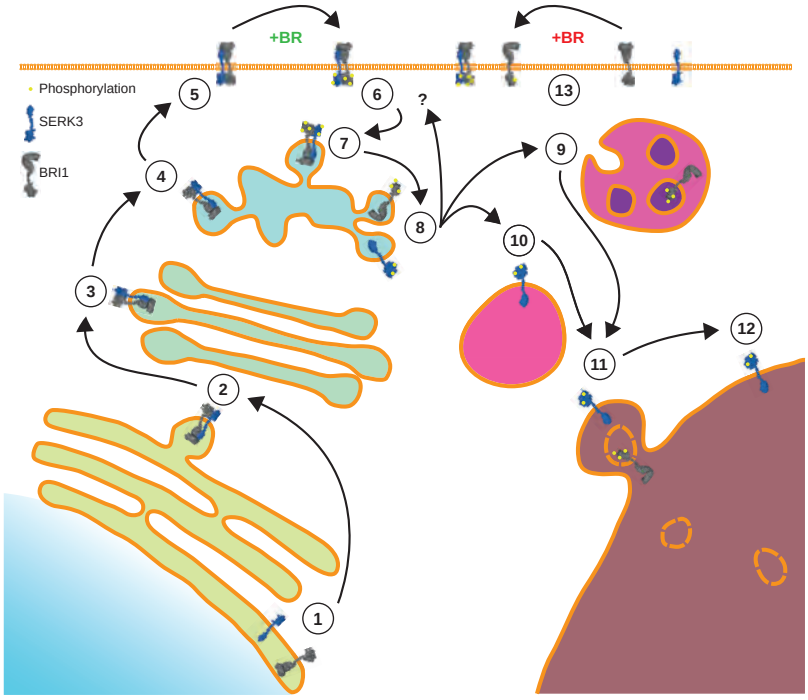

Figure 1: Schematic overview of the endosomal trafficking of BRI1-SERK3 hetero-oligomers.
After the translation of BRI1 and SERK3 (1) subpopulations of the two LRR-RLKs hetero-oligomerize in restricted ER regions (2). Targeted transport via the Golgi apparatus (3) and trans-Golgi network (4) leads to PM insertion (5) of preformed receptor complexes. Binding of brassionsteroids (BR) results in activation and trans-phosphorylation of the cytosolic kinase domains of BRI1 and SERK3 (6), followed by the initiation of downstream signaling. Activated hetero-oligomers are endocytosed and sorted in the trans-Golgi network/early endosome compartment (7). Here, the disassembly of activated BRI1-SERK3 hetero-oligomers may occur (8). Subsequently, early endosomes mature to late endosomes/multi-vesicular bodies, accompanied by the uptake of BRI1 into the multivesicular body lumen (9). SERK3 instead is sorted into prevacuolar compartments (10). Alternatively, partial recycling of hetero-oligomers or the individual BRI1 and SERK3 receptors may occur, marked by "?". The fusion of prevacuolar compartments and multi-vesicular bodies with the vacuole (11) leads to incorporation of activated SERK3 into the tonoplast, whereas BRI1 is released into the vacuolar lumen. Tonoplast-residing SERK3 may exhibit autonomous functions (12) prior to its degradation.
This scheme represents a model for BRI1-SERK3 hetero-oligomers that transduce stimulatory signaling under low BR concentrations. However, high concentrations of BRs may induce the de novo formation of BRI1-SERK3 hetero-oligomers, which initiate inhibitory BR signaling (13).
For simplicity only BRI1 and SERK3 are shown in the schematic representation, without referring to other regulators of BR signal transduction. Also the transport of individual BRI1 and SERK3 receptors, which most likely follow the same secretory pathway, is not shown.

Therefore preformed BRI1-SERK3 hetero-oligomers may contain additional regulatory or signaling components, and even about the preformation of whole signalosomes organized around scaffold proteins and including positive as well as negative regulators can be speculated.

Future Perspectives

We have to keep in mind that the presented model is only a snapshot of the current knowledge and like the signaling event itself of transient nature. Likewise the described receptor interactions are only transient and are subject to the dynamics of living matter. To improve our understanding of BR signal transduction, and signaling mechanisms in general, more multi-dimensional and spatiotemporally resolved experimental setups are required, like recently shown for the FLS2 signal transduction pathway by Beck et al. (2012). The complexity of primary and derivative receptor interactomes, which eventually dictate the cellular and organism fate, is inaccessible by one-dimensional approaches but requires the integration of complementary technologies (Poorgholi Belverdi et al., 2012).

Here, mainly aspects of PM-associated signal transduction were discussed, but increasing evidence accumulates for the correlation of endosomal trafficking and signaling outputs (Lemmon and Schlessinger, 2010). Local interactions between signaling components and fluctuations in their densities are crucial for cell survival and adaptation (Dehmelt and Bastiaens, 2010). Whereas signal transduction was traditionally seen as a linear sequence of signal relay processes, especially the introduction of novel imaging technologies changed this concept into a more holistic view of interconnected, spatially organized states of the cell that are dynamically regulated (Dehmelt and Bastiaens, 2010). Hence, signal transduction can also be considered as the communication of changes in the organization of supramolecular structures (Dehmelt and Bastiaens, 2010). Such supramolecular structures could be formed around hub receptors with moonlighting characteristics and could act similar to computational processors that integrate and transmit different signaling inputs concurrently into the cell (Ciruela et al., 2010). A likely candidate for a moonlighting receptor, thus a protein that exhibits various distinct functions based on the same amino acid sequence (Jeffery, 2003; Borroto-Escuela et al., 2011), is SERK3.

In summary, this thesis highlights how fluorescence microscopy as a low invasive methodology can deepen our understanding of signal transduction processes in the natural environment of signaling components. Colocalization and FRET-FLIM approaches allowed us to investigate the BR signaling pathway in more detail and extended our view on the regulation of RLK signaling in different aspects. Nonetheless, future investigations are needed to illuminate further mechanistic details and the real-time dynamics of BR signaling under physiological conditions.

REFERENCES

Afzal, A.J., Wood, A.J., and Lightfoot, D.A. (2008). Plant receptor-like serine threonine kinases: roles in signaling and plant defense. Mol. Plant Microbe Interact. **21**: 507–517.

Albrecht, C., Boutrot, F., Segonzac, C., Schwessinger, B., Gimenez-Ibanez, S., Chinchilla, D., Rathjen, J.P., de Vries, S.C., and Zipfel, C. (2012). Brassinosteroids inhibit pathogen-associated molecular pattern-triggered immune signaling independent of the receptor kinase BAK1. Proc. Natl. Acad. Sci. U.S.A. **109**: 303–308.

Albrecht, C., Russinova, E., Kemmerling, B., Kwaaitaal, M., and de Vries, S.C. (2008). Arabidopsis SOMATIC EMBRYOGENESIS RECEPTOR KINASE proteins serve brassinosteroid-dependent and -independent signaling pathways. Plant Physiol. **148**: 611–619.

Bader, A.N., Hofman, E.G., Voortman, J., en Henegouwen, P.M.P.V.B., and Gerritsen, H.C. (2009). Homo-FRET imaging enables quantification of protein cluster sizes with subcellular resolution. Biophys. J. **97**: 2613–2622.

Bai, M. (2004). Dimerization of G-protein-coupled receptors: roles in signal transduction. Cell. Signal. **16**: 175–186.

Beck, M., Zhou, J., Faulkner, C., Maclean, D., and Robatzek, S. (2012). Spatio-Temporal Cellular Dynamics of the Arabidopsis Flagellin Receptor Reveal Activation Status-Dependent Endosomal Sorting. Plant Cell. doi: 10.1105/tpc.112.100263

Borroto-Escuela, D.O., Tarakanov, A.O., Guidolin, D., Ciruela, F., Agnati, L.F., and Fuxe, K. (2011). Moonlighting characteristics of G protein-coupled receptors: focus on receptor heteromers and relevance for neurodegeneration. IUBMB Life **63**: 463–472.

Caesar, K., Elgass, K., Chen, Z., Huppenberger, P., Witthöft, J., Schleifenbaum, F., Blatt, M.R., Oecking, C., and Harter, K. (2011). A fast brassinolide-regulated response pathway in the plasma membrane of Arabidopsis thaliana. Plant J. **66**: 528–540.

Canals, M., Lopez-Gimenez, J.F., and Milligan, G. (2009). Cell surface delivery and structural reorganization by pharmacological chaperones of an oligomerization-defective alpha(1b)-adrenoceptor mutant demonstrates membrane targeting of GPCR oligomers. Biochem. J. **417**: 161–172.

Caño-Delgado, A. and Wang, Z.-Y. (2009). Binding assays for brassinosteroid receptors. Methods Mol. Biol. **495**: 81–88.

Chinchilla, D., Shan, L., He, P., de Vries, S., and Kemmerling, B. (2009). One for all: the receptor-associated kinase BAK1. Trends Plant Sci. **14**: 535–541.

Ciruela, F., Vilardaga, J.-P., and Fernández-Dueñas, V. (2010). Lighting up multiprotein complexes: lessons from GPCR oligomerization. Trends Biotechnol. **28**: 407–415.

Clouse, S.D. (2011). Brassinosteroid signal transduction: from receptor kinase activation to transcriptional networks regulating plant development. Plant Cell **23**: 1219–1230.

Cui, F., Liu, L., Zhao, Q., Zhang, Z., Li, Q., Lin, B., Wu, Y., Tang, S., and Xie, Q. (2012). Arabidopsis Ubiquitin Conjugase UBC32 Is an ERAD Component That Functions in Brassinosteroid-Mediated Salt Stress Tolerance. Plant Cell **24**: 233-244.

Dehmelt, L. and Bastiaens, P.I.H. (2010). Spatial organization of intracellular communication: insights from imaging. Nat. Rev. Mol. Cell Biol. **11**: 440–452.

Dunn, K.W., Kamocka, M.M., and McDonald, J.H. (2011). A practical guide to evaluating colocalization in biological microscopy. AJP: Cell Physiol. **300**: C723–C742.

Ebine, K., Fujimoto, M., Okatani, Y., Nishiyama, T., Goh, T., Ito, E., Dainobu, T., Nishitani, A., Uemura, T., Sato, M.H., Thordal-Christensen, H., Tsutsumi, N., Nakano, A., and Ueda, T.

(2011). A membrane trafficking pathway regulated by the plant-specific RAB GTPase ARA6. Nat. Cell Biol. **13**: 853–859.

Ehrlich, M., Gutman, O., Knaus, P., and Henis, Y.I. (2012). Oligomeric interactions of TGF-β and BMP receptors. FEBS Letters **586**: 1885–1896.

Ehrlich, M., Horbelt, D., Marom, B., Knaus, P., and Henis, Y.I. (2011). Homomeric and heteromeric complexes among TGF-β and BMP receptors and their roles in signaling. Cell. Signal. **23**: 1424–1432.

Etxeberria, E., Pozueta-Romero, J., and Gonzalez, P. (2012). In and out of the plant storage vacuole. Plant Sci. **190**: 52–61.

Flajolet, M., Wang, Z., Futter, M., Shen, W., Nuangchamnong, N., Bendor, J., Wallach, I., Nairn, A.C., Surmeier, D.J., and Greengard, P. (2008). FGF acts as a co-transmitter through adenosine A(2A) receptor to regulate synaptic plasticity. Nat. Neurosci. **11**: 1402–1409.

French, A.P., Mills, S., Swarup, R., Bennett, M.J., and Pridmore, T.P. (2008). Colocalization of fluorescent markers in confocal microscope images of plant cells. Nat. Protoc. **3**: 619–628.

Friedrichsen, D.M., Joazeiro, C.A., Li, J., Hunter, T., and Chory, J. (2000). Brassinosteroid-insensitive-1 is a ubiquitously expressed leucine-rich repeat receptor serine/threonine kinase. Plant Physiol. **123**: 1247–1256.

Fuxe, K., Dahlström, A., Höistad, M., Marcellino, D., Jansson, A., Rivera, A., Diaz-Cabiale, Z., Jacobsen, K., Tinner-Staines, B., Hagman, B., Leo, G., Staines, W., Guidolin, D., Kehr, J., Genedani, S., Belluardo, N., and Agnati, L.F. (2007). From the Golgi-Cajal mapping to the transmitter-based characterization of the neuronal networks leading to two modes of brain communication: wiring and volume transmission. Brain Res. Rev. **55**: 17–54.

Gadella, T.W. and Jovin, T.M. (1995). Oligomerization of epidermal growth factor receptors on A431 cells studied by time-resolved fluorescence imaging microscopy. A stereochemical model for tyrosine kinase receptor activation. J. Cell Biol. **129**: 1543–1558.

Geldner, N., Hyman, D.L., Wang, X., Schumacher, K., and Chory, J. (2007). Endosomal signaling of plant steroid receptor kinase BRI1. Genes Dev. **21**: 1598–1602.

Gou, X., Yin, H., He, K., Du, J., Yi, J., Xu, S., Lin, H., Clouse, S.D., and Li, J. (2012). Genetic evidence for an indispensable role of somatic embryogenesis receptor kinases in brassinosteroid signaling. PLoS Genet. **8**: e1002452.

Grove, M.D., Spencer, G.F., Rohwedder, W.K., Mandava, N., Worley, J.F., Warthen, J.D., Steffens, G.L., Flippen-Anderson, J.L., and Cook, J.C. (1979). Brassinolide, a plant growth-promoting steroid isolated from Brassica napus pollen. Nature **281**: 216–217.

Hacham, Y., Holland, N., Butterfield, C., Ubeda-Tomas, S., Bennett, M.J., Chory, J., and Savaldi-Goldstein, S. (2011). Brassinosteroid perception in the epidermis controls root meristem size. Development **138**: 839–848.

Hara-Nishimura, I. and Hatsugai, N. (2011). The role of vacuole in plant cell death. Cell Death Differ. **18**: 1298–1304.

Hart, Y. and Alon, U. (2013). The Utility of Paradoxical Components in Biological Circuits. Mol. Cell **49**: 213–221.

Hartung, A., Bitton-Worms, K., Rechtman, M.M., Wenzel, V., Boergermann, J.H., Hassel, S., Henis, Y.I., and Knaus, P. (2006). Different routes of bone morphogenic protein (BMP) receptor endocytosis influence BMP signaling. Mol. Cell. Biol. **26**: 7791–7805.

He, K., Gou, X., Yuan, T., Lin, H., Asami, T., Yoshida, S., Russell, S.D., and Li, J. (2007). BAK1 and BKK1 regulate brassinosteroid-dependent growth and brassinosteroid-independent cell-death pathways. Curr. Biol. **17**: 1109–1115.

Hong, Z., Hong, Z., Jin, H., Jin, H., Tzfira, T., Tzfira, T., Li, J., and Li, J. (2008). Multiple mechanism-mediated retention of a defective brassinosteroid receptor in the endoplasmic reticulum of Arabidopsis. Plant Cell **20**: 3418–3429.

Hong, Z., Hong, Z., Kajiura, H., Kajiura, H., Su, W., Su, W., Jin, H., Jin, H., Kimura, A., Kimura, A., Fujiyama, K., Fujiyama, K., Li, J., and Li, J. (2012). Evolutionarily conserved glycan signal to degrade aberrant brassinosteroid receptors in Arabidopsis. Proc. Natl. Acad. Sci. U.S.A. **109**: 11437–11442.

Hong, Z., Jin, H., Fitchette, A.-C., Xia, Y., Monk, A.M., Faye, L., and Li, J. (2009). Mutations of an alpha1,6 mannosyltransferase inhibit endoplasmic reticulum-associated degradation of defective brassinosteroid receptors in Arabidopsis. Plant Cell **21**: 3792–3802.

Hsieh, M.-Y., Yang, S., Raymond-Stinz, M.A., Edwards, J.S., and Wilson, B.S. (2010). Spatiotemporal modeling of signaling protein recruitment to EGFR. BMC Syst. Biol. **4**: 57.

Irani, N.G., Di Rubbo, S., Mylle, E., Van den Begin, J., Schneider-Pizoń, J., Hniliková, J., Síša, M., Buyst, D., Vilarrasa-Blasi, J., Szatmari, A.-M., Van Damme, D., Mishev, K., Codreanu, M.-C., Kohout, L., Strnad, M., Caño-Delgado, A.I., Friml, J., Madder, A., and Russinova, E. (2012). Fluorescent castasterone reveals BRI1 signaling from the plasma membrane. Nat. Chem. Biol. **8**: 583–589.

Issafras, H., Angers, S., Bulenger, S., Blanpain, C., Parmentier, M., Labbé-Jullié, C., Bouvier, M., and Marullo, S. (2002). Constitutive agonist-independent CCR5 oligomerization and antibody-mediated clustering occurring at physiological levels of receptors. J. Biol. Chem. **277**: 34666–34673.

Jaillais, Y., Belkhadir, Y., Balsemão-Pires, E., Dangl, J.L., and Chory, J. (2011a). Extracellular leucine-rich repeats as a platform for receptor/coreceptor complex formation. Proc. Natl. Acad. Sci. U.S.A. **108**: 8503–8507.

Jaillais, Y., Hothorn, M., Belkhadir, Y., Dabi, T., Nimchuk, Z.L., Meyerowitz, E.M., and Chory, J. (2011b). Tyrosine phosphorylation controls brassinosteroid receptor activation by triggering membrane release of its kinase inhibitor. Genes Dev. **25**: 232–237.

Jeffery, C.J. (2003). Moonlighting proteins: old proteins learning new tricks. Trends Genet. **19**: 415–417.

Jones, J.D.G. and Dangl, J.L. (2006). The plant immune system. Nature **444**: 323–329.

Karlova, R., Boeren, S., Russinova, E., Aker, J., Vervoort, J., and de Vries, S. (2006). The Arabidopsis SOMATIC EMBRYOGENESIS RECEPTOR-LIKE KINASE1 protein complex includes BRASSINOSTEROID-INSENSITIVE1. Plant Cell **18**: 626–638.

Kemmerling, B., Halter, T., Mazzotta, S., Mosher, S., and Nürnberger, T. (2011). A genome-wide survey for Arabidopsis leucine-rich repeat receptor kinases implicated in plant immunity. Front. Plant Sci. **2**: 88.

Kinoshita, T., Caño-Delgado, A., Seto, H., Hiranuma, S., Fujioka, S., Yoshida, S., and Chory, J. (2005). Binding of brassinosteroids to the extracellular domain of plant receptor kinase BRI1. Nature **433**: 167–171.

Kutschera, U., Deng, Z., Oses-Prieto, J.A., Burlingame, A.L., and Wang, Z.Y. (2010). Cessation of coleoptile elongation and loss of auxin sensitivity in developing rye seedlings: A quantitative proteomic analysis. Plant Signal Behav. **5: 509-517**.

Kutschera, U.U. and Wang, Z.-Y.Z. (2012). Brassinosteroid action in flowering plants: a Darwinian perspective. J. Exp. Bot. **63**: 3511–3522.

Lemmon, M.A. and Schlessinger, J. (2010). Cell signaling by receptor tyrosine kinases. Cell **141**: 1117–1134.

Li, J. and Chory, J. (1997). A putative leucine-rich repeat receptor kinase involved in brassinosteroid signal transduction. Cell **90**: 929–938.

Margeta-Mitrovic, M., Jan, Y.N., and Jan, L.Y. (2000). A trafficking checkpoint controls GABA(B) receptor heterodimerization. Neuron **27**: 97–106.

Martin-Fernandez, M., Clarke, D.T., Tobin, M.J., Jones, S.V., and Jones, G.R. (2002). Preformed oligomeric epidermal growth factor receptors undergo an ectodomain structure change during signaling. Biophys. J. **82**: 2415–2427.

Massague, J., Pilch, P.F., and Czech, M.P. (1980). Electrophoretic resolution of three major insulin receptor structures with unique subunit stoichiometries. Proc. Natl. Acad. Sci. U.S.A. **77**: 7137–7141.

Monaghan, J. and Zipfel, C. (2012). Plant pattern recognition receptor complexes at the plasma membrane. Curr. Opin. Plant Biol. **15**: 349–357.

Nam, K.H. and Li, J. (2002). BRI1/BAK1, a receptor kinase pair mediating brassinosteroid signaling. Cell **110**: 203–212.

Nebenführ, A., Ritzenthaler, C., and Robinson, D.G. (2002). Brefeldin A: deciphering an enigmatic inhibitor of secretion. Plant Physiol. **130**: 1102–1108.

Nürnberger, T., Brunner, F., Kemmerling, B., and Piater, L. (2004). Innate immunity in plants and animals: striking similarities and obvious differences. Immunol. Rev. **198**: 249–266.

Oh, M.-H., Kim, H.S., Wu, X., Clouse, S.D., Zielinski, R.E., and Huber, S.C. (2012a). Calcium/calmodulin inhibition of the Arabidopsis BRASSINOSTEROID INSENSITIVE 1 receptor kinase provides a possible link between calcium- and brassinosteroid-signaling. Biochem. J. **443**: 512-523.

Oh, M.-H., Wang, X., Clouse, S.D., and Huber, S.C. (2012b). Deactivation of the Arabidopsis BRASSINOSTEROID INSENSITIVE 1 (BRI1) receptor kinase by autophosphorylation within the glycine-rich loop. Proc. Natl. Acad. Sci. U.S.A. **109**: 327–332.

Peiter, E. (2011). The plant vacuole: emitter and receiver of calcium signals. Cell Calcium **50**: 120–128.

Pines, G., Köstler, W.J., and Yarden, Y. (2010). Oncogenic mutant forms of EGFR: lessons in signal transduction and targets for cancer therapy. FEBS Letters **584**: 2699–2706.

Poorgholi Belverdi, M., Krause, C., Guzman, A., and Knaus, P. (2012). Comprehensive analysis of TGF-β and BMP receptor interactomes. Eur. J. Cell Biol. **91**: 287–293.

Reynolds, A.R., Tischer, C., Verveer, P.J., Rocks, O., and Bastiaens, P.I.H. (2003). EGFR activation coupled to inhibition of tyrosine phosphatases causes lateral signal propagation. Nat. Cell Biol. **5**: 447–453.

Rozenfeld, R. and Devi, L.A. (2010). Functional Role(s) of Dimeric Complexes Formed from G-Protein-Coupled Receptors. Handbook of Cell Signaling, Three-Volume Set 2 ed, pp. 185–194.

Russinova, E., Borst, J.W., Kwaaitaal, M., Caño-Delgado, A., Yin, Y., Chory, J., and de Vries, S.C. (2004). Heterodimerization and endocytosis of Arabidopsis brassinosteroid receptors BRI1 and AtSERK3 (BAK1). Plant Cell **16**: 3216–3229.

Saitoh, S.-I., Akashi, S., Yamada, T., Tanimura, N., Matsumoto, F., Fukase, K., Kusumoto, S., Kosugi, A., and Miyake, K. (2004). Ligand-dependent Toll-like receptor 4 (TLR4)-oligomerization is directly linked with TLR4-signaling. J. Endotoxin Res. **10**: 257–260.

Schulze, B., Mentzel, T., Jehle, A.K., Mueller, K., Beeler, S., Boller, T., Felix, G., and Chinchilla, D. (2010). Rapid heteromerization and phosphorylation of ligand-activated plant transmembrane receptors and their associated kinase BAK1. J. Biol. Chem. **285**: 9444–9451.

Shimada, Y., Goda, H., Nakamura, A., Takatsuto, S., Fujioka, S., and Yoshida, S. (2003). Organ-specific expression of brassinosteroid-biosynthetic genes and distribution of endogenous brassinosteroids in Arabidopsis. Plant Physiol. **131**: 287–297.

Shimizu, T., Nakano, T., Takamizawa, D., Desaki, Y., Ishii-Minami, N., Nishizawa, Y., Minami, E., Okada, K., Yamane, H., Kaku, H., and Shibuya, N. (2010). Two LysM receptor molecules, CEBiP and OsCERK1, cooperatively regulate chitin elicitor signaling in rice. Plant J. **64**: 204–214.

Shiu, S.H. and Bleecker, A.B. (2003). Expansion of the receptor-like kinase/Pelle gene family and receptor-like proteins in Arabidopsis. Plant Physiol. **132**: 530–543.

Shiu, S.H. and Bleecker, A.B. (2001). Receptor-like kinases from Arabidopsis form a monophyletic gene family related to animal receptor kinases. Proc. Natl. Acad. Sci. U.S.A. **98**: 10763–10768.

Springael, J.-Y., Urizar, E., and Parmentier, M. (2005). Dimerization of chemokine receptors and its functional consequences. Cytokine Growth Factor Rev. **16**: 611–623.

Su, W., Liu, Y., Xia, Y., Hong, Z., and Li, J. (2011). Conserved endoplasmic reticulum-associated degradation system to eliminate mutated receptor-like kinases in Arabidopsis. Proc. Natl. Acad. Sci. U.S.A. **108**: 870–875.

Symons, G.M., Ross, J.J., Jager, C.E., and Reid, J.B. (2008). Brassinosteroid transport. J. Exp. Bot. **59**: 17–24.

Uberti, M.A., Hague, C., Oller, H., Minneman, K.P., and Hall, R.A. (2005). Heterodimerization with beta2-adrenergic receptors promotes surface expression and functional activity of alpha1D-adrenergic receptors. J. Pharmacol. Exp. Ther. **313**: 16–23.

Ueda, T., Uemura, T., Sato, M.H., and Nakano, A. (2004). Functional differentiation of endosomes in Arabidopsis cells. Plant J. **40**: 783–789.

Van Craenenbroeck, K. (2012). GPCR Oligomerization: Contribution to Receptor Biogenesis. Subcell. Biochem. **63**: 43–65.

Van Craenenbroeck, K., Borroto-Escuela, D.O., Romero-Fernandez, W., Skieterska, K., Rondou, P., Lintermans, B., Vanhoenacker, P., Fuxe, K., Ciruela, F., and Haegeman, G. (2011). Dopamine D4 receptor oligomerization--contribution to receptor biogenesis. FEBS J. **278**: 1333–1344.

van Esse, G.W., van Mourik, S., Stigter, H., Hove, ten, C.A., Molenaar, J., and de Vries, S.C. (2012). A mathematical model for BRASSINOSTEROID INSENSITIVE1-mediated signaling in root growth and hypocotyl elongation. Plant Physiol. **160**: 523–532.

van Esse, G., Westphal, A.H., Surendran, R.P., Albrecht, C., van Veen, B., Borst, J.W., and de Vries, S.C. (2011). Quantification of the brassinosteroid insensitive1 receptor in planta. Plant Physiol. **156**: 1691–1700.

Viotti, C., Bubeck, J., Stierhof, Y.-D., Krebs, M., Langhans, M., van den Berg, W., van Dongen, W., Richter, S., Geldner, N., Takano, J., Jürgens, G., de Vries, S.C., Robinson, D.G., and Schumacher, K. (2010). Endocytic and secretory traffic in Arabidopsis merge in the trans-Golgi network/early endosome, an independent and highly dynamic organelle. Plant Cell **22**: 1344–1357.

Wang, J. and Norcross, M. (2008). Dimerization of chemokine receptors in living cells: key to receptor function and novel targets for therapy. Drug Discov. Today **13**: 625–632.

Wang, X., Goshe, M.B., Soderblom, E.J., Phinney, B.S., Kuchar, J.A., Li, J., Asami, T., Yoshida, S., Huber, S.C., and Clouse, S.D. (2005). Identification and functional analysis of in vivo phosphorylation sites of the Arabidopsis BRASSINOSTEROID-INSENSITIVE1 receptor kinase. Plant Cell **17**: 1685–1703.

Wang, X., Kota, U., He, K., Blackburn, K., Li, J., Goshe, M.B., Huber, S.C., and Clouse, S.D. (2008). Sequential transphosphorylation of the BRI1/BAK1 receptor kinase complex impacts early events in brassinosteroid signaling. Dev. Cell **15**: 220–235.

Wang, Z.-Y., Bai, M.-Y., Oh, E., and Zhu, J.-Y. (2012). Brassinosteroid signaling network and regulation of photomorphogenesis. Annu. Rev. Genet. **46**: 701–724.

Yu, X., Sharma, K.D., Takahashi, T., Iwamoto, R., and Mekada, E. (2002). Ligand-independent dimer formation of epidermal growth factor receptor (EGFR) is a step separable from ligand-induced EGFR signaling. Mol. Biol. Cell **13**: 2547–2557.

Zajac, M., Law, J., Cvetkovic, D.D., Pampillo, M., McColl, L., Pape, C., Di Guglielmo, G.M., Postovit, L.M., Babwah, A.V., and Bhattacharya, M. (2011). GPR54 (KISS1R) transactivates EGFR to promote breast cancer cell invasiveness. PLoS ONE **6**: e21599.

Chapter 7

Samenvatting in het Nederlands

De Oostenrijkse fysicus en medegrondlegger van de kwantummechanica Erwin Schrödinger karakteriseert het leven als volgt: "Levende materie vermijdt verval naar een evenwichtstoestand"[1]. Het begrip evenwichtstoestand heeft betrekking op de fysisch-chemische samenstelling waaruit volgt dat levende materie op een hoger fysisch-chemisch niveau staat dan haar omgeving. Een verlaging van dit hogere niveau naar dat van de omgeving zou daarom tot stilstand en uiteindelijk tot de dood leiden.

Om voor een hoog fysisch-chemisch niveau te zorgen moeten levende organismen, waaronder eencelligen, mens, dier en planten voortdurend de dynamische toestand van de omgeving waarnemen. Hiervoor zijn in de loop van de evolutie een scala van sensoren, receptoren genoemd, ontwikkeld. Deze receptoren zijn eiwitten die zich ofwel binnen in de cel of aan het oppervlak bevinden, daar waar signalen zoals licht, temperatuur ionen, voedingsstoffen, pathogenen of hormonen kunnen worden waargenomen. De waarneming van een externe fysische of chemische prikkel opgevangen door een receptor heeft als gevolg dat er een reactie binnenin de cel plaats vindt die er voor zorgt dat de fysiologisch toestand van de cel of organisme zal veranderen tijdens gewijzigde omstandigheden. De verschillende stappen van signaalwaarneming, overdracht en vertaling in een cellulaire respons staan bekend als signaaltransductie-route.

In dit proefschrift is een dergelijke route onderzocht van het plantenhormoon brassinosteroïde waarbij *Arabidopsis thaliana* (ook wel zandraket genoemd) als modelorganisme wordt gebruikt. Net als bij de werking van steroïden bij dieren hebben brassinosteroïden ook invloed op de ontwikkeling en groei van planten. De brassinosteroïden en dierlijke hormonen tonen ook grote gelijkenis op structureel gebied. In tegenstelling tot dierlijke cellen die de aanwezigheid van hormonen intracellulair kunnen waarnemen, hebben planten receptoren die aan het oppervlak of buitenkant van de cel opereren. Een van de belangrijkste plantenreceptor die het hormoon brassinosteroïde herkent is Brassinosteroid insensitive 1 (BRI1). Deze receptor behoort tot de leucine rijke repeats receptor achtige kinases (LRR-RLKs voor leucine-rich repeat receptor-like kinases) welke tot een van de grootste receptor families in planten behoort. De schematische architectuur van de BRI1 receptor omvat een extracellulair LRR domein met een regio waar het homoon kan binden, een intracellulair domein met kinaseactiviteit die er voor zorgt dat het signaal wordt doorgegeven en een membraantussenstuk die de extracellulaire en intracellulaire domeinen met elkaar verbindt (zie hoofdstuk 1). Genetisch en biochemisch onderzoek hebben aangetoond dat deze receptor die het hormoon brassinosteroïde bindt alleen maar goed kan functioneren wanneer een samenwerking met een ander LRR-RLK aanwezig is. Deze LRR-RLK is de Somatic embryogenesis receptor-like kinase 3 (SERK3) receptor, die ook onder een andere naam bekend is, BAK1 voor BRI1-geassocieerde Kinase 1 (BRI1-associate kinase 1). De schematische opbouw van SERK3 is hetzelfde als die van BRI1,

1 uit "Was ist Leben?" van Erwin Schrödinger en Ernst Peter Fischer (1989)

echter is het extracellulaire domein van deze RLK beduidend kleiner. Huidige modellen die de functie van beide receptoren proberen te verklaren gaan ervan uit dat bij het ontbreken van brassinosteroïden, BRI1 en SERK3 aanwezig zijn als inactieve dimeren in de PM van plantencellen. Hierbij wordt de kinaseactiviteit van BRI1 kinase geremd door binding van een "inhibitor" molecuul BRI1 kinase inhibitor 1 (BKI1), die tegelijkertijd de associatie van BRI1 met SERK3 voorkomt.

Binding van het brassinosteroïde aan de extracellulaire domein van BRI1 heeft een conformatieverandering van het BRI1 dimeer tot gevolg. Deze structurele verandering geeft een basale activering van het intracellulaire BRI1 kinase domein wat resulteert in de fosforylatie en dissociatie van BKI1. Daaropvolgend wordt SERK3 "gerekruteerd" en vormt een hetero oligomeer met BRI1. Door fosforylatie binnen het receptorcomplex worden beide kinase domeinen volledig geactiveerd die voor "downstream" signaal transmissie en brassinosteroïde afhankelijke genregulatie zorgt.

Echter nieuwe experimentele data hebben twijfel gebracht over het huidige model over de vorming van BRI1-SERK hetero-oligomeren. Genetische data hebben aangetoond dat SERK3 en andere leden van de SERK familie niet alleen de kinase activiteit van BRI1 versterken maar deze zijn essentieel voor brassinosteroid signaaltransductie route. Additionele data over de moleculaire structuur van de BRI1 ectodomein spreekt het huidige beeld tegen dat BRI1 dimeren voor de hormoonbinding verantwoordelijk zijn. Hierover kan men speculeren of SERK3 niet een belangrijk element van het hormoon bindend receptorcomplex is.

De huidige modellen over de brassinosteroïde signaaltransductieroutes zijn volledig op biochemisch en genetisch onderzoek gebaseerd. In dit proefschrift is voor een andere aanpak gekozen namelijk fluorescentie microscopie welke de mogelijkheid geeft om de subcellularie signaatransductieroute te belichten in een levende plant.

In het **eerste hoofdstuk** wordt naast een gedetailleerde introductie over de brassinosteroïde signaaltransductieroute ook een beschrijving van de gebruikte fluorescentie microscopie technieken weergeven. In **hoofdstuk 2** wordt een bijzondere methode gedetailleerd beschreven die ons in staat stelt de interactie van eiwitten of receptoren zichtbaar te maken.

Het gaat hierbij om een speciale techniek met de afkorting FRET-FLIM welke een acroniem is voor Förster Resonantie-Energietransfer (FRET) gemeten met behulp van fluorescentie levensduurmicroscopie (FLIM voor fluorescence lifetime imaging microscopy). Dit type microscopie stelt ons in staat om interacterende eiwitmoleculen te visualiseren in levende cellen van een compleet organisme. In dit onderzoek is FRET-FLIM gebruikt om de complexformatie tussen BRI1 en SERK3 in levende wortelpuntjes van Arabidopsis te onderzoeken. In overeenstemming met de huidige modellen kon worden aangetoond dat na activering van de BRI1 signaaltransductieroute een tijdsafhankelijke complexformatie

met SERK3 zichtbaar werd (**hoofdstuk 3**). Echter, niet alleen de tijdsafhankelijke vorming van receptor complexen werd aangetoond, maar in afwezigheid van brassinosteroïden kwamen BRI1 en SERK3 ook al als hetero-oligomeer voor in het plasmamembraan.

In **hoofdstuk 4** wordt een nieuwe methode beschreven waarbij kwantificering van FRET-FLIM data informatie over receptor complexen geeft. Dit heeft geresulteerd dat rond 70% van BRI1 en SERK3 hetero-oligomeren onafhankelijk van hormoon in het plasmamembraan van Arabidopsis wortels aanwezig zijn.

Nu vroegen wij ons af waar en wanneer deze receptorcomplexen gevormd worden. Om hier een antwoord op te vinden wordt in **hoofdstuk 5** verschillende cellulaire markers gebruikt om de compartimenten waar BRI1 en SERK3 bevinden vast te stellen. Het eerste compartiment waar BRI1 en SERK3 colocaliseren was het endoplasmatisch reticulum (ER) wat de eerste plaats is waar eiwitten geproduceerd worden. De FRET-FLIM methode heeft het mogelijk gemaakt om de hetero-oligomerisatie van BRI1 en SERK3 in dit vroege stadium te demonstreren. Deze experimenten konden echter alleen in geïsoleerde plantencellen (protoplasten) worden uitgevoerd. Deze resultaten worden ondersteund door recent onderzoek in Arabidopsis worteltjes waar de handhaving van BRI1-SERK3 complexen op de transport route naar de plasmamembraan wordt aangetoond. Hiermee kan worden geconcludeerd dat BRI1 en SERK3 al in een vroeg stadium na de biosynthese als hetero-oligomeer aanwezig kunnen zijn en als receptorcomplex naar het plasmamembraan getransporteerd worden waar ze als brassinosteroid transductie unit kunnen functioneren.

In het **laatste hoofdstuk** worden de resultaten van het gehele proefschrift samengevat en een nieuwe visie op de signaleringsroute van BRI1 bediscussieerd.

Samengevat toont dit proefschrift aan hoe met behulp geavanceerde fluorescentie microscopie methoden meer inzicht in signaaltransductie gebeurtenissen kan worden verkregen. Echter om een volledig beeld van biologische processen te verkrijgen, is het gebruik van interdisciplinaire methoden noodzakelijk.

Chapter 8

Zusammenfassung in Deutsch

Der österreichische Physiker und Mitbegründer der Quantenmechanik Erwin Schrödinger charakterisierte Leben wie folgt: „Die lebende Materie entzieht sich dem Abfall in den Gleichgewichtszustand“[1]. Der Begriff Gleichgewicht bezieht sich in diesem Zusammenhang auf physikalisch-chemische Potentiale, woraus folgert, dass belebte Materie ein höheres physikalisch-chemisches Potential aufweist als deren Umgebung. Ein Abfall in den Gleichtwichtszustand, das heißt, ein Ausgleich der Potentiale zwischen lebender Materie und deren Umgebung, würde unweigerlich zu einem Stillstand, in anderen Worten, zum Tod führen.

Um sich diesem Ausgleich der Potentiale zu entziehen, müssen Lebewesen jeglicher Art, ob Einzeller, Mensch oder Pflanze, ständig den dynamischen Zustand ihrer Umgebung beobachten. Zu diesem Zweck haben Zellen und Organismen im Laufe der Evolution ein beträchtliches Repertoire an Sensoren, sogenannte Rezeptoren, erworben. Diese Rezeptoren, welche ihrer chemischen Natur nach meist der Klasse der Eiweiße (Proteine) angehören, befinden sich entweder im Inneren von Zellen oder an deren Oberfläche und dienen zur Wahrnehmung unterschiedlichster Signale, wie etwa Licht, Temperatur, Nahrung, Krankheitserreger, Ionen oder auch Hormonen. Das Wahrnehmen eines physikalischen oder chemischen Reizes durch einen dafür spezialisierten Rezeptor löst eine intrazelluläre Abfolge von Reaktionen aus, welche in einer Anpassung des physiologischen Zustandes der Zelle oder des Organismus an die veränderte Umgebung mündet. In ihrer Gesamtheit werden die verschiedenen Schritte der Signalwahrnehmung, Reizweiterleitung und –umwandlung in eine zelluläre Antwort als Signaltransduktionswege bezeichnet.

In dieser Dissertation wurde der Signaltransduktionsweg der pflanzlichen Steroidhormone, der sogenannten Brassinosteroide, untersucht, wobei *Arabidopsis thaliana* (Acker-Schmalwand oder auch Schotenkresse) als Modelorganismus diente. Ähnlich der Wirkungsweise tierischer Steroide beeinflussen Brassinosteroide Entwicklung und Wachstum des pflanzlichen Organismus. Auch strukturell zeigen sich Gemeinsamkeiten zwischen Brassinosteroiden und der tierischen Hormonklasse. Im Gegensatz zu tierischen Zellen, welche die Anwesenheit von Steroiden durch Rezeptoren im Zellinneren wahrnehmen, verwenden Pflanzen allerdings Rezeptoren an der Zelloberfläche. Der wichtigste Rezeptor zur Erkennung von Brassinosteroiden in Pflanzen ist Brassinosteroid insensitive 1 (BRI1). Er gehört der Familie der Leucin-reichen Wiederholung Rezeptor-ähnlichen Kinasen (LRR-RLKs für leucine-rich repeat receptor-like kinases) an, einer der größten Familien an pflanzlichen Rezeptoren. Die schematische Architektur des BRI1 Rezeptors umfasst eine extrazelluläre LRR-Domäne zur Hormonbindung, eine intrazelluläre Domäne mit Kinaseaktivität zur Signalweiterleitung und eine Region innerhalb der Plasmamembran, welche beide Domänen verknüpft und den Rezeptor in der Plasmamembran verankert (siehe Kapitel 1). Genetische

1 aus “Was ist Leben?” von Erwin Schrödinger und Ernst Peter Fischer (1989)

und biochemische Untersuchungen haben gezeigt, dass dieser Rezeptor zwar Brassinosteroide binden kann, jedoch zur Signaltransduktion auf das Zusammenwirken mit einem weiteren Vertreter der LRR-RLK Familie angewiesen ist. Bei dieser weiteren LRR-RLK handelt es sich um den Somatic embryogenesis receptor-like kinase 3 (SERK3) Rezeptor, der auch unter dem Namen BAK1 für BRI1-assozierte Kinase 1 (BRI1-associate kinase 1) bekannt ist. Der schematische Aufbau von SERK3 ist jenem von BRI1 sehr ähnlich, allerdings ist die extrazelluläre Domain deutlich kleiner. Gegenwärtige Modelle, welche versuchen die Funktionsweise dieser beiden Rezeptoren zu erklären, gehen davon aus, dass in Abwesenheit von Brassinosteroiden BRI1 und SERK3 getrennt von einander als inaktive Dimere in der PM von Pflanzenzellen vorliegen. Die Hemmung der Kinaseaktivität von BRI1 wird dabei durch die Anlagerung eines Inhibitors, BRI1 kinase inhibtor 1 (BKI1), gewährleistet, der zugleich die Assoziation mit SERK3 unterbindet. Den Modellen zu folge äußert sich das Binden von Hormonen an die extrazelluläre Domäne in einer Konformationsänderung der BRI1-Dimere. Dieser strukturelle Wandel wiederum bewirkt eine basale Aktivierung der intrazellulären BRI1-Kinasedomäne und resultiert in der Phosphorylierung und Dissoziation des Inhibitors BKI1. Daraufhin erfolgt die Rekrutierung von SERK3 und die Ausbildung von BRI1-SERK3 Hetero-Oligomeren. Durch gegenseitige Phosphorylierung innerhalb dieser Rezeptorkomplexe erlangen beide Kinasen ihre volle Funktionsfähigkeit, was schließlich die intrazelluläre Signalweiterleitung und Brassinosteroid-abhängige Genregulation ermöglicht.

Neueste experimentelle Ergebnisse haben allerdings gewisse Zweifel an diesen Modellen geweckt, vor allem in Hinsicht auf die Bildung von BRI1-SERK3 Komplexen. Genetische Daten konnten zeigen, dass SERK3 und weitere Mitglieder der SERK-Familie nicht nur die Kinaseaktivität von BRI1 steigern, sondern unabdingbar für den Brassinosteroid- Signaltransduktionsweg sind. Weitere Erkenntnisse, gewonnen aus der Aufklärung der molekularen Struktur der BRI1-Ektodomäne, widersprechen zudem der Ansicht, dass BRI1-Dimere für die Hormonbindung verantwortlich sind. Vielmehr wird darüber spekuliert, ob nicht SERK3 bereits Bestandteil des Hormon-bindenden Rezeptorkomplexes ist.

Wie bereits erwähnt, basieren die derzeitigen Modelle des Brassionsteroid- Signaltransduktionsweges vorwiegend auf genetischen und biochemischen Untersuchungen. In der vorliegenden Dissertation wurde deshalb ein Fluoreszenz-mikroskopischer Ansatz gewählt, um diesen Signalweg auf subzellulärer Ebene zu beschreiben.

Das **erste Kapitel** dieser Arbeit umfasst eine detaillierte Einführung in die Brassionsteroid-Signaltransduktionskaskade und eine Beschreibung Fluoreszenz-mikroskopischer Methoden, die zur Untersuchung molekularer Signaltransduktionsvorgänge verwendet werden können.

Eine besondere Methode, welche es ermöglicht die Interaktion von Proteinen beziehungsweise wie im vorliegenden Fall von Rezeptoren zu analysieren, wurde tiefergehend in **Kapital 2** erläutert. Dabei handelt es sich um FRET-FLIM, ein Akronym aus Förster Resonanz-Energietransfer (FRET) und Fluorezenzlebensdauer-abbildende Mikroskopie

(FLIM für fluorescence lifetime imaging microscopy). Diese Art der Mikroskopie erlaubt die Visualisierung von wechselwirkenden Proteinen in lebenden Zellen oder Organismen und gestattet ferner, diese Proteinkomplexe innerhalb einer zweidimensionalen mikroskopischen Abbildung zu lokalisieren.

Nachfolgend wurde FRET-FLIM zur Untersuchung der Hetero-Oligomerizierung von BRI1 und SERK3 in lebenden Arabidopsis-Wurzeln angewendet. In Übereinstimmung mit den bisherigen Modellen zur BR Signaltransduktion konnte gezeigt werden, dass die Aktivierung dieses Signalweges tatsächlich zu einer zeitabhängigen Formierung von BRI1-SERK3 Rezeptorkomplexen führt (**Kapitel 3**). Allerdings wurde nicht nur die Ausbildung neuer Proteinkomplexe beobachtet. Im Gegensatz zu bisherigen Annahmen konnte mit Hilfe von FRET-FLIM auch die Existenz von konstitutiven BRI1-SERK3 Hetero-Oligomeren enthüllt werden.

Zur Quantifizierung dieser Rezeptorkomplexe wurde in **Kapitel 4** eine neue Methode zur FRET-FLIM Datenanalyse eingeführt. Dies ermöglichte abzuschätzen, dass in etwa 70% der BRI1-SERK3 Hetero-Oligomere unabhängig von aktivierend Hormonen innerhalb der Plasmamembran von epidermalen Wurzelzellen vorliegen.

Nun stellte sich die Frage, wann oder wo diese Rezeptorkomplexe gebildet werden. Um eine Antwort darauf zu finden, wurden in **Kapitel 5** zunächst die verschiedenen zellulären Kompartimente definiert, welche beide Rezeptoren zugleich beherbergen. Das erste Kompartiment, in dem BRI1 und SERK3 kolokalisierten, war das endoplasmatische Reticulum (ER), der Ort, an dem beide Rezeptoren synthetisiert werden. Die Anwendung von FRET-FLIM ermöglichte überdies, die Hetero-Oligomerisierung von BRI1 and SERK3 in diesem frühen Stadium der Rezeptorbiogenese zu demonstrieren. Diese Experimente wurden jedoch in isolierten Pflanzenzellen (Protoplasten) durchgeführt. Aber auch nachfolgende Untersuchungen in Wurzeln unterstützen die Ergebnisse der Protoplasten-Studien, indem die Aufrechterhaltung von BRI1-SERK3 Rezeptorkomplexen auf dem zellulären Transportweg zur Plasmamembran nachgewiesen werden konnte. Dies führte zur Schlussfolgerung, dass BRI1 und SERK3 bereits kurz nach ihrer Biosynthese im ER hetero-oligomerisieren und als Rezeptorkomplexe zur PM transportiert werden, dem Kompartiment, in welchem sie ihre Funktion als Brassinosteroid-Signaltransduktionseinheit erfüllen.

Im abschließenden **Kapitel 6** dieser Arbeit wurden die Ergebnisse dieser Fluoreszenzmikroskopischen Studien zusammengefasst und die Auswirkungen auf das Model der Brassinosteroid-Signaltransduktionskaskade ausführlich diskutiert.

Zusammenfassend zeigt diese Dissertation eindrücklich, wie die Anwendung von Fluoreszenz-Mikroskopie das Verständnis von Signaltransduktionsvorgängen vertiefen kann. Sie zeigt aber auch, dass ein umfassendes Bild biologischer Vorgänge nur durch interdisziplinäres Vorgehen zu bewerkstelligen ist.

ACKNOWLEDGMENTS

"Nothing endures but change" (Heraclitus of Ephesus)

This quote has never been so present in my daily life than during the years of my PhD studies in Wageningen, both in the laboratory and in private. The changes I have experienced here are inseparably connected to the personal encounters along my path to this thesis. Therefore I would like to thank all of you, who helped me to navigate through the days and nights along this path.

My first personal encounter here in Wageningen was Prof. Dr. Sacco de Vries, who has been at the same time the promoter of my PhD studies. Thank you so much for giving me the opportunity to follow a PhD program in your group within the Laboratory of Biochemistry at Wageningen University. Thank you for your time and patience, the scientific guidance and discussions, and your trust. I will never forget when you picked me up at this "remote" train station and showed me the way around in Wageningen. Sacco, dank je wel voor het zijn van mijn "Doktor-Vater"!

To continue in the chronological order, I would like to thank Dr. Jan Willem Borst, who was my daily supervisor and co-promoter. We met for the first time in this particular dark room in the basement of the Transitorium, which turned out to be one of the places I would spend most of my time during my PhD studies. You showed me the pleasure of microscopy and this I will take with me on my scientific track. It was a pleasure to follow your way while developing your "Biomolecular Networks" group within the Laboratory of Biochemistry. You not only fulfilled your task as daily supervisor in a literal sense, but you also have always had an open ear for all my other concerns. I appreciate you as a scientific supervisor, a colleague, and friend. Hartelijk bedankt, Jan Willem! Je hebt echt een groot hart!

Even though Jan Willem and Sacco guided me through my thesis, this work would not have been possible without all the people of the "Signal Transduction" and "Biomolecular Networks" groups. Lisette and Danny, you were amazing colleagues and I enjoyed being part of our little familiar group led by our captain Jan Willem. Wilma, Marije, Colette, Esther, Rumyana, Kirsten, Maurijn, and Walter I thank you for all our discussions, your assistance, your patience and scientific input. Wilma, thanks a lot for your contributions to this work. Also a special thank to Marije and Colette. You are both impressive personalities with such a neat balance between scientific ambition and social understanding.

This brings me to Dr. Catherine Albrecht, who enormously contributed to this work, both in practice and theory. The discussions we had are unpayable. Merci beaucoup, Cathy, et chapeau!

Less involved in the scientific part, but the more in the administrative work was Laura van Egmond. Dank je wel voor je hulp met de Wageningse and Nederlandse bureaucratie!

Furthermore, I would like to thank Prof. Dr. Dolf Weijers. I really appreciate that you spent time with me and discussed openly about my work, even though I was not part of your group.

And this also accounts for the previous and present Weijers-group members. Thank you all for your help and discussions.

Moreover, I would like to thank Prof. Dr. Willem van Berkel, Dr. Carlo van Mierlo, and Adrie Westphal for our discussion mainly during the meetings in Veldhoven.

A pleasant encounter within the Laboratory of Biochemistry was also Dr. Jacques Vervoort, who introduced me to the field of international relations. Thank you and your group members.

Besides the people in our own department I also would like to thank the people involved in the Microspectroscopy Centre. Without you most of my work would not have been possible. It was a pleasure to work together with you, especially with Arie van Hoek and Boudewijn van Veen.

Since my PhD studies were part of the European Marie Curie network "BRAVISSIMO" I also would like to thank all the people, who made it possible and turned it into an inspiring experience. A special thank you to Dr. Jenny Russinova, who led the project. But also to all the PostDocs and PhD participants, I really enjoyed our meetings and discussions, especially with you guys Simone, Thierry, and Emanuele.

A special thank you also to the groups of Prof. Dr. Karin Schumacher and Prof. Dr. David Robinson at the Rupprecht Karls University of Heidelberg, who hosted me for colocalization studies. In particular, I would like to thank Falco Krüger, Dr. Melanie Krebs, Dr. David Schürring, and Dr. Corrado Viotti.

The last part of my acknowledgements I want to dedicate to the people, who were close to me inside, but also outside the lab. You made me enjoy the breaks in between my basement sessions. Therefore thank you to:

Stefania Montersino, Alessandra Lillo, Cristina Llavata Peris, Norma Fabregas, Tatyanna Radoeva, Taicia Marques, Monika Haag, Simon Lindhoud, Eike Rademacher, Benjamin Schwessinger, Fabrizio Assenza, Joakim Palovaara, Misha Denis, Vangelis Kouklos, Johan van Woggelum, Adrian Tartia, Matthias Weiß, Marco Martinez, Michael Ziereis, Christian Kiefer, Daniel Aberle, Marco Bischof, and Thomas Oesch.

You really helped me to navigate along my path!

Eventually, I want to thank the people, who have made this path possible in the first place. And these are my parents and family.

Euer Vertrauen, Eure Unterstützung und Wärme haben mir die Kraft und Freitheit gegeben, diesen Weg zu gehen! Deshalb möchte ich Euch allen herzlich danken!

Still, I want to thank two more people in particular.

Jakob, I cannot thank you enough for your love and care! "Navigated by heart" – let's continue our journey without a particular destination! Bruderherz!

Roxana, you make my eyes sparkling, my heart beating, and my soul feeling in ease! My love!

LIST OF PUBLICATIONS

Bücherl, C., Aker, J., de Vries, S., and Borst, J. W. (2010). Probing protein-protein Interactions with FRET-FLIM. Methods in molecular biology (Clifton, N.J.), 655, 389–399. doi:10.1007/978-1-60761-765-5_26

Bücherl, C.A., van Esse, G.W., Kruis, A., Luchtenberg, J., Westphal, A.H., Aker, J., van Hoek, A., Albrecht, C., Borst, J.W., de Vries, S.C. (2013). Visualization of BRI1 and BAK1(SERK3) Membrane Receptor Heterooligomers during Brassinosteroid Signaling. Plant Physiology 162(**4**):1911-25

Halter, T., Mazzotta, S., Wierzba, M., Imkampe, J., Postel, S., **Bücherl, C.**, Kiefer, C., Stahl, M., Chinchilla, D., Nürnberger, T., Zipfel, C., Clouse, S., Borst, J. W., de Vries, S. C., Tax, F., and Kemmerling, B.; The leucine-rich repeat receptor kinase BIR2 regulates complex formation of the multifunctinonal co-receptor BAK1. *submitted*

Laptenok, S. P., Snellenburg, J. J., **Bücherl, C.**, Konrad, K. R., and Borst, J. W.; Global analysis of FRET-FLIM data in live plant cells. *in press*

Bücherl, C., Lingzi, L., Viotti, C., de Vries, S. C., and Borst, J. W.; Illuminating BRI1 and BAK1(SERK3) endosomal trafficking. *manuscript in preparation*

Bücherl, C., and Borst, J. W.; FRET-FLIM in plants. *manuscript in preparation*

Education Statement of the Graduate School
Experimental Plant Sciences

Issued to: Christoph Albert Bücherl
Date: 11 September 2013
Group: Laboratory of Biochemistry, Wageningen University & Research Centre

1) Start-up phase	date
► **First presentation of your project**	
Visualization of receptor kinase interactions in situ/in vivo	Sep 09, 2009
► **Writing or rewriting a project proposal**	
► **Writing a review or book chapter**	
Probing Protein-Protein Interactions with FRET -FLIM, Methods Mol. Biol. 2010; 655: 389-399. 10.1007/978-1-60761-5_26.	2010
► **MSc courses**	
► **Laboratory use of isotopes**	
Subtotal Start-up Phase	*4.5 credits**

2) Scientific Exposure	date
► **EPS PhD Student Days**	
EPS PhD Student Day, Leiden University	Feb 26, 2009
EPS Expectations Day 2010, W ageningen University	Nov 19, 2010
EPS Expectations Day 2011, Wageningen University	Nov 18, 2011
► **EPS Theme Symposia**	
EPS Theme Symposium 'Developmental Biology of Plants', Leiden University	Jan 30, 2009
EPS Theme Symposium 'Developmental Biology of Plants', W ageningen University	Jan 28, 2010
EPS Theme Symposium 'Developmental Biology of Plants', W ageningen University	Jan 19, 2012
► **NWO Lunteren days and other National Platforms**	
ALW/EPW Annual meeting, Lunteren	Apr 06-07, 2009
ALW/EPW Annual meeting, Lunteren	Apr 19-20, 2010
ALW/EPW Annual meeting, Lunteren	Apr 05, 2011
Spring symposium: In singulo biochemistry: biology one molecule at a time, Groningen	May 27, 2011
ALW/EPW Annual meeting, Lunteren	Apr 02-03, 2012
► **Seminars (series), workshops and symposia**	
Invited Seminars Biochemistry: Thorsten Nürnberger (Tübingen, Germany) and Anna Koltunow (Adelaide, Australia)	Dec 2008
Invited Seminars Biochemistry: Ana Cano Delgado (Barcelona, Spain), Sabrina Sabatini (Rome, Italy), Cyril Zipfel (Norwich, Unit ed Kingdom), Dorus Gadella (Amsterdam, Netherlands), Bruno Mueller (Zürich, Switzerland) and Klaus Harter (Tübingen, Germany)	Feb-Dec 2009
EPS Flying Seminar: David Baulcombe (Cambridge, United Kingdom)	2010
Invited Seminars Biochemistry: Roeland de Boer (Barcelona, Spain), Teva Vernoux (Lyon, France) and Richard Smith (Bern, Switser land)	Apr-Nov 2010
Invited Seminar Biochemistry: Keiko Torii (Washington, USA)	Dec 15, 2011
EPS Flying Seminar: V eronica Grieneisen (Norwich, United Kingdom)	Dec 17, 2011
Invited Seminars Biochemistry: Jacco van Rheenen (Utrecht, Netherlands) and David Robinson (Heidelberg, Germany)	Mar-Sep 2012
► **Seminar plus**	
► **International symposia and congresses**	
20th International Conference on Arabidopsis Research (Edinburg, United Kingdom)	Jun 30- Jul 4, 2009
10th EMBL/EMBO Joint Conference on Science and Society (Heidelberg, Germany)	Nov 06-07, 2009
NWO meeting 'Chemistry related to biological and medical science' (V elthoven, Netherlands)	Dec 07-09, 2009
Keystone symposium 'Receptors and Signaling in Plant Development and Biotic Interactions' (T ahoe, USA)	Mar 14-18, 2010
35th FEBS Congress 'Molecules of Life' (Goteborg, Sweden)	Jun 26-Jul 01, 2010
NWO meeting 'Cellular Biophysics and Biochemistry' (V elthoven, Netherlands)	Oct 04-05, 2010
NWO meeting 'Biophysics and life sciences' (V elthoven, Netherlands)	Oct 03-04, 2011
EIMI meeting (Leuven, Belgium)	Jun 05-08, 2012
1st International Brassinosteriod Conference (Barcelona, Spain)	Jun 27-29, 2012
► **Presentations**	
Oral presentation: PhD retreat Laboratory of Biochemistry (Barcelona, Spain)	Apr 21, 2009
Oral presentation: BRA VISSIMO Symposium 'All hormones - all phenotypes' (Lausanne, Switzerland)	March 20, 2010
Oral presentation: ALW/EPW Annual meeting (Lunteren, Netherlands)	Apr 05, 2011
Oral presentation: TSL seminars (Norwich, United Kingdom)	Mach 20, 2012
Poster presentation: ALW/EPW Annual meeting (Lunteren, Netherlands)	Apr 19, 2010
Poster presentation: NWO meeting (V eldhoven, Netherlands)	Oct 03-04, 2010
Poster presentation: ELMI meeting (Leuven, Belgium)	Jun 06, 2012
Poster presentation: 1st International Brassinosteriod Conference (Barcelona, Spain)	Jun 27-29, 2012
► **IAB interview**	Dec 04, 2011
► **Excursions**	
PhD retreat Laboratory of Biochemistry to CSIC-IR TA (Barcelona, Spain)	Apr 21-25, 2009
CropDesign (Ghent, Belgium)	Sep 08, 2011
KeyGene (Wageningen, Netherlands)	Jan 26, 2011
Subtotal Scientific Exposure	*26.2 credits**

3) In-Depth Studies	date
► **EPS courses or other PhD courses**	
FEBS Advanced Course: "Microspectroscopy: Probing Protein Dynamics and Interactions in Living Cells"	Sep 14-23, 2010
FEBS Advanced Course: "Microspectroscopy: V isualization of Protein Dynamics in Living Cells"	Sep 04-13, 2012
► **Journal club**	
Journal club Signal Transduction group, Laboratory of Biochemistry	2008-2012
► **Individual research training**	
Germany)	Feb 20-24, 2012
Subtotal In-Depth Studies	*9.9 credits**

4) Personal development	date
► **Skill training courses**	
PhD Competence assesment	2009
Communication with Media and the General Public	Oct-Nov 2010
Dutch for Employees	May-Jul 2011
Scientific W riting	2011
► **Organisation of PhD students day , course or conference**	
BRAVISSIMO workshop: Microspectroscopy - Monitoring Cellular Biochemistry in vivo	2009
Lab-Outing Laboratory of Biochemistry	2009
EPS Expectations Day 2011	Nov 2011
► **Membership of Board, Committee or PhD council**	
Subtotal Personal Development	*8.1 credits**

TOTAL NUMBER OF CREDIT POINTS*	**48.7**

Herewith the Graduate School declares that the PhD candidate has complied with the educational requirements set by the Educatio nal Committee of EPS which comprises of a minimum total of 30 ECTS credits

** A credit represents a normative study load of 28 hours of study .*

The research described in this thesis was financially supported by the Marie Curie initial training network (ITN) BRAssinosteroid Venture Increasing StudentS' International MObility (BRAVISSIMO) grant number 215118.

Financial support from Wageningen University for printing this thesis is gratefully acknowledged.